

9 CIRCULATION AND STRATIFICATION WITHIN CONTAINMENT

Design basis accident (DBA) evaluations of AP600 and AP1000 containment pressurization transients follow an approach that bounds uncertainties in parameters important for containment response. In this regard, the assessment of circulation and stratification examined a range of possible break elevations, orientations, and momentum to determine the worst case set of assumptions. A summary of the evaluation results and a cross reference to supporting subsections is given in Table 9-1.

The effect of break parameters on mass transfer to heat sinks, the dominant means of pressure mitigation, is evaluated. The evaluation results in both the selection of a limiting scenario for large-scale circulation, and also a conservative handling of potential effects of stratification. The objective is to perform a bounding, or worst case analysis. The effects of circulation and stratification do not lend themselves readily to quantification of a bias and distribution for uncertainty, such as would be done for a best-estimate analysis. For example, it would be very difficult to quantify the probability of a break being directed in any particular direction. Rather the simplest DBA approach is to examine the range of possible break conditions, to select a limiting scenario, and use modeling techniques to bound the potential for reduced heat sink mass transfer.

For equipment qualification (SSAR Appendix 3D.5.5.1.5), the simple bounding approach is taken which uses the temperature in the break compartment as input to the qualification envelope. This temperature is the maximum value in containment. For containment pressure, the evaluation in this section has been performed, summarized as follows.

The containment pressure transient is potentially affected by parameters which influence the dominant heat removal mechanism, mass transfer. Mass transfer has as its primary parameters steam concentration, and, in the case of forced convection conditions, velocity. Large-scale circulation and entrainment into jets or plumes can drive circulation and can affect local values of steam concentration and velocity near heat transfer surfaces. Jet and plume entrainment within compartments or the above-deck region can also result in stratification, or the existence of a vertical steam concentration gradient. Therefore, an assessment of the effects of circulation and stratification should focus on how the steam concentration and velocity are affected. Since the Evaluation Model assumes only free convection inside the containment, the potential benefit of forced convection, when it exists, is neglected. Therefore, the assessment can be further focused on the potential effects on steam concentration distributions.

For the main steamline break (MSLB), the containment vessel shell never becomes the dominant heat removal mechanism before break releases are over; therefore, known biases inherent in the lumped parameter Evaluation Model are used to minimize the internal heat sink effectiveness. Lumped parameter model biases, supported with LST comparisons, are used to impose a conservative break release boundary condition location in the Evaluation Model for MSLB pressure responses.

For the loss of coolant accident double-ended cold leg guillotine break (LOCA DECLG), temporal partitioning has been used to further refine the evaluation for blowdown (0-30 sec.), refill (30 to 90 sec.), peak pressure (90 to 1200 sec.), and long-term (1200 sec. and beyond). During blowdown, volume pressurization is the dominant energy absorber, so the details of mixing and stratification effects are not dominant. During the long-term, the passive containment cooling system (PCS) is the dominant heat removal mechanism, so that increasing the concentration of noncondensables in the above-deck region would reduce the PCS heat removal capability and result in higher calculated containment pressures. The peak pressure period, where both the below-deck heat sinks and the PCS surface are significant contributors, has been assessed by examining extreme release scenarios and examining the range of conditions to select a limiting scenario for peak pressure. The evaluation includes a logical sorting and organization of extreme break scenarios that are quantified by various analytical models and selected experimental results. The analytical models include hand calculations and the use of the WGOTHIC AP600 Containment Evaluation Model for sensitivities to the range of the extreme break scenarios considered.

Entrainment into a jet or plume and large-scale, density-driven circulation between compartments can force some degree of homogenization between and within compartments. Entrainment into a jet or plume can reduce the vertical density gradient occurring due to stratification because of the induced circulation. The assessment of large-scale circulation and compartment density gradients is summarized below.

Large-scale circulation is evaluated by examining a range of extreme release scenarios, including break location, elevation, orientation, and momentum. A limiting, large-scale circulation scenario for the peak pressure period can be shown to result from the assumption of dissipation of the break momentum within the steam generator compartment, at the elevation of the primary system pipe. The scenario is limiting because other scenarios were shown to have improved heat sink utilization, and thus lower peak pressures. For example, the extreme postulated scenario of an undissipated forced jet exiting the upper steam generator compartment opening would drive significantly more convection on the steel shell (PCS) surface, and data indicates that the kinetic energy exiting the steam generator compartment would drive circulation below deck. Mass transfer would be greater than that for a buoyant plume. For a buoyant source and a break low in containment, it is reasonable to use a lumped parameter formulation to model the large-scale, or intercompartment circulation. A review of possible release locations and the expected circulation patterns led to the selection of four potentially limiting cases for further evaluation. The lumped parameter WGOTHIC AP600 Containment Evaluation Model was then used to examine those potentially limiting buoyant source release locations. Results from the sensitivity cases were consistent with the expected circulation patterns in each case, which supports the use of the WGOTHIC lumped parameter model for those sensitivities. Results also showed that the postulated scenarios examined a wide range of possible transient evolutions of steam concentrations throughout the dominant circulating compartments. An assumption of a buoyant release within the broken steam generator compartment reduced the steam access to a large fraction of heat sinks compared to the other locations for a buoyant release, which reduced below-deck heat sink effectiveness and led to the maximum calculated containment pressure.

The use of lumped parameter models can introduce a bias in heat and mass transfer calculations when details within a compartment or region may be important. The simplified momentum formulation can lead to overmixing when multiple lumped parameter nodes are used to represent a single region, such as is done for the above-deck region in the Evaluation Model. Thus, density gradients larger than those predicted by the model in the above-deck region are expected and are assessed independently from the Evaluation Model. The calculation uses a single calculational node to represent each below-deck compartment. The single node representing each compartment allows only an average value of steam concentration for that compartment. For both above- and below-deck regions, density gradients larger than those predicted by the Evaluation Model are evaluated to gain insight into the effects of extreme gradients on heat sink utilization. Showing how sensitive the heat sink utilization is to extreme gradients provides greater confidence that the simplifications inherent in the Evaluation Model have been conservatively bounded.

Since stratification within compartments is not considered explicitly in the WGOTHIC lumped parameter model, it has been evaluated for its effect on total compartment heat sink utilization. The potential for degraded heat sink effectiveness has been examined using a simple calculation for the vertical heat sink distribution and an extreme vertical density gradient. Results show that the total heat sink effectiveness within a compartment or region is affected by the assumed vertical gradients. Evaluations also showed that mass transfer to upward facing surfaces in circulating compartments may be degraded very early in the transient, and heat sink effectiveness within dead-ended compartments may be overestimated by the lumped parameter model after blowdown. Biases have been introduced into the Evaluation Model to bound these effects.

The conclusion of the circulation and stratification assessment provides specific guidelines for the Evaluation Model to bound the effects. The guidelines are summarized in Table 9-1, noted in the conclusions in Section 9.5, and are implemented as noted in Section 4 in the Special Modeling Assumptions subsection for each compartment or region.

9.1 INTRODUCTION

The rupture of the primary system or main steamline piping has the potential to release a significant amount of mass and energy into the containment atmosphere. The passive containment is designed to withstand a loss-of-coolant accident (LOCA) or a main steamline break (MSLB) through a combination of a high containment design pressure and passive heat removal mechanisms. The passive heat removal systems include energy absorption by internal heat sinks as well as heat removal by the passive containment cooling system (PCS).

A containment analysis is performed to verify the adequacy of the containment heat removal mechanisms to maintain post-accident containment pressure below the design limit. In this regard, the WGOTHIC code (Reference 9.1) has been developed as the containment code for performing the design basis containment analysis. Appropriate Evaluation Models (Sections 4 and 13) have been created. These models consider important input parameters such as mass and energy releases, containment volume, internal heat sinks, and PCS heat removal to calculate post-LOCA and post-MSLB containment pressure and temperature response.

To obtain a conservative containment analysis, the effects of circulation and stratification must be bounded by the Evaluation Model. Circulation and stratification are natural processes that occur inside the passive containment during postulated containment pressurization transients and have been identified as important phenomena to be addressed in support of the Evaluation Model for containment pressure calculations (Reference 9.2). The circulation and stratification that occur during a high energy pipe break transient, have the potential to reduce heat and mass transfer rates by transporting and concentrating noncondensables. The degradation of heat and mass transfer may reduce the effectiveness of the heat sinks and the PCS at mitigating the peak containment pressure. The effects of circulation and stratification must be addressed to justify the approach used in the containment Evaluation Model.

This section presents an overview of the effects of circulation and stratification for the containment Evaluation Model for the LOCA and MSLB events. The evaluation results are summarized in Table 9-1. As the table shows, the LOCA and MSLB events are evaluated separately. The LOCA event is divided into four temporal phases based on heat sink utilization: the blowdown phase, the refill phase, the peak pressure phase, and the long-term phase. During each of these phases, important phenomena, such as mass and energy release rates, break source direction, and heat removal mechanisms are considered for impact on circulation and stratification. Unlike the LOCA events, the MSLB events are not divided into temporal phases. The MSLB is characterized by a single, high-intensity blowdown phase. However, different piping rupture locations are considered in the MSLB evaluation.

Table 9-1 Circulation and Stratification Evaluation Summary			
Element	Summary of Evaluation	Relevant PIRT Parameter ⁽¹⁾	WCAP-14407 Section Reference
General Approach			
	Circulation and stratification evaluated because of the potential to degrade heat sink effectiveness via the condensation parameters: <ul style="list-style-type: none"> • Steam concentration • Velocity 	Circulation/stratification (2A), condensation (3F, 7C)	9.0
	High kinetic energy sources, such as during LOCA blowdown and MSLB result in forced convection component of mass transfer	Circulation (2A), condensation (3F)	9.0
	Effects of velocity eliminated in calculation by assuming only free convection internally. Focus, therefore, is on impact of circulation and stratification on steam and noncondensable distributions	Circulation/stratification (2A)	9.0
	Equipment qualification temperature is conservatively taken from the break compartment (containment pressure is therefore, the focus of the evaluation in Section 9)	Circulation/stratification (2A)	9.0
	For the DBA LOCA, volume compliance is the primary pressure mitigator during blowdown, internal heat sinks and the containment steel shell are the primary mitigators during the peak pressure phase, and the steel shell surface is the dominant mitigator during the long-term phase	Gas compliance (2C), condensation (3F, 7C)	9.0, 9.3, 9.3.2.1, 9.3.2.4
	For the DBA MSLB, the internal heat sinks are the dominant pressure mitigators.	Condensation (3F)	9.0, 9.4.3

Table 9-1 (cont.) Circulation and Stratification Evaluation Summary			
Test Data			
A. Method to Address Distortions in the LST for Circulation and Stratification Assessment	Power to volume ratio: using only quasi-steady-state data for circulation and stratification, therefore, no impact of this distortion on these results.	Stratification (2A), int. heat sink conduction (3D), shell conduction (7F)	9.2.3
	Power to area ratio: <ul style="list-style-type: none"> • Steam flow was ranged and external boundary conditions were ranged • Considering the matrix of the LST, a range of power-to-area (or condensation rate) ratios were considered, which minimizes the degree of the distortion • Distortion addressed by considering stratification and condensation data from LST matrix tests and supplementing LST with assessment of international test data for stratification 	Circulation/Stratification (2A)	9.2.3, 1.4.1
	Circulation path impact on <i>circulation</i> : cannot use the LST data for assessment of circulation. Addressed by supplementing LST with assessment of international test data for circulation	Circulation (2A), intercomp flow (2B)	9.2.3
	Circulation path impact on <i>stratification</i> : <ul style="list-style-type: none"> • Lack of LST SG compartment circulation results in LST stratification more extreme than if a circulation path existed • Addressed by supplementing LST with assessment of using international test data for stratification 	Stratification (2A), intercomp flow (2B)	9.2.3

Table 9-1 (cont.) Circulation and Stratification Evaluation Summary			
B. Usage of LST Data for Circulation and Stratification Assessment	LST above-deck separate effects style data for condensation and stratification is considered	Mass and energy (1A), direction and elevation (1B), momentum (1C), Circulation/stratification (2A)	9.2.1, 9.2.2
	LOCA - applicable tests had diffuser under the SG, reference case had elevated diffuser. Key LST result - above-deck stratification data used to support development of a bounding stratification gradient for evaluation of heat sink utilization for peak pressure/long-term phases	Stratification (2A)	9.2.1
	MSLB - applicable tests had elevated 3" pipe pointing vertically/horizontally. Key LST results - kinetic energy drives circulation below-deck, forced convection significantly enhances mass transfer (factor of 1 to 10 over shell surface relative to free convection mass transfer)	Circulation/stratification (2A)	9.2.2
Lumped Parameter Biases Implemented in WGOTHIC Evaluation Model			
A. International/ Industry Experience	Lumped-parameter modeling uses a simplified momentum formulation, which biases calculated pressure with respect to circulation and stratification. These biases are evaluated and bounded by the Evaluation Model.	Circulation/stratification (2A)	9.1.2
	NUPEC modeling experience is applied to Evaluation Model compartment flow connections, resulting in reasonably predicted circulation patterns.	Circulation (2A) Inter-compartment Flow (2B)	9.2.4, Appendix C Section 9.C.3

Table 9-1 (cont.) Circulation and Stratification Evaluation Summary			
B. LOCA Biases	The effects of stratification on heat sink utilization are negligible for compartments experiencing downflow of heavier ambient atmosphere mixture	Stratification (2A)	9.3.1.1
	<ul style="list-style-type: none"> • Dead-ended compartments with no assumed thermal gradients stratify • Condensation and convective heat transfer turned off in dead-ended compartments after 30 seconds 	Stratification (2A)	9.3.2.1
	<ul style="list-style-type: none"> • Effect of stratification on steel shell condensation assessed with extreme gradient • Stratification effect bounded by removing upward facing surface of operating deck as a heat sink 	Stratification (2A)	9.3.1.1
	<ul style="list-style-type: none"> • Effect of stratification on heat sinks in a below-deck compartment assessed with extreme gradient • CMT room (most heat sinks) evaluated for case in which LOCA plume is rising in room • Stratification effect bounded by removing floor as heat sink (bias applied in all compartments regardless of assumed break location) 	Stratification (2A)	9.3.1.3
C. MSLB Biases	LST data indicates: <ul style="list-style-type: none"> • Kinetic energy drives some circulation below-deck • Forced convection is driven by high kinetic energy jet above-deck • No significant stratification above-deck, therefore no bias required 	Circulation/stratification (2A)	9.4.2

Table 9-1 (cont.) Circulation and Stratification Evaluation Summary			
	<p>Lumped parameter model code biases:</p> <ul style="list-style-type: none"> • Evaluation Model places break node at operating deck level minimizing circulation and steam access to below-deck heat sinks • Momentum dissipated in each node (Evaluation Model uses only free convection) • Density-driven circulation as plume rises resulting in relatively homogeneous region above modeled break node <ul style="list-style-type: none"> – results in steam-rich region above modeled break node and steam-deficient region below modeled break node, which bounds effects of stratification – conservatively, the LOCA stratification biases are included for the MSLB Evaluation Model 	Circulation/ stratification (2A)	9.4.2
LOCA Evaluation Results			
A. Considerations by Time Phase for Evaluation Model	<p>LOCA blowdown (0 to 30 seconds):</p> <ul style="list-style-type: none"> • Blowdown pressurizes compartments and drives significant circulation above and below-deck • Lumped parameter modeling adequate for pressure-driven flow • Containment pressure insensitive to noding (multi-node vs. one-node model) • Low sensitivity to heat sinks because volume storage is dominant pressure mitigator • Fr indicates significant forced convection on steel shell, Evaluation Model conservatively assumes only free convection • Steam driven into dead-ended compartments. Assuming thermally uniform heat sinks results in no circulation, therefore, condensation and convection heat transfer in dead-ended compartments neglected after 30 seconds. 	<p>Intercompartment Flow (2B)</p> <p>Gas compliance (2C)</p> <p>Break source momentum (1C)</p>	<p>9.3.2, 9.3.2.1</p> <p>9.2.2</p>
	<p>LOCA refill (30 to 90 seconds):</p> <ul style="list-style-type: none"> • Break releases are negligible • Containment depressurizes during this phase • Conservatively ignore containment pressure reduction by neglecting this phase to maximize initial pressure for the peak pressure phase 	Break source mass and energy (1A)	9.3.2.2

Table 9-1 (cont.) Circulation and Stratification Evaluation Summary			
	Jet to RCDT cavity - dissipated plume rises in CMT North room <ul style="list-style-type: none"> • Good steam access to below-deck room with most internal heat sinks 	Break source (1B, 1C)	9.3.1.3
	Jet to RCDT cavity - dissipated plume rises in SG West compartment <ul style="list-style-type: none"> • Same scenario as dissipated jet rising in SG East compartment 	Break source (1B, 1C)	9.3.1.3
	Jet dissipates in RCDT cavity <ul style="list-style-type: none"> • Flow split based on flow area and loss coefficients • Better steam access to CMT room and SG West compartment compared to break in SG East compartment 	Break source (1B, 1C)	9.3.1.3
C. Sensitivity Cases Run with the Evaluation Model	Break locations (all located low in containment): <ul style="list-style-type: none"> • Jet undissipated in SG East compartment - forced convection benefit on steel shell assessed to estimate effect of undissipated jet • Jet dissipated in SG East compartment - limiting case for maximum containment pressure • Jet into RCDT cavity - plume rises in CMT North room • Jet dissipated in RCDT cavity - plume rise determined by flow path resistances 	Intercompartment Flow (2B)	9.3.2.5
	Loss coefficients: <ul style="list-style-type: none"> • Loss coefficients for several flow paths changed to modify blowdown-predicted flow direction • Modeled dissipated jet in SG East compartment • End of blowdown conditions changed with negligible change to maximum containment pressure 	Intercompartment Flow (2B)	9.3.2.1

Table 9-1 (cont.) Circulation and Stratification Evaluation Summary			
	Thermal and circulation effects of drops: <ul style="list-style-type: none"> • Drops only created during LOCA blowdown • Thermal effects <ul style="list-style-type: none"> - 5 percent drop formation enough to saturate containment atmosphere - 0 percent drops less limiting for maximum containment pressure - Negligible change in containment pressure between 100 percent drops and Evaluation Model (approximately 50 percent drops) • Circulation effects examined for 0 and 100 percent drop formation <ul style="list-style-type: none"> - Presence of drops increases density of atmosphere increasing relative buoyancy of plume - Containment atmosphere entrainment into plume is significant for both 0 and 100 percent cases 	Break source droplet/liquid flashing (1E) Stratification (2A) Intercompartment Flow (2B) Containment volume fog (2D)	9.2.3.6 5.8 9.2.3.6
D. Conclusions	<ul style="list-style-type: none"> • Evaluation Model with dissipated break in SG East compartment is the limiting scenario <ul style="list-style-type: none"> - Calculated containment pressure is not very sensitive to break location due to heat sink utilization prior to maximum pressure • Biases included in Evaluation Model to bound effects of stratification 		9.2.3.5, 9.5
MSLB Evaluation Results			
A. Break Location Scenarios and Effects	<ul style="list-style-type: none"> • Selected based on routing of steamline pipe • MSLB above-deck <ul style="list-style-type: none"> - High kinetic energy release with relatively short duration, which drives circulation below the source - High Fr number (comparison provided to LST Fr number) - LST data indicates forced convection enhancement to mass transfer (only free convection modeled) - Break in MSLB Evaluation Model located in node just above-deck, which limits steam access to below-deck heat sinks 	Stratification (2A) Intercompartment Flow (2B) Break source (1B, 1C)	9.4, 9.4.1, 9.4.1.1, 9.4.2

Table 9-1 (cont.) Circulation and Stratification Evaluation Summary			
	<ul style="list-style-type: none"> • MSLB in CMT North room <ul style="list-style-type: none"> - Break in CMT room would significantly dissipate due to equipment in room and rise as a plume - CMT room contains most of the internal heat sinks - Good steam access to CMT room heat sinks, therefore case is expected to be less limiting 		9.4.1.2
B. Sensitivity Cases	<ul style="list-style-type: none"> • MSLB located just above deck • MSLB in CMT North room 		9.4.3
C. Conclusions	<ul style="list-style-type: none"> • MSLB in CMT North room calculated containment pressure significantly less limiting • MSLB located just above-deck used for the MSLB Evaluation Model 		9.4.3, 9.5

(1) PIRT parameters are identified in Reference 9.2, Table 4-1

9.1.1 Definitions

Several terms used to discuss circulation and stratification are defined, as they relate to containment analysis.

Stratification is a state characterized by strata, or horizontal layers, of different density. Stratification is stable when the lower layers are increasingly dense due to composition and/or temperature. The term stratification does not indicate the magnitude of the density gradient.

Mixing is a collective term for convective transport processes that reduce temperature and/or concentration differences within a volume or between volumes. Convective transport processes in containment include jets, plumes, wall layers, turbulent diffusion, and entrained flow. Molecular diffusion also contributes to mixing but is considerably less effective than convection, except in boundary layers. Diffusion also contributes to mixing in stratified conditions.

Circulation is a term used to describe gross, overall convective flow patterns that occur on a compartment scale and on a large scale (or containment scale). The compartment-scale circulation is due to wall layers, jets, plumes, and entrained flow. The large-scale circulation is due to interactions between compartments induced by pressure, density, elevation, and momentum differences such as intercompartment flow. The break source jet or plume can induce both compartment-scale and large-scale circulation.

Segregation is a state characterized by a different air/steam concentration in one compartment than in another. For example, the heavier air may reach different concentrations in separate compartments, especially the dead-ended compartments if the intercompartment circulation is low.

9.1.2 Lumped Parameter Biases and Capabilities

Lumped parameter biases and capabilities have been identified based on industry experience, as documented in the literature (Appendix 9.C, Section 9.C.3.4). The documented experience base includes facilities at different geometric scales, from that of the LST to nearly full-scale AP600 height (Appendix 9.C, Figure 9.C.2-1). The lumped parameter biases and capabilities, summarized below, have been reported consistently across the range of facilities, indicating that the biases and capabilities are applicable to the Containment Evaluation Model. The consistency across scales also indicates that the LST facility is a reasonable basis on which to study the biases and capabilities as they apply to AP600, reported in WCAP-14382 (Reference 9.1). The following provides a summary of the method used in the development of the Containment Evaluation Model to address each documented bias and capability.

1. Single node models were not capable of modeling stratification, or the passing of a stratification front through horizontal vents.

(a,c)

2. Sump liquid level and sump temperature were not well predicted

(a,c)

3. Some codes produced results which were not correct due to missing or oversimplifying buoyancy terms

(a,c)

4. To account for recirculation flows, the applied lumped parameter model used double junctions in the horizontal direction. (This did not help in the case of an elevated release and resulting stratified containment.)

See discussion for item 3 above regarding the impact of lumped volume static pressure profile on the use of double junctions in the Evaluation Model. All of the LOCA cases have releases in the lower compartments (below the operating deck). This break location results in good circulation throughout containment. The main steamline break releases contain high kinetic energy. Therefore, the break node used in the lumped parameter model is a node that minimizes kinetic energy driven circulation to below-deck heat sinks, thus overestimating calculated containment pressure.

5. For releases low in containment, typical for the LOCA DECLG, the lumped parameter model well-predicted pressure, temperature, and helium concentrations inside the compartments, which were affected by the global circulation loop, while predictions needed improvements to account for postulated circulation effects inside dead-ended compartments

(a,c)

6. Scenarios with homogeneous containment atmosphere (like HDR E11.4 and E11.5) can be simulated successfully with lumped parameter models. (Such conditions typically result from breaks located within the bottom 20 percent of the containment height.)

See discussion for item 5 regarding the use of lumped parameter models for bounding design basis analyses.

7. Circulation effects due to sump boiling (releases generated at the bottom of containment) were well-simulated.

Sump boiling is not a consideration for containment DBA, since long-term primary system energy rejection is through the ADS Stage 4 valves and the sump is therefore a relatively insignificant heat source.

8. The order of magnitude of computed velocities matches data and it can be concluded that trends in the direction of the flow are predicted well; however, predicted velocities differ by as much as a factor of two.

Calculated velocities using lumped parameter codes are strongly dependent on the noding used. Experience with validating the WGOTHIC lumped parameter model of the LST (Reference 9.1, Section 8.2) shows that the noding used can result in calculated velocities that differ from measured by an order of magnitude, showing that the particular test facility and noding used can have a strong influence on calculated velocities. Therefore, a bounding approach is used in the WGOTHIC Evaluation Model, as follows. The effects of predicted velocities in the containment pressure transient are eliminated by considering only free convection heat and mass transfer in the containment. This conservatively biases the Evaluation Model when forced convection would occur during the LOCA blowdown and the MSLB transients.

9. The lumped parameter method does not have the capability to predict the hydrogen distribution in a stratified containment atmosphere, as in HDR E11.2 with high-positioned release. In a break scenario with buoyant plume (released at about 50 percent of containment height), the steam and gas transport to the lower parts of the containment were over-predicted. (Artificial limitation of convective flows by decreasing flow areas improved predicted concentrations in the lower regions, but overestimated the containment pressure in upper compartments.)

Hydrogen distribution predictions are not a consideration for containment DBA (Reference 9.2, Section 4.4.2E).

9.2 LARGE-SCALE TEST RESULTS

In the passive containment design, interest is focused on how much the jet kinetic energy affects gradients inside containment. If the jet kinetic energy is sufficient to disrupt stable stratification, it may also be sufficiently energetic to virtually eliminate vertical gradients in the upper containment volume and to induce circulation between the above-deck and below-deck regions. The Westinghouse Large-Scale Test (LST) data was used to understand the effect of jet kinetic energy on stratification gradients above the operating deck.

The Westinghouse large-scale PCS test facility was built to provide integral test data for a geometrically similar model of the AP600 containment vessel and PCS. The tests provide experimental data that can be used for evaluating the physics in containment, determining the relative importance of various parameters that affect heat and mass transfer, and validating computer codes. Three series of tests (References 9.5 and 9.6) were run at the Westinghouse large-scale PCS test facility. The steady-state pressure, annulus air flow rate, water coverage, steam flow rate, injection velocity, location and orientation, and noncondensable gas concentration were varied between the tests.

It is desirable to use a Froude number formulation that relates momentum phenomena in both the AP600 and the LST to permit scaled inferences between the tests and the AP600. A volumetric Froude number can be defined as the square of the jet Reynolds number, divided by the containment Grashof number:

$$Fr_v = \frac{\rho_a U_o^2 d_o^2}{g(\rho_a - \rho_o)H^3}$$

where ρ_a = density of ambient containment
 U_o = velocity of jet at source
 d_o = hydraulic diameter of jet at source
 g = gravitational acceleration
 ρ_o = density of jet source
 H = height of volume above steam source

The following sections first describe test configurations as they represent LOCA and MSLB configurations and then provide data that can be used to examine gradients in the above-deck region.

9.2.1 LOCA Configuration

Twenty-five LSTs were conducted in the LOCA configuration with the diffuser located under the steam generator model. A diffuser was used to provide a uniform velocity profile. The tests do not apply to the LOCA blowdown phase, but they do apply to the peak pressure and long-term phases. The volumetric Froude numbers ranged from approximately 5×10^{-6} to 5×10^{-3} . Steam concentrations just above the deck and below the deck near the bottom of the vessel are presented in Figure 9-1, which can be used to see test-to-test variation in above-deck gradients. The plotted values are the ratios of the measured local steam partial pressure to the partial pressure of steam assuming perfect mixing. A value of 1.0 indicates perfect mixing. The values show the above-deck ratios generally range from 0.6 to 1.0 and below-deck values range from 0.1 to 0.4. The below-deck values are an indication of the distortion in the LST due to lack of a simulated steam generator compartment flow path. The distortion leads to an air-rich mixture in the LST below-deck.

Stratification data for LSTs with the diffuser under the simulated steam generator compartment are shown in Figures 9-2 through 9-25. Tests have been grouped by steam flow and plotted so that the temperature axis spans the same range for all the tests to simplify test-to-test comparison. For each group of tests, three plots are shown. First is the azimuthally-averaged temperature data from thermocouples located one inch inside the vessel shell, called the "fluid thermocouples." Data is available from nine elevations above the operating

deck; fluid thermocouple data was not taken below the deck. Second is a plot of the saturation temperature obtained based on the third plot of measured steam mole fractions, or pressure ratio ($p_{\text{stm}}/P_{\text{vessel}}$).

Also, a reference test to examine the physics of stratification (test 222.2), with an elevated diffuser, is included as Figures 9-26 through 9-28. These test data are reviewed in Section 9.2.3 to develop insight into an appropriate bounding stratification gradient.

9.2.2 MSLB Configuration

Phase 3 of the LST program included a series of tests designed to simulate a main steamline pipe rupture. LST data from baseline and Phase 2 tests suggested that noncondensable concentrations increase dramatically below the elevation of steam injection with considerable steam mixing above the operating deck. One could postulate that the effect of the higher steamline elevation could be to create a larger volume of rich air mixture which extends above the operating deck, and reduces the active heat transfer area. Test series 222 addressed the impact of the elevation and direction of the steamline break on the response of the test vessel and included a high flow transient to a steady-state condition. The kinetic energy available in an MSLB is seen to be an important parameter.

The four configurations in this test series were:

- 222.1 Low velocity steam flow from under the operating deck
- 222.2 Low velocity steam flow above the operating deck (a reference condition to examine the physics, not a realistic AP600 configuration)
- 222.3 High velocity steam flow with horizontal discharge above the operating deck
- 222.4 High velocity steam flow above the operating deck directed upward

Stratification data for LSTs with high kinetic energy above the operating deck are shown in Figures 9-29 through 9-34, also grouped by steam flow, and showing measured internal fluid temperature, saturation temperature, and measured steam pressure ratio, as described in Section 9.2.1 for the LOCA configuration. These data are referenced in the development of a bounding MSLB Evaluation Model (Section 9.4.2).

To understand the effects of kinetic energy on circulation and stratification, it is useful to note the stratification pattern observed for a test with a buoyant source (low Froude number) versus a test with a high Froude number. For example, test 222.4 can be used to assess the effects of steam releases with Froude numbers representative of an MSLB occurring above the steam generator. Test 222.4 is compared to test 222.2, which had a similar setup, but a diffuser was used to provide a low velocity elevated steam source.

The elevated buoyant source in test 222.2 produced a significantly stratified vessel, with very little steam penetration below the elevation of the break. In contrast, the high kinetic energy-elevated source of test 222.4 induced a substantial amount of circulation in the test vessel, including substantial steam ingress into the below-deck regions. The decrease in the steam concentration stratification for test 222.4 compared to test 222.2 is due to the high kinetic energy of the injected fluid because that is the only significant difference between the two tests.

Mass transfer data from LSTs with high velocity jets (forced convection) has been compared to that from the low velocity diffuser under the simulated steam generator (dominated by free convection) in Reference 9.9, Figure 3.9-5. The referenced figure includes shell condensation data above the operating deck for the elevated high momentum source LST compared to the mean of such data from the diffuser under the steam generator. The elevated diffuser LST is not included in the referenced figure due to its atypical condition of a low Froude number elevated source - the elevated releases which may be postulated for an MSLB are of a higher Froude number similar to that of the tests for which data are plotted, as described earlier in this section. Results indicate that in the LST forced convection effects enhanced the mass transfer rate by a factor of 1 to a factor of 10 in the direction the jet is directed.

9.2.3 Method to Address Distortions in LST Stratification Data

Internal momentum effects were distorted in the LST due to the lack of a simulated flow path for entrainment near the bottom of the steam generator compartment. Thus in the LOCA DECLG configuration, the LST effectively stratified into two regions - separated at the elevation of the steam generator compartment exit (Section 9.2.1). Therefore, the LST cannot be used to examine intercompartment circulation.

There is also a system level distortion in the LST with respect to power-to-volume and power-to-area (Reference 9.7, Section 11). Since only quasi-steady state data for circulation and stratification were used, there is no impact of power-to-volume distortion on this evaluation. The LST quasi-steady data was taken with a range of break flow rates, and the external wall boundary condition was ranged using controllable variables (turning external water and fan on and off). The internal release configuration also allowed varying the release elevation, momentum, and direction. Initial noncondensable content ranged from near vacuum to two atmospheres. Thus the LST provides a valuable database to examine the physics of potential stratification mechanisms that may be postulated to occur in a passive containment.

Because of the momentum-related distortions in the LST, available international test data has been reviewed (Appendix 9.C, Section 9.C.2) to supplement the database for examining stratification effects. The supplementing of LST data with additional tests at various scales, combined with the use of LST matrix tests, sufficiently addresses the system level power-to-area distortion. The following summarizes conclusions that may be drawn from LST and the international databases, leading to the selection of an extreme stratification gradient to be considered in thermal calculations of Appendix 9.B.

It is desired to gain insight into vertical steam concentration gradients that may occur within the region above the operating deck and within compartments below-deck during a LOCA. (The bounding approach for an MSLB is given in Section 9.4.2.) The region above the operating deck in the LST can be considered to be an enclosure with a plume and wall boundary layers (Appendix 9.C, Section 9.C.1.4.1). The relevant vertical profile data is presented in Figures 9-2 through 9-25. Comparisons of internal fluid thermocouple data (1-inch inside the vessel wall) and steam concentration measurements show that the gas is within a few degrees of saturation, so that the vertical temperature profiles provide a good measure of the vertical steam concentration gradient during the LSTs. Clearly, for the diffuser under the steam generator model, there is only about a 3 to 12°F temperature gradient from the steam generator exit elevation to the dome. The plotted data is at the fluid thermocouple location. A review of the internal rake temperature data shows that the bulk fluid vertical temperature difference is equal to or several degrees less than that given by the fluid thermocouples.

Comparison of the vertical temperature profile from the elevated diffuser case in the LST (Figure 9-26) shows that the stratification in the above-deck region is more pronounced than that in any of the tests with the LOCA configuration. Such stratification from an elevated diffuser is similar to that observed in the CVTR tests (Appendix 9.C, Section 9.C.2.3) which had a similarly elevated, low momentum source. Tests in the much larger HDR and NUPEC facilities indicate that stratification gradients from diffuse releases low in containment in fact produce temperature gradients above the operating deck similar in magnitude to those quoted above in the LST with a low diffuser. However, because of the distortions in LST mentioned above and uncertainties in transferring stratification data from HDR and NUPEC to AP600 and AP1000, an extreme stratification gradient, well beyond that which would occur in a containment with natural convection and a low elevation release, has been considered for thermal calculations.

The steam concentrations used for thermal calculations presented in Appendix 9.B assume a three region distribution — nearly pure steam at the top (steam fraction 0.98), the average value at the middle (steam fraction 0.63), and the balance of the air content at the bottom (steam fraction 0.28). The elevated diffuser case in the LST shows a steam pressure ratio (equal to steam mole fraction) of 0.10 near the operating deck and 0.90 under the dome. The distribution chosen is consistent with that indicated by the LST elevated diffuser, considering that the Appendix 9.B calculation represents an average steam concentration calculated for AP600 transient conditions. It should be noted that the LST elevated diffuser test produces an extreme, or bounding, test configuration for the real situation of a buoyant plume released low in containment, such as for the LOCA DECLG post-blowdown. Thermal calculations in Appendix 9.B are used to develop appropriate biases to bound the effects of stratification within the AP600 and AP1000 lumped parameter compartment nodes and the above-deck region.

9.2.4 Application of Modeling Methods Developed for NUPEC M-4-3 Lumped Parameter Model

The following is a brief summary of the experience gained in developing the WGOTHIC lumped parameter model of the NUPEC natural circulation test, M-4-3, and application of the experience to development of the WGOTHIC lumped parameter Evaluation Model. Justification is provided for using the lumped parameter Evaluation Model for performing sensitivity studies. The sensitivities are used to examine the effects of circulation in containment from a LOCA DECLG.

NUPEC Lumped Parameter Modeling Experience

Actual circulation was interpreted based on data provided by NUPEC for the detailed time history for gas temperature and hydrogen concentration as well as a video of processed data to aid visualization.

As shown in Figures 9.C.2-32 (flow pattern) and 9.C.2-38 (data for one circulation loop) of Appendix 9.C, the break flow rose from the affected steam generator loop, spread through the upper portion of the large vertical opening into the adjacent steam generator loop, and rose from those two compartments into the dome. The large-scale natural convection loop continued with continuity driving circulation down through the opposite steam generator compartments and other openings through the operating deck, and then down to the level of the break release. From the break release level, the convection loop was closed by entrainment into the rising plume. This result is consistent with results of international tests at several scales and is rather simple and straightforward. However, careful development of the lumped parameter noding structure is necessary to allow the code to predict the observed qualitative behavior, as follows.

It should first be noted that for the M-4-3 calculations, best estimate condensation correlations were used to better isolate the biases of lumped parameter noding on predicted parameter distributions and the effect of those biases on containment pressure.

For general application of WGOTHIC lumped parameter, it is necessary that the vertical noding be defined by a set of horizontal planes that cut through the entire modeled region, as described in Reference 9.4, Section 16.12.1. This is done to prevent artificial flows driven solely by the method used to estimate a static pressure profile using the single value of density available within a lumped parameter cell. The successful elimination of such artificial circulation is confirmed when a new model is developed by running a null problem (uniform temperatures in heat sinks and volumes, and no heat or mass source) and verifying that there is no predicted circulation.

(a,c)

Application of NUPEC Test Experience to Containment Evaluation Model

The Evaluation Model has been verified to have no significant artificial flows in a null problem. In the further development of the WGOTHIC lumped parameter noding used in the containment pressure Evaluation Model, experience with the NUPEC tests was used qualitatively in representing the CMT compartment.

(a,c)

+a,c

9.3 CIRCULATION AND STRATIFICATION ASSESSMENT FOR THE LOSS-OF-COOLANT ACCIDENT

The rupture of primary system piping can lead to a significant release of mass and energy into the containment. A containment analysis is performed to verify the ability of the passive containment systems to mitigate the consequences of a hypothetical LOCA. The WGOTHIC code, in conjunction with the Containment Evaluation Model, is used for the containment analysis. The effects of circulation and stratification must be bounded by the containment analysis calculations to ensure a conservative containment analysis. For purposes of evaluating the effects of circulation and stratification on the LOCA containment analysis, the LOCA event is divided into four temporal phases: the blowdown phase, the refill phase, the peak pressure phase, and the long-term phase, based on Section 3.4.2.2 of Reference 9.2.

The blowdown phase is the period immediately following the rupture of the primary system piping: For the design basis event, a double-ended, cold leg guillotine (DECLG) break is assumed, which results in the complete severance of the pipe. This phase is characterized by a rapid depressurization of the reactor coolant system (RCS), as the RCS inventory is expelled into the containment volume. The containment gas volume rapidly pressurizes due to the tremendous release of mass and energy. This phase is short in duration (about 30 seconds) and ends when the RCS pressure has equilibrated with containment.

The refill phase immediately follows blowdown. After blowdown, the accumulators refill the lower plenum of the reactor with a high flow rate of cold water. The resulting steam and water flow rates from the break are very low and increase with time. The mass and energy release rates are two orders of magnitude less than the blowdown rates, and can be approximated as 0 from approximately 30 to 90 seconds into the event. With a negligible steam source rate and a high condensation rate, the containment pressure drops by a few psi from its peak at the end of blowdown to the end of the refill phase at approximately 90 seconds. (It should be noted that the Evaluation Model used for sensitivity studies conservatively neglects the refill period.)

The phase following refill is the peak pressure phase. During the beginning of the peak pressure phase, a continuing pressurization of the containment building accompanies the release of mass and energy. Containment pressurization is mitigated by the containment volume and the presence of the substantial number of heat sinks inside containment. Hot steam condenses on the cold steel and concrete surfaces, which transfers energy into the heat sinks. As this phase continues, the temperature of the internal heat sinks increases and their effectiveness is reduced. By this time, however, water flow onto the containment shell has initiated. The PCS provides the path to the ultimate heat sink, and represents the only assumed path through which energy can be removed from inside the containment building. A key feature of the peak pressure phase is the second, more limiting, pressure peak. The combination of internal heat sinks and the PCS act to limit the containment pressurization, and containment pressure begins to drop. Later in this phase, the PCS becomes clearly dominant. The peak pressure phase extends from 90 seconds to about

1500 seconds when the containment pressure reaches its peak. During this phase, ADS Stage 4 actuates and becomes the source of mass and energy release.

The long-term phase is the period after the peak pressure occurs out to twenty-four hours and beyond. During the long-term phase, core decay heat continues to create steam, which exits the fourth stage automatic depressurization system (ADS) as a buoyant plume. The containment continues to depressurize as a result of energy removed by the PCS. As containment pressure drops, internal heat sinks may begin to reject some of their heat back into the containment atmosphere. Thus the long-term phase depressurization is governed by PCS heat removal.

To facilitate an understanding of the relative positions of the various compartments, a simplified AP600 compartment diagram is provided in Figure 9-36. Figure 9-36 shows the relative location of various important compartments, such as the steam generator compartment, the core makeup tank (CMT) compartment, and the above-deck volume. Noding used to represent these compartments within the Evaluation Model is described in Section 4. The compartment features are discussed in Section 4 and summarized in Table 3-1 of Reference 9.2.

Figure 9-35 presents a diagram of the CMT compartment. The CMT room contains most of the below-deck containment heat sinks (approximately 52 percent of below-deck heat sinks by area). Although 48 percent of the heat sinks are not in the CMT room, no other single below-deck compartment contains as many heat sinks. Also, the CMT room is the largest (volume) of the below deck compartments and contains many flow paths. These flow paths mean that the CMT room is of significant importance with respect to both above- and below-deck circulation patterns. Therefore, the effect of circulation and stratification on heat sink utilization in the CMT room plays an important part in the transient pressure mitigation.

9.3.1 LOCA Break Scenarios

The DECLG rupture is the design basis LOCA event for the AP600 and AP1000. The circulation and stratification patterns associated with this break will depend on the direction of the break jet momentum. Although leak-before-break has been implemented, the conservative design basis analysis evaluation assumes the broken pipe can be pointed in any direction from its nominal position. Three scenarios may be postulated: the jet momentum is locally dissipated in the steam generator compartment, the jet exits undissipated up through the steam generator compartment, or the jet momentum is dissipated in the reactor coolant drain tank (RDCT) cavity (stairwell).

9.3.1.1 Jet Momentum Locally Dissipated in Steam Generator Compartment

During the blowdown phase, a tremendous amount of mass is released as shown in Figures 4-96 and 4-98 of Section 4.5.2 for AP600. For the case where the jet momentum is locally dissipated, the source flow rate is so high that it increases the local pressure by several psi. This results in a high-pressure source in the break compartment, with the fluid flow distribution governed by the relative resistances through flowpaths. This forces the source mixture through the RCDT cavity, CMT room, the steam generator compartments, and into the above-deck volume. Pressurization will also drive steam into dead-ended compartments during blowdown (See subsection 9.3.2.1). As the event progresses into the peak pressure phase, the source flow rate drops by two orders of magnitude. The jet momentum locally dissipates. This brings the source flow velocity to near zero, including a local pressure increase that is the same order of magnitude as the buoyant forces. The pressure source may be opposed or aided by buoyancy in other flow paths. The resulting flow pattern is the solution to the flow in a network with buoyancy and heat/mass transfer in the network branches. Superimposed on the large-scale flow, the mixture within a given compartment is most likely stratified (Reference 9-8).

Within compartments, the gas may stratify with air concentrating in lower regions and steam concentrating in upper regions, resulting in a vertical steam concentration gradient. If the circulation is sufficient to entrain significant bulk mixture, the gradient may be expected to be small. Entrainment-driven circulation rates in the CMT room are shown, for example, in Section 9.3.1.3. Significant circulation occurs over the height of the CMT room.

Stratification is expected in the containment based on LST data. Low Froude numbers during the long-term indicate a low kinetic energy buoyant plume source. This type of plume is not sufficiently energetic to disrupt stratification. The physics of buoyant plumes and wall layers leads to the existence of recirculating stratification (Appendix 9.C, Section 9.C.1.4.1) in the above-deck region. Plumes rise from the release point and entrain significant volume of mixture as they rise. The heavier bulk air/steam mixture is drawn through the top of the CMT and other deck openings and through compartments to be entrained into the rising plume. Stratification is assumed to have a negligible impact on heat removal in compartments which experience the already air-rich downflow. A very conservative assessment of the effects of stratification on heat removal through the steel shell by the PCS has been performed (Appendix 9.B). An extreme stratification gradient is assumed, to bound the potential for distortions in test data (9.2.3). The homogeneous case total heat sink utilization results are nearly equal to those for the stratified case, with the homogeneous case giving less than 0.5 percent less instantaneous heat removal rates. A simple bias of removing operating deck floors is included in the Evaluation Model to bound this effect.

The containment pressure was calculated for this case using the WGOTHIC AP600 Evaluation Model, (Section 4). It was assumed that the jet was dissipated in the East steam generator compartment, so no

specific break orientation was modeled. The break was located in Volume []^(a,c) at elevation []^(a,c). The results are discussed in Section 9.3.2.5.

9.3.1.2 Jet Directed Up With No Dissipation

A jet directed upward, that passes through the steam generator compartment undissipated, is considered unlikely. Releases are initially from the break and, later in the transient, releases exit from the fourth stage ADS and the break pipe is covered with liquid. The containment design calls for a steel plate to cover half the flow area in the steam generator compartment above the cold leg pipe and ADS Stage 4 valves. This plate and other structures in the steam generator compartment such as gratings, supports, and the steam generator itself make it doubtful that the break jet could pass through the steam generator compartment unobstructed. Despite the improbability of this scenario, it will be considered as an extreme case to support the selection of a limiting scenario for circulation and stratification.

For the case in which a jet is postulated to pass undissipated up through the steam generator compartment, there is no entrainment into the Steam Generator compartment due to chimney or momentum effects because these effects would act to dissipate the jet. An undissipated jet would enter the above-deck region at the top of the Steam Generator compartment with approximately the same diameter as the broken cold leg pipe. This scenario is similar to two of the LST MSLB configuration tests 222.3 and 222.4. To assess the effects relative to the mass transfer in the above-deck region, volumetric Froude numbers (Fr_v) for the undissipated jet are determined and compared to the LST. An examination of the magnitude of AP600 pressure improvements is provided with sensitivities, relative to condensation results discussed in Reference 9.9, Section 3.9.

For a LOCA DECLG, a postulated undissipated jet will have the same mass flow rate as the design basis LOCA DECLG exiting the top of the steam generator compartment. The two cases differ in the flow area and exit velocity. For the design basis case, the flow area is the area at the top of the Steam Generator compartment. For the undissipated jet, the flow area is the area of the cold leg pipe. For a constant mass flow rate, the product of the flow area times the exit velocity will be equal for the two cases ($U_{DECL} \times A_{DECL} = U_{UNDIS} \times A_{UNDIS}$, where U is the velocity, A is the area, subscript $DECL$ designates the design basis case, and subscript $UNDIS$ designates the undissipated jet case). Fr_v , defined in Section 9.2 is proportional to $U^2 d^2$, and is therefore proportional to $U^2 A^2$. For the two cases, the other terms in the Fr_v equation will be the same and $Fr_{v-UNDIS}$ can be expressed in terms of Fr_{v-DECL} , using $U_{DECL} \times A_{DECL} = U_{UNDIS} \times A_{UNDIS}$. The relationship is $Fr_{v-UNDIS} = Fr_{v-DECL} (A_{DECL} / A_{UNDIS})^2$. The area of the top of the Steam Generator compartment is approximately []^(a,c) and the area of the cold leg pipe is approximately []^(a,c). This results in $Fr_{v-UNDIS} \approx Fr_{v-DECL} \times []^{(a,c)}$

Reference 9.7, Section 6.5.2 presents Fr_v as a function of time for the design basis LOCA in Figure 6-2. At 24 hours Fr_v is approximately $3E-06$ (the minimum value during the transient excluding the refill phase). For an undissipated jet, Fr_v is estimated to be $3E-06 \times []^{(a,c)}$ which equals $[]^{(a,c)}$. This value is at the lower end of the LST Fr range in the MSLB configuration as shown in Reference 9.7, Figure 6-3. For such high values of Fr , data from the LST in the MSLB configuration (Section 9.2.2) shows that there is minimal deviation from a homogeneous steam concentration in the above-deck region. For the MSLB, Reference 9.9, Figure 3.9-5 shows that use of the Evaluation Model free convection correlation underpredicts condensation on shell surfaces by a factor of $[]^{(a,c)}$ for the LST. A multiplier of $[]^{(a,c)}$ is a reasonable factor to assess based on the data. To address postulated uncertainty in scaling the LST condensation results to AP600, a range of potential forced convection benefits in AP600 shell heat transfer are considered by examining the sensitivity of predicted containment pressure to condensation multipliers in the Evaluation Model. A sensitivity study examined the effects on containment pressure of using condensation multipliers of $[]^{(a,c)}$. These sensitivity cases show that taking credit for improved condensation provides a significant benefit in the calculated containment pressure. The results are discussed in Section 9.3.2.5.

9.3.1.3 Jet into RCDT Cavity (Stairwell)

During the blowdown phase, a jet into the RCDT cavity will create a pressure source in the RCDT cavity compartment. As with the jet dissipation in the East steam generator compartment, the high-pressure source will force fluid through all available openings. The source mixture will flow into the above-deck volume through both the CMT room and steam generator compartments. Following the blowdown phase, the source will rise from the RCDT cavity as a buoyant plume and split, based upon flow areas and resistances, with part of the flow rising through the West steam generator compartment and the remaining fluid flowing through the CMT compartment.

The post-blowdown flow split between the West steam generator and the CMT compartment will depend on flow areas and loss coefficients associated with both flow paths. A range of flow splits can be postulated varying from all the fluid rising through the steam generator compartments to all of the fluid rising through the CMT room and everything in between.

The first scenario is an extreme case which postulates that all the fluid rises through the West steam generator compartment. This scenario is identical to the scenario that assumes the jet momentum is locally dissipated in the East steam generator compartment. The case of the jet momentum dissipated in the East steam generator compartment is discussed in Section 9.3.1.1. The buoyant plume rising from the RCDT cavity into the West steam generator compartment is essentially the same scenario.

The second scenario is a split of the flow entering the RCDT cavity, with part of the break flow rising through the West steam generator compartment and part rising through the CMT compartment. The flow split is dependent on the relative flow path resistances. In this scenario, both the steam generator compartments and the CMT compartment would be subjected to a steam-rich break plume. The CMT and steam generator compartments contain the majority of the below-deck heat sinks. The flow split will result in good heat sink utilization subjecting both the steam generator compartments and the CMT compartment to the steam source. Thus, the case with the jet momentum dissipated in the RCDT cavity and a plume flow split between the CMT and steam generator compartments, will not be limiting. This is confirmed in the sensitivity calculations of Section 9.3.2.5.

The third scenario is an extreme case which postulates that the plume from the RCDT cavity rises into the CMT room. For this scenario, the buoyant plume rises from the floor to the ceiling of the CMT room, entraining gas from the bulk concentration present in the CMT room. An examination of entrainment into a CMT plume can be used to gain insight into the potential for stratification.

Calculation of CMT Room Plume Entrainment Rates

For the case of the LOCA jet being dissipated in the CMT room, the rate of entrainment of mixture in the CMT into the incoming break flow plume, Q_e , can be estimated based on the work of Peterson (Reference 9.15). In particular, Peterson gives the following relation for the volumetric entrainment rate into a buoyant plume,

$$Q_e = k_\mu B^{1/3} z^{5/3} \quad (9-1)$$

where k_μ is a constant equal to approximately 0.15, z is the height of the plume, and B is the buoyancy flux, given by:

$$B = g \frac{(\rho_a - \rho_o)}{\rho_a} Q_b \quad (9-2)$$

In this equation, g is acceleration due to gravity, ρ_a and ρ_o are the ambient fluid and injected fluid densities respectively, and Q_b is the volumetric flow rate from the plume source.

Substitution of equation (9-2) into equation (9-1) gives:

$$Q_e = k_\mu \left[g \frac{(\rho_a - \rho_o)}{\rho_a} Q_b \right]^{1/3} z^{5/3} \quad (9-3)$$

The ratio of entrained flow to break flow is therefore:

$$\frac{Q_e}{Q_b} = k_\mu \left[g \frac{(\rho_a - \rho_o)}{\rho_a} \frac{1}{Q_b^2} \right]^{1/3} z^{5/3} \quad (9-4)$$

AP600 break flow rates for a LOCA DECLG at transient times of 460 seconds and 1,000 seconds are 1,070 ft³/sec and 266 ft³/sec respectively for steam. The injected fluid density is taken as the density of saturated steam at the CMT room pressure. These densities are 0.128 lb/ft³ (based on 54.6 psia at 460 seconds) and 0.135 lb/ft³ (based on 58 psia at 1,000 seconds). Ambient fluid density is taken as the total density of gas mixture in the CMT room at the times of interest. Inspection of the WGOTHIC output, from the sensitivity case which modeled the break in the CMT room (see Section 9.3.2.5), indicates densities of 0.158 lb/ft³ at 460 seconds and 0.165 lb/ft³ at 1,000 seconds in the CMT room. The height of the CMT room is 28.1 feet. Based on this data the applicable entrainment ratios, Q_e/Q_b , are 0.68 at t=460 seconds, and 1.7 at t = 1000 seconds.

An entrainment-driven circulation time constant for the CMT room is calculated by dividing the entrainment flow rate into the volume of the CMT. From above Q_e/Q_b is 0.68 when Q_b is 1066 ft³/sec and 1.7 when Q_b is 266 ft³/sec. Solving for Q_e gives a range of 725 to 452 ft³/sec for the entrainment rate. The volume of the CMT room is approximately 157200 ft³ and the resulting circulation time constant ranges from 217 seconds to 348 seconds (3.6 to 5.8 minutes). This range is relatively short compared to the time of ADS Stage 4 actuation (approximately 1000 seconds), when the steam source is relocated to the steam generator compartments.

Assessment of CMT Room Entrainment Circulation

The entrainment rate for this case is relatively large, increasing to over a factor of two relative to break flow later in time. Thus, a significant amount of CMT room mixture is entrained into the break as the plume rises to the ceiling. It may be concluded that vertical concentration gradients in the CMT room would be relatively small due to circulation within the room. It also may be concluded that the break flow circulates within the room, significantly increasing the room average steam concentration. Thus, high steam concentrations are expected in the CMT room compared to other break scenarios. The high steam concentrations for this scenario will result in high heat sink utilization for heat sinks in this important room.

With such low density mixture in the North CMT room, the chimney effect induces flow to the room from connecting flow paths at the floor elevation. Connecting flow paths from the Section 4 Evaluation Model are []^(a,c) horizontally connecting to the steam generator compartments, and until the liquid level closes the path, []^(a,c) from the RCDT cavity (see Figure 9-47). The density head over almost 30 feet of height outside the CMT room strongly drives circulation through the CMT and upward in this scenario, suggesting that the flow should rise from the North CMT room into the above-deck region. There is little resistance to flow navigating past the CMT room pinch point to access the ceiling openings on the South CMT room opposite the stairwell, suggesting that flow would spread as it rises into the South CMT room, and then rise from all CMT deck openings. It is known from studies of building fires that very little pressure driving force is necessary to drive horizontal flow in a stratified room (References 9.10, 9.11, 9.12).

The effect of stratification on heat sink utilization is also evaluated. Room pressure, temperature, and steam concentrations were input into a separate calculation to assess the potential effect of stratification in the CMT room. For the calculation, the CMT room was divided vertically into three equal sections. Using free convection heat and mass transfer correlations, room heat sink energy removal was calculated for a room with a homogeneous steam concentration. The applied steam fraction was .63. For the second scenario, the CMT room was subjected to a stratified condition. The top region was assumed to be nearly all steam (steam fraction = 0.98), the middle region was assumed to have a nominal steam fraction (0.63), and the bottom region steam fraction was determined by conserving the total amount of steam in the total volume (0.28). Figure 9.B-3 shows the energy absorbed by the heat sinks in the CMT room for; 1) a stratified steam concentration with the CMT floor included, 2) a homogeneous steam concentration with the CMT floor included, and 3) a homogeneous steam concentration without the CMT floor included. As Figure 9.B-3 shows, the homogeneous concentration with the floor results in the most energy absorbed in the CMT room (top curve). The curve for the stratified concentration with the floor is close to the curve for the homogeneous concentration without the floor. The curve for the homogeneous concentration without the floor is more conservative (less energy absorbed) after 2000 seconds. Given the relative closeness of these two curves, and considering the extreme cases they represent, it is concluded that the lumped parameter Evaluation Model (which uses a homogeneous steam concentration in each volume) without floors provides a reasonably conservative model for heat sink utilization, accounting for the thermal effects of potential stratification. Information on the heat sink utilization calculations is presented in Appendix 9.B.

The break scenario with a buoyant plume flowing into the CMT compartment will not be a limiting scenario. The evaluation of this scenario has shown only small vertical concentration gradients are expected in the CMT compartment while a bias has nevertheless been implemented by removing the floor. Furthermore, high steam concentrations are expected in this compartment due to the large amount of entrainment and subsequent circulation driven by the break plume. The high steam concentrations will yield improved heat sink usage in this room. The scenario discussed in Section 9.3.1.1, with the jet momentum dissipated in the steam generator compartment, will have lower steam concentrations in the CMT room. Thus, the break scenario with a buoyant plume flowing into the CMT compartment will be bounded by the case with the

break jet locally dissipated. To further confirm this conclusion, the results of a WGOTHIC analysis using the AP600 Containment Evaluation Model (Section 4), for a buoyant plume flowing into the CMT compartment, are discussed in Section 9.3.2.5. The analysis confirms that the buoyant plume rising into the CMT compartment is not a limiting scenario.

9.3.2 WGOTHIC Containment Evaluation Model for LOCA

The WGOTHIC Containment Evaluation Model uses lumped parameter nodding. Lumped parameter nodding simplifies the calculation by assuming homogeneous conditions in each network node. Lumped parameter formulation uses what may be called a scalar form of the momentum equations as follows. Here, momentum flow into each volume is parallel to the junction, and the terms perpendicular to the junction are discarded while junction momentum is dissipated within the volume. Momentum orientation is not tracked, and no turning losses are represented. During the LOCA blowdown phase, the high break mass flow pressurizes the steam generator compartment and flow exits based on relative loss coefficients. Such pressure-driven flows are reasonably modeled by the lumped parameter node-network formulation. Lumped parameter reasonably represents buoyancy and pressure-driven flows and the resulting large-scale circulations. The effects of stratification within each compartment or region can then be superimposed on the large-scale circulation solution. The Containment Evaluation Models are described in Section 4 (AP600) and Section 13 (AP1000).

Comparison of lumped parameter GOTHIC results to test data, has shown lumped parameter nodding to be acceptable for LOCA breaks occurring in low zones of containment. Reference 9.13 discusses the test results and subsequent GOTHIC evaluation of the German Heissdampfreaktor (HDR) hydrogen mixing and distribution experiment E11.5. This experiment simulated a large-break LOCA in the lowest region of the HDR containment. The authors conclude that accident scenarios initiated by large-break LOCAs in the low zones of containments can be reliably predicted by the GOTHIC lumped parameter model using only a modest number of nodes (Appendix 9.C, Section 9.C.3.3). The DBA LOCA case models the break in []^(a,c) (lower East steam generator compartment) at the []^(a,c) elevation.

The conclusions concerning the use of a lumped parameter for low breaks modeled by GOTHIC, can be readily applied to WGOTHIC because of the similarity between the two codes. WGOTHIC is a descendant of the GOTHIC code. The difference between the two codes relates to the heat and mass transfer correlations applied to WGOTHIC by Westinghouse, to model the PCS phenomena for the passive containment design. Thus, since the LOCA scenarios of interest are breaks in the lower region of containment, it is reasonable to use WGOTHIC lumped parameter to model these events.

As discussed previously, the LOCA event is divided into four phases: the blowdown phase, the refill phase, peak pressure phase, and the long-term phase. These phases are discussed in Subsections 9.3.2.1 through 9.3.2.4.

9.3.2.1 Blowdown Phase (0 to 30 seconds)

The lumped parameter solution during blowdown is a node-network solution, governed by pressure differences and flow resistances between nodes. The mass and energy release in the Evaluation Model acts as a high-pressure source that forces the steam out through flowpaths connected to the source node. The Evaluation Model also assumes only free convection on inner containment surfaces. Based on high kinetic energy during blowdown (Ref. 9.7, Figure 6-2) significant enhancement to mass transfer due to forced convection occurs (Section 9.2.2). The steam is driven into the below-deck region and the above-deck volume. Figure 9-37 shows the calculated steam concentration of various containment regions during the blowdown phase, using the Evaluation Model described in Section 4 with a dissipated break in the SG East compartment.

The paragraphs in this subsection describe several sensitivity cases and an evaluation performed to examine various aspects of the blowdown phase. The first sensitivity case examines the effect of modeling a containment with a homogeneous steam concentration on the calculated containment pressure. The second sensitivity case examines the effect of removing all internal heat sinks on the calculated containment pressure. Following this sensitivity case, an evaluation of heat sink utilization in dead-ended compartments is performed. The final sensitivity case examines the effect of varying the flow pattern and steam concentrations on the calculated containment pressure.

To show the relative insensitivity to stratification, or heat and mass transfer coefficient during blowdown, a comparison is needed between the containment pressure response predicted by this node-network solution, and the containment response predicted for a homogeneous containment. Section 8, Figure 8-1 compares the LOCA blowdown pressure results of a one-node WGOTHIC AP600 model to the node-network solution. The one-node model assumes the same total containment volume and containment heat sinks as the multi-node model. Both models predict essentially identical containment pressure responses during the blowdown phase. Therefore, the details of the flow connections and heat mass transfer rates for the multi-node Evaluation Model are not important with respect to the containment pressure results because volume compliance is the dominant pressure mitigator during blowdown.

During the blowdown phase, the mass and energy release is mitigated primarily by containment volume via the rapid pressurization of the containment building. Figure 8-2 shows a comparison of the AP600 Evaluation Model results for the blowdown phase versus an identical model with all internal heat sinks removed. At the end of blowdown (30 seconds), the difference between these two cases is about 3 psi, accounting for only 10 percent of the pressurization. Thus, in the Evaluation Model, the blowdown mass and energy release increases containment pressure by about 35 psi, while the containment heat sinks absorb approximately 3 psi worth of energy. Clearly, the dominant mechanism during blowdown is the pressurization of containment.

The heat sink effectiveness in the presence of a stratification gradient is evaluated in Appendix 9.B. To conservatively account for the reduced effectiveness of heat sinks in lower room areas, floors are eliminated in the WGOTHIC Containment Evaluation Model throughout the transient.

The effectiveness of heat sinks in dead-ended compartments is also evaluated. Since only one opening exists for these compartments, interaction with overall containment volume is expected to be minimal unless the compartments have non-uniform temperatures. During blowdown, these compartments pressurize along with the rest of containment. Steam/air mixture from the bulk containment volume flows into the dead-ended compartments during the initial pressurization. Once pressurized, additional steam/air flow into the dead-ended compartments only occurs to make up for steam condensing in the compartment. Analysis of the Nuclear Power Engineering Corporation (NUPEC) natural circulation test, M-4-3, showed that asymmetric heating of dead-ended compartment walls can lead to natural circulation flows within the compartment (Reference 9.14). However, a conservative evaluation of dead-ended compartments would consider no thermally driven circulation. In such a case, inside the compartments, the condensation of steam leaves behind a heavier air-rich mixture. The air flows to the bottom and blankets the lower heat sinks. The poor circulation within the dead-ended compartments leaves the air-rich layer relatively undisturbed. As steam continues to condense, the air-rich layer continues to build up and will result in significant stable stratification within the dead-ended compartments. Although the heat sinks in the dead-ended compartments will contribute somewhat to containment heat removal, to conservatively bound the effects of stratification, condensation and convection on the heat sinks in the dead-ended compartments are neglected after 30 seconds in the Evaluation Model.

Based on the results of the evaluation, it has been demonstrated that blowdown pressure history is relatively insensitive to the effects of circulation and stratification. The internal heat sinks do heat up during blowdown, however, as discussed above, containment volume pressurization is the dominant mechanism for absorbing the energy released. Since volume pressurization is the governing process, blowdown pressure response is not sensitive to circulation and stratification effects. The Evaluation Model utilizes a conservative lower estimate of containment free volume. Thus, the uncertainties in heat and mass transfer or stratification, and flow path effects, do not significantly impact the LOCA blowdown pressure history and the Evaluation Model adequately models the LOCA blowdown phase.

To assess the effects of varying the steam concentrations and flow rates on the calculated containment pressure, a sensitivity was performed which varied several loss coefficients in the Evaluation Model. This sensitivity shows how changes in conditions during the blowdown phase affect the later phases and, in particular, the calculated containment pressure. For this sensitivity, the AP600 Containment Evaluation Model (Section 4), with a dissipated jet in the SG East compartment, was used and the loss coefficients

[

](a,c)

Figure 9-38 shows the pressure transient for this sensitivity case. The maximum calculated pressure is 43.8 psig, which is 0.1 psi less than the 43.9 psig reported in Section 9.3.2.5.

Circulation plots for this sensitivity case are presented in Figures 9-39 through 9-42. Compared to the circulation plots for the dissipated jet in the SG East compartment (Figures 9-47 through 9-50), the effects of the revised loss coefficients are evident. At 20 seconds, Figure 9-39 shows that most of the break flow goes from the SG East compartment to the SG West compartment, and through the RCDT cavity to the North CMT room. At 1000 seconds (Figure 9-40), flow is rising from both SG compartments and a steam/air mixture is flowing down into the North and South CMT volumes. Figure 9-48, shows flow rising only from the SG East compartment. At 1550 and 80050 seconds (Figures 9-41 and 9-42) the ADS Stage 4 valves are the source of the steam releases and the flow patterns are similar to those in Figures 9-49 and 9-50. This sensitivity altered the flow patterns and steam concentrations early in the transient by changing some of the flow path loss coefficients. The change in calculated maximum pressure was negligible.

9.3.2.2 Refill Phase (30 to 90 seconds)

The refill phase immediately follows blowdown. After blowdown, the accumulators refill the lower plenum of the reactor with a high flow rate of cold water. The resulting steam and water flow rates from the break are very low and increase with time. The mass and energy release rates are two orders of magnitude less than the blowdown rates, and can be approximated as 0 from approximately 30 to 90 seconds into the event. With a negligible steam source rate and a high condensation rate, the containment pressure drops by a few psi from its peak at the end of blowdown to the end of the refill phase at approximately 90 seconds. For the calculation of maximum containment pressure, the Evaluation Model conservatively neglects the refill period.

9.3.2.3 Peak Pressure (90 to 1200 seconds)

During the peak pressure phase, the location of the steam releases changes from the break to the ADS Stage 4 valves in both steam generator compartments. The Evaluation Model includes this change in steam release location. In addition, the lower compartments begin to fill with liquid from the break. The reduced heat transfer area due to filling is accounted for in the Evaluation Model. Figure 9-43, for a jet dissipated in the SG East compartment, shows that the condensation on the steel becomes the dominant mechanism for heat removal towards the end of the peak pressure phase.

The evaluation of break scenarios in Section 9.3.1 led to the conclusion that the case with jet momentum dissipated in the steam generator compartment may lead to stratification within compartments after the blowdown phase. Given this possibility, it is necessary to show that the Evaluation Model bounds the possible effects of this stratification. Lumped parameter models assume no gradients within each volume of the network. Thus, in the Evaluation Model, all heat sinks within a compartment volume see identical environmental conditions. In contrast, actual conditions may lead to a stratified compartment with a region of higher steam concentration on top and lower steam concentration near the bottom. For the effects of stratification on heat sink utilization, the most significant heat sinks are the above-deck region (containment shell) and the CMT room (steel and jacketed concrete). The compartment features are discussed in Sections 4 and 13 and summarized in Table 3-1 of Reference 9.2. In Section 9.3.1.3, the CMT room was assessed for its sensitivity to stratification. In this calculation, heat sink usage was calculated for a homogeneous room and a severely stratified room. A bias has been defined to bound the potential effects of stratification in compartments as discussed in 9.3.1.3. In Section 9.3.1.1, the containment shell was assessed for its sensitivity to stratification. A bias has been defined to bound the potential effects of stratification above-deck as discussed in Section 9.3.1.1. Appendix 9.B discusses the calculations performed.

Based upon the results of the evaluation, a method to bound circulation and stratification effects for the peak pressure phase has been developed. In the Evaluation Model, all floors are neglected throughout the transient and condensation and convection on all heat sinks in dead-ended compartments are neglected after 30 seconds (refer to Section 9.3.2.1).

9.3.2.4 Long-Term Phase (1200 seconds to 24 hours)

Figure 9-43 shows the condensation on the steel shell remains the dominant mechanism for heat removal during the long-term. The results shown are from the AP600 Containment Evaluation Model (Section 4) with a dissipated jet in the SG East compartment. During early portions of the transient, internal heat sinks are the primary path of containment heat removal. As the transient progresses, the temperature of the heat sinks increases and their heat removal effectiveness is reduced. PCS heat removal, which dominates in the long-term, is dependant on steam concentrations. The effects of stratification on the containment shell heat removal have been evaluated in Section 9.3.1.1 and a bias of removing operating deck floors has been included in the Evaluation Model.

In addition, WGOTHIC predicts a slight gradient between the upper and lower compartments (excluding dead-ended compartments). Figure 9-44 shows WGOTHIC predicted steam concentrations for various compartments in the AP600, using the Evaluation Model (Section 4) with a dissipated jet in the SG East compartment. As Figure 9-44 shows, at 24 hours WGOTHIC predicts a homogeneous above-deck region. However, WGOTHIC predicts a slightly lower steam concentration below the operating deck, excluding the SG compartments which continue to have steam release through the ADS Stage 4 valves.

The trend over time for the WGOTHIC calculations leads to a very small steam density gradient between above- and below-deck compartments. The WGOTHIC predicted average steam concentration above the operating deck is approximately 0.47 at 24 hours. Below the operating deck, the average is approximately 0.46 at 24 hours excluding the SG compartments. The calculated steam concentration for a homogeneous condition between the above-deck region and the below-deck open compartments is approximately 0.468. There is a negligible change between the WGOTHIC calculated above-deck steam concentration and the calculated homogeneous concentration (excluding dead-ended and SG compartments). Since the predicted stratification is slight, and since the volume of the above-deck regions is significantly greater than the below-deck open compartments, mixing the above-deck volume with the below-deck open compartments does not significantly change the above-deck steam concentrations. Thus, the WGOTHIC predictions as the transient calculation passes through 24 hours are essentially similar to the assumption of a homogeneous containment. It is conservative to not include the steam generator compartment steam concentration in the homogeneous calculation.

It is concluded that WGOTHIC predicts a slight segregation between the above- and below-deck regions, but the deviation from the homogeneous assumption is insignificant. Based upon the results of the evaluation, it has been shown that the Evaluation Model adequately bounds the effects of circulation and stratification during the long-term phase.

9.3.2.5 Evaluation Model Results

Sensitivities have been performed using the lumped parameter AP600 Containment Evaluation Model (Section 4) for several postulated, plausible break locations. An evaluation of the sensitivities leading to selection of a limiting scenario for design basis accident calculations follows.

It has been determined that to bound circulation and stratification effects, floors are neglected throughout the transient, and condensation and convection on all heat sinks in the dead-ended compartments are neglected after blowdown. The stratification of steam and air within compartments may reduce heat sink effectiveness. These biases are included in the Evaluation Model used to perform sensitivities.

Undissipated Jet Rising in SG East Compartment

The postulated, undissipated jet directed up the Steam Generator compartment results in increased heat and mass transfer, possibly as high as a factor of []^(a,b) over the steel shell surface based on the LST, compared to that using the free convection correlation in the Evaluation Model, as discussed in Section 9.3.1.2. To estimate the potential benefit for AP600, the heat transfer coefficient multipliers for the inner surfaces of the clime conductors (that is, only the steel shell mass transfer is enhanced) were increased to []^(a,c) times the Evaluation Model values. The Evaluation Model with the break in the steam generator East compartment was used for the sensitivity cases. The postulated, undissipated jet will only

occur until the ADS Stage 4 valves are opened at approximately 1000 seconds. Therefore the containment pressure response is plotted for the first 1000 seconds of the LOCA. The containment pressure sensitivity results are shown in Figure 9-45, along with the Evaluation Model results. The results show that the pressure response during the blowdown phase is the same for all cases. This is expected because volume compliance is the dominant pressure mitigator during blowdown (Section 9.3.2.1). Compared to the Evaluation Model results at 1000 seconds, the calculated containment pressure for the [

]^(a,c) These results show that a substantial benefit in containment pressure is gained when the heat transfer coefficient is increased to account for the forced convection from an undissipated jet. Therefore, this case will be less limiting than the other postulated break scenarios in which the jet is dissipated.

Dissipated Jet Rising in SG East Compartment

Another postulated break scenario, the design basis case, is a dissipated jet in the SG East compartment (Volume 107, elevation 100 ft.). Figure 9-46 shows the results of the WGOTHIC AP600 Containment Evaluation Model which includes the circulation and stratification biases. Assuming the break momentum is dissipated in the broken loop steam generator compartment, a maximum containment pressure of 43.9 psig is calculated, which is below the design pressure of 45 psig. The pressure transients for compartments directly connected to the SG East compartments are shown in Figure 9-46A. Figures 9-47 through 9-50 show the circulation pattern predicted by WGOTHIC for this case at different times during the transient. The figures show the Evaluation Model flow path connections for the below-deck volumes, the flow rates and directions, volume steam pressure ratio, and liquid level. Figure 9-51 is a depiction of each of the flow connections to the above-deck volumes. In subsequent figures, total flows through the ceiling of each compartment are shown for simplicity. Flow paths that have been grouped have the same flow direction. Figure 9-47 presents data at 20 seconds which is near the end of blowdown. Flow is forced into all of the below-deck volumes and into the above-deck volumes from the East and West steam generator compartments and the North and South CMT rooms. Figure 9-48 presents data at 1000 seconds which is near the time of maximum pressure and prior to ADS Stage 4 valve actuation. Flow to the dead-ended compartments has stopped. The general circulation pattern is fluid from the break flowing up through the SG East compartment while a steam/air mixture is drawn into and through the SG West compartment, the North and South CMT rooms, and the RCDT cavity into the SG East compartment. At 1500 seconds, Figure 9-49 shows the change in circulation pattern due to the actuation of the ADS Stage 4 valves. The steam releases flow up through both steam generator compartments while a steam/air mixture is drawn into and through the CMT rooms and the RCDT cavity. This flow pattern develops less than 2 minutes after ADS Stage 4 activation. Figure 9-50 shows the circulation pattern near 24 hours. The flow rate out of the ADS Stage 4 valves is approximately one-fourth of the flow at 1500 seconds. The flow pattern remains out of the SG compartments and into the CMT rooms, however, flow through the RCDT cavity has ceased, due to liquid level rising above the top of the flow path.

Plume Rising in CMT Room

In Section 9.3.1.3, the LOCA with jet dissipation in the RCDT cavity was postulated. It was postulated that the entire buoyant plume rises into the North CMT compartment. The evaluation concluded this scenario was not limiting because of the higher steam concentrations expected in the CMT compartment, which would result in better internal heat sink utilization. Furthermore, the evaluation concluded that the relative steam densities would drive the steam to navigate the bend in the CMT compartment. This would lead to a steam-rich environment for the heat sinks in the south end of the CMT room opposite the stairwell. To confirm that this scenario is not bounding, a WGOTHIC calculation was performed using the AP600 Containment Evaluation Model (Section 4). The calculation assumed a LOCA where the jet plume dissipates and rises into the North CMT compartment. This was simulated by applying the break boundary conditions to the North CMT node (Volume 6, elevation 107 ft.), the only change made to the Evaluation Model. The circulation and stratification biases of neglecting floors throughout the transient and condensation and convection in dead-ended compartments following blowdown were included. The containment pressure results of this evaluation are shown in Figure 9-52. The maximum pressure was calculated to be 43.7 psig. As expected, this pressure is below the previous scenario where momentum is dissipated in the East steam generator compartment. The circulation pattern predicted by WGOTHIC is shown in Figures 9-53 and 9-54.

Figure 9-53 presents data at 1000 seconds which is near the time of maximum pressure and prior to ADS Stage 4 valve actuation. Compared to Figure 9-48 (break in SG East compartment), Figure 9-53 shows flow out of the North and South CMT rooms into the above-deck region, while a steam/air mixture flows down into both SG compartments and up through the RCDT cavity into the North CMT room. Figure 9-54, at 1400 seconds, shows the change in flow pattern due to ADS Stage 4 valve actuation. The flow rates and pattern are similar to those in Figure 9-49, as expected. Figure 9-55 shows the heat sink utilization for this sensitivity case. As expected, Figure 9-55 shows a greater CMT room (Volumes 6 and 104) heat sink utilization than that shown in Figure 9-43 for a break in the SG East compartment. Both figures show that the PCS shell is the dominant heat sink at the time of maximum containment pressure and beyond.

Plume Rising in RCDT Cavity

In Section 9.3.1.3, a LOCA with jet dissipation in the RCDT cavity was postulated. This scenario assumed the break flow splits between the CMT and steam generator compartments. The evaluation concluded that good below-deck heat sink utilization is expected because of the high steam concentrations in the CMT and steam generator compartments. A WGOTHIC calculation was performed for this scenario using the AP600 Containment Evaluation Model (Section 4). The calculation simulated the flow split by placing the break boundary condition directly in the RCDT cavity []^(a,c) The circulation and stratification biases were included. The pressure prediction from the evaluation is shown in Figure 9-56. The maximum pressure was calculated to be 43.4 psig. This pressure is below both of the previously discussed sensitivities. The WGOTHIC predicted circulation pattern is shown in Figures 9-57 and 9-58.

Figure 9-57 presents data at 1000 seconds which is near the time of maximum pressure and prior to ADS Stage 4 valve actuation. With the break in the RCDT cavity, the bulk flow distribution is based on the path areas and loss coefficients. Consequently, at 1000 seconds, the steam flow from the break goes up through the CMT rooms, while a steam/air mixture flows down through both SG compartments and into the North CMT room and RCDT cavity. Figure 9-58, at 1500 seconds, shows the change in flow pattern due to ADS Stage 4 valve actuation. The flow rates and pattern are similar to those in Figure 9-49, as expected. Figure 9-59 shows the heat sink utilization for this sensitivity case. Compared to Figure 9-43 for a break in the SG East compartment, Figure 9-59 shows a small delay in the heat absorption from the SG East compartment and the CMT rooms. The heat absorption from the SG West compartment starts a little sooner in Figure 9-59. The effects are due to the break location differences. Consistent with the other cases, Figure 9-59 shows that the PCS shell is the dominant heat sink at the time of maximum containment pressure and beyond.

9.3.2.6 Evaluation of Drops During a LOCA

Drops, or fog particles, are created when the blowdown break source steam velocity is large enough to disperse a fraction of the break liquid along with the gas. As discussed in Reference 9.2, Section 4.4.2D and Reference 9.7, Section 7.1, drops will be formed during the LOCA blowdown phase. For the post-blowdown phases of a LOCA and for the main steamline break (MSLB), there will not be any significant drop formation. The thermal and circulation effects of drops on LOCA containment pressure are examined in Appendix 9.A and summarized below.

Drop fall times for various size drops were determined in Appendix 9.A, which only account for the gravitational effects on the drops. Fall times range from seconds to hours depending on the drop size and fall height. This provides an indication that the drops will exist long enough that their effect on containment pressure must be considered. In addition, Appendix 9.A estimated plume entrainment rates for 0 percent and 100 percent of the break liquid converted to drops. The entrainment rates and subsequent circulation time constant for both 0 and 100 percent drops show that a large fraction of the containment volume will be entrained in the plume within a few minutes, which is relatively short compared to the time to reach maximum pressure (at approximately 1200 seconds), and very short compared to long-term cooling. A relatively large entrainment rate within the above-deck region indicates that the steam density gradients above-deck are not large whether drops exist or not. Therefore, the presence of drops will not significantly affect the general circulation and stratification patterns in the containment atmosphere.

Section 5.8 shows the results of sensitivity cases to assess the Evaluation Model treatment of the thermal effects of drops with respect to containment pressure. The results that show the Evaluation Model assumption of 50 percent of the break liquid being converted into drops provides essentially the same containment maximum calculated pressure as assuming 100 percent of the liquid is converted into drops.

The 50 and 100 percent drop fractions are both more limiting with respect to maximum pressure than assuming none of the break liquid is converted into drops.

The formation of drops during the LOCA blowdown phase is a physically real phenomenon which may influence the maximum containment pressure calculated by the Evaluation Model. Drop formation increases the effective density of the containment atmosphere due to the close coupling between small drops and gas by shear forces, making the post-blowdown releases relatively more buoyant. A small percentage ($\geq 5\%$) of the blowdown break liquid formed into drops is sufficient to saturate the containment atmosphere, at which point, additional drop density has a minor thermal effect. The Evaluation Model treatment of drops, as described in Section 4.5.2.1 and Section 13.5.2.1, provides a sufficiently bounding calculation for maximum and long-term containment pressure.

9.4 MAIN STEAMLINE BREAK (MSLB)

The main steamline transports steam from the steam generators within the containment building to the turbine generators in the auxiliary building. The main steamline path begins at the top of the steam generator, where it bends 180° and follows a downward path to the CMT room. In the CMT room, the steamline bends 90°, crosses through the CMT room, and exits the building through a penetration in the containment shell. Rupture of the main steamline inside containment would release high energy steam into the containment. To confirm the design adequacy of the containment, various MSLB scenarios are examined to develop a conservative model accounting for the effects of circulation and stratification in the containment pressure calculations.

9.4.1 Break Locations

An evaluation of circulation and stratification must allow for the consideration of possible break locations. For the MSLB, two distinct break locations may be postulated: a break in the steamline above the operating deck or a break in the steamline in the CMT compartment.

9.4.1.1 MSLB Above the Operating Deck

An MSLB above the operating deck could occur anywhere in the steamline piping from the top of the steam generator to the operating deck penetration into the CMT compartment.

The design basis MSLB mass and energy releases for containment pressure assume a 1.388 ft² break (due to integral flow limiters). The MSLB event is characterized by a high energy release of short duration. Reference 9.7, Figure 6-3 shows the calculated Froude numbers for the event compared to Froude numbers calculated for the LST. The high Froude numbers indicate a high kinetic energy source which is expected to drive circulation above and below the jet source elevation. High Froude numbers also indicate that a significant forced convection enhancement to mass transfer occurs during an MSLB.

An examination of releases from smaller sized breaks in main steamlines indicates that the reduction in mass flow is more than offset by the reduction in exit flow area. Therefore, the larger size breaks have the lowest Froude numbers. The double-ended rupture MSLB has the limiting combination of mass and energy release and Froude numbers.

9.4.1.2 MSLB in the CMT Compartment

A steamline rupture in the CMT compartment would propel a high momentum steam jet into the CMT room. Since the break is within an enclosed compartment, momentum from the jet would be dissipated by the equipment, walls, floors, and ceilings of the CMT room. The effect would create a pressure source in the

CMT compartment with the fluid following the path of resistance through the node network into adjacent compartments and the above-deck volume.

The steam source in the CMT compartment will create a steam-rich environment for this room which contains many heat sinks. The high steam concentration will result in excellent heat sink utilization for this scenario.

The MSLB in the CMT compartment case is bounded by the scenario of an MSLB occurring above the operating deck. While the break above the operating deck does produce substantial circulation, the steam concentrations in the CMT compartment will not approach the steam levels for a break directly within the CMT room. Thus, the MSLB in the CMT compartment is not the bounding scenario. To confirm this conclusion, Section 9.4.3 presents the results of a WGOTHIC analysis for a break in the CMT compartment. As expected, the containment peak pressure is lower for the MSLB in the CMT compartment than for an MSLB above the operating deck.

9.4.2 WGOTHIC Containment Evaluation Model for MSLB

In creating an appropriate and conservative Evaluation Model, it is necessary to understand how the code handles circulation, to bias the model to produce bounding but reasonably representative results. Investigation of the lumped parameter AP600 Containment Evaluation Model (Section 4) has shown that this noding structure tends to mix upwards from the break elevation.

The lumped parameter calculational bias may be attributed to the use of multiple, relatively large lumped parameter nodes to represent the above-deck region in the Evaluation Model. Lumped parameter formulation uses what may be called a scalar form of the momentum equations, as follows. Here, momentum flow into each volume is parallel to the junction, and the terms perpendicular to the junction are discarded while junction momentum is dissipated within the volume. Momentum orientation is not tracked, and no turning losses are represented. This momentum dissipation is the characteristic of the lumped parameter noding which results in the calculated stratification above/below the jet. With momentum diffused throughout the volume node, the vigorous circulation from the high kinetic energy jet does not occur in the model. Circulation above the jet source in the lumped parameter model is driven by the density head terms in the momentum equation which cannot drive flow below the source. Thus, lumped parameter noding predicts a steam-rich atmosphere above the assumed source elevation, and a steam-deficient atmosphere below this source elevation (simulating stratification).

With an understanding of both the physics, and lumped parameter model biases, a WGOTHIC representation is constructed which conservatively represents the accident scenario. The high kinetic energy of the MSLB will tend to circulate steam through the above-deck portion of the containment vessel and lead to forced convection conditions for the shell. The lumped parameter Evaluation Model, however, calculates a steam-

rich region above the injection point and an air-rich region below this point. Figure 9-60 shows the steam concentration results of a WGOTHIC MSLB calculation using the AP600 Containment Evaluation Model with the source entering []^(a,c) which is just above the operating deck (refer to Section 4.5.2.2). The model predicts a small steam density gradient above-deck, consistent with the expectation of only small gradients in the AP600, based on LST data (see Section 9.2.2). Evaluation has shown that the effect on shell mass transfer of even extreme stratification, beyond that expected for the AP600 or AP1000 (see Section 9.3.1.3), is very small. Very little steam penetrates into the below-deck region in the model. Steam access into the below-deck compartments in the model is governed only by the volume pressurization. As the mass and energy releases pressurize the above-deck region, a steam/air mixture from above-deck is pushed into the below-deck compartments. The use of the WGOTHIC lumped parameter model, with an injection point just above the operating deck, results in a conservative Evaluation Model for the steam line break as a result of reduced steam access to the below-deck heat sinks. The reduced steam access is due to the momentum dissipation in the model which reduces the calculated circulation to the nodes below the operating deck. The Evaluation Model neglects any heat and mass transfer contribution from forced convection, so above-deck velocity predictions become unimportant. Mass transfer is seen to be underestimated by as much as a factor of []^(a,c) on the steel shell surface relative to forced convection in the LST. To add an additional conservative bias, the stratification heat sink biases developed for LOCA scenarios are also included

9.4.3 MSLB Sensitivity Results

Based on an evaluation of circulation and stratification, an MSLB Evaluation Model has been constructed to bound circulation and stratification effects. The limiting MSLB scenario assumes a pipe break above the operating deck. In this scenario, test data indicates that the high kinetic energy source jet induces circulation above and below the jet elevation, including substantial steam penetration into below-deck compartments. The lumped parameter Evaluation Model, that bounds circulation and stratification, places the break source directly above the operating deck []^(a,c) This results in a well-circulated upper region with little steam access to the heat sinks below the operating deck. To further bound circulation and stratification effects, stratification heat sink biases developed for LOCA scenarios are included (see Table 9-1). Figure 9-61 shows the results of the AP600 WGOTHIC MSLB Evaluation Model described above. A containment peak pressure of 44.8 psig is calculated, which is below the design pressure of 45 psig.

In Section 9.4.1.2, the MSLB in the CMT compartment scenario was evaluated, concluding that increased circulation below the operating deck would reduce the calculated containment pressure. This scenario was determined not to be the limiting scenario, because of the high steam concentrations expected in the CMT compartment. The high steam concentration would result in improved heat removal rates by the heat sinks in the CMT compartment. To confirm this hypothesis, a WGOTHIC analysis was performed for a break in the CMT compartment []^(a,c) As with the break above the operating deck, LOCA stratification biases were included. Figure 9-62 shows the results of the WGOTHIC calculation.

A containment peak pressure of 43.2 psig is calculated, which is 1.6 psi less than the peak pressure for the MSLB above the operating deck. As expected, the Evaluation Model predicts the MSLB above-deck to be the limiting location.

9.5 CONCLUSIONS

A WGOTHIC Containment Evaluation Model is used which considers circulation and stratification in the calculation of LOCA and MSLB containment pressures and temperatures. The effects of circulation and stratification on the calculated containment pressure have been examined, and biases have been defined for the Evaluation Model. The Evaluation Model input deck and specific biases are described in Sections 4 and 13. In addition, break locations have been examined for LOCA and MSLB to determine the limiting location for each transient with respect to calculated containment pressure.

The following biases have been incorporated into the Evaluation Model for the LOCA analysis based on the circulation and stratification evaluations documented in this section:

- Heat and mass transfer from floors of compartments and the operating deck have been removed to bound the potential reduction in heat transfer due to stratification. Refer to Sections 9.3.1.1, 9.3.1.3, and Appendix 9.B.
- Condensation and convective heat transfer in dead-ended compartments are turned off after 30 seconds (i.e., after blowdown) to bound the potential reduction in heat transfer due to stratification. The basis for this bias is provided in Section 9.3.2.1.
- The lumped parameter Evaluation Model considers only free convection for internal heat sinks and shell surfaces and, therefore, conservatively neglects the increase in mass transfer to the containment steel shell due to forced convection during blowdown. Refer to Section 9.3.2.1.

Ranges of LOCA break locations and jet directions were evaluated to determine the limiting case with respect to containment pressure. The limiting scenario is the DECLG break in the East steam generator compartment with the jet momentum locally dissipated. Other break locations, or jet directions, result in increased heat sink utilization which results in lower calculated containment pressures. Based on the results presented in Section 9.3.5.2, the calculated maximum LOCA containment pressure from a dissipated jet is not very sensitive to the break location since internal heat sinks "reach maximum effectiveness" well before the time of maximum pressure.

The following biases have been incorporated into the Evaluation Model for the MSLB analysis based on the circulation and stratification evaluations documented in this section:

- The break is placed in a node at the operating deck level to minimize circulation and steam access to below-deck heat sinks, which bounds the potential reduction in heat transfer in below-deck compartments due to stratification. This is discussed in Section 9.4.2.

- The lumped parameter Evaluation Model considers only free convection for internal heat sinks and shell surfaces and, therefore, conservatively neglects the increase in mass transfer to the containment steel shell due to forced convection during the entire transient. Refer to Section 9.4.2.
- The above listed LOCA biases (relative to floors and dead ended compartments) have been included in the MSLB Evaluation Model to further conservatively bound potential reductions in heat transfer due to stratification. Refer to Section 9.4.3.

Based on the routing of the steamline pipe, two MSLB locations were evaluated; a break above the operating deck and a break in the CMT room. As discussed in Section 9.4.3, the break above-deck resulted in the higher calculated containment pressure. The break in the CMT room had increased heat sink utilization in the CMT room which resulted in the lower calculated containment pressure.

The above biases are incorporated into the Evaluation Model as described in Sections 4.2 and 13.2, subsections entitled "Special Modeling Assumptions." Therefore, the effects of circulation and stratification have been conservatively bounded in the WGOTHIC containment pressure calculations.

9.6 REFERENCES

- 9.1 WCAP-14382, "WGOTHIC Code Description and Validation," May 1995.
- 9.2 WCAP-14812, "Accident Specification and Phenomena Evaluation for AP600 Passive Containment Cooling System," Revision 2, April 1998.
- 9.3 NTD-NRC-95-4563, "GOTHIC Version 4.0 Documentation, Enclosure 2: Technical Manual," September 21, 1995.
- 9.4 NTD-NRC-95-4563, "GOTHIC Version 4.0 Documentation, Enclosure 3: User Manual," September 21, 1995.
- 9.5 WCAP-13566, "AP600 1/8th Large-Scale Passive Containment Cooling System Heat Transfer Test Baseline Data Report," October 1992.
- 9.6 WCAP-14135, "Final Data Report for PCS Large-Scale Tests, Phase 2 and Phase 3," Revision 1, April 1997.
- 9.7 WCAP-14845, "Scaling Analysis for AP600 Containment Pressure During Design Basis Accidents," Revision 3, March 1998.
- 9.8 Wolf, L., Gavrilas, M., Mun, K., 1996, "Overview of Experimental Results for Long-Term, Large-Scale Natural Circulations in LWR-containments after Large LOCAs," DOE - Project, Order Number: DE-AP07-96ID10765, University of Maryland at College Park, July 1996.
- 9.9 WCAP-14326, "Experimental Basis for the AP600 Containment Vessel Heat and Mass Transfer Correlations," Revision 2, April 1998.
- 9.10 Jaluria, Y. "Buoyancy Driven Wall Flows in Enclosure Fires," Twenty-first Symposium (International) on Combustion, The Combustion Institute, 151-157 (1986).
- 9.11 Goldman, D., Jaluria, Y., "Effect of Opposing buoyancy on the Flow in Free and Wall Jets," *Journal of Fluid Mechanics*, 166, 41-56 (1986).
- 9.12 Jaluria, Y., Cooper, L.Y., "Negatively Buoyant Wall Flows Generated in Enclosure Fires," *Progress in Energy and Combustion Science*, 15, 159-182 (1989).

- 9.13 Fisher, K., Schall, M., and Wolf, M., "Simulations of GOTHIC Large-Scale Containment Experiments," published by Battelle Ingenieurtechnik GmbH, October 1995.
- 9.14 Ofstun, R.P., Woodcock, J., Paulsen, D.L., "Westinghouse - GOTHIC Modeling of NUPEC's Hydrogen Mixing and Distribution Test M-4-3," Third International Conference on Containment Design and Operation, October 1994, Toronto, Canada.
- 9.15 Peterson, P.F., "Scaling and Analysis of Mixing in Large Stratified Volumes," *International Journal of Heat and Mass Transfer*, Vol. 37, Suppl. 1, pp 97-106, 1994.

(a,c)

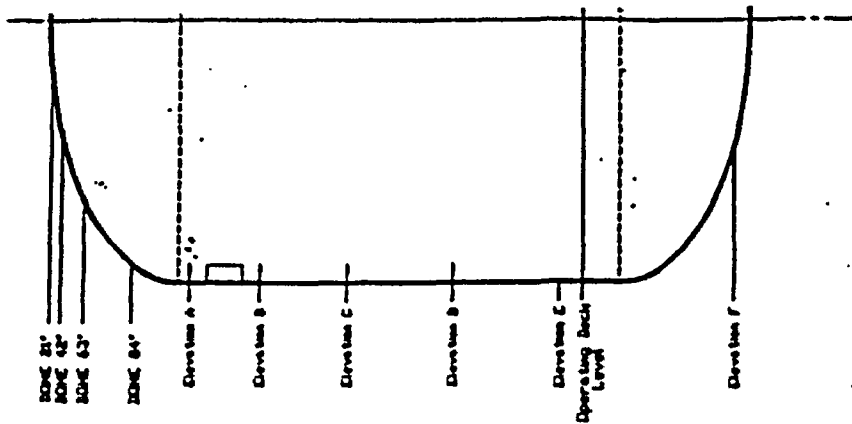


Figure 9-1 Measured Steam Concentrations for LST

(a,b)

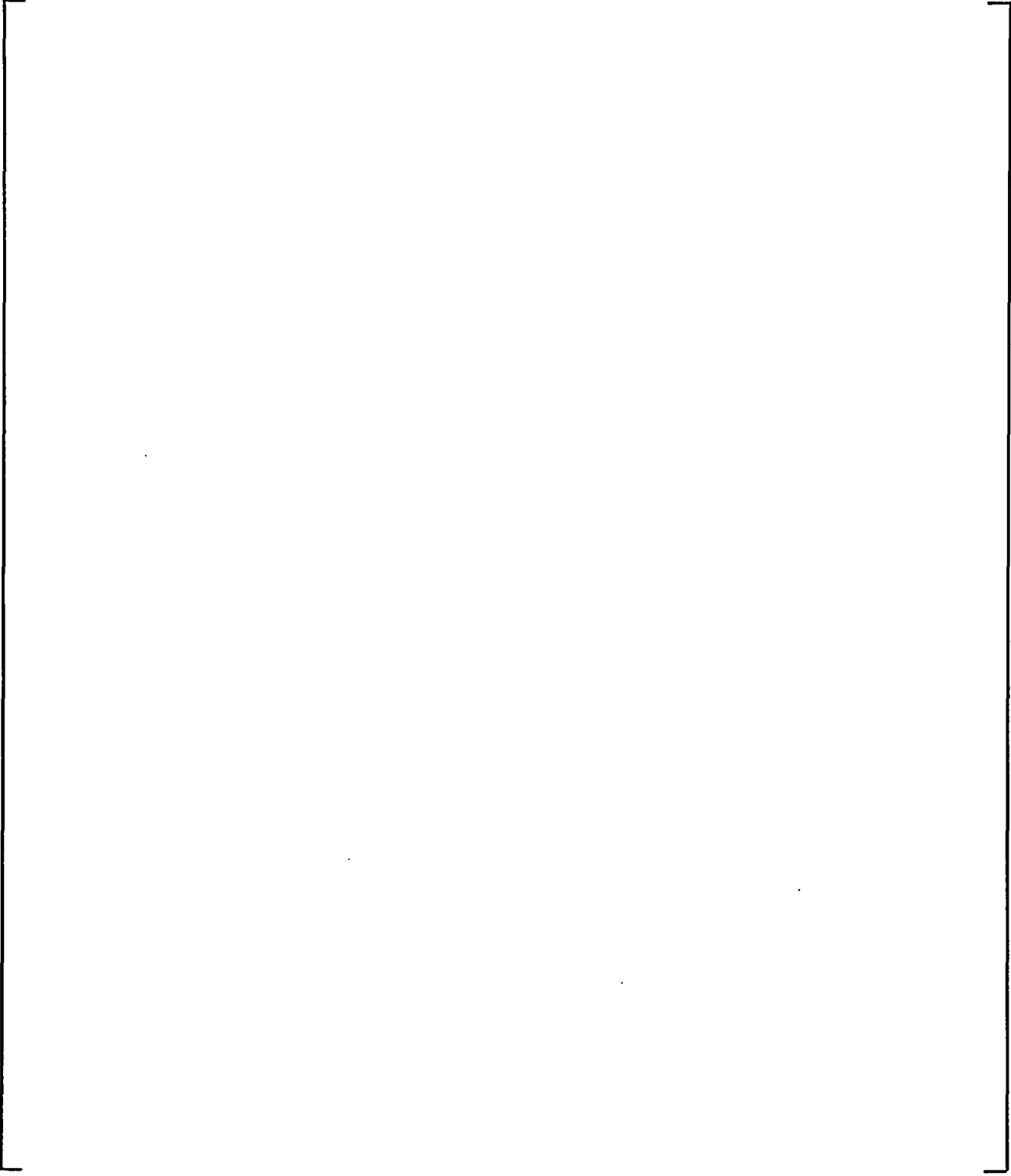


Figure 9-2 LST with Diffuser Under Steam Generator - Steam Flow 0.11-0.17 lb/sec - Internal Fluid Temperature - Group 1

(a,b)

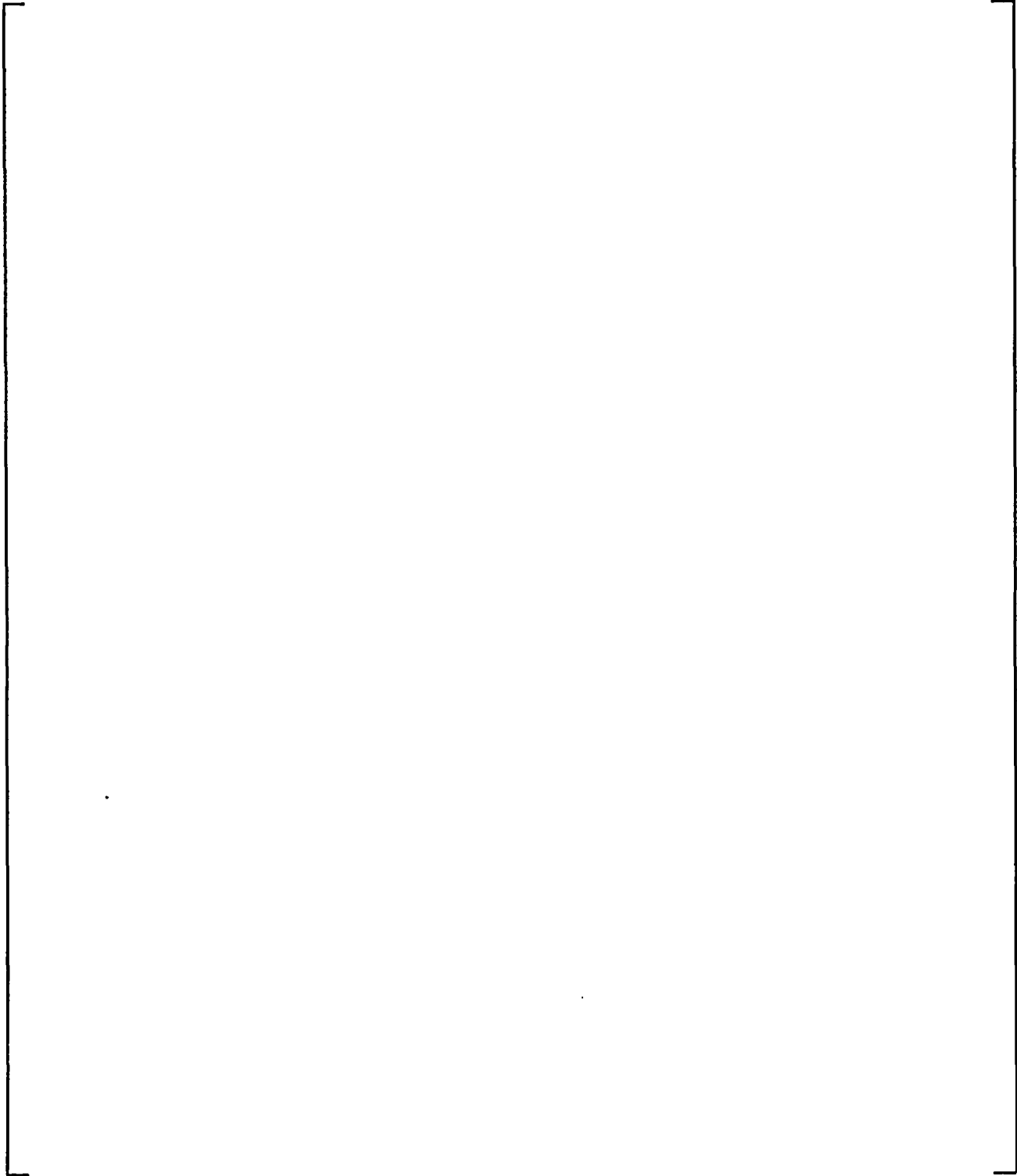


Figure 9-3 LST with Diffuser Under Steam Generator - Steam Flow 0.11-0.17 lb/sec - Saturation Temperature - Group 1

(a,b)

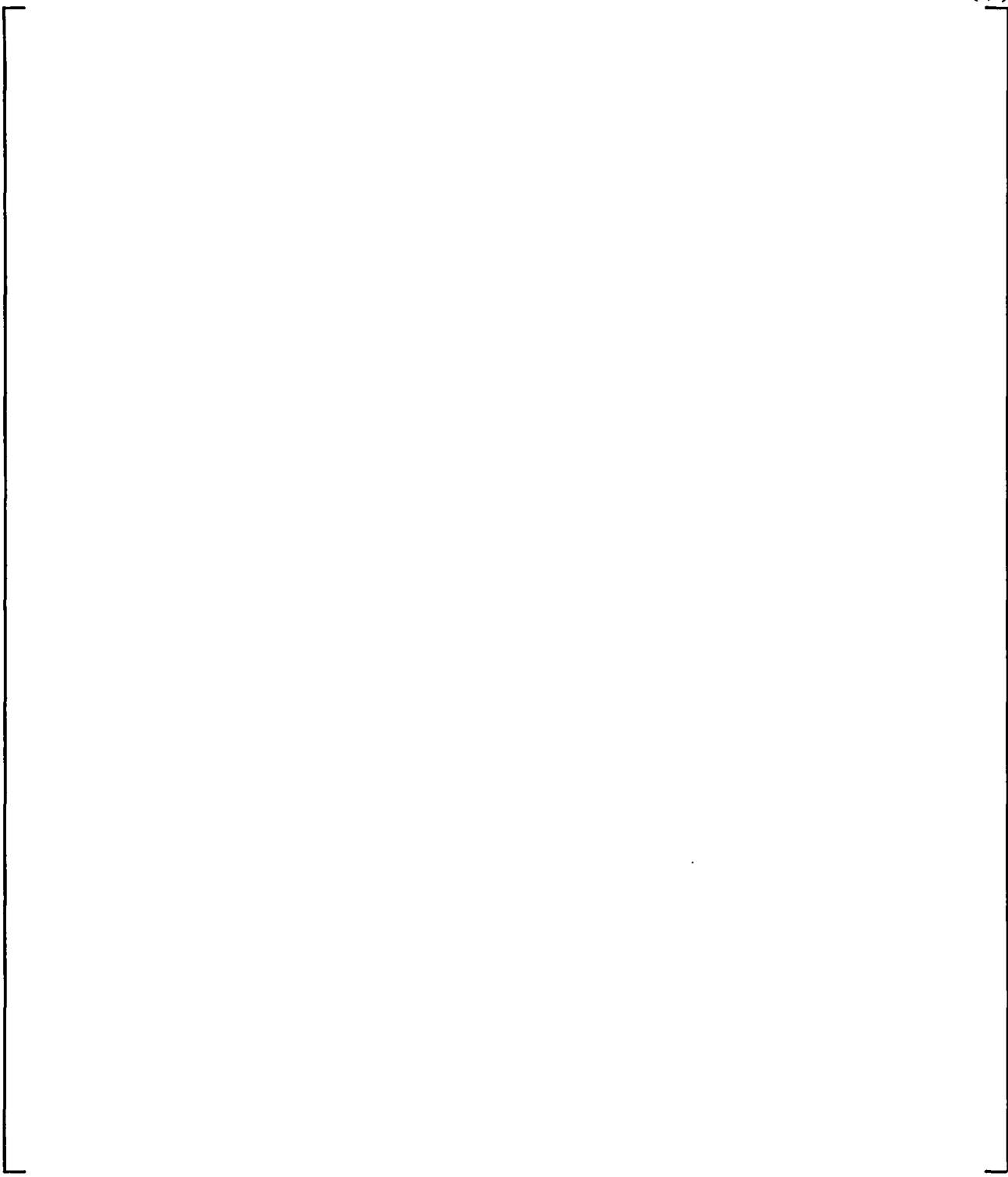


Figure 9-4 LST with Diffuser Under Steam Generator - Steam Flow 0.11-0.17 lb/sec - Internal Steam Pressure Ratio - Group 1

(a,b)

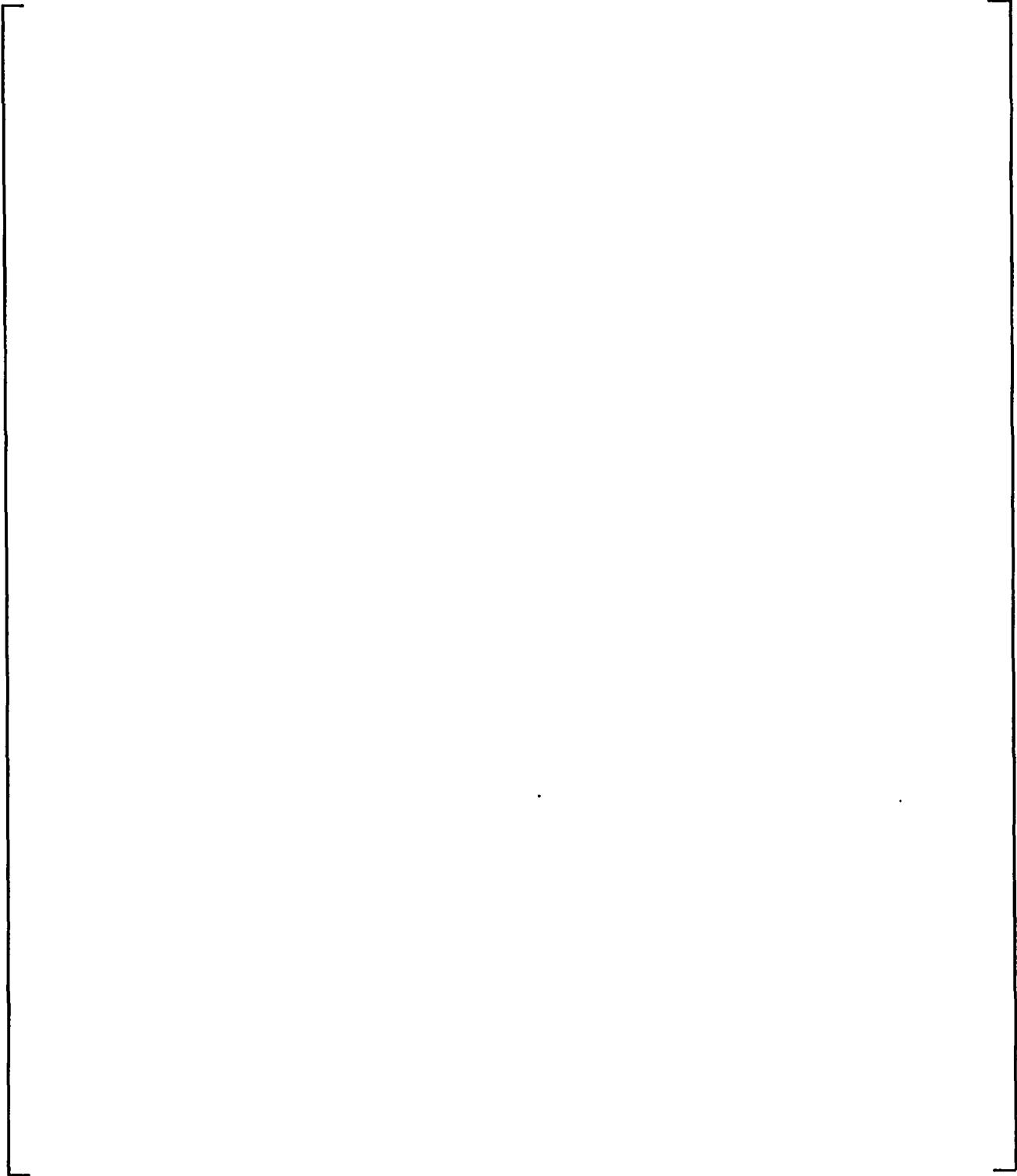


Figure 9-5 LST with Diffuser Under Steam Generator - Steam Flow 0.11-0.17 lb/sec - Internal Fluid Temperature - Group 2

(a,b)

Figure 9-6 LST with Diffuser Under Steam Generator - Steam Flow 0.11-0.17 lb/sec - Saturation Temperature - Group 2

(a,b)

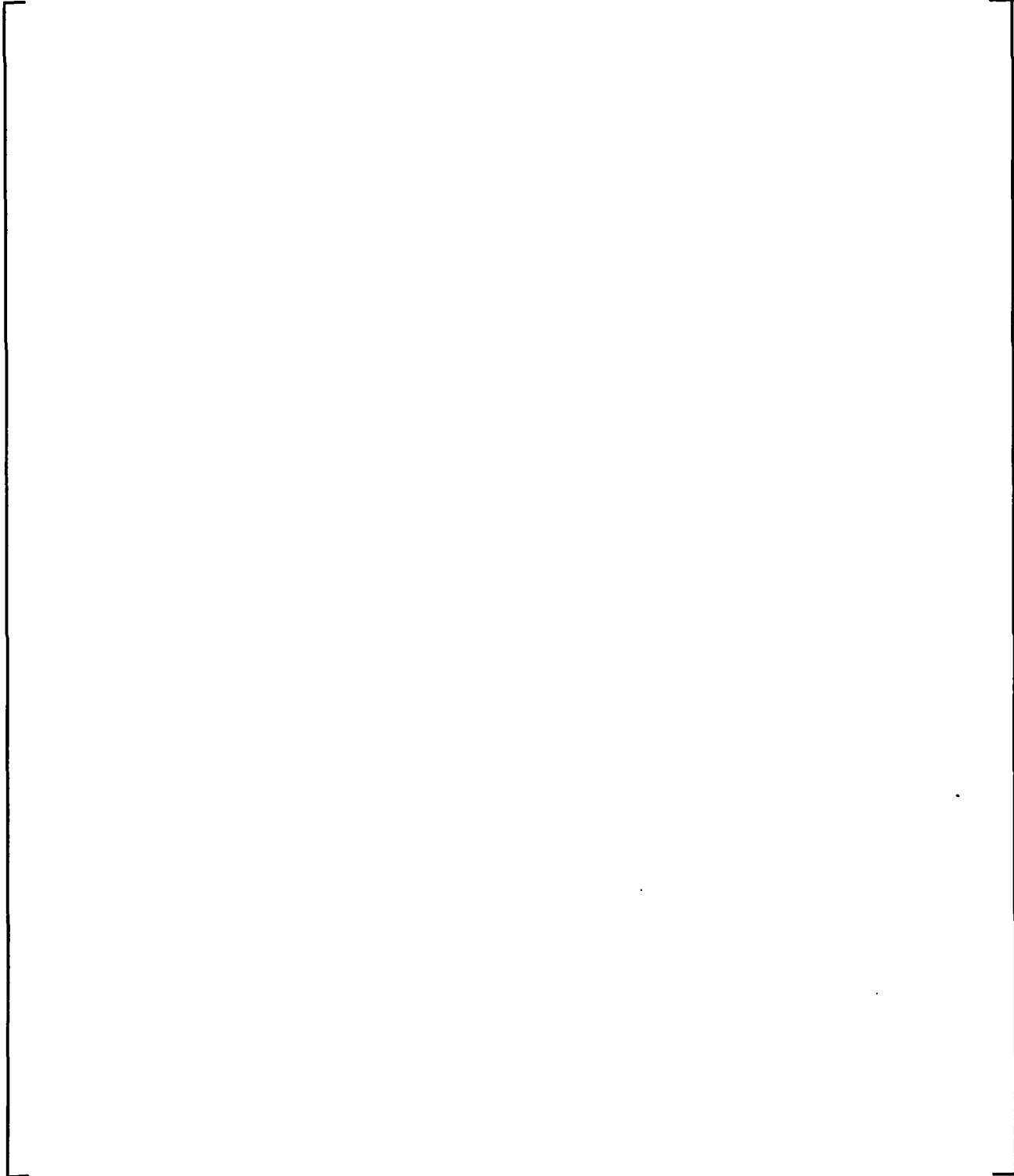


Figure 9-7 LST with Diffuser Under Steam Generator - Steam Flow 0.11-0.17 lb/sec - Internal Steam Pressure Ratio - Group 2

(a,b)

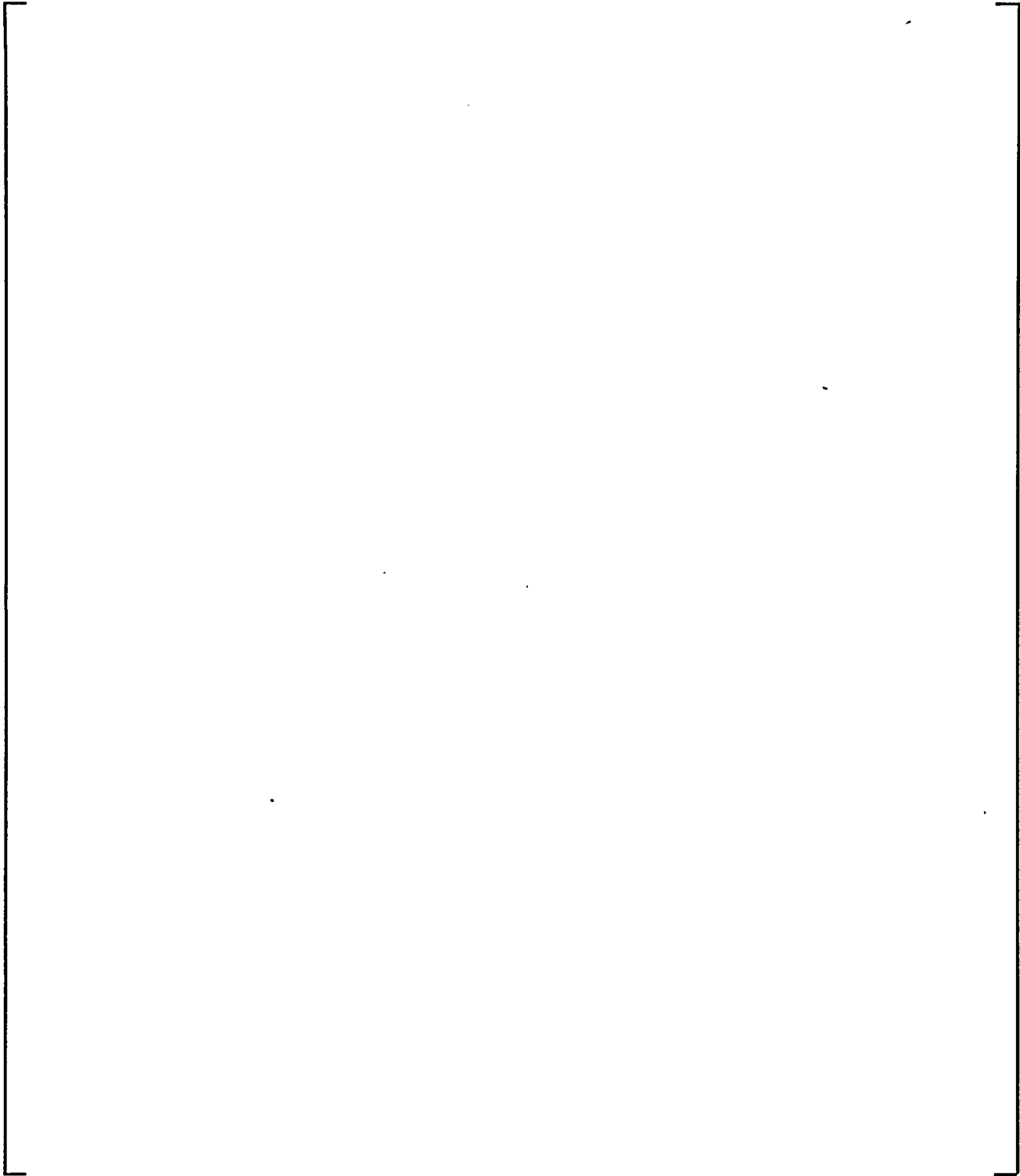


Figure 9-8 LST with Diffuser Under Steam Generator - Steam Flow 0.27-0.36 lb/sec - Internal Fluid Temperature

(a,b)

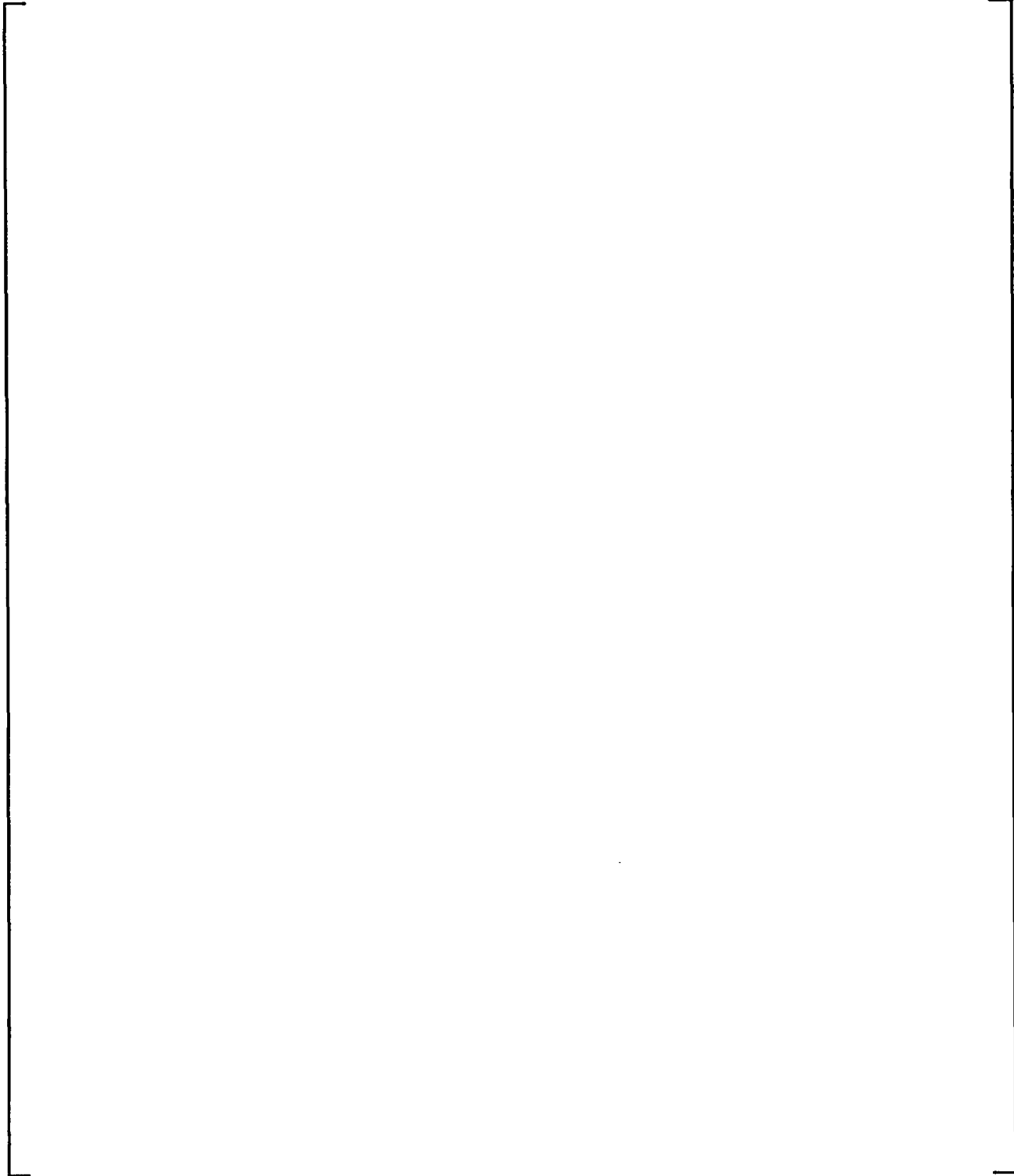


Figure 9-9 LST with Diffuser Under Steam Generator - Steam Flow 0.27-0.36 lb/sec - Saturation Temperature

(a,b)

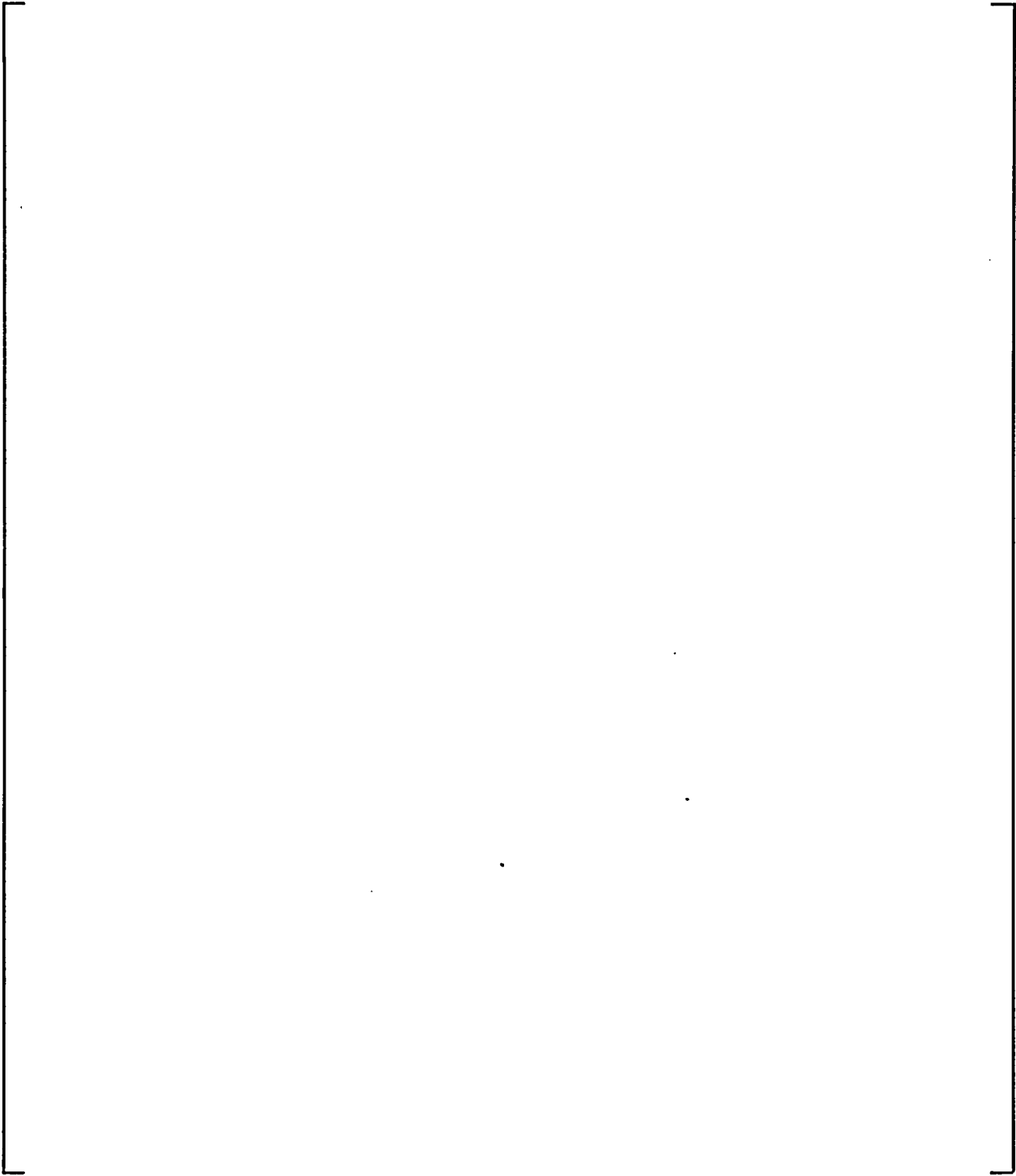


Figure 9-10 LST with Diffuser Under Steam Generator - Steam Flow 0.27-0.36 lb/sec - Internal Steam Pressure Ratio

(a,b)

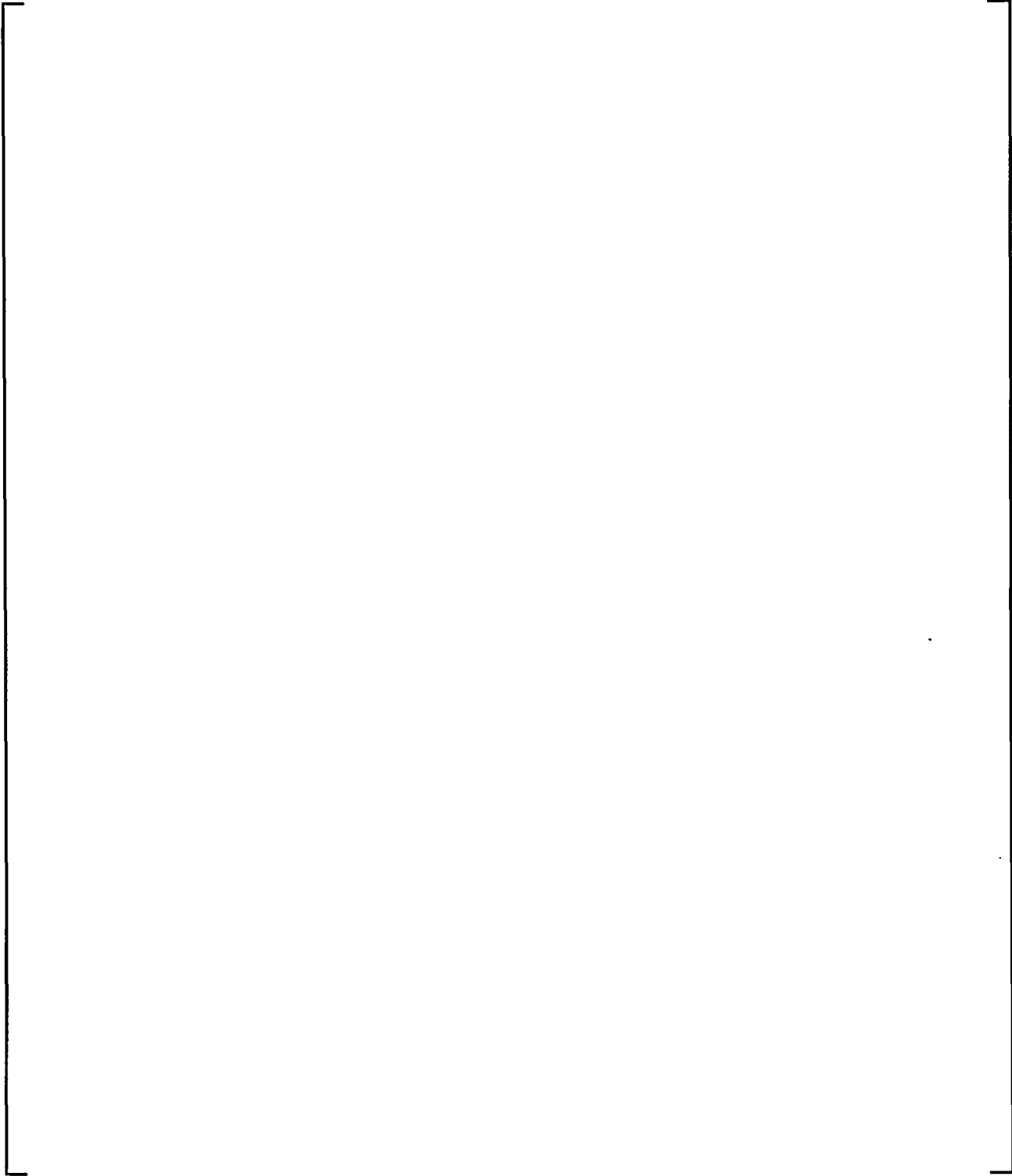


Figure 9-11 LST with Diffuser Under Steam Generator - Steam Flow 0.49-0.62 lb/sec - Internal Fluid Temperature - Group 1

(a,b)

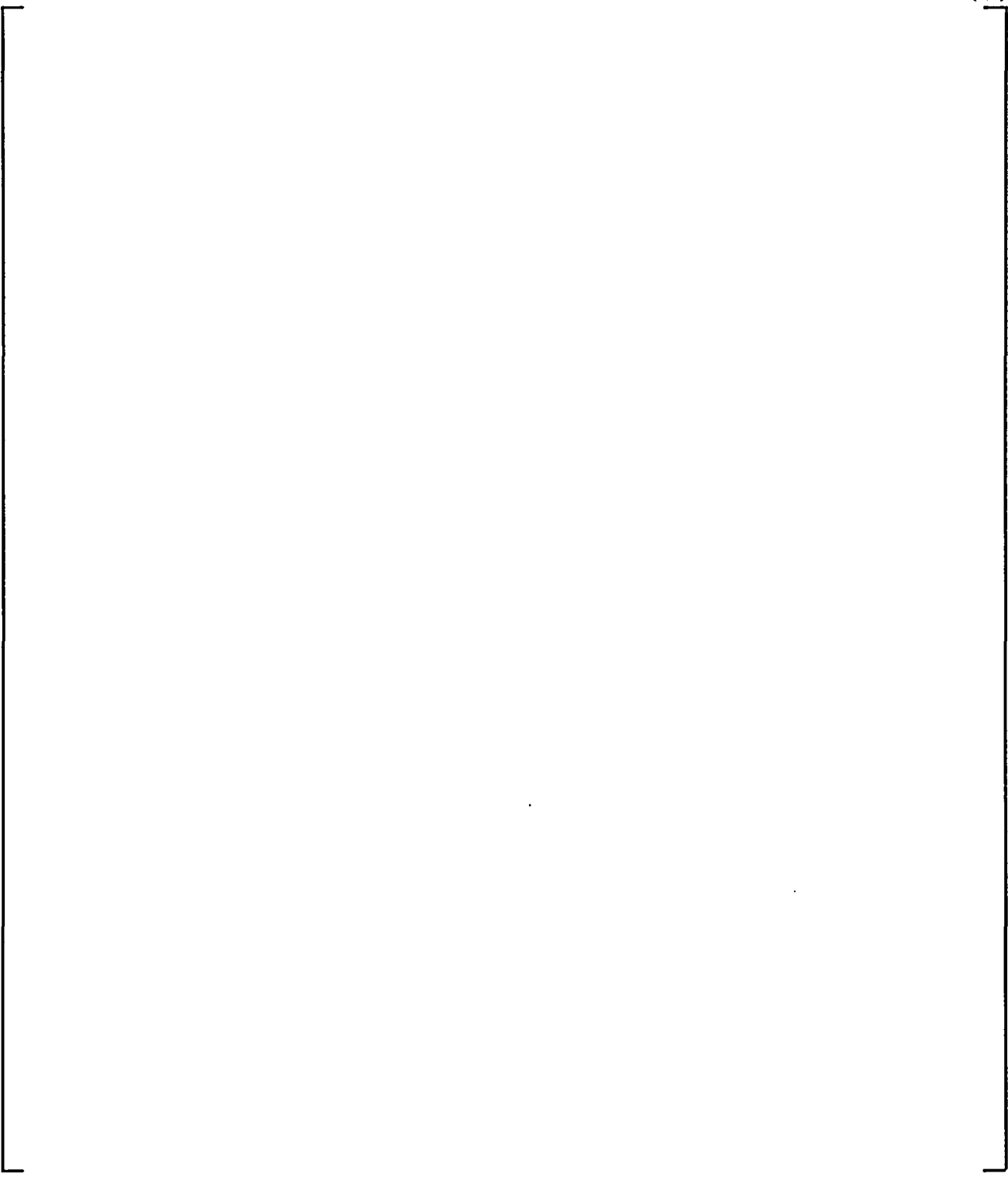


Figure 9-12 LST with Diffuser Under Steam Generator - Steam Flow 0.49-0.26 lb/sec - Saturation Temperature - Group 1

(a,b)

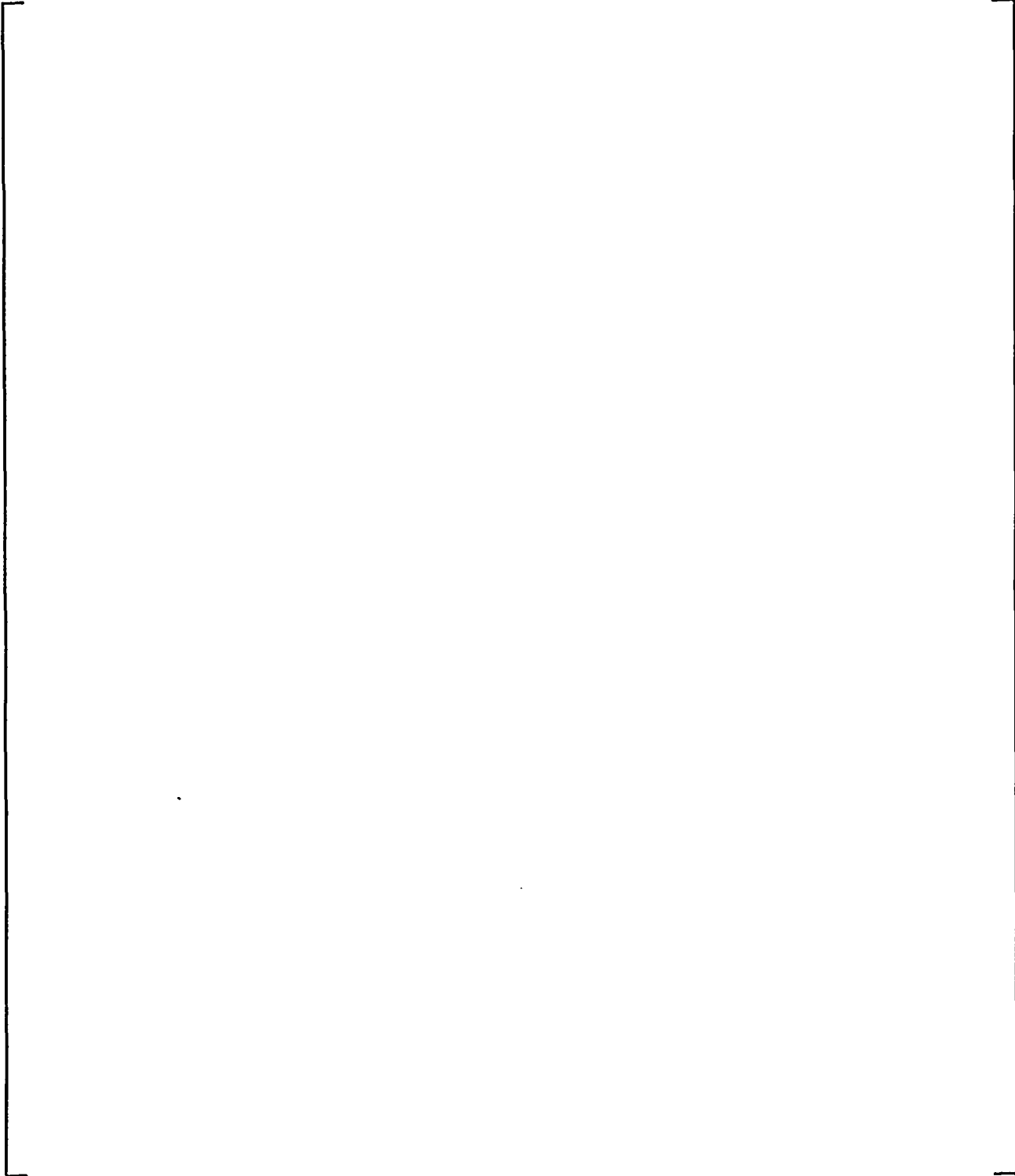


Figure 9-13 LST with Diffuser Under Steam Generator - Steam Flow 0.49-0.62 lb/sec - Internal Steam Pressure Ratio - Group 1

(a,b)

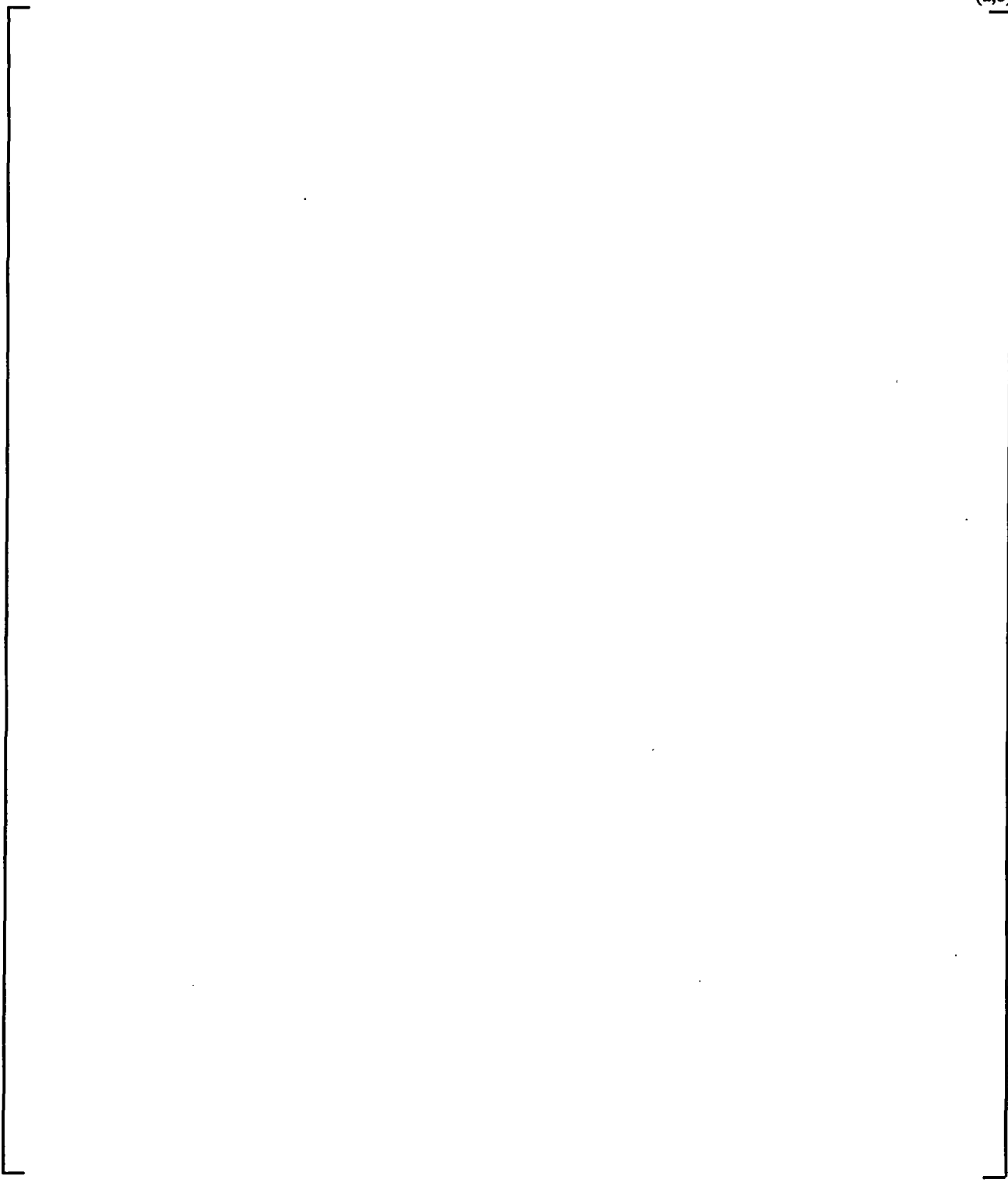


Figure 9-14 LST with Diffuser Under Steam Generator - Steam Flow 0.49-0.62 lb/sec - Internal Fluid Temperature - Group 2

(a,b)

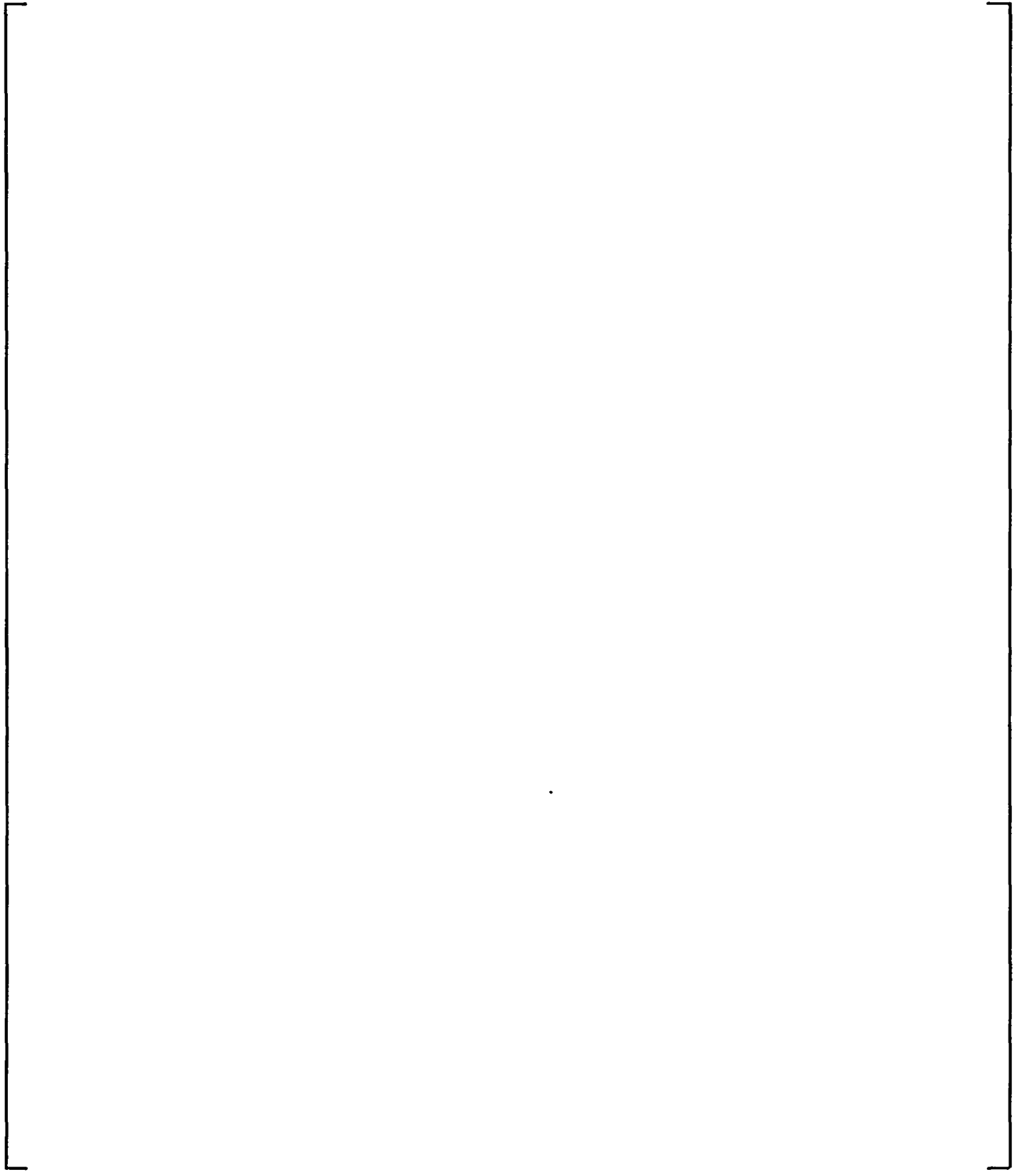


Figure 9-15 LST with Diffuser Under Steam Generator - Steam Flow 0.49-0.62 lb/sec - Saturation Temperature - Group 2

(a,b)

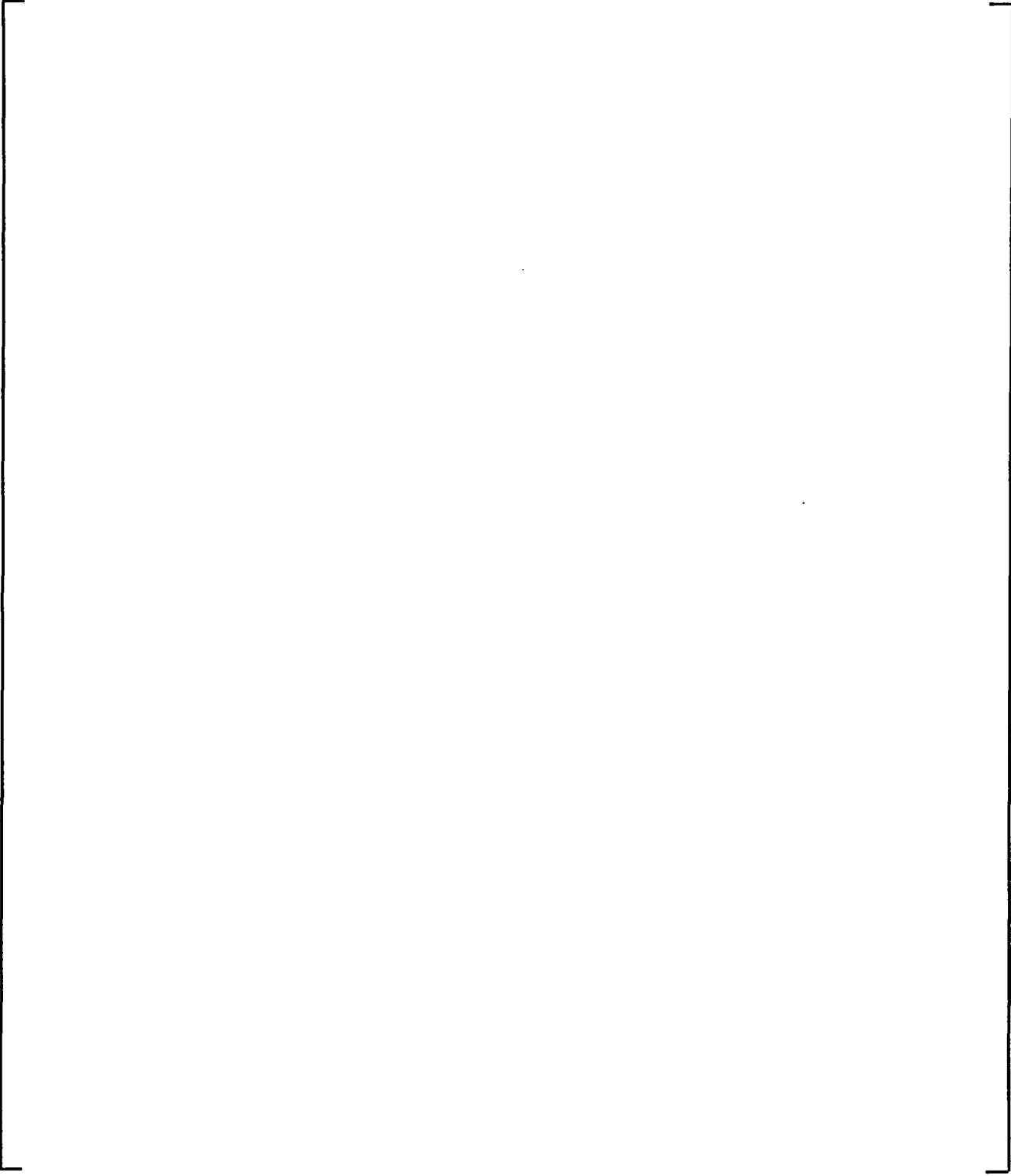


Figure 9-16 LST with Diffuser Under Steam Generator - Steam Flow 0.49-0.62 lb/sec - Internal Steam Pressure Ratio - Group 2

(a,b)

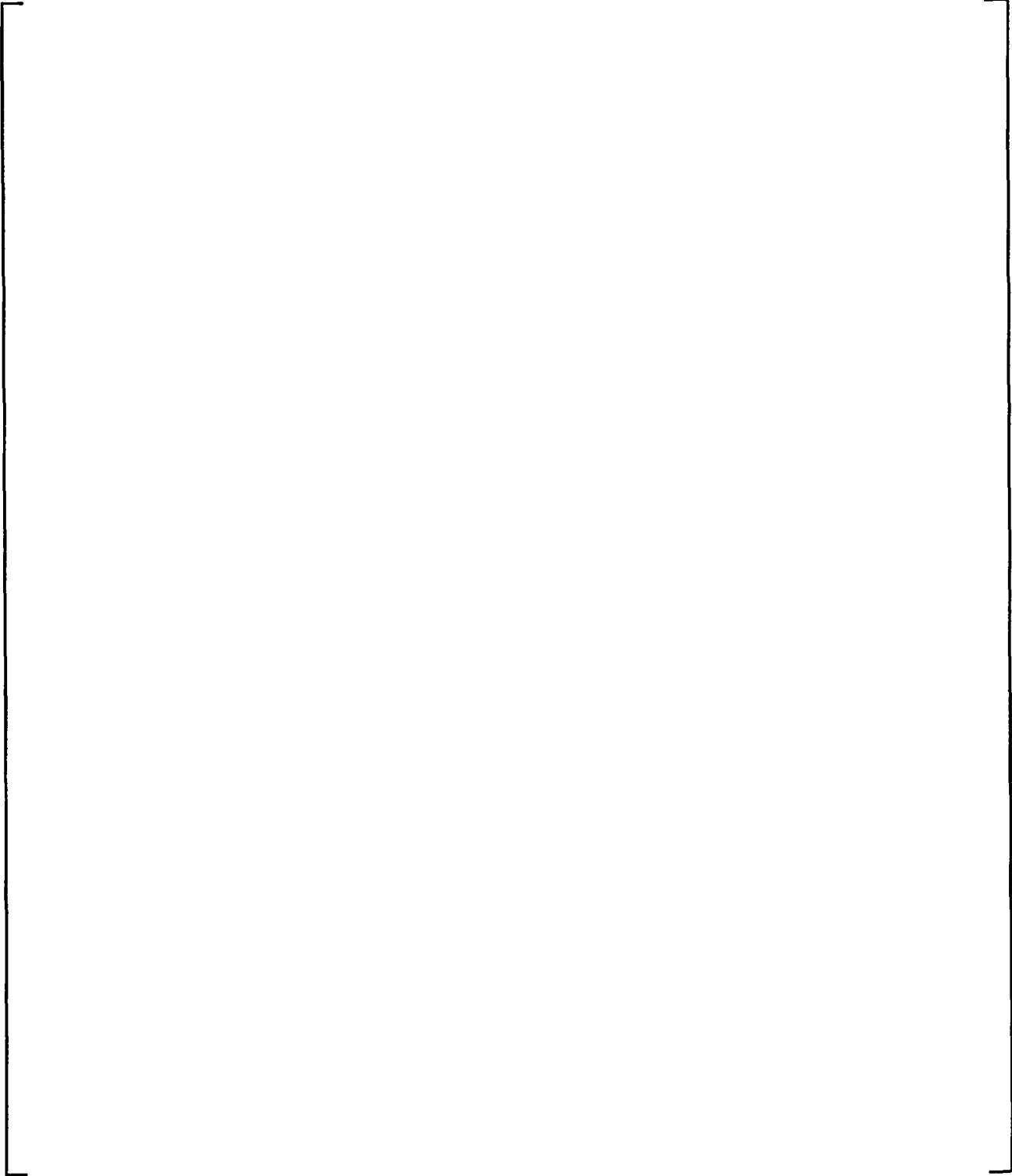


Figure 9-17 LST with Diffuser Under Steam Generator - Steam Flow 0.76-0.84 lb/sec - Internal Fluid Temperature

(a,b)



Figure 9-18 LST with Diffuser Under Steam Generator - Steam Flow 0.76-0.84 lb/sec - Saturation Temperature

(a,b)

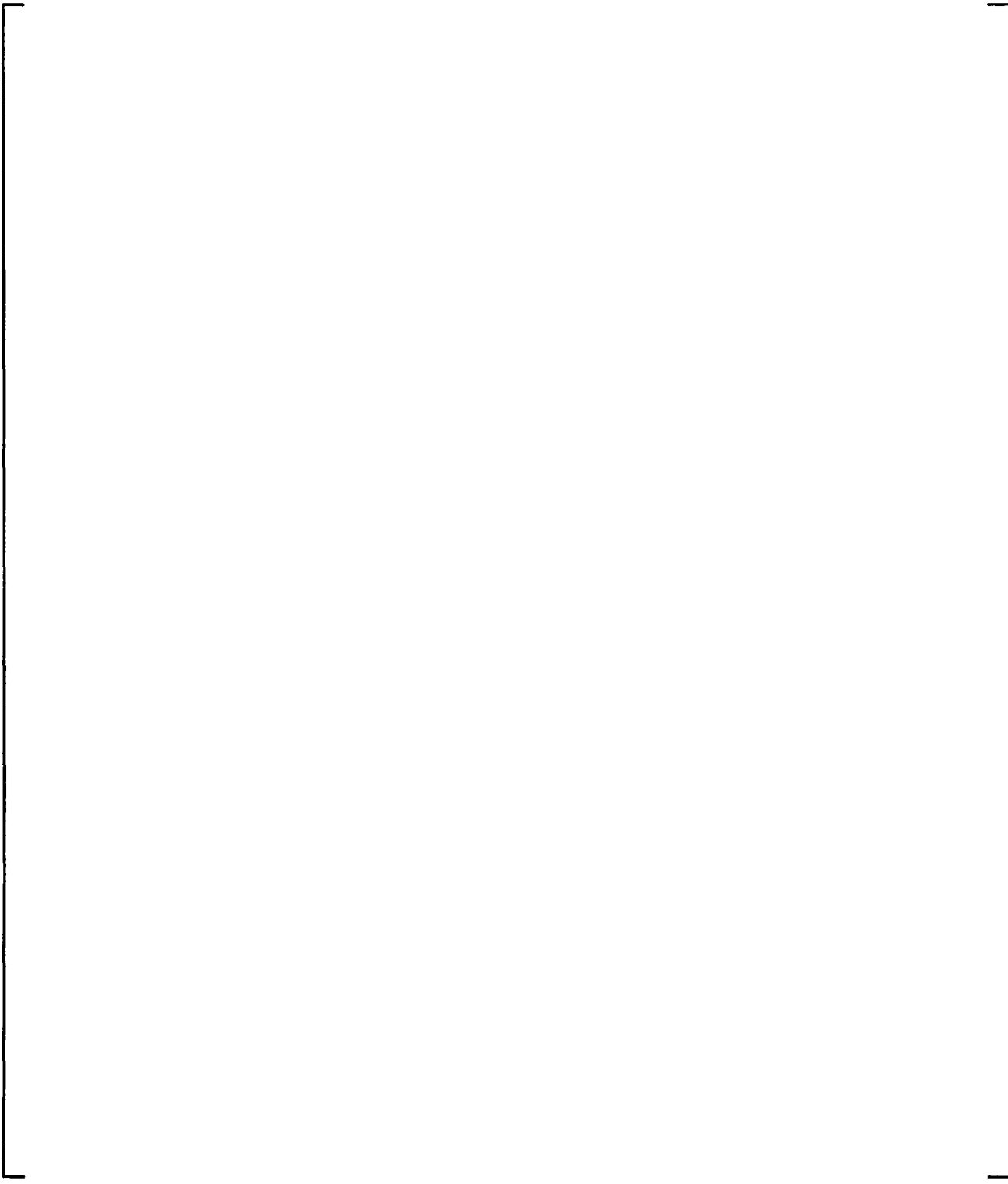


Figure 9-19 LST with Diffuser Under Steam Generator - Steam Flow 0.76-0.84 lb/sec - Internal Steam Pressure Ratio

(a,b)

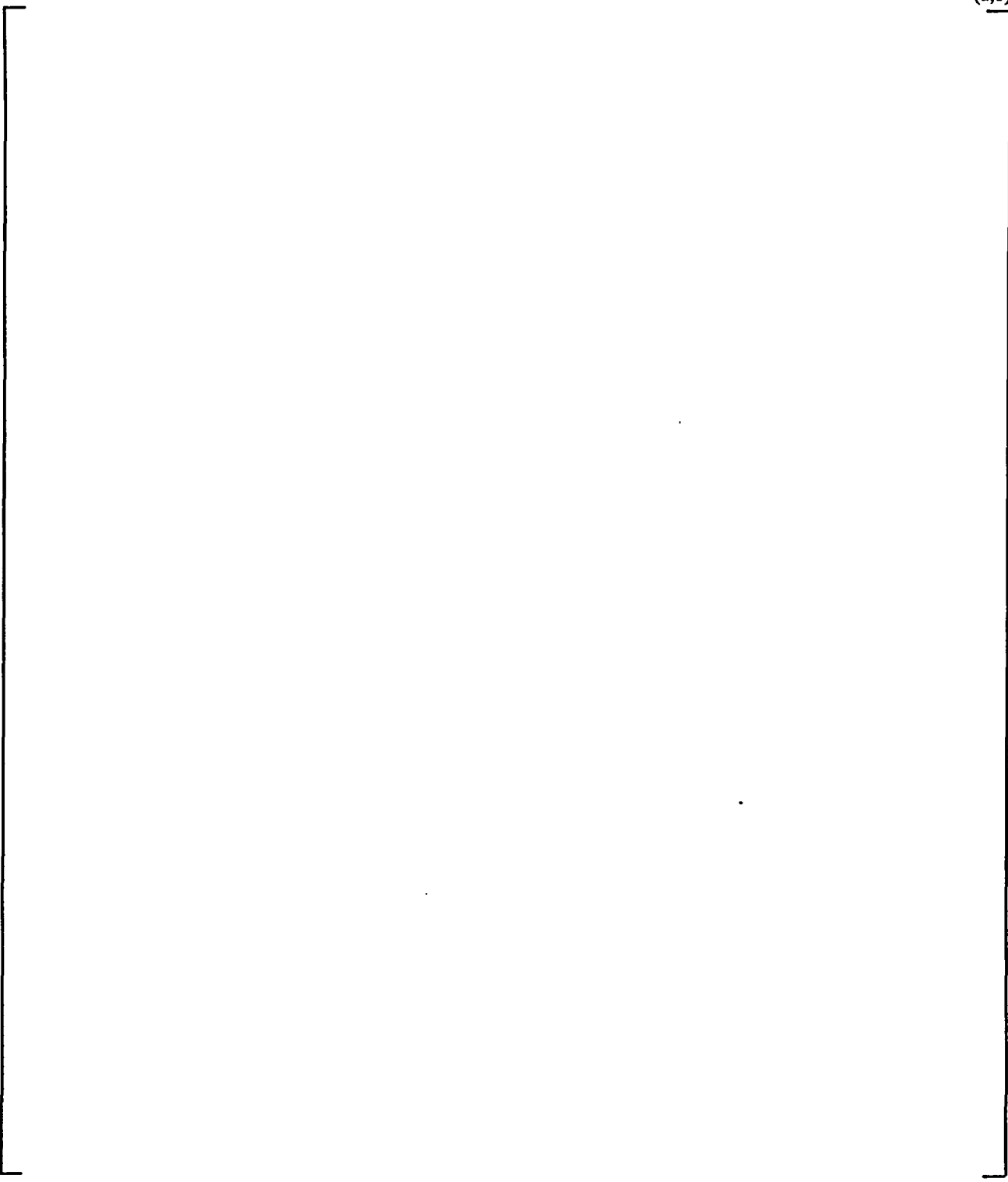


Figure 9-20 LST with Diffuser Under Steam Generator - Steam Flow 1.10-1.20 lb/sec - Internal Fluid Temperature

(a,b)

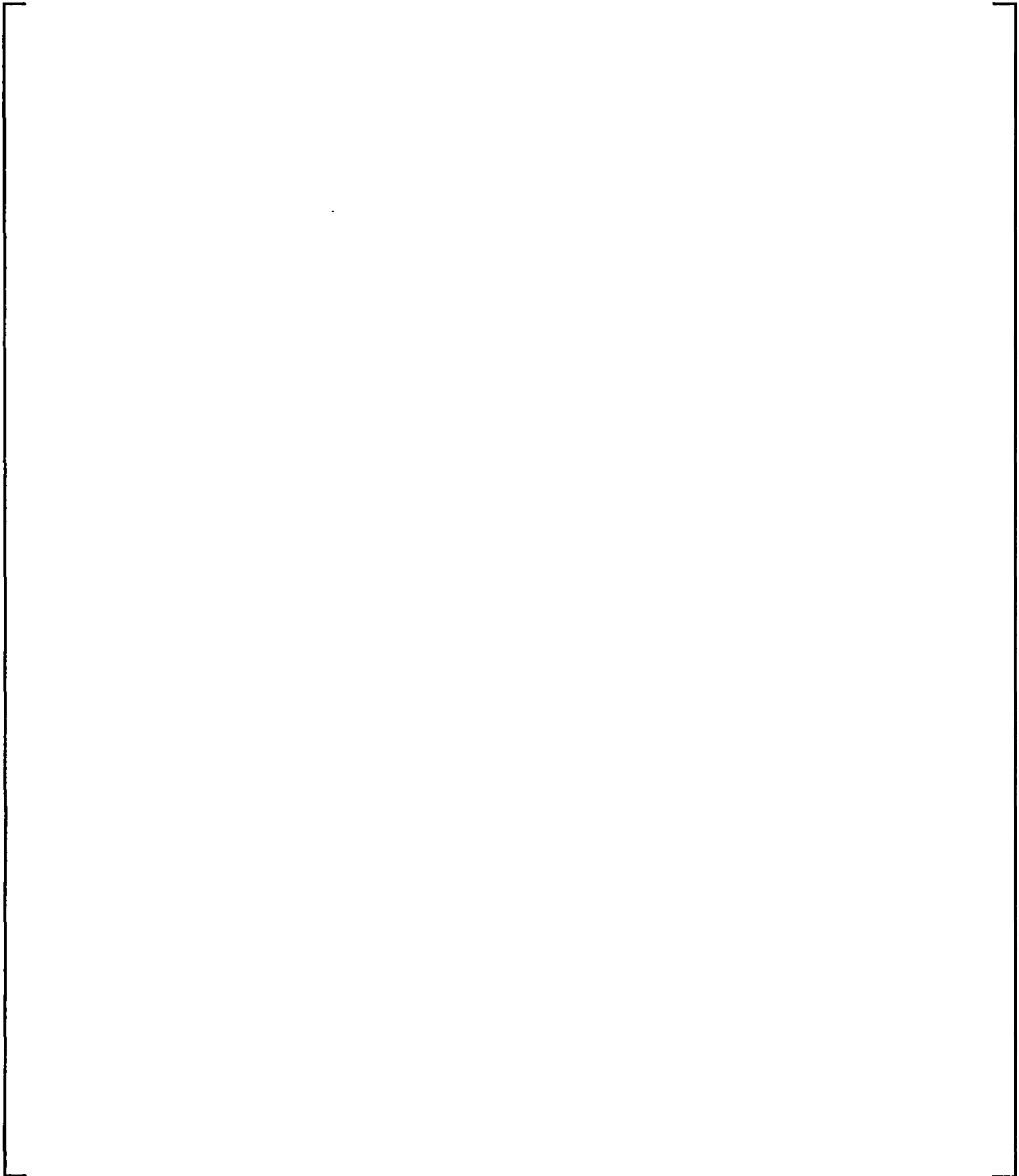


Figure 9-21 LST with Diffuser Under Steam Generator - Steam Flow 1.10-1.20 lb/sec - Saturation Temperature

(a,b)

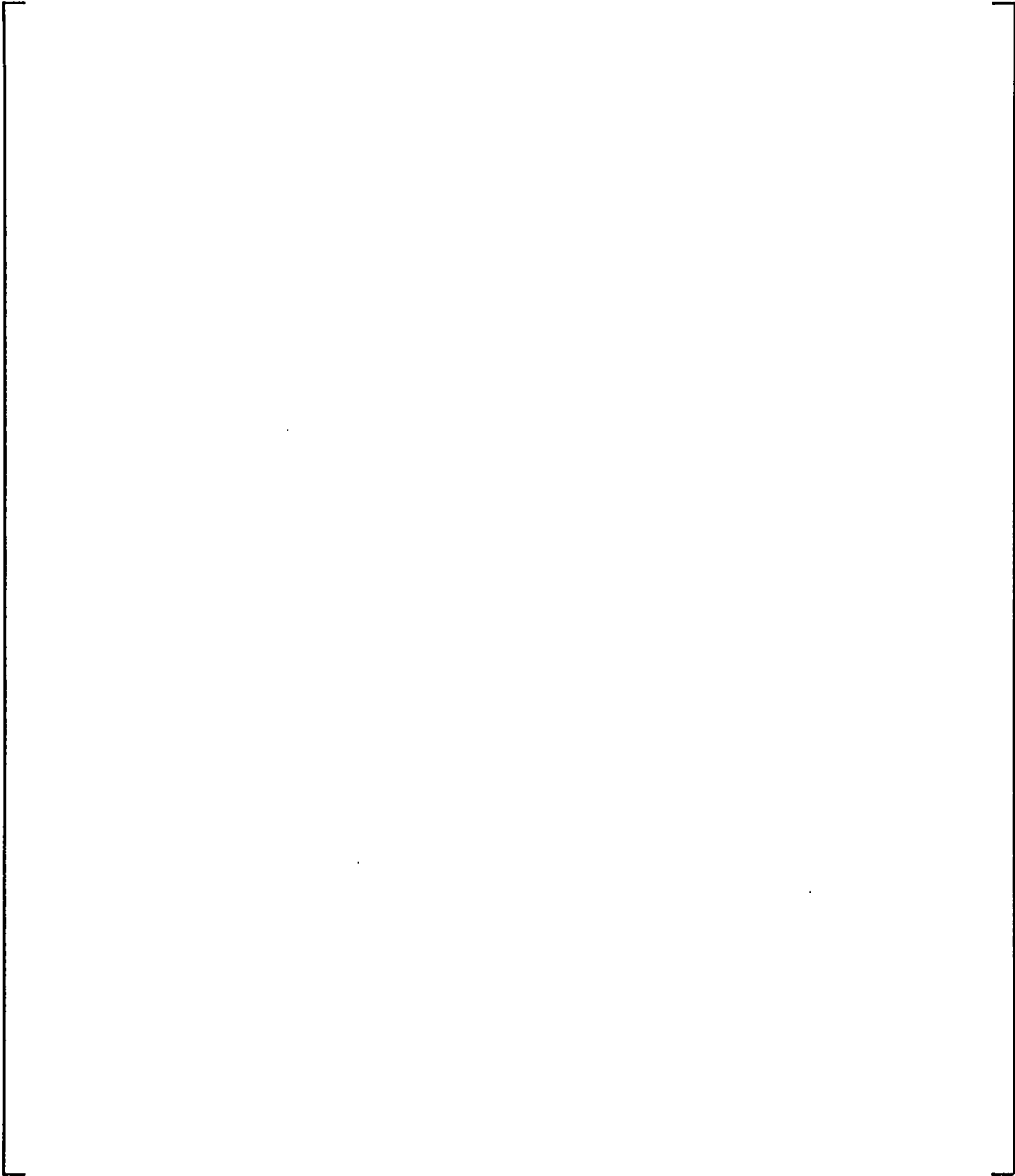


Figure 9-22 LST with Diffuser Under Steam Generator - Steam Flow 1.10-1.20 lb/sec - Internal Steam Pressure Ratio

(a,b)

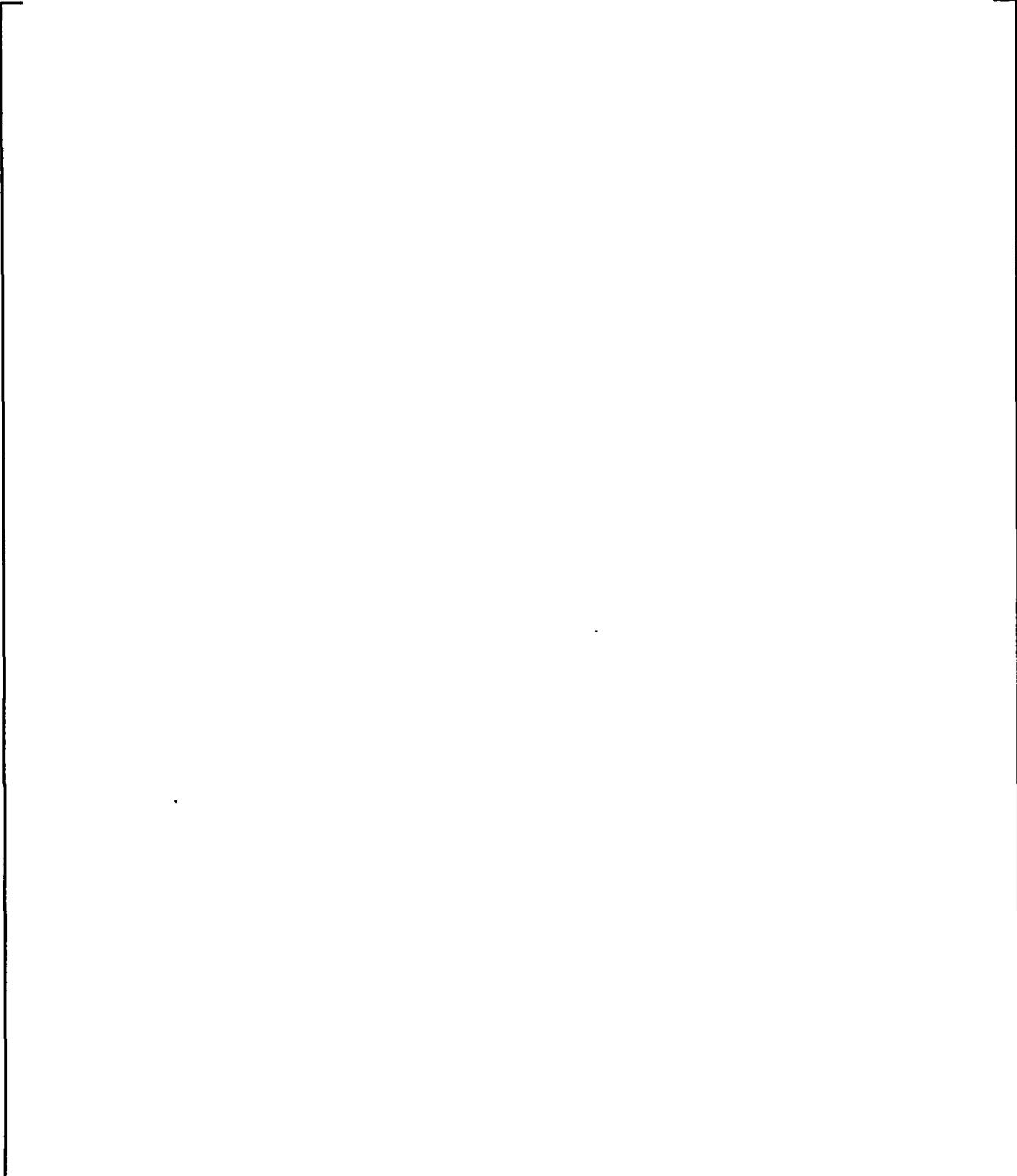


Figure 9-23 LST with Diffuser Under Steam Generator - Steam Flow 1.54-1.68 lb/sec - Internal Fluid Temperature

(a,b)

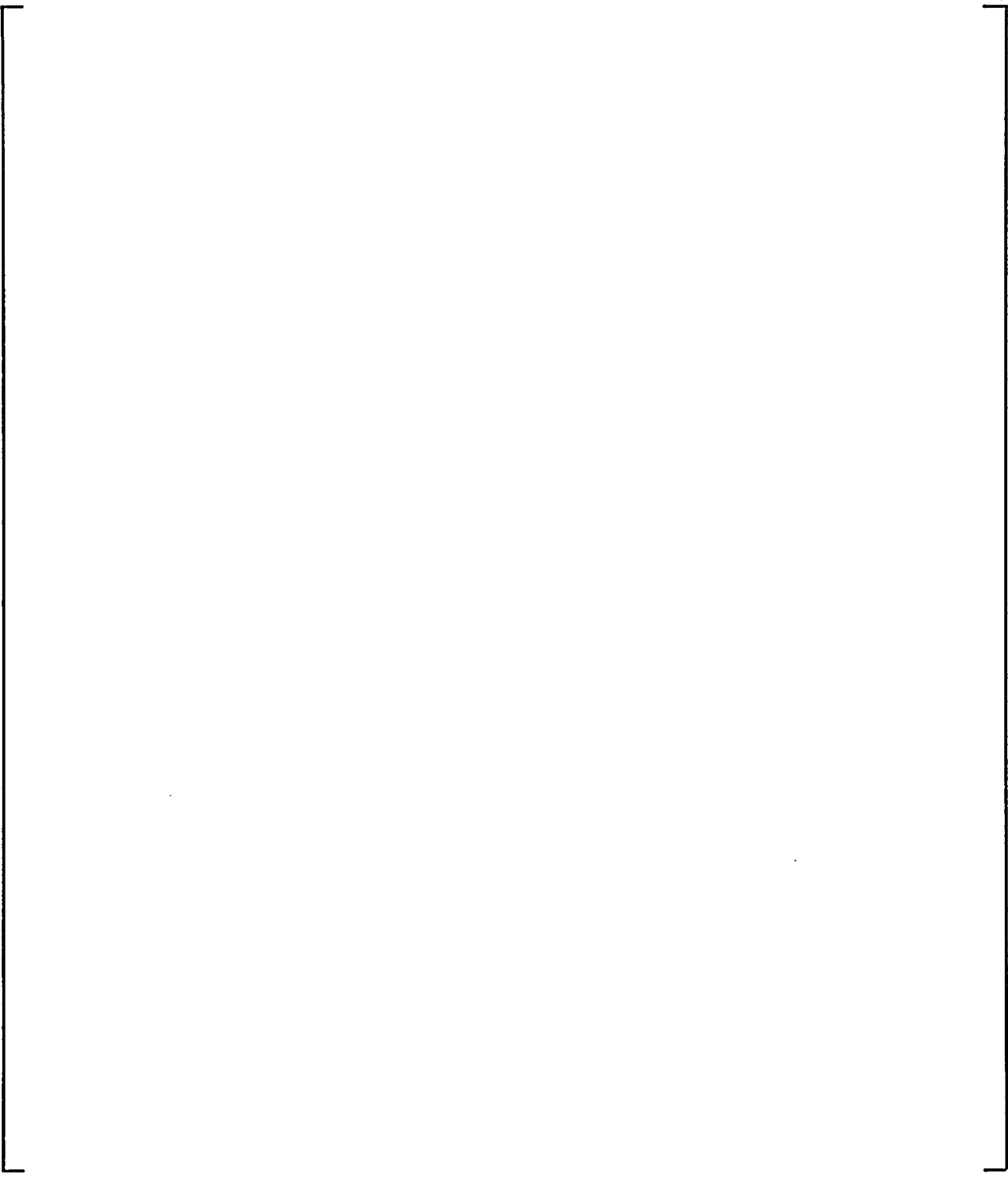


Figure 9-24 LST with Diffuser Under Steam Generator - Steam Flow 1.54-1.68 lb/sec - Saturation Temperature

(a,b)

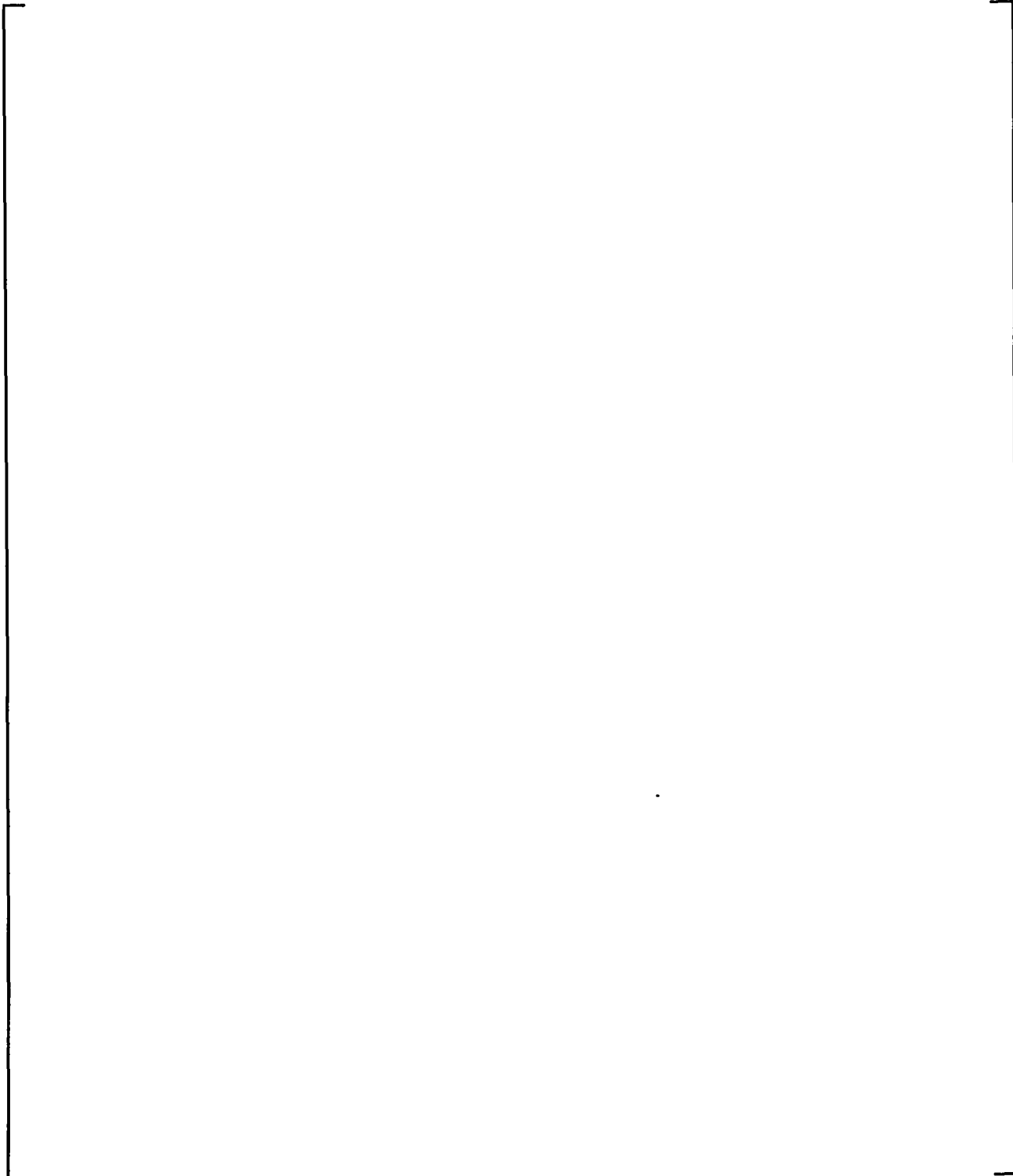


Figure 9-25 LST with Diffuser Under Steam Generator - Steam Flow 1.54-1.68 lb/sec - Internal Steam Pressure Ratio

(a,b)

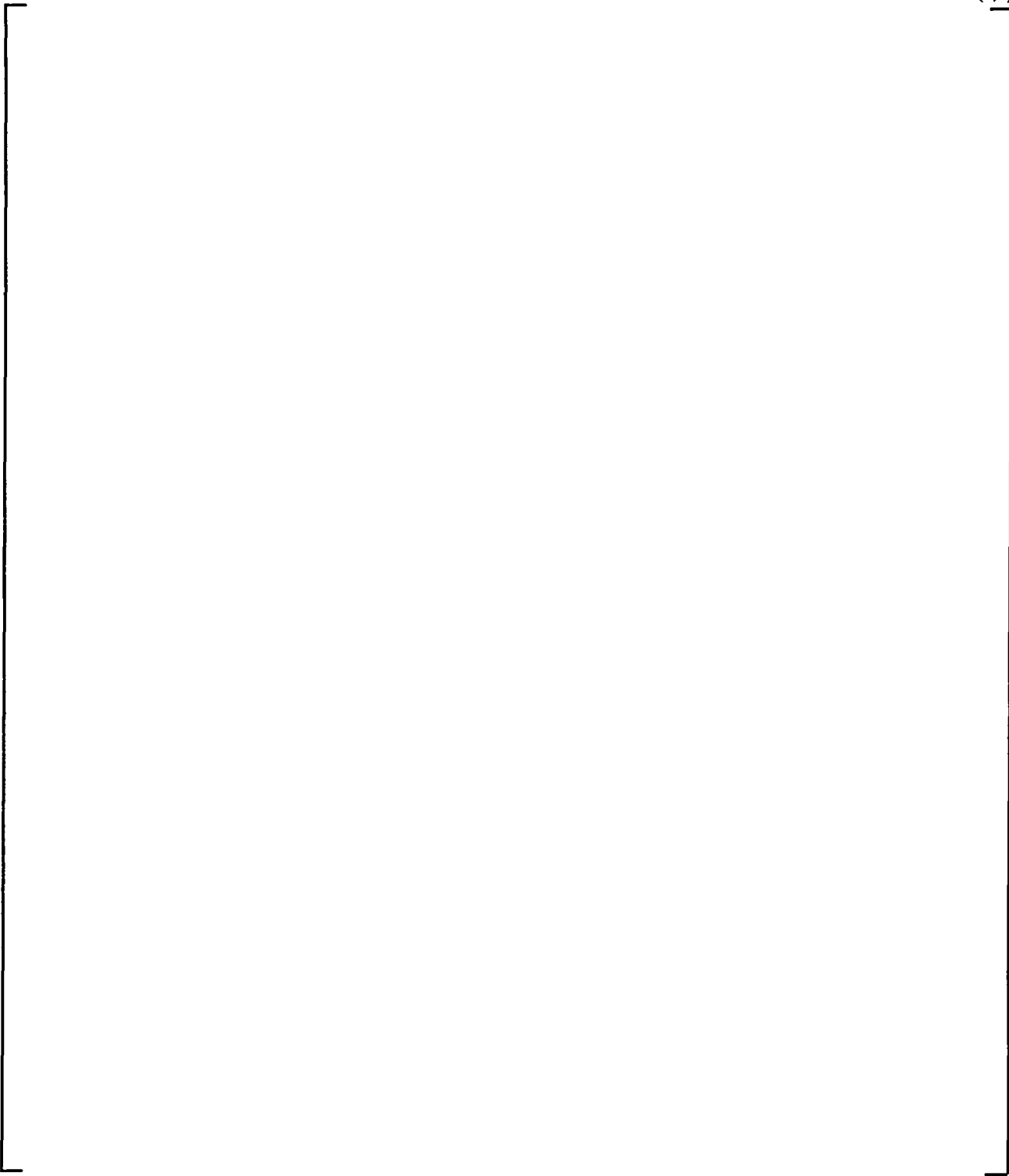


Figure 9-26 LST with Diffuser Up 6 Feet - Steam Flow 0.76 & 1.68 lb/sec - Internal Fluid Temperature

(a,b)

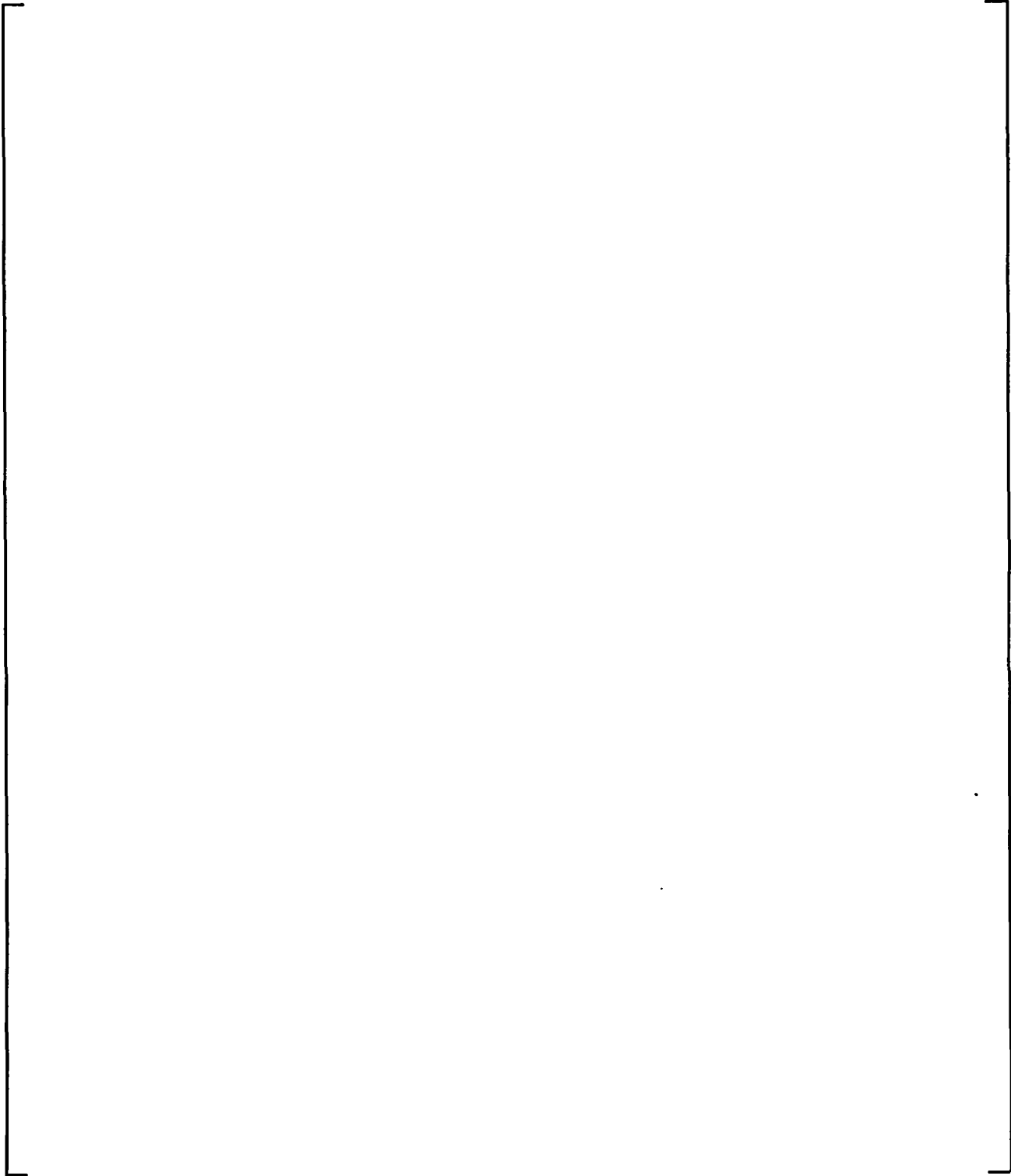


Figure 9-27 LST with Diffuser Up 6 Feet - Steam Flow 0.76 & 1.68 lb/sec - Saturation Temperature

(a,b)

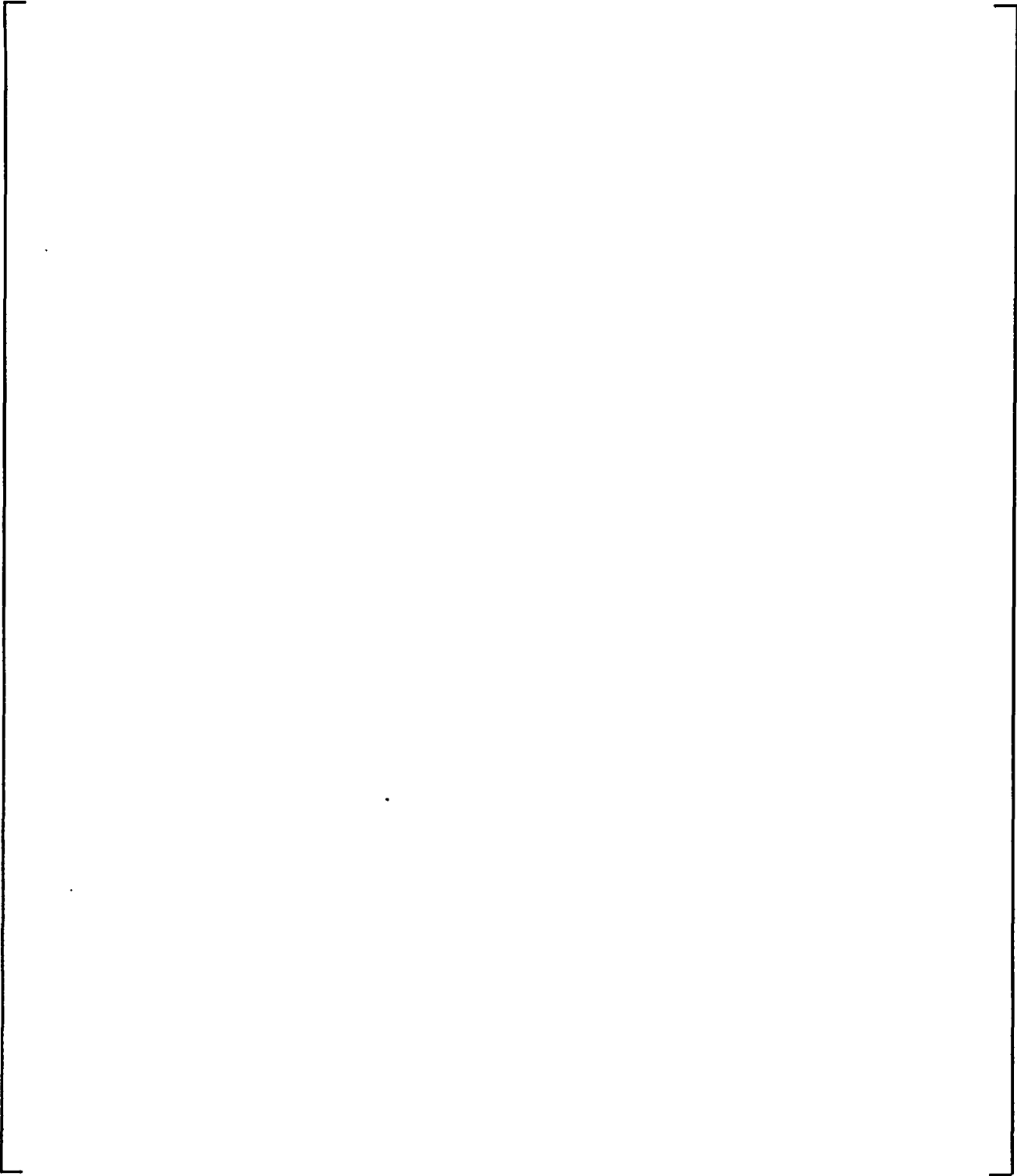


Figure 9-28 LST with Diffuser Up 6 Feet - Steam Flow 0.76 & 1.68 lb/sec - Internal Steam Pressure Ratio

(a,b)

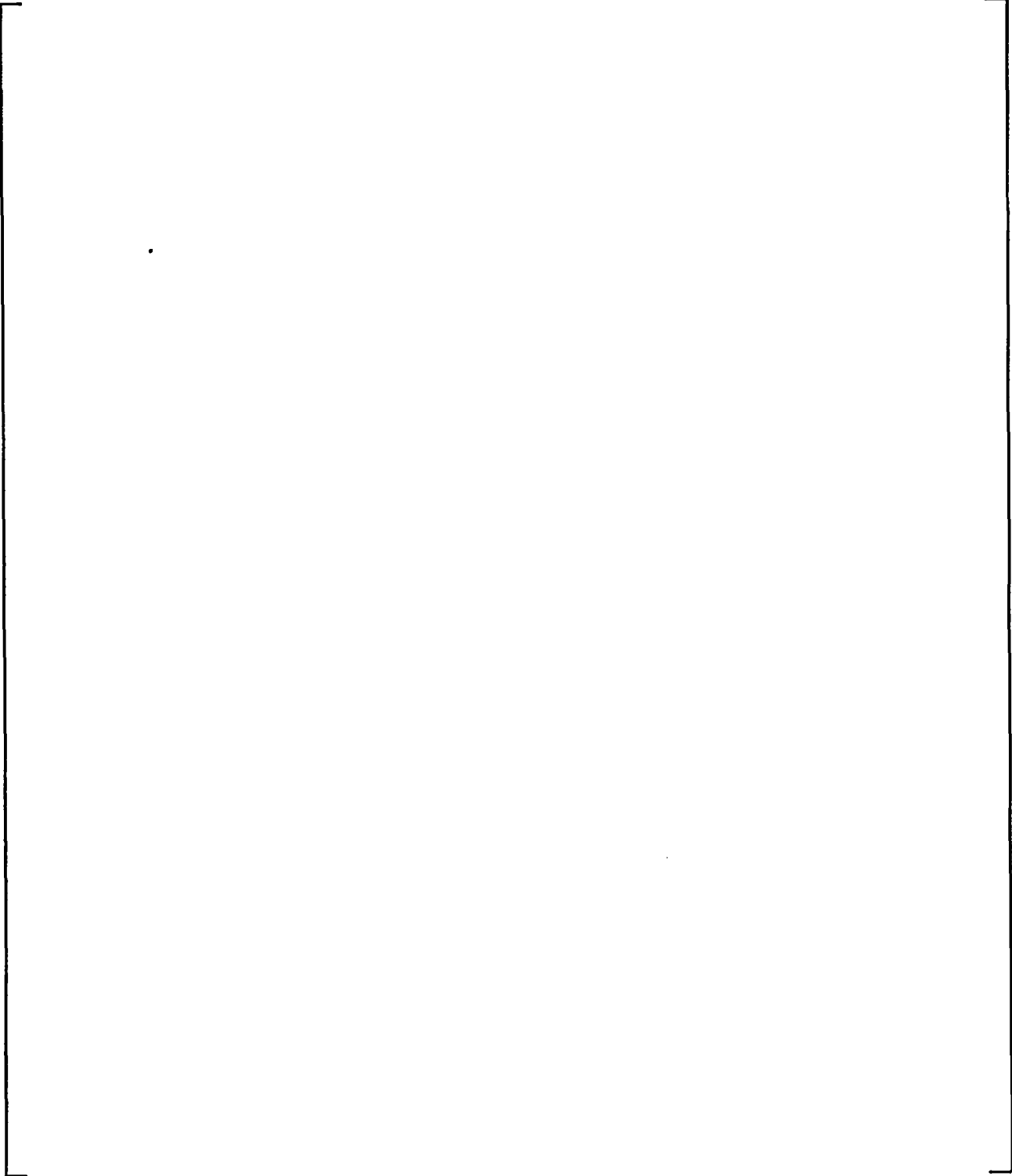


Figure 9-29 LST with Steam Injection: 3 Inch Pipe - Steam Flow 0.76 - 0.95 lb/sec - Internal Fluid Temperature

(a,b)

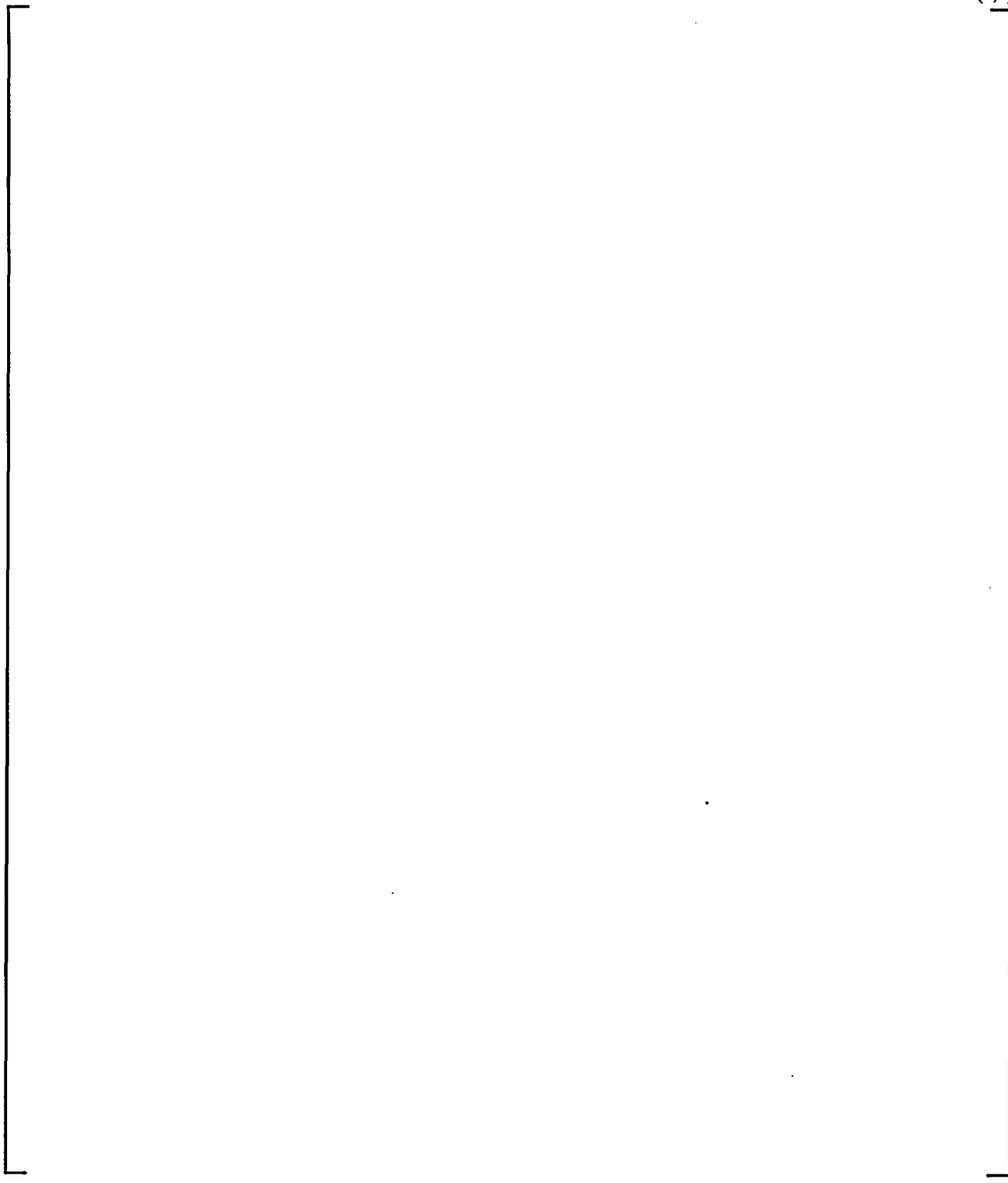


Figure 9-30 LST with Steam Injection: 3 Inch Pipe - Steam Flow 0.76 - 0.95 lb/sec - Saturation Temperature

(a,b)

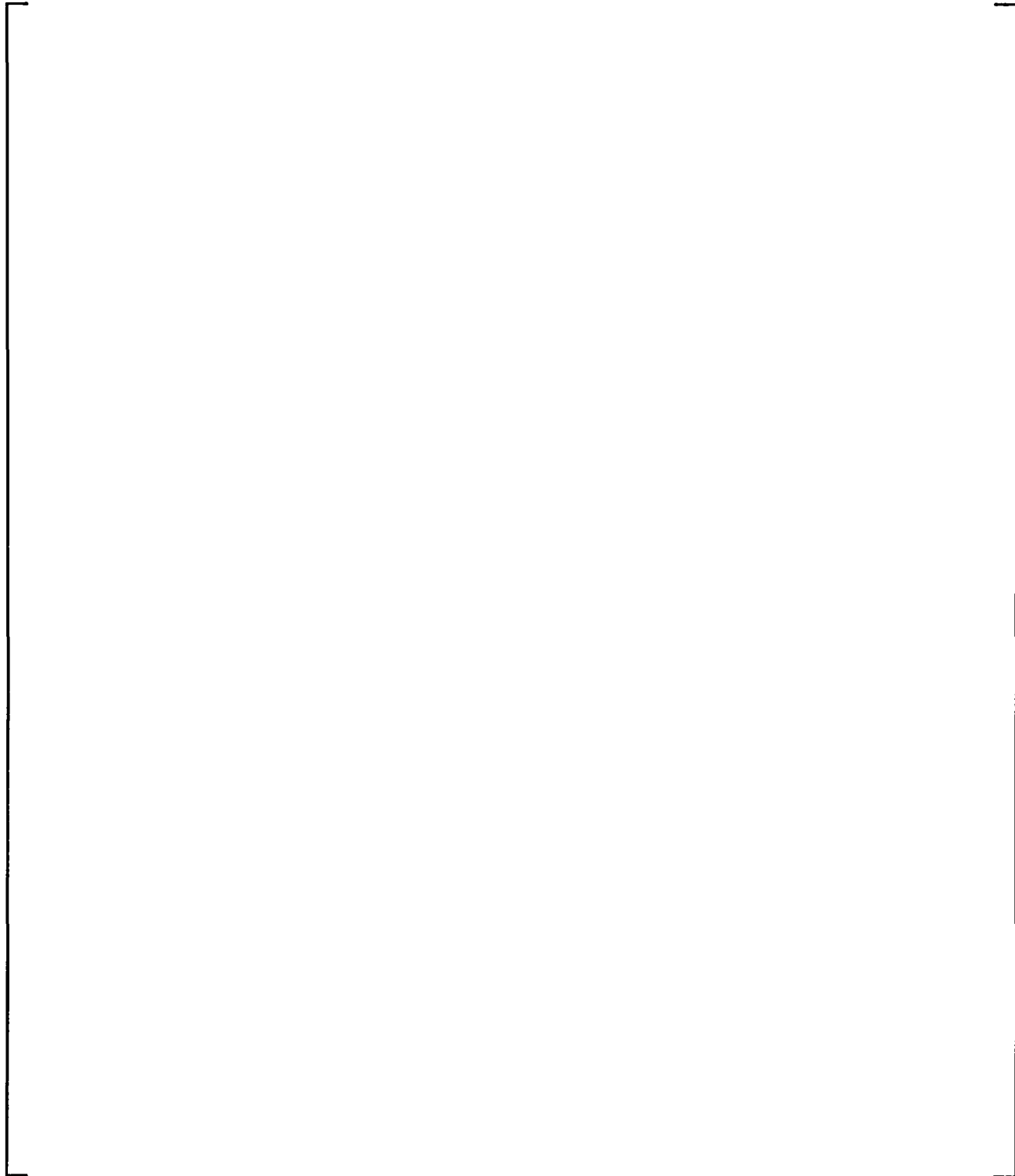


Figure 9-31 LST with Steam Injection: 3 Inch Pipe - Steam Flow 0.76 - 0.95 lb/sec - Internal Steam Pressure Ratio

(a,b)

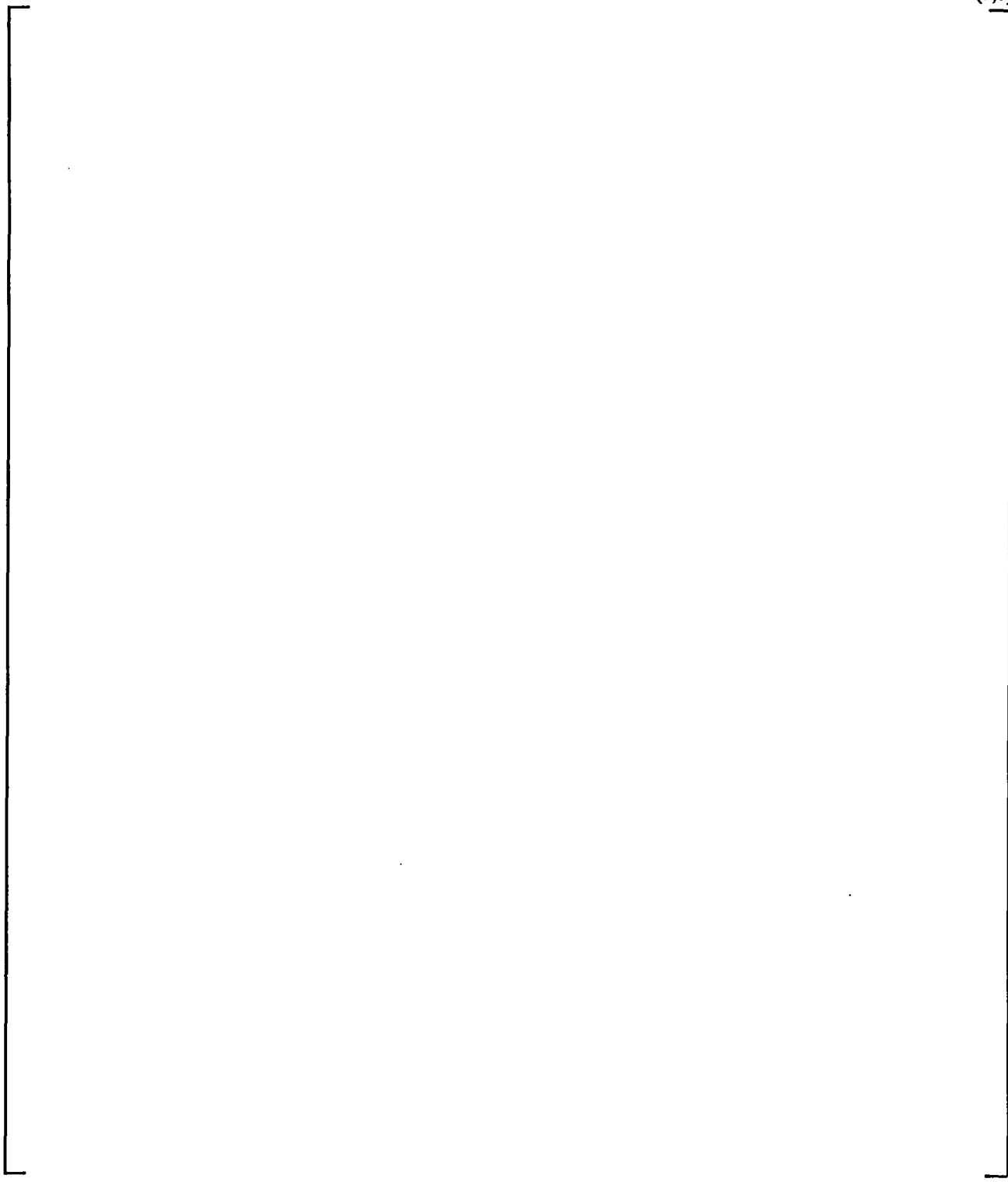


Figure 9-32 LST with Steam Injection: 3 Inch Pipe - Steam Flow 1.25 - 1.31 lb/sec - Internal Fluid Temperature

(a,b)

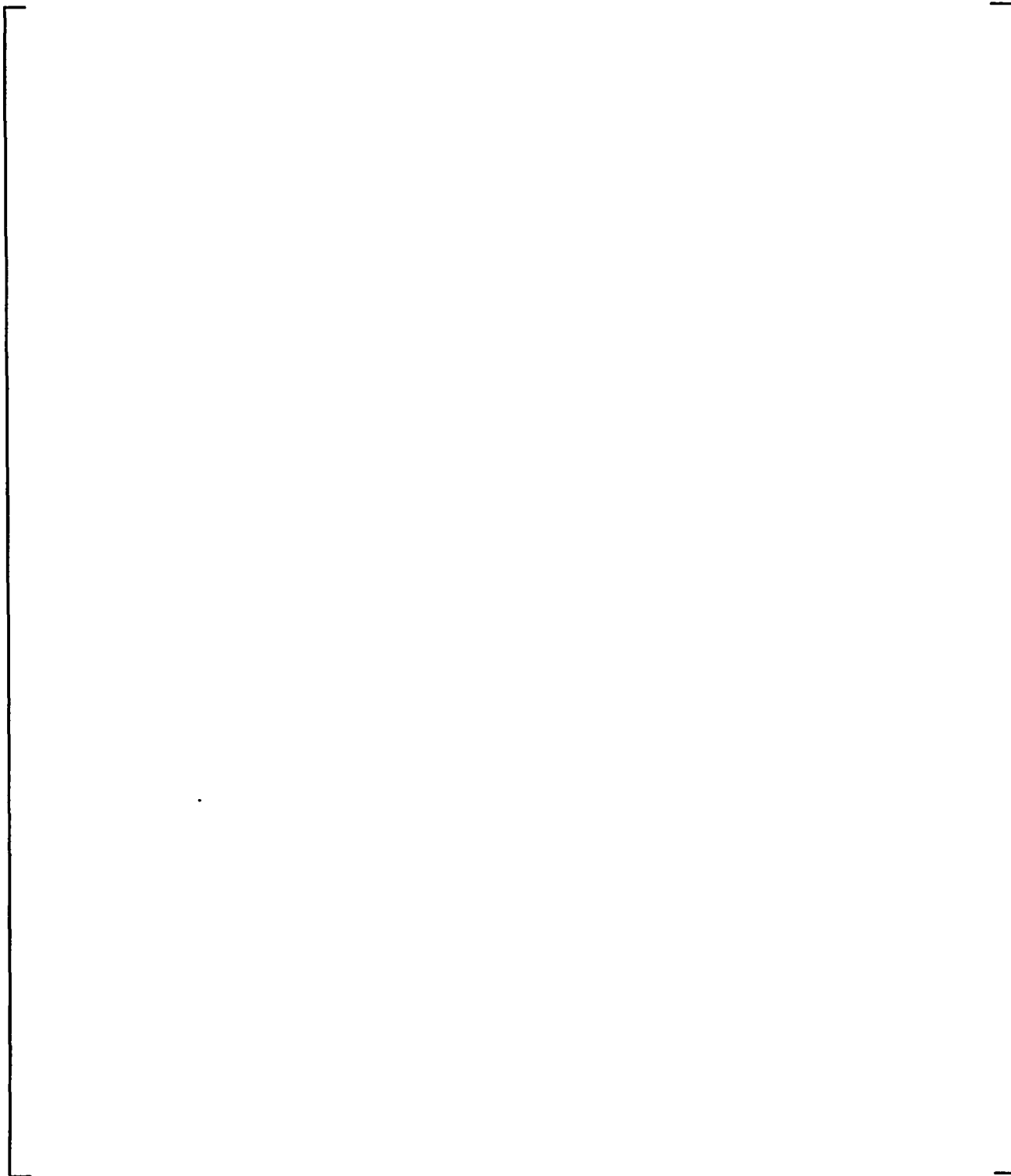


Figure 9-33 LST with Steam Injection: 3 Inch Pipe - Steam Flow 1.25 - 1.31 lb/sec - Saturation Temperature

(a,b)

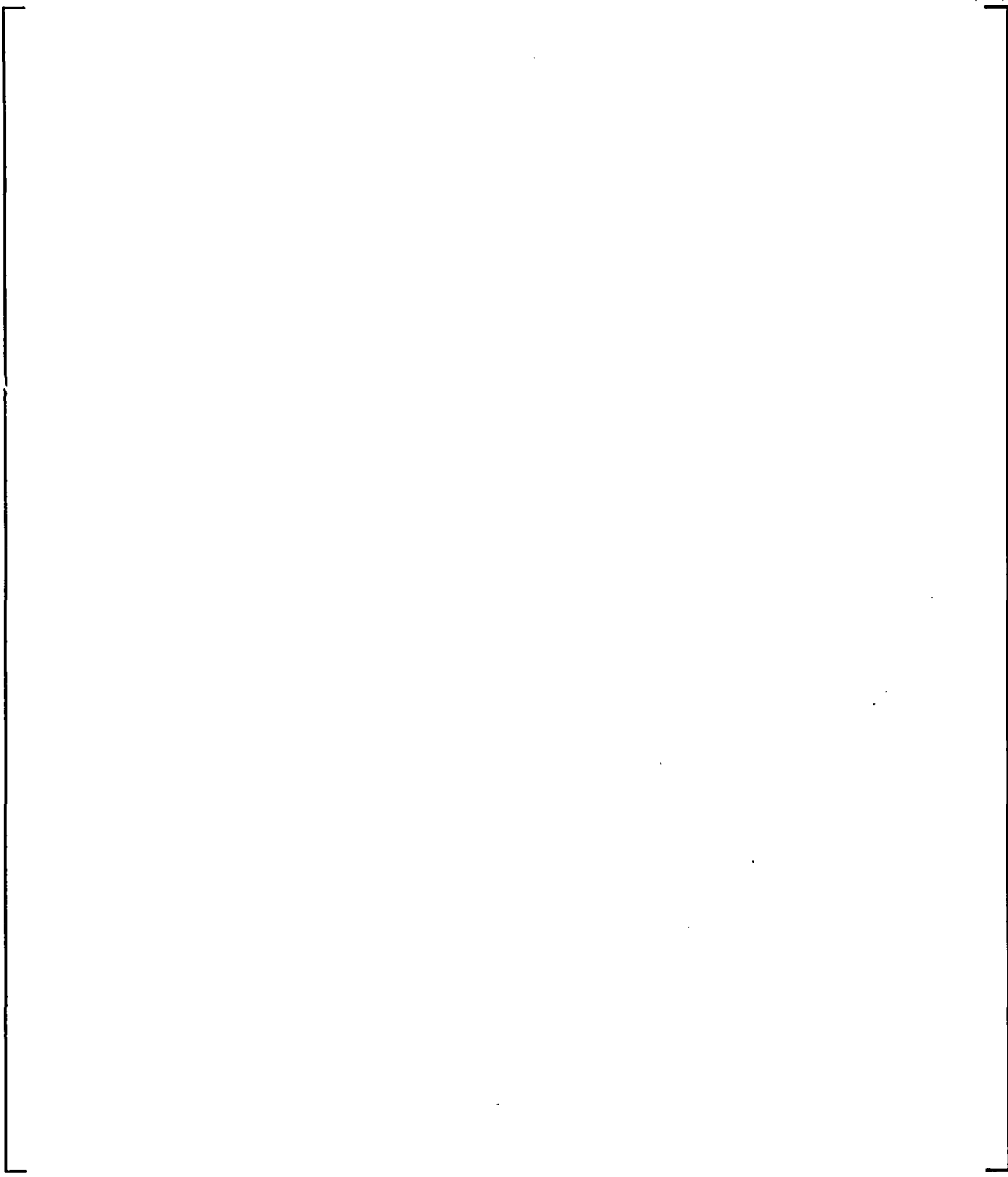


Figure 9-34 LST with Steam Injection: 3 Inch Pipe - Steam Flow 1.25 - 1.31 lb/sec - Internal Steam Pressure Ratio

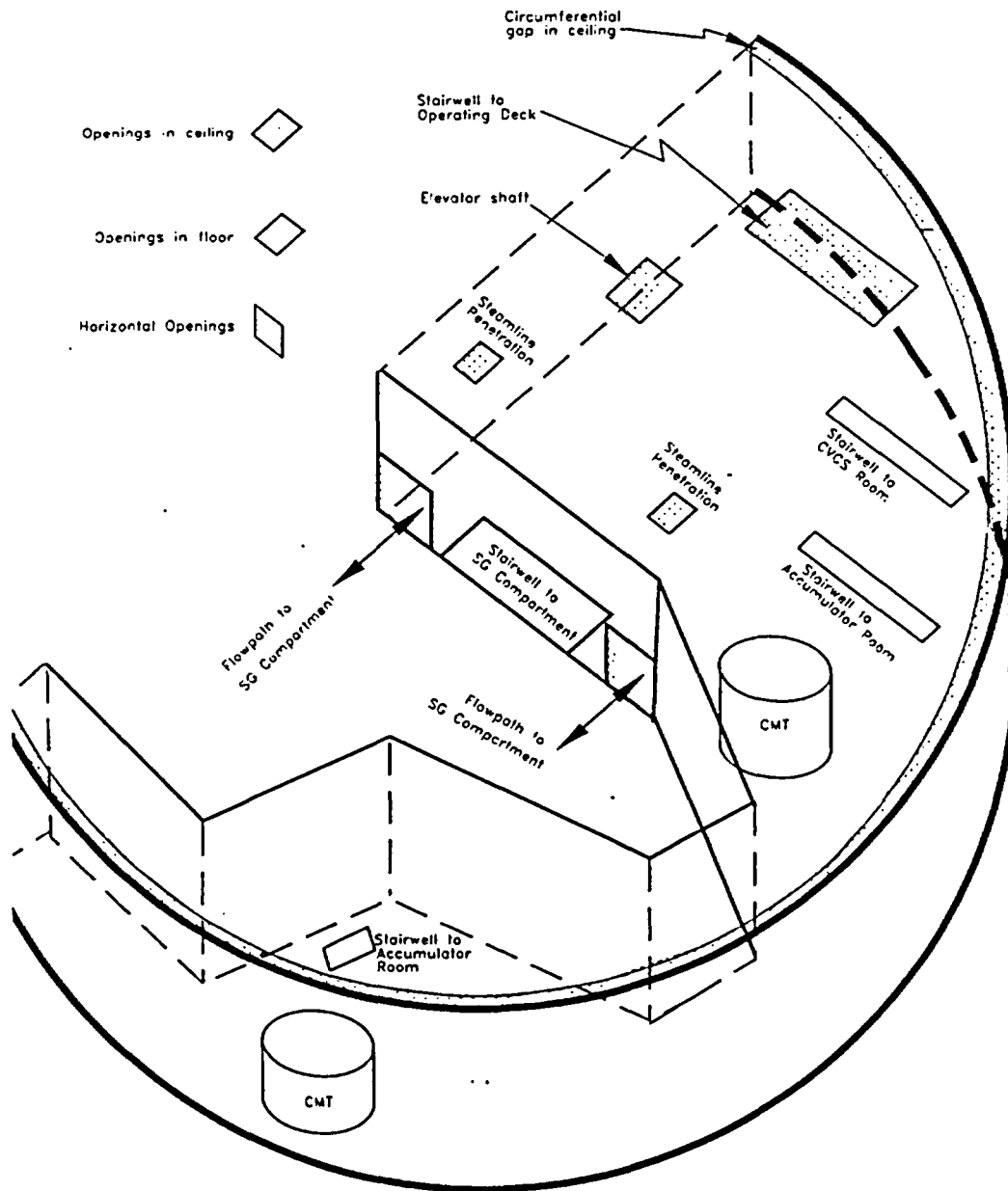


Figure 9-35 CMT Compartment Layout

(a,c)

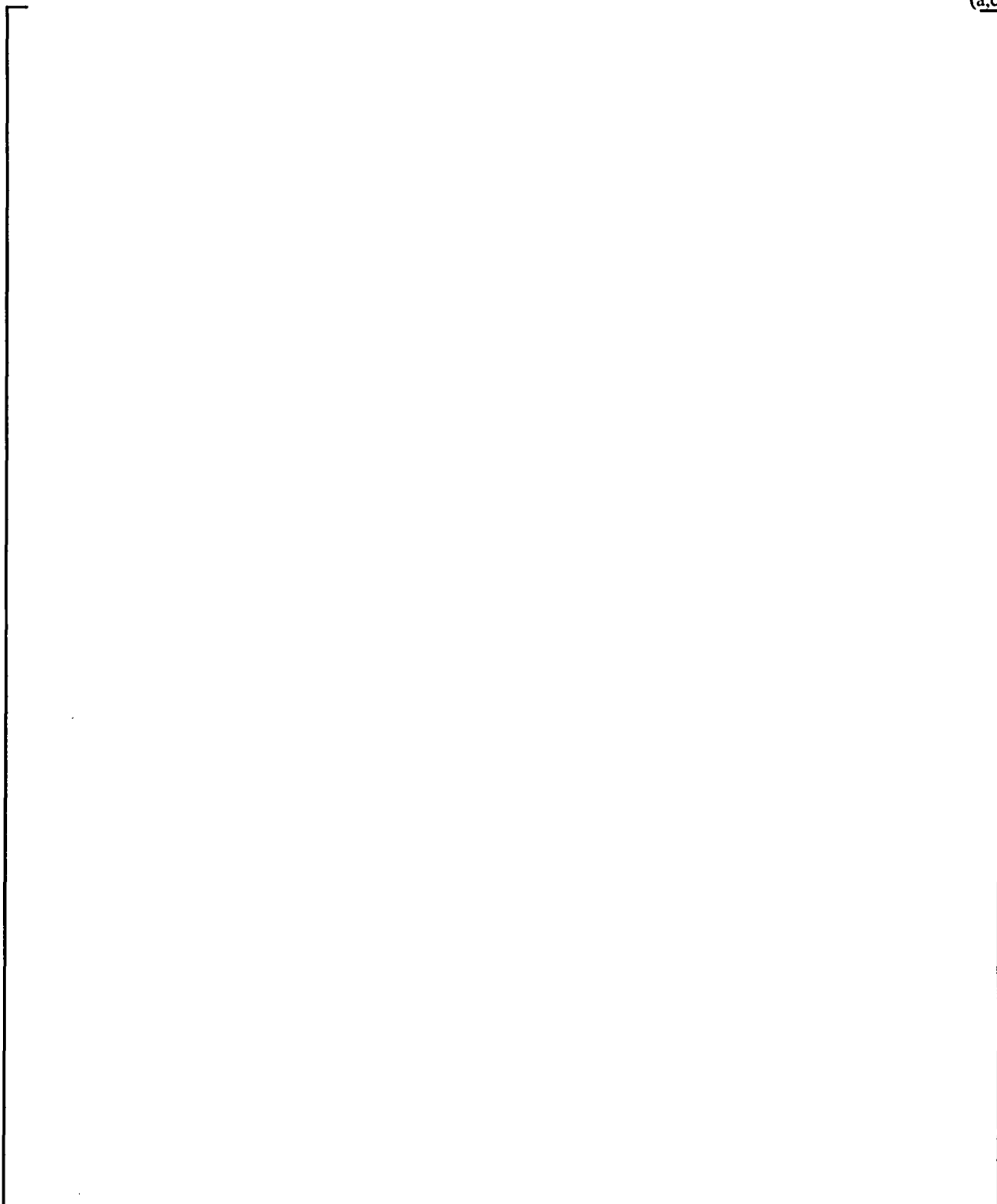


Figure 9-36 **Simplified AP600 Containment Diagram**

(a,c)

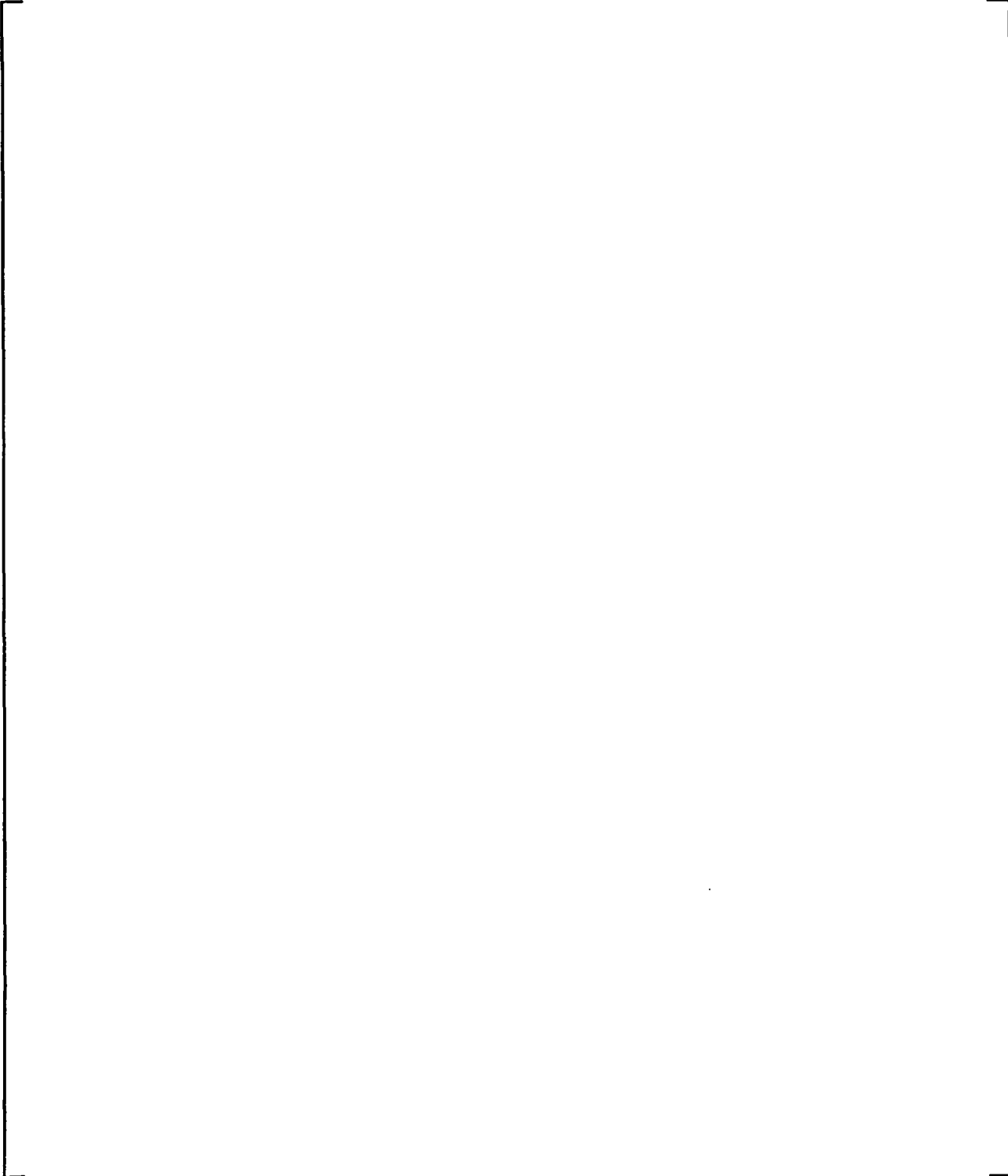


Figure 9-37 WGOTHIC Calculated LOCA Blowdown Steam Pressure Ratio for Jet Momentum Dissipated in SG East Compartment

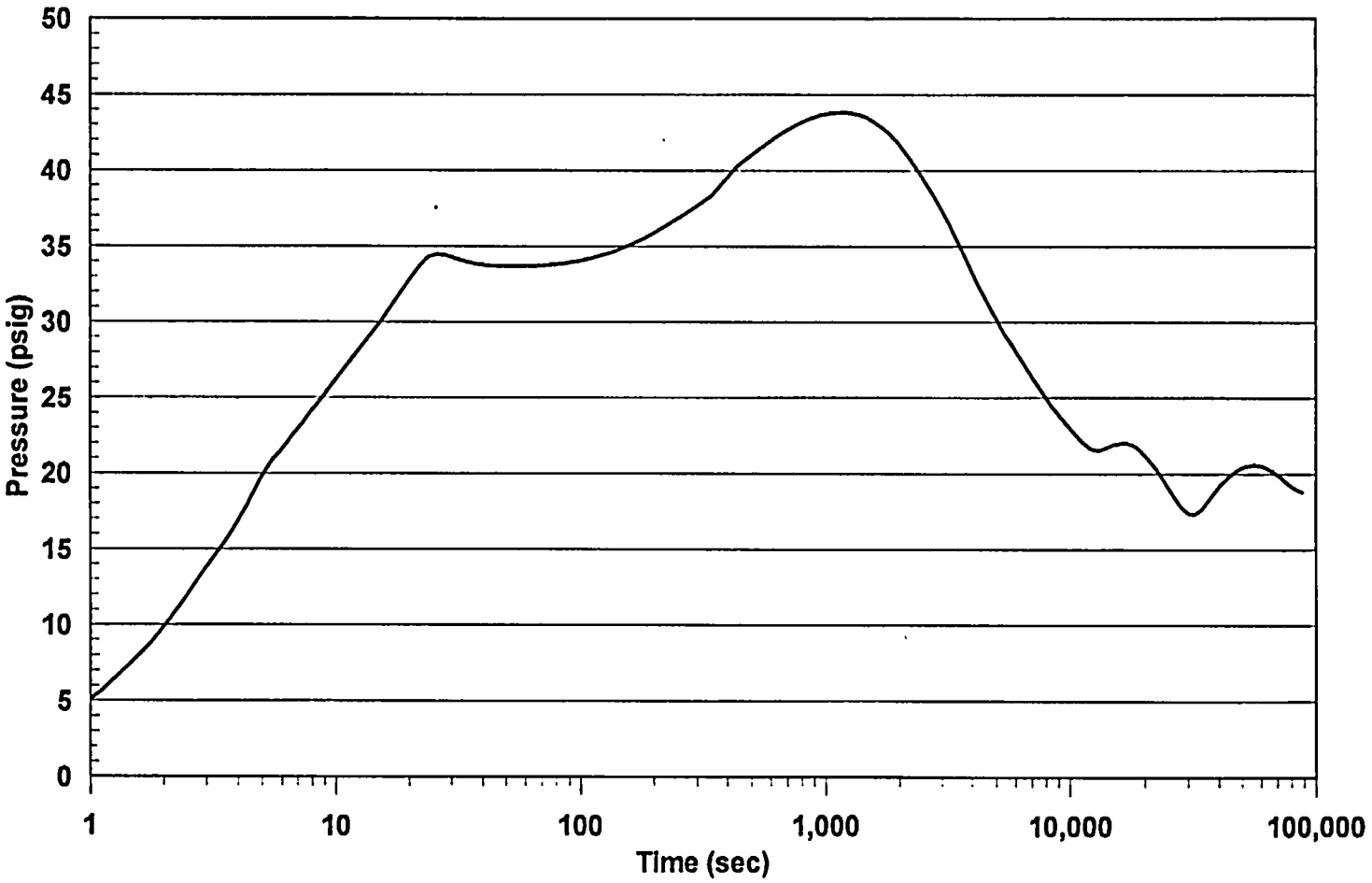


Figure 9-38 WGOIHIC Calculated AP600 Containment Pressure - Sensitivity to Loss Coefficients for LOCA Jet Momentum Dissipated in SG East Compartment

(a,c)



Figure 9-39 WGOTHIC Calculated Flow Pattern - Sensitivity to Loss Coefficients for LOCA
Jet Momentum Dissipated in SG East Compartment at 20 Seconds

(a,c)

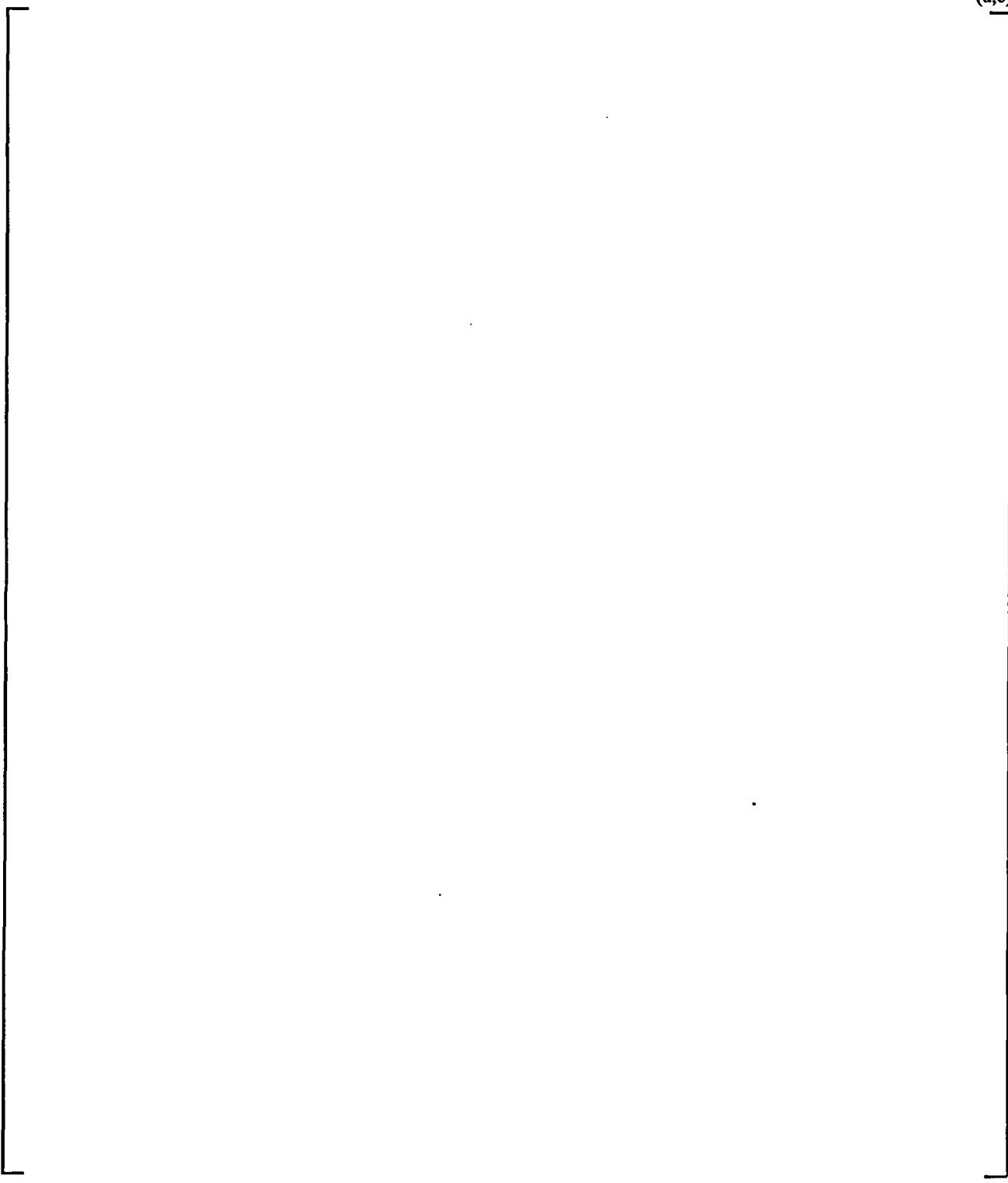


Figure 9-40 WGOTHIC Calculated Flow Pattern - Sensitivity to Loss Coefficients for LOCA
Jet Momentum Dissipated in SG East Comp. at 1000 Seconds

(a,c)

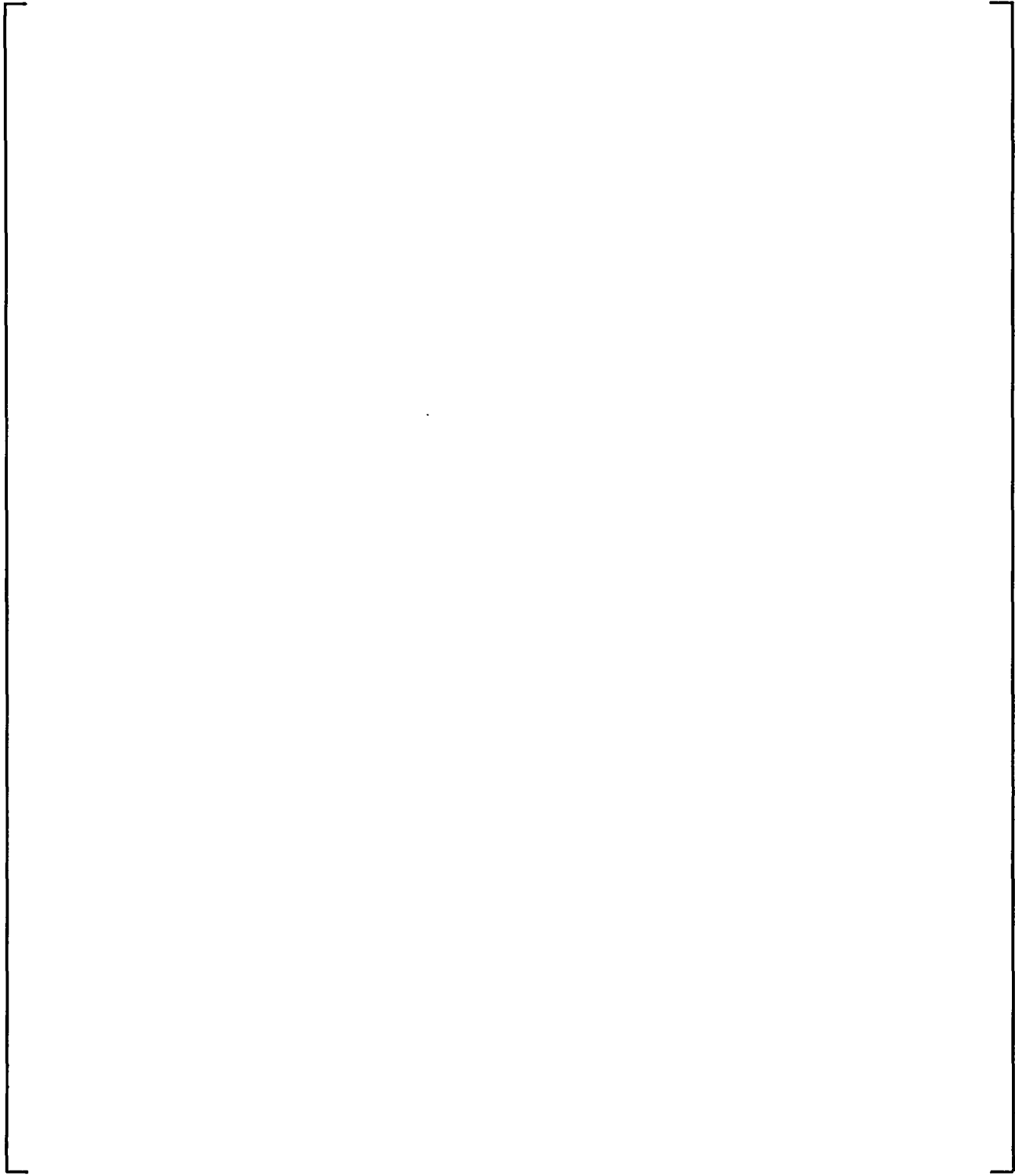


Figure 9-41 WGOTHIC Calculated Flow Pattern - Sensitivity to Loss Coefficients for LOCA
Jet Momentum Dissipated in SG East Comp. at 1550 Seconds

(a,c)

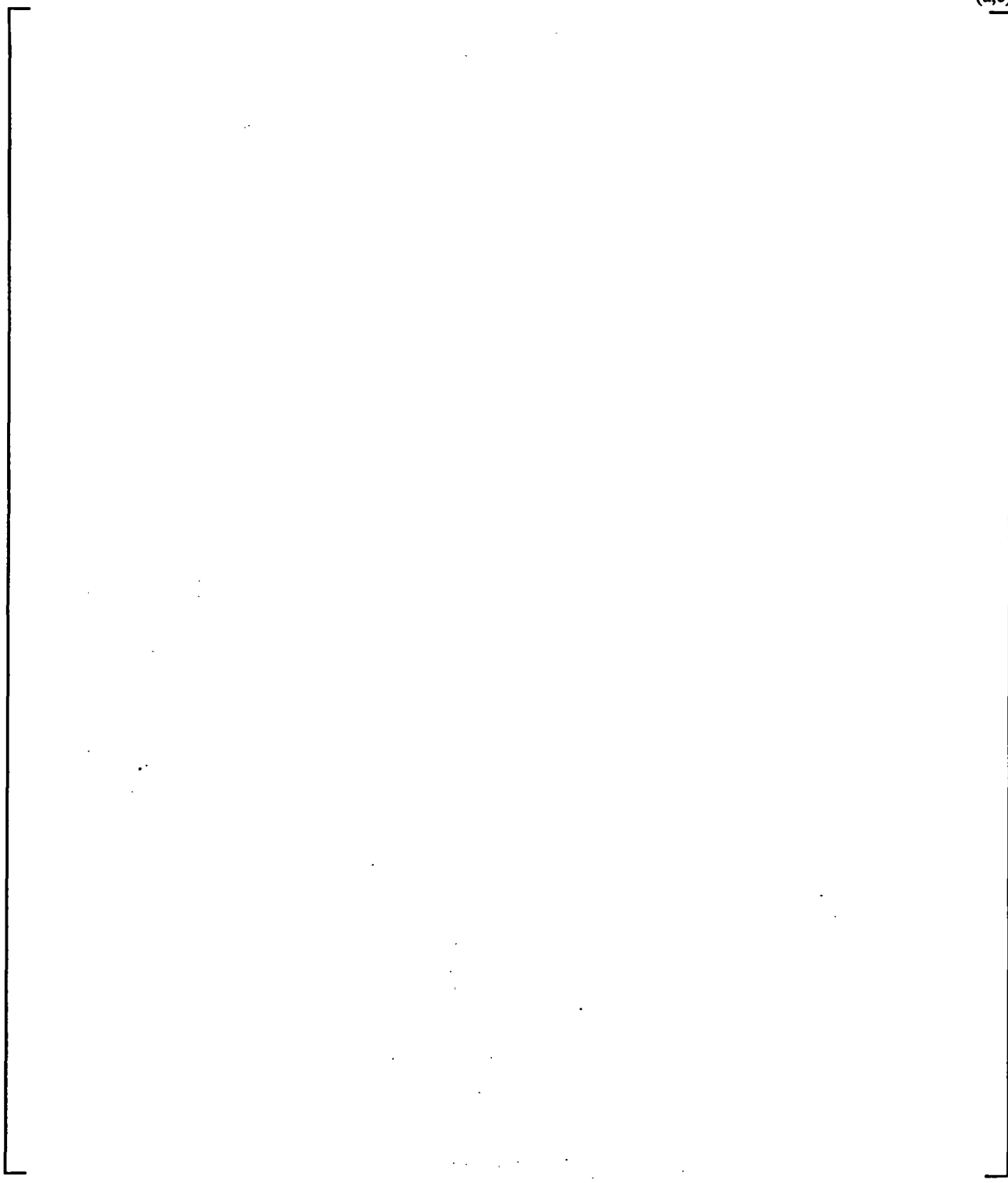


Figure 9-42 WGOTHIC Calculated Flow Pattern - Sensitivity to Loss Coefficients for LOCA
Jet Momentum Dissipated in SG East Comp. at 80050 Seconds

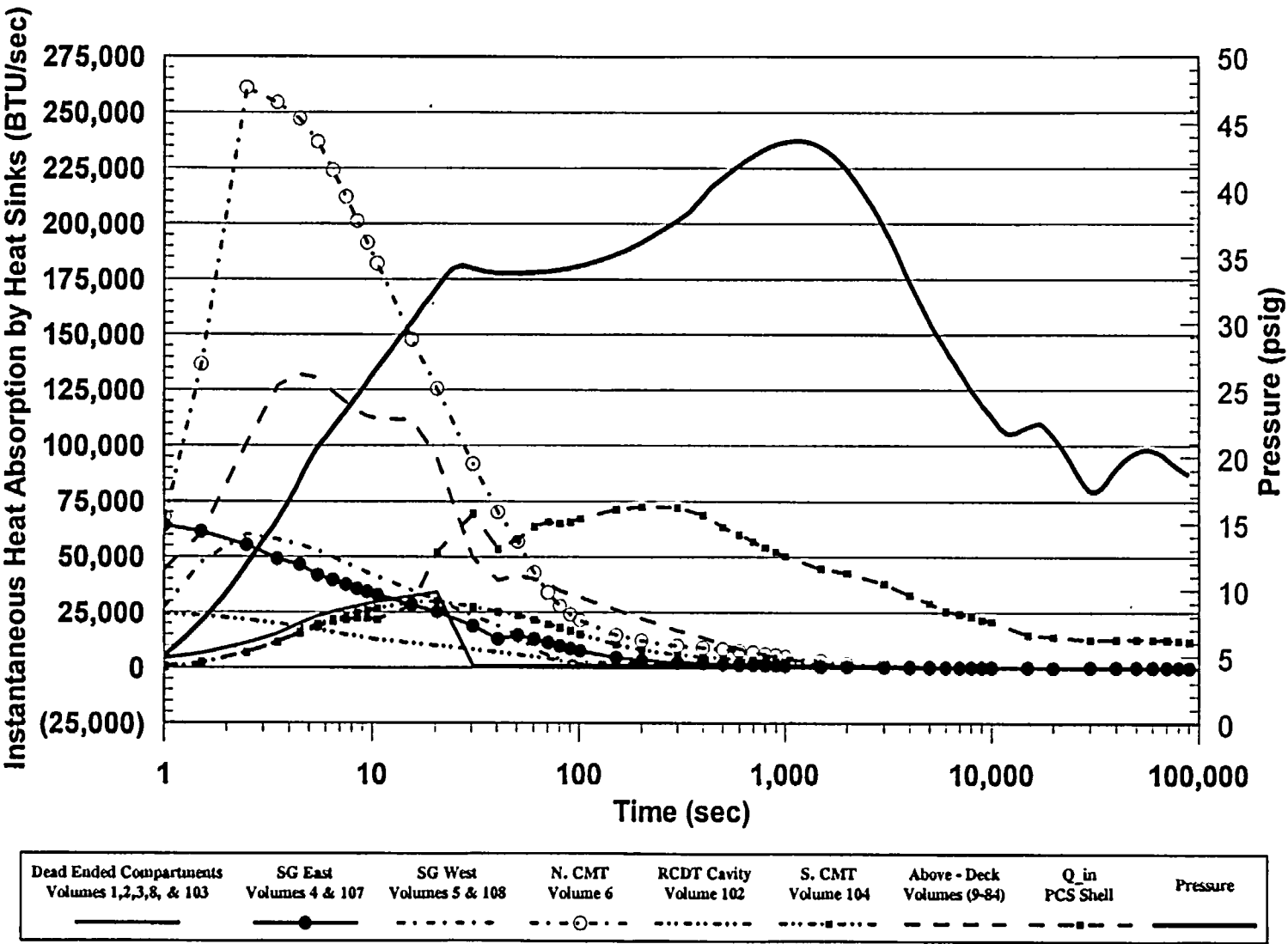


Figure 9-43 WGTIHC Calculated AP600 Containment Heat Removal Rates - LOCA Jet Momentum Dissipated in SG East Compartment

(a,c)

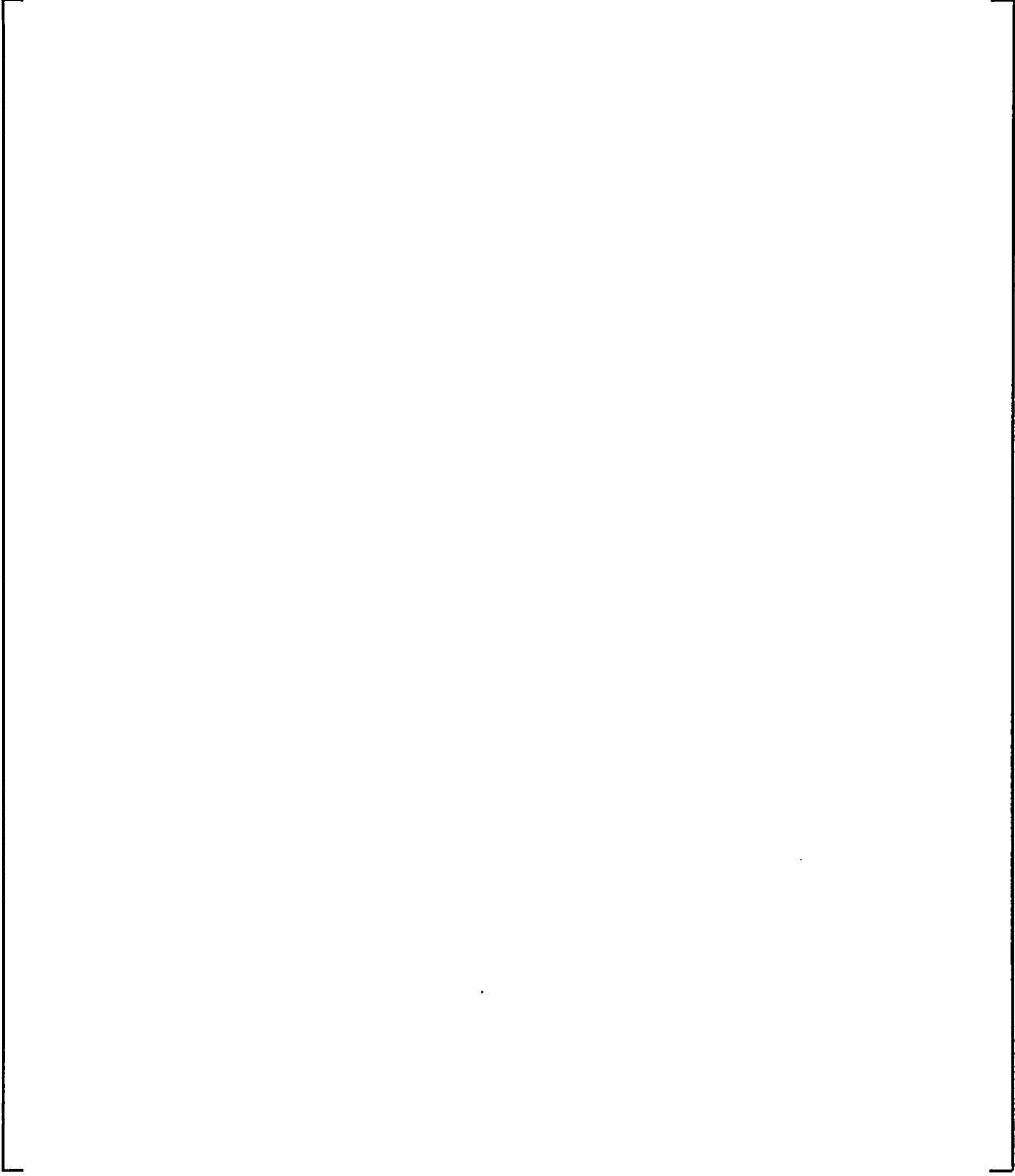


Figure 9-44 WGOTHIC Calculated AP600 Containment Steam Pressure Ratio for LOCA Jet Momentum Dissipated in SG East Compartment

(a,c)

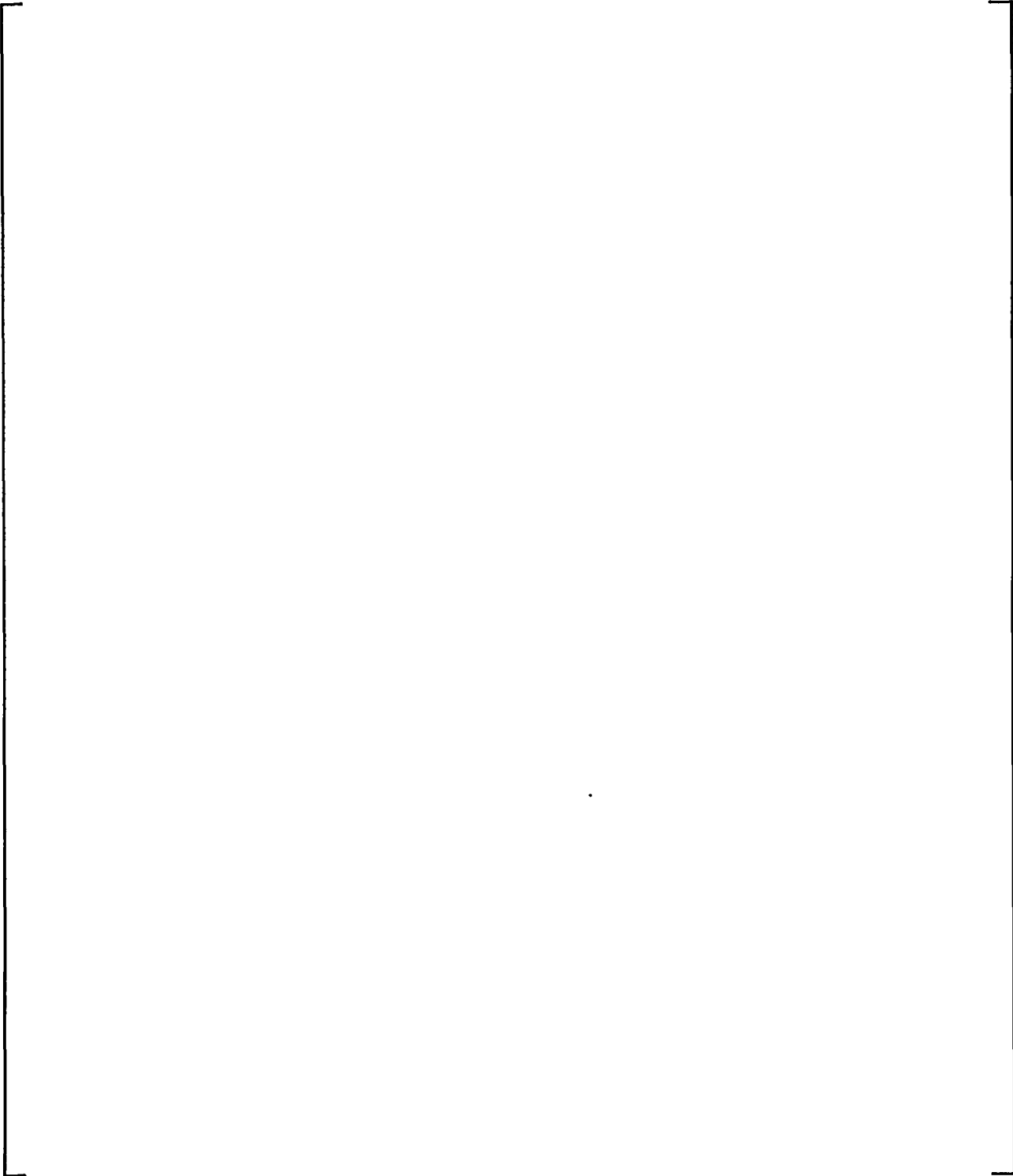


Figure 9-45 WGOTHIC Calculated AP600 Cont. Pressure - Sensitivity to Heat Transfer Coefficient for Study of Undissipated Jet Effects During a LOCA

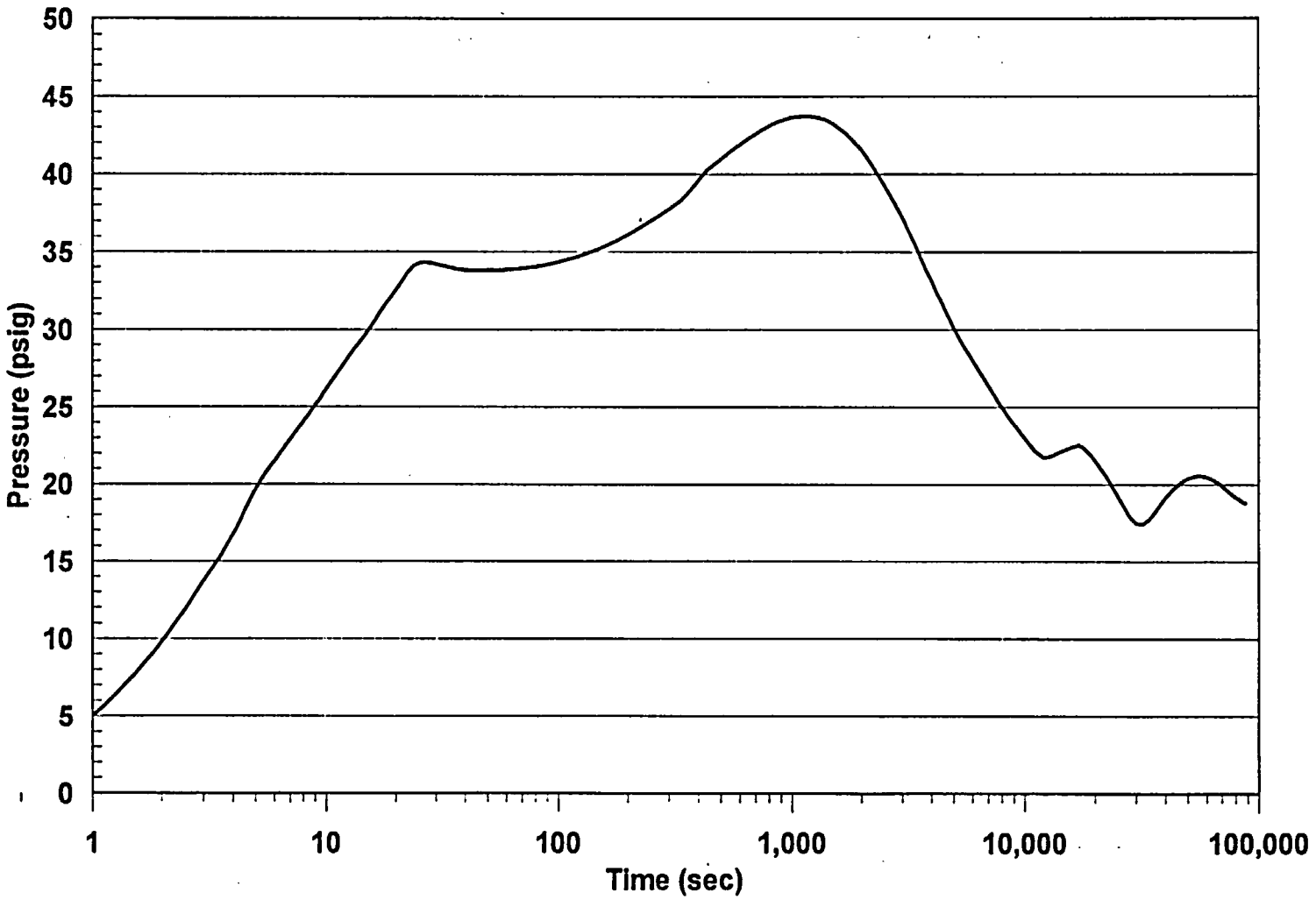
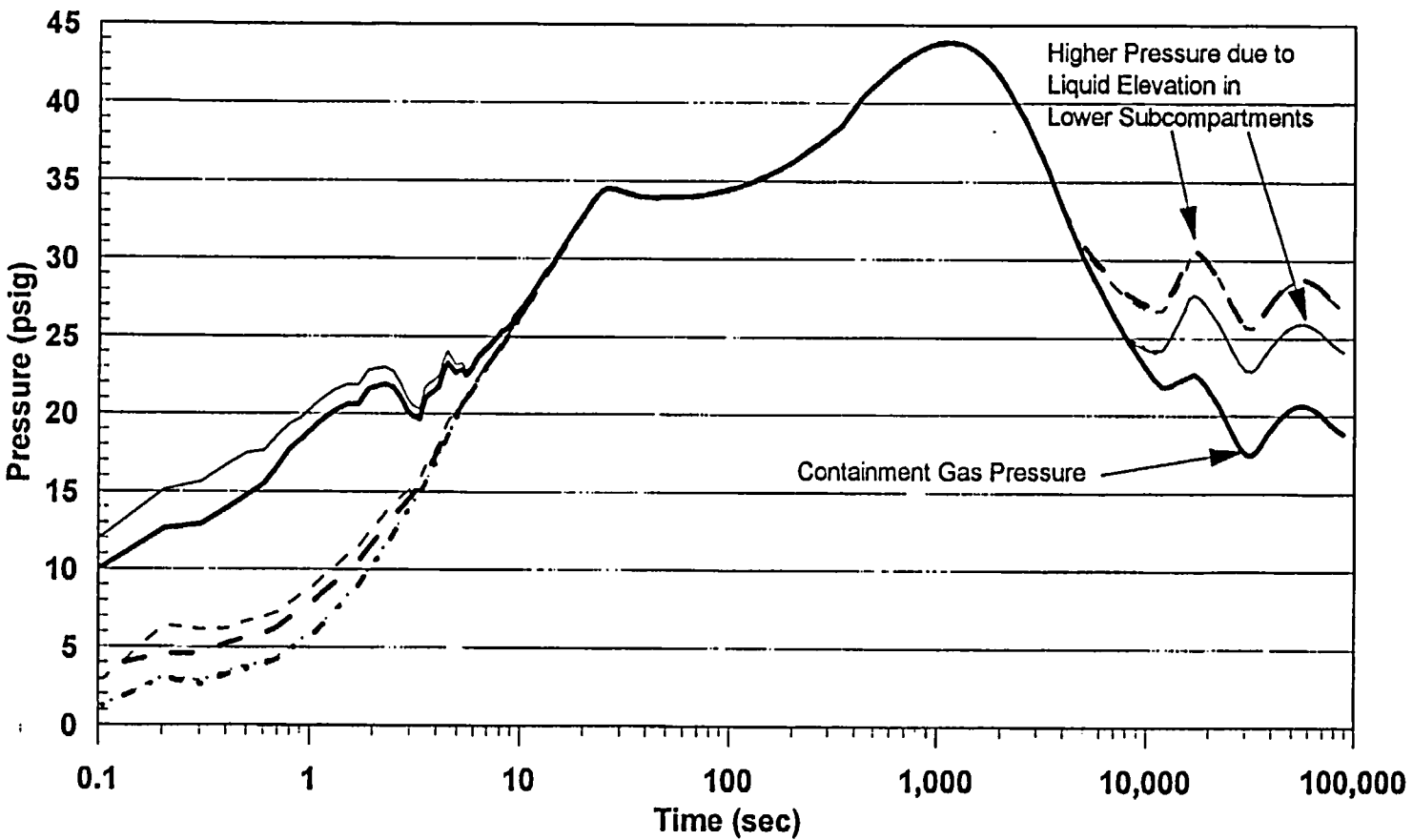


Figure 9-46 WGO THIC Calculated AP600 Containment Pressure-LOCA Jet Momentum
Dissipated in SG East Compartment



SG East Lower Volume 107	SG East Upper Volume 4	SG West Lower Volume 108	SG West Upper Volume 5	Reactor Cavity Volume 1	RCDT Cavity Volume 102
—————	—————	- - - - -	—————	—————

Figure 9-16A WCAP Calculated AP600 Containment Below-Deck Compartment Pressure for LOCA Jet Momentum Dissipated in SG East Compartment

(a,c)

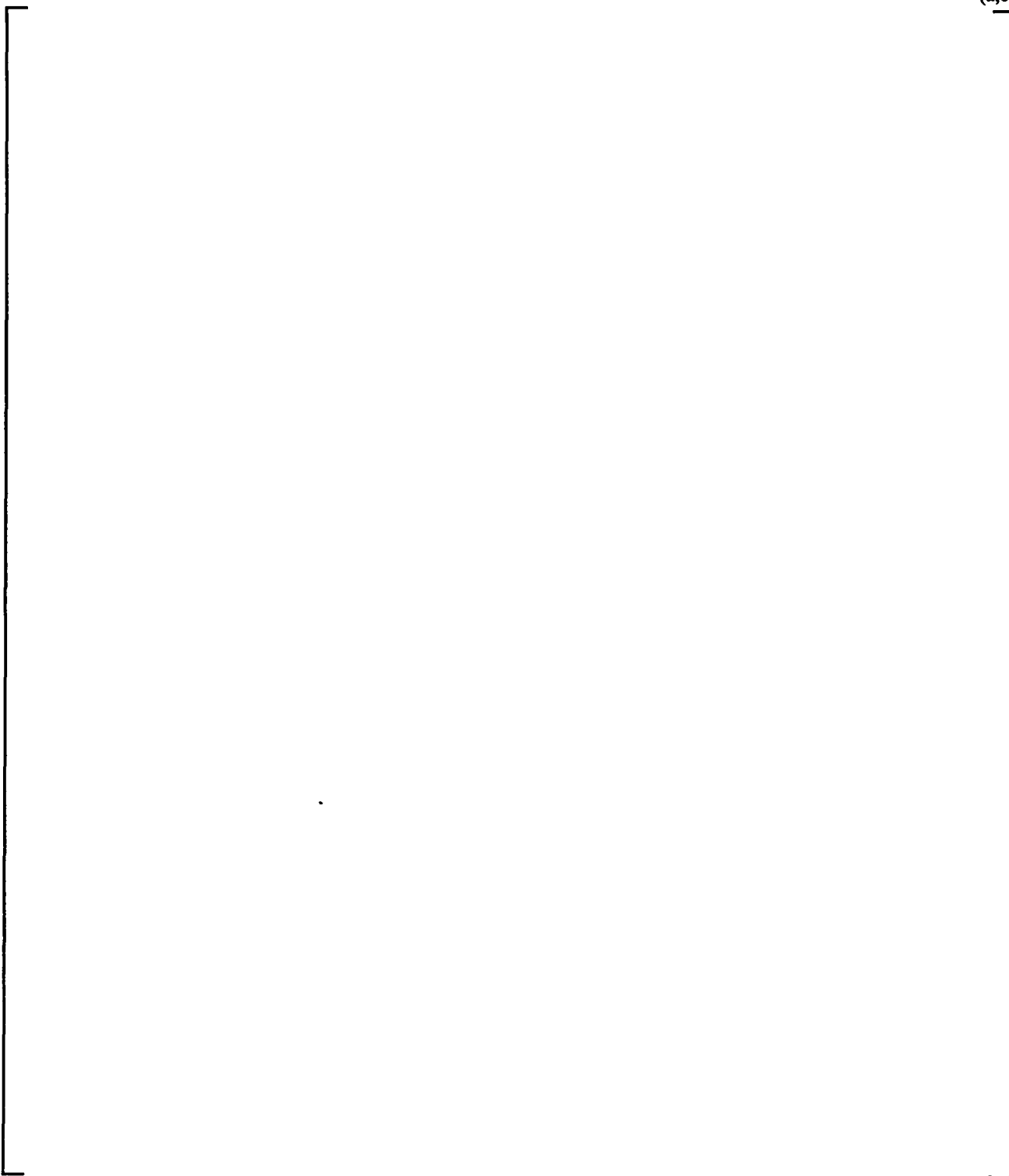


Figure 9-47 WGOTHIC Calculated Flow Pattern - LOCA Jet Momentum Dissipated in SG East Compartment at 20 Seconds

(a,c)

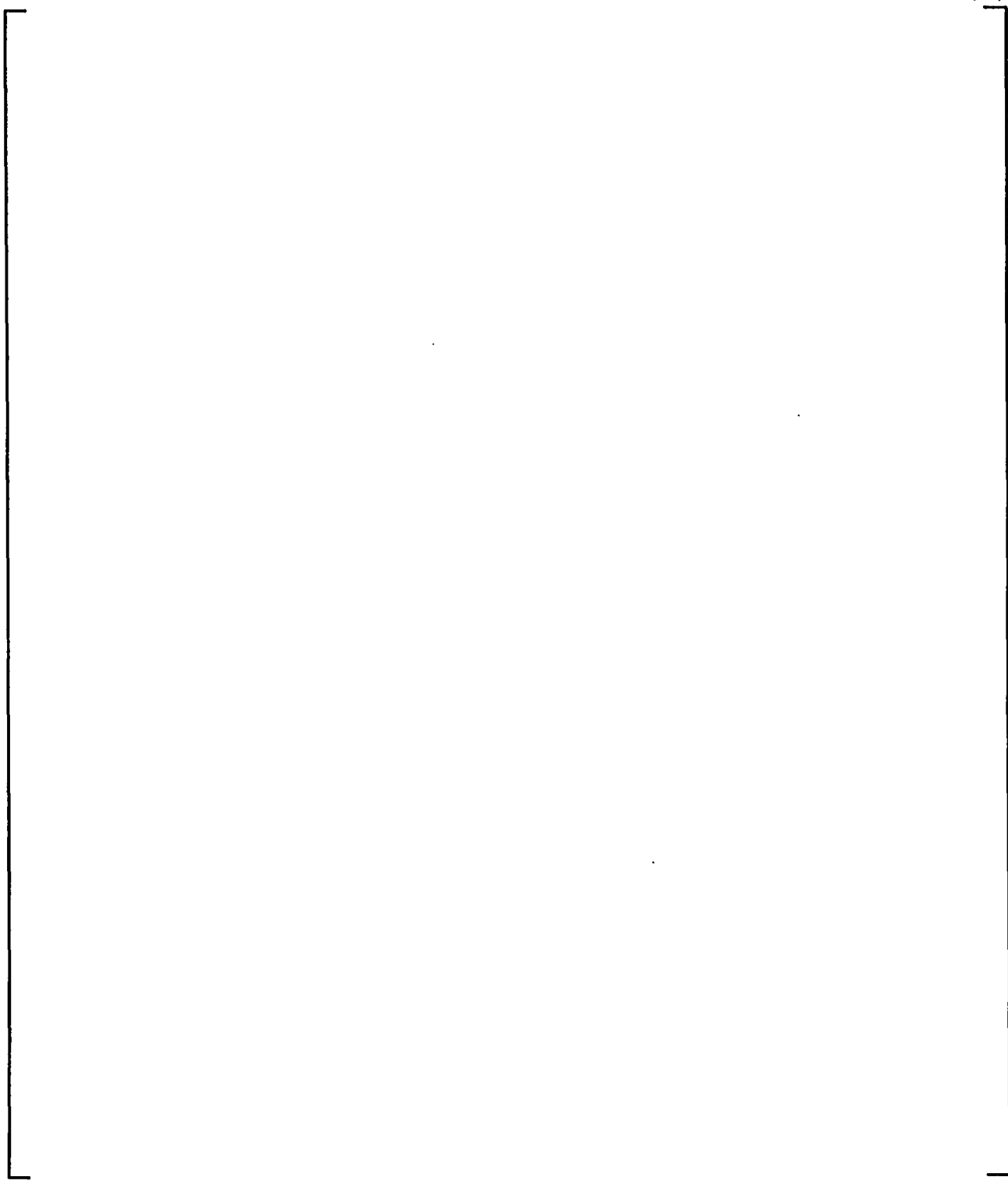


Figure 9-48 WGOTHIC Calculated Flow Pattern - LOCA Jet Momentum Dissipated in SG
East Compartment at 1000 Seconds

(a,c)

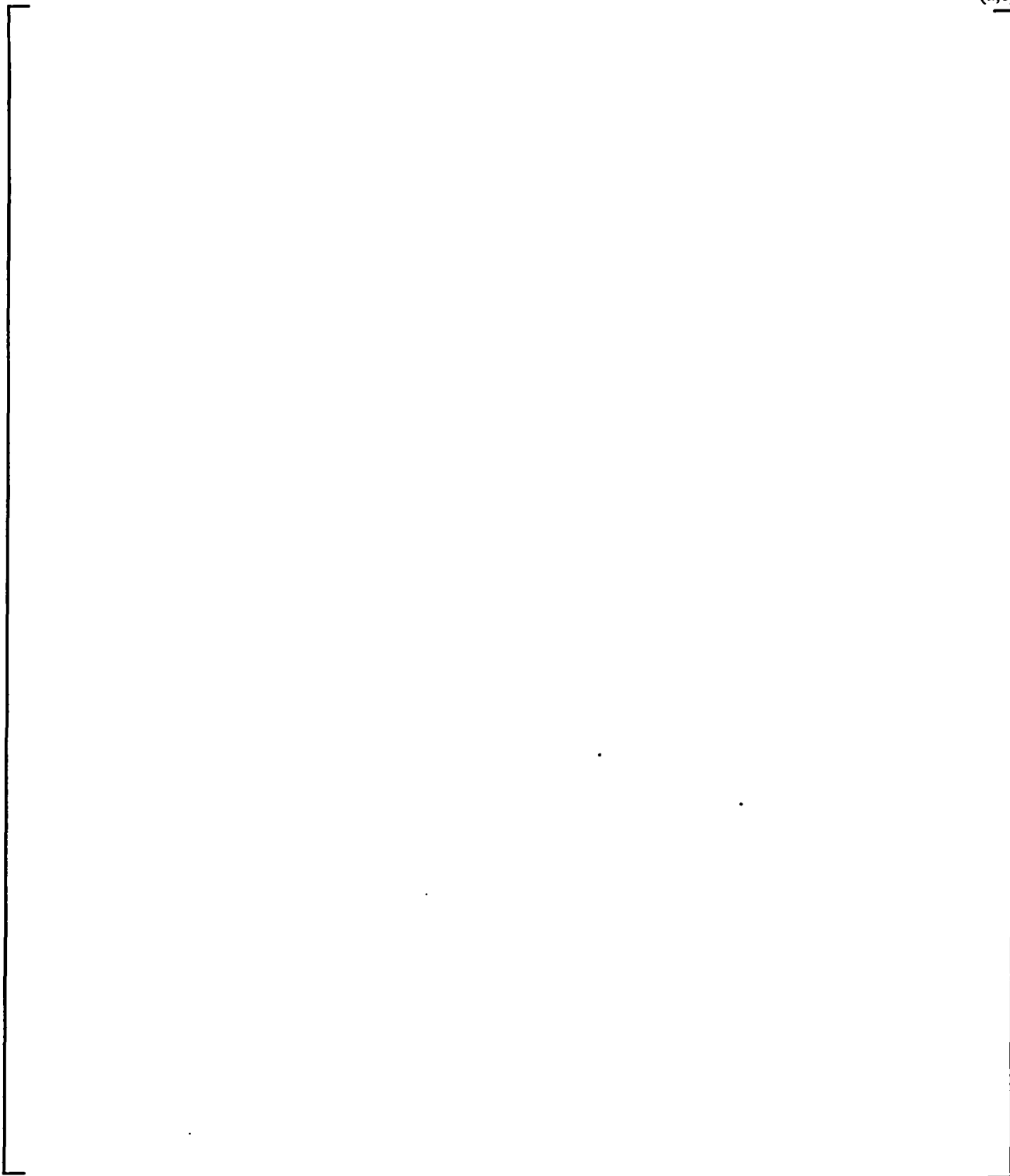


Figure 9-49 WGOTHIC Calculated Flow Pattern - LOCA Jet Momentum Dissipated in SG East Compartment at 1500 Seconds

(a,c)

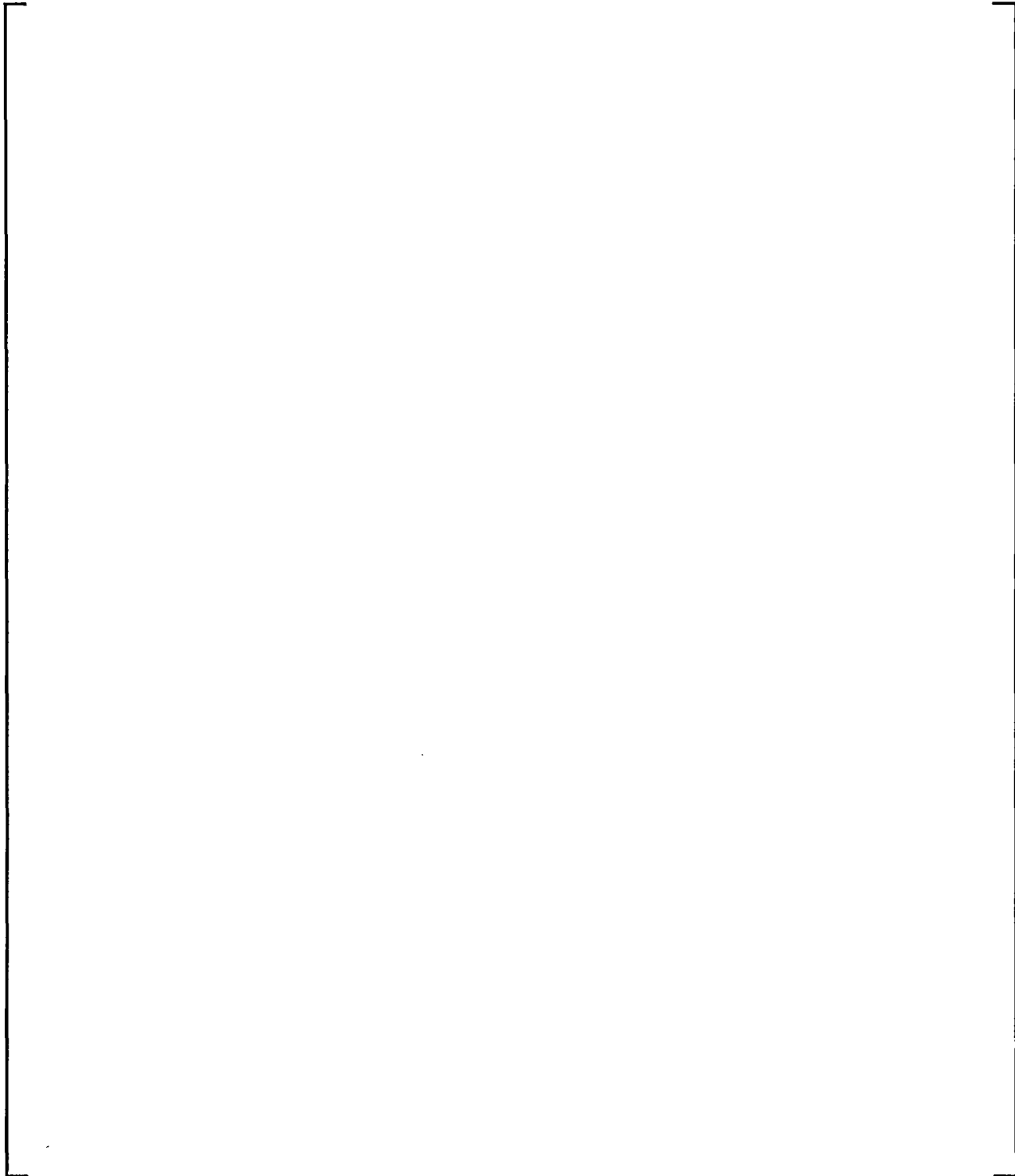


Figure 9-50 **W**GOTHIC Calculated Flow Pattern - LOCA Jet Momentum Dissipated in SG East Compartment at 8000 Seconds

(a,c)

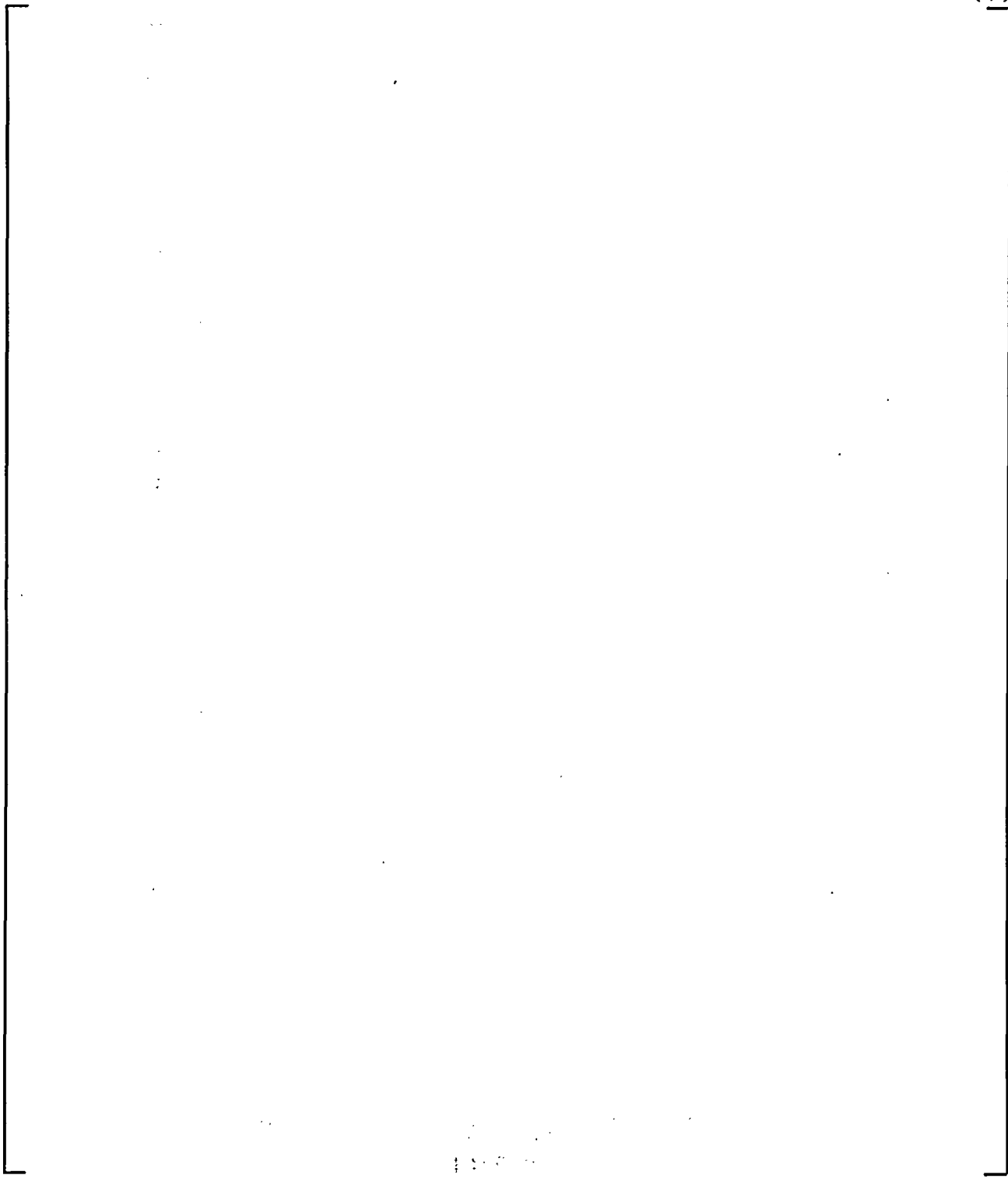


Figure 9-51 Details of WGOTHIC Flow Paths to Above-Deck Region from CMT, Refueling Canal, and IRWST

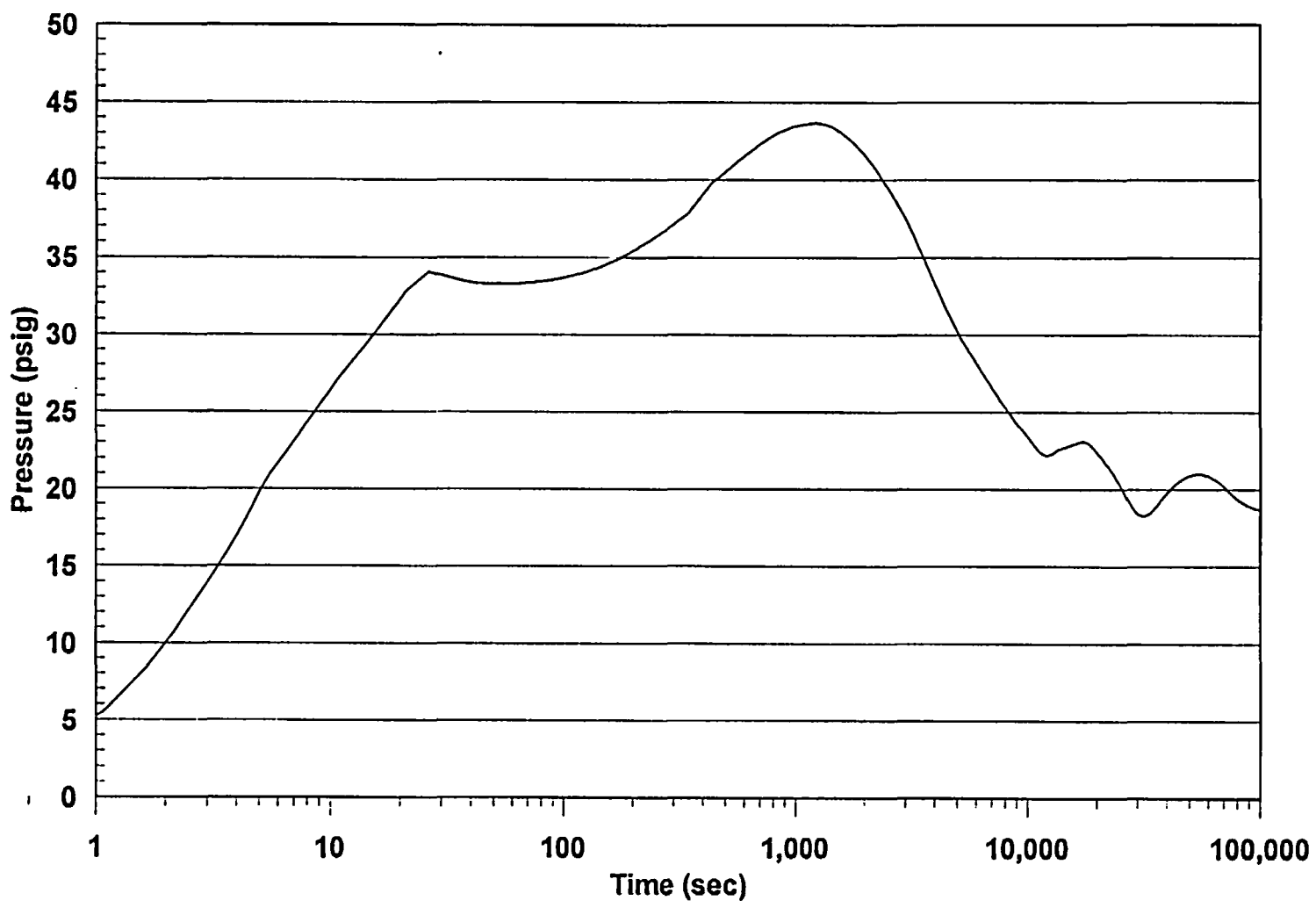


Figure 9-52 WCAP-15862
CMT Room
WCAP-15862 Calculated AP600 Containment Pressure - LOCA Plume Rising into

(a,c)

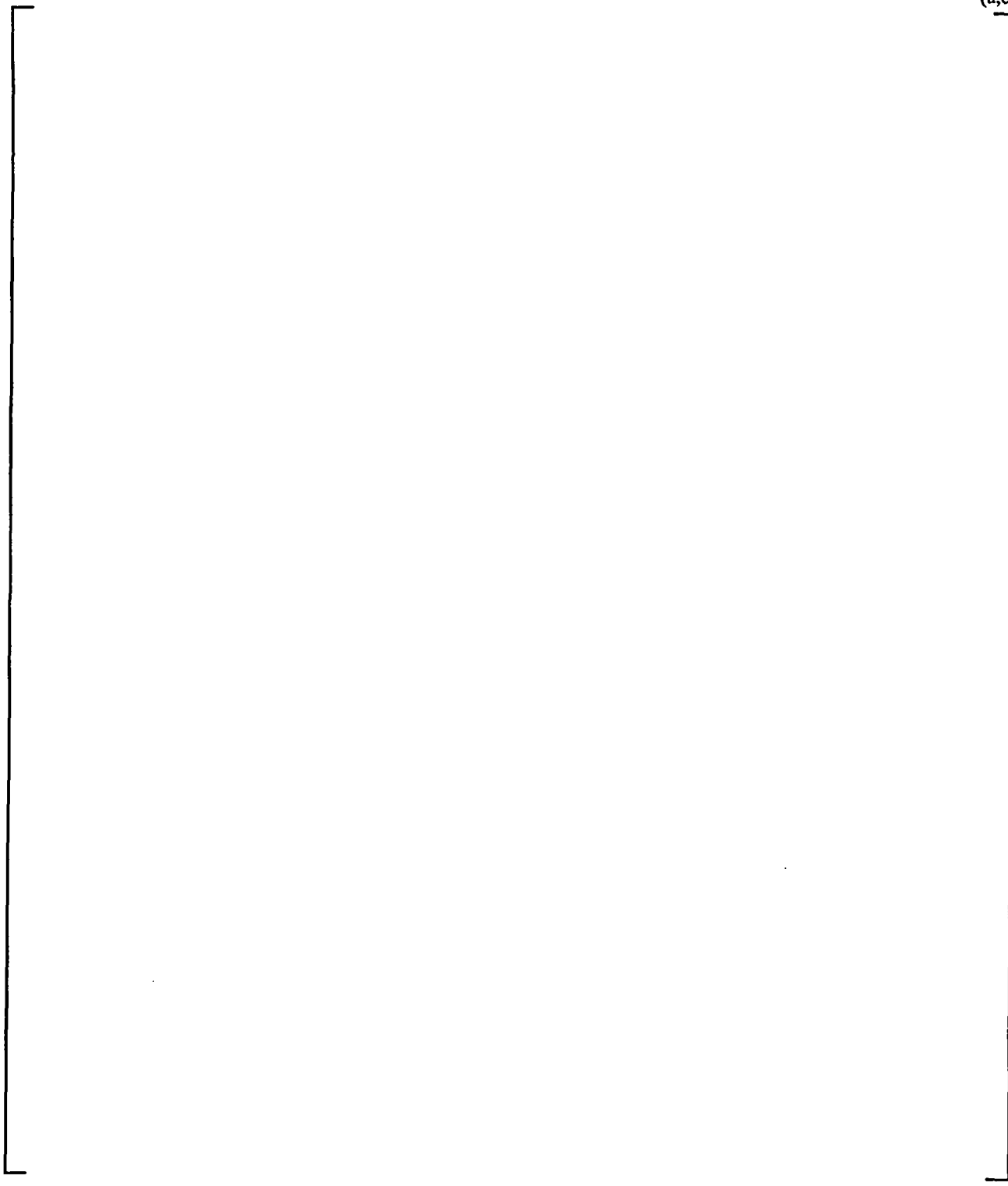


Figure 9-53 WGOTHIC Calculated Flow Pattern - LOCA Plume Rising into CMT Room at 1000 Seconds

(a,c)

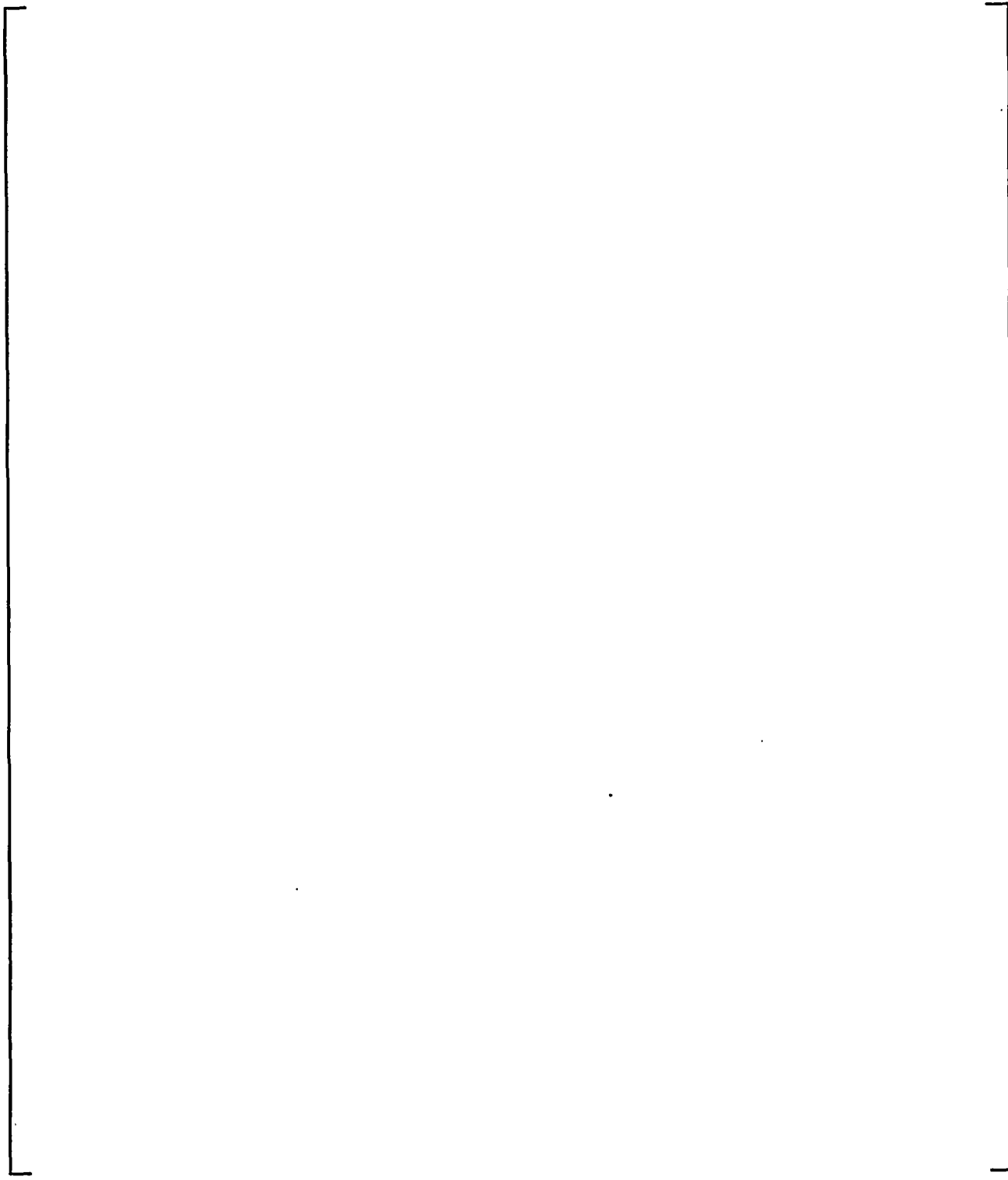


Figure 9-54 WGOTHIC Calculated Flow Pattern - LOCA Plume Rising into CMT Room at 1400 Seconds

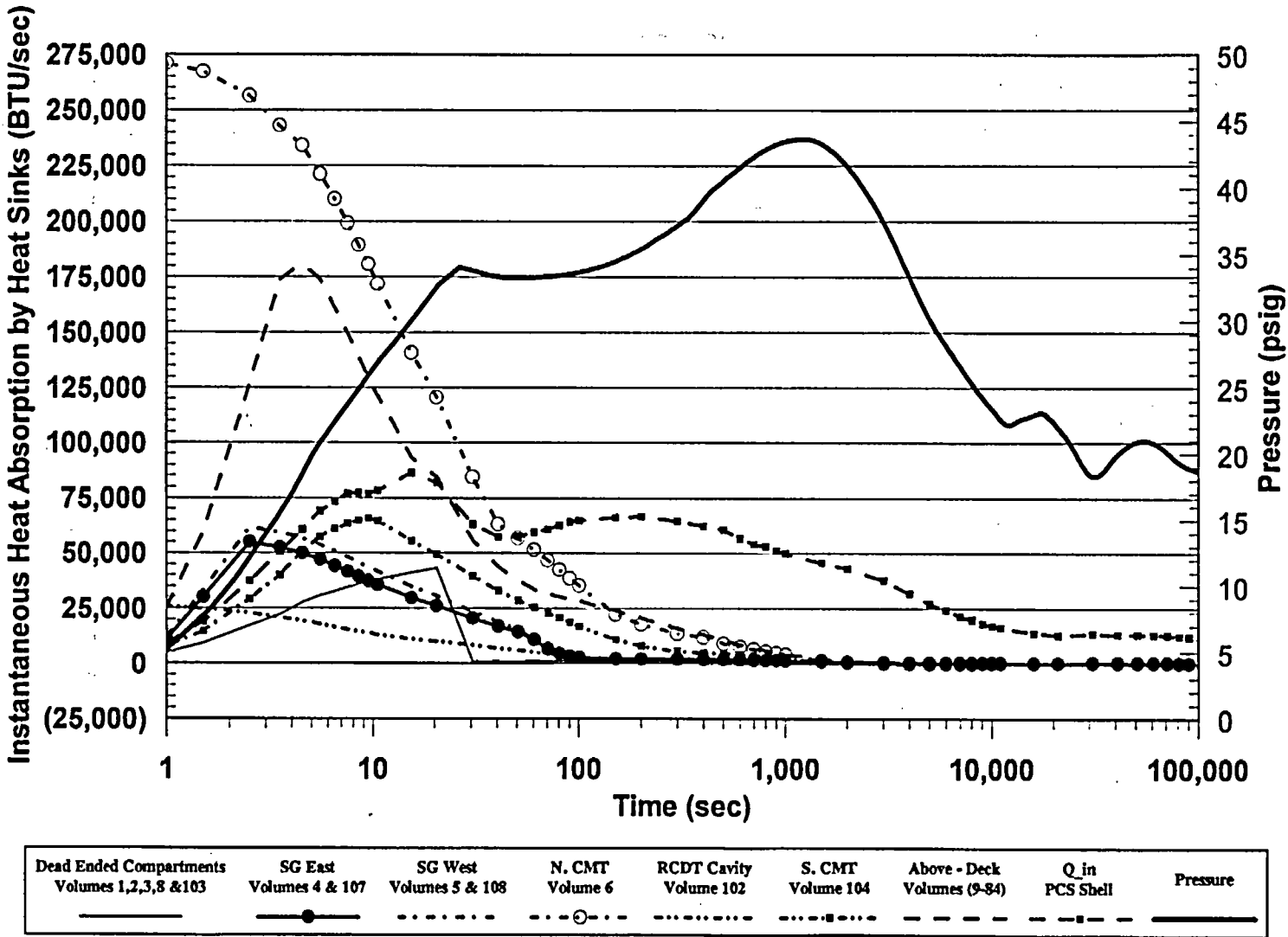


Figure 9-55 WGOTHIC Calculated AP600 Containment Heat Removal Rates - LOCA Plume Rising into CMT Room

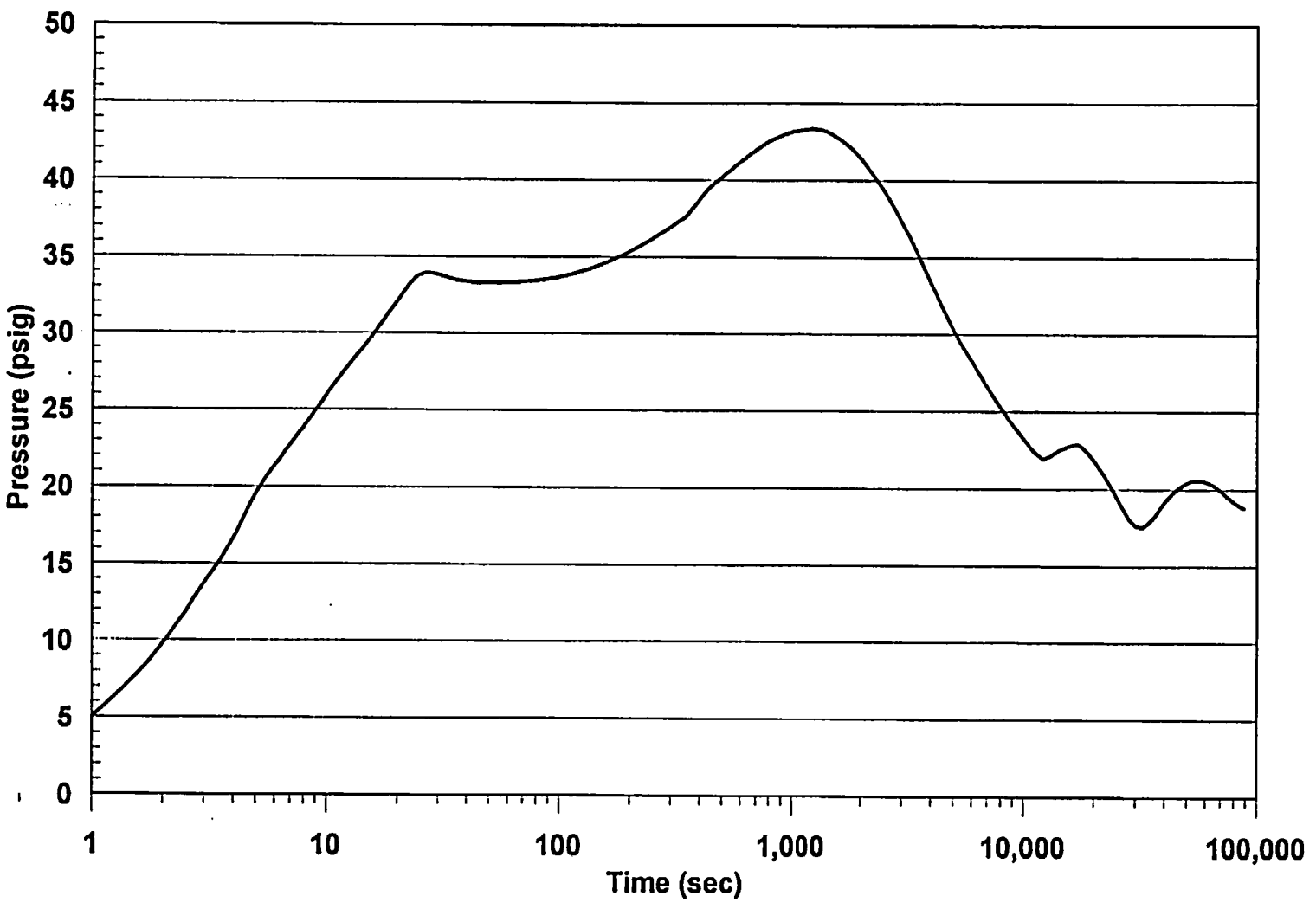


Figure 9-56 WEGOTHIC Calculated AP600 Containment Pressure - LOCA Plume Rising Into CMT Room and SG Compartments

(a,c)

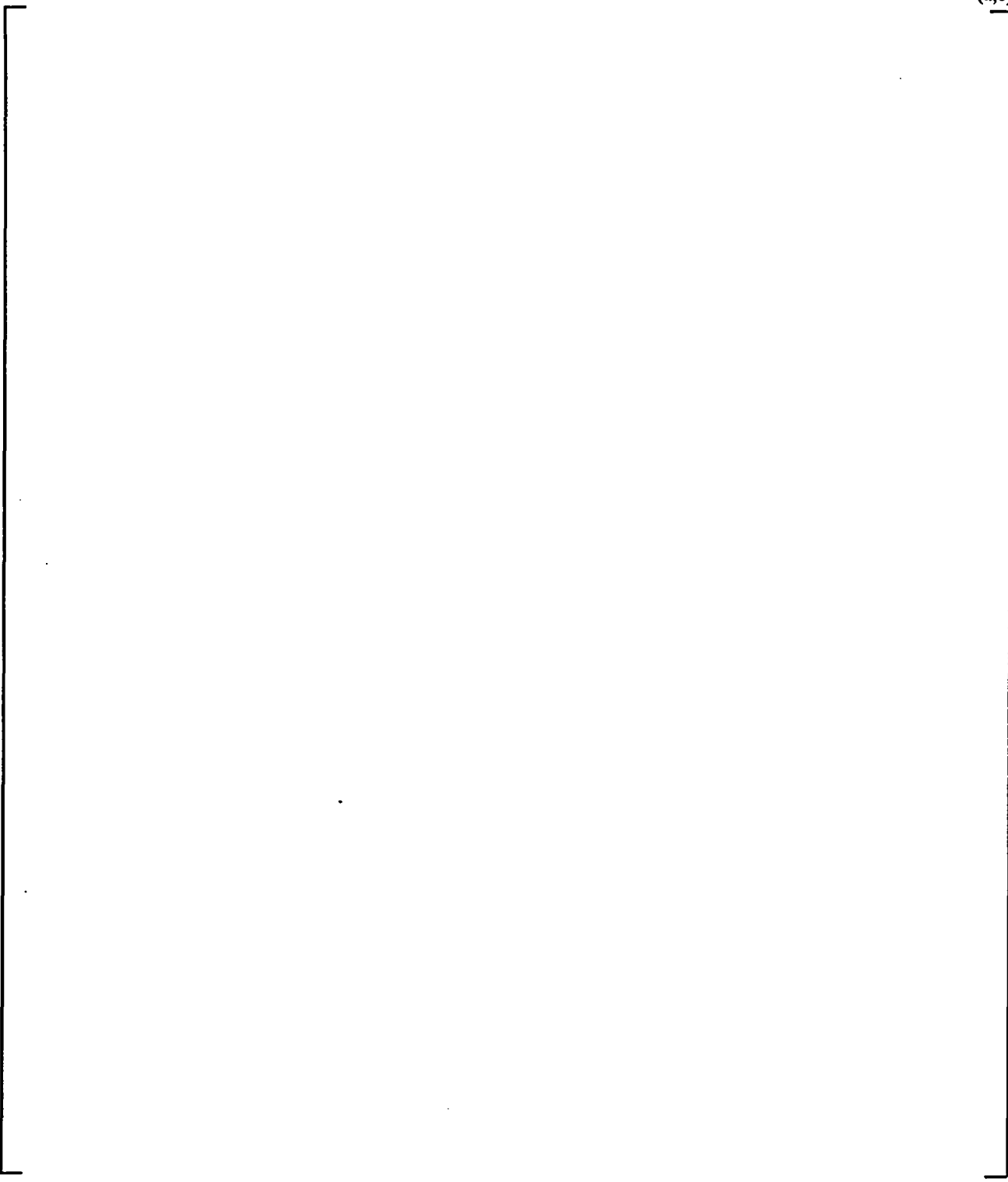


Figure 9-57. WGOTHIC Calculated Flow Pattern - LOCA Plume Rising into CMT Room and SG Compartments at 1000 Seconds

(a,c)

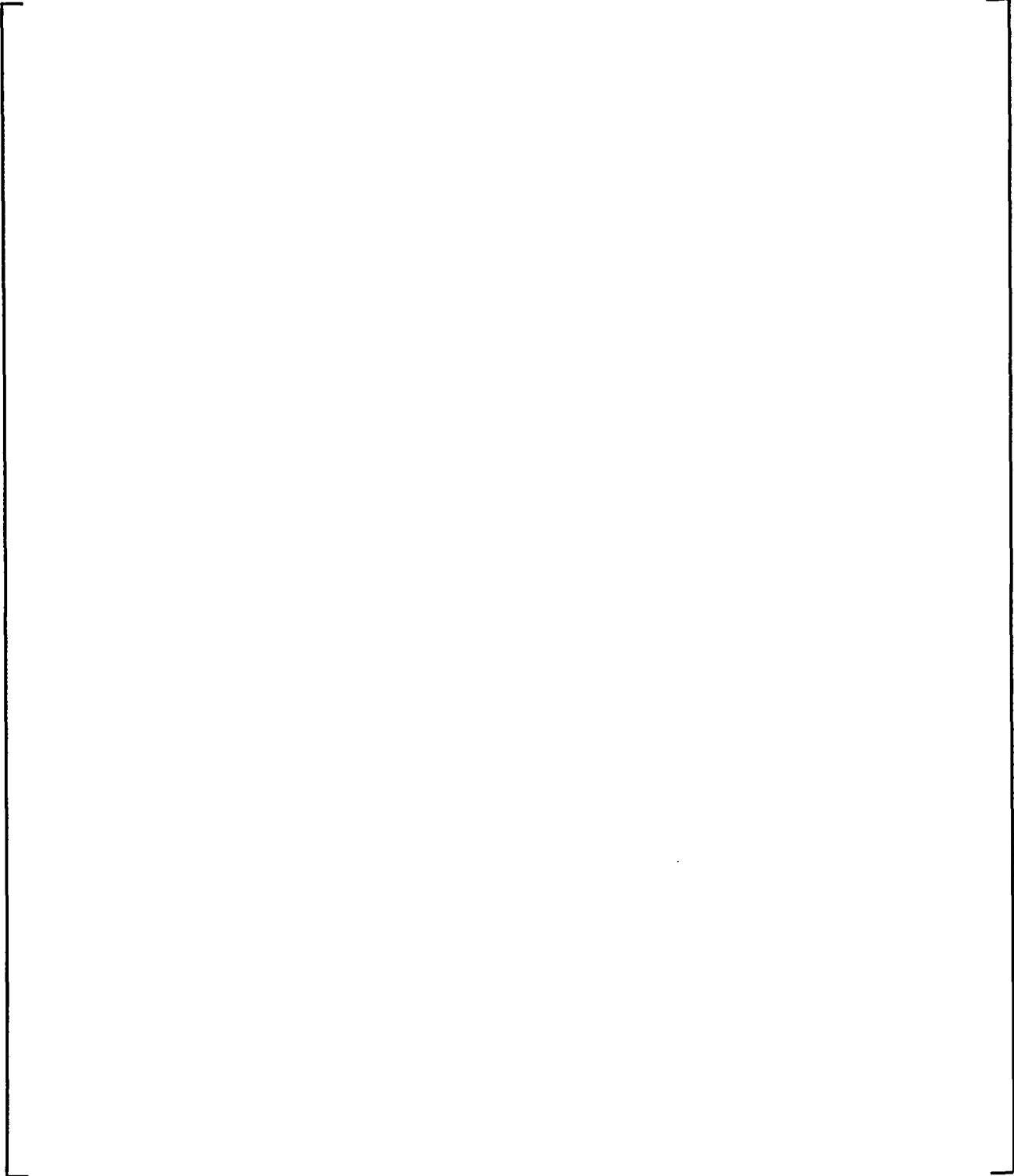


Figure 9-58 VGOTHIC Calculated Flow Pattern - LOCA Plume Rising into CMT Room and SG Compartments at 1500 Seconds

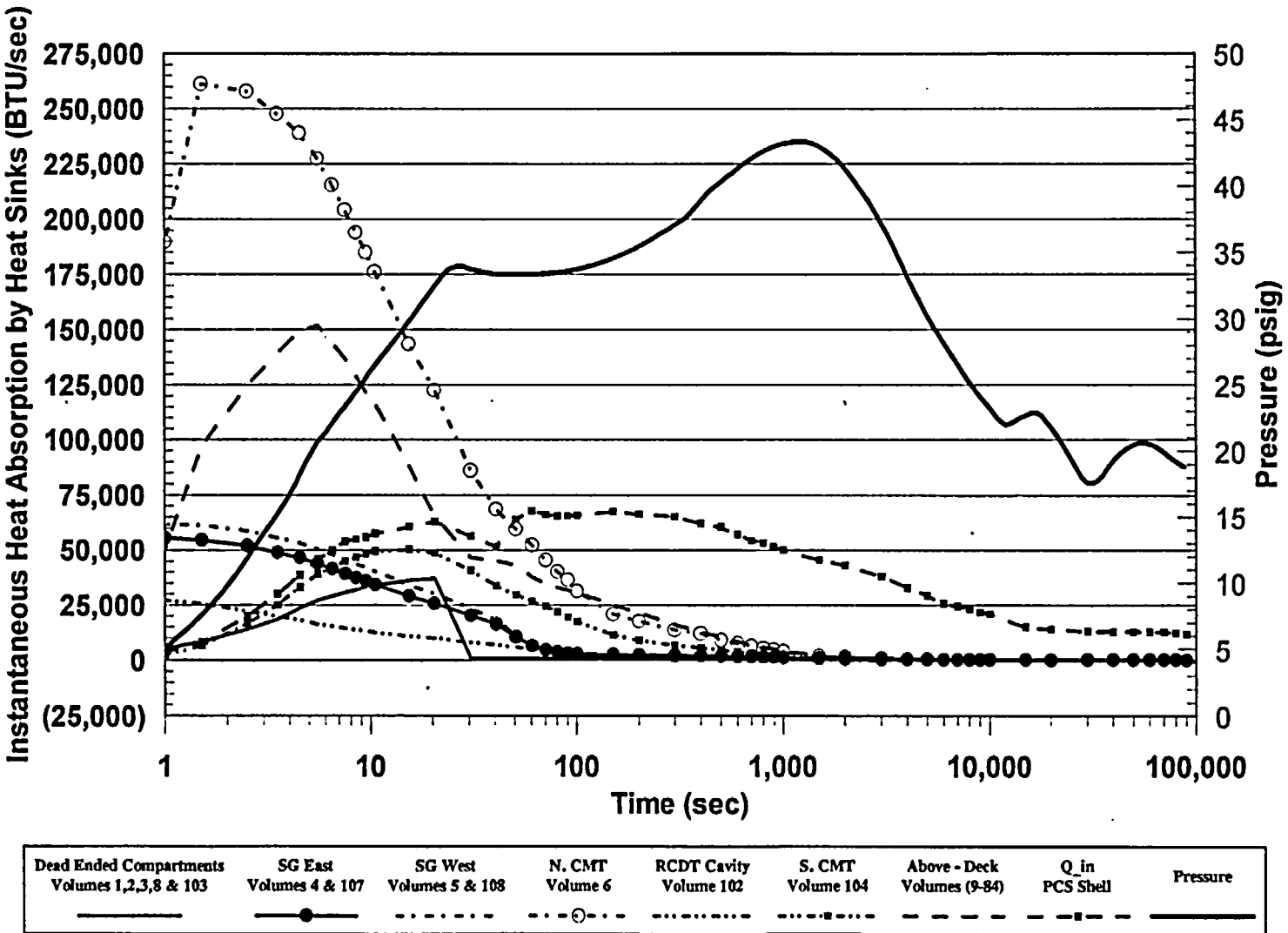


Figure 9-59 WGOIHIC Calculated AP600 Containment Heat Removal Rates - LOCA Plume Rising into CMT Room and SG Compartments

(a,c)

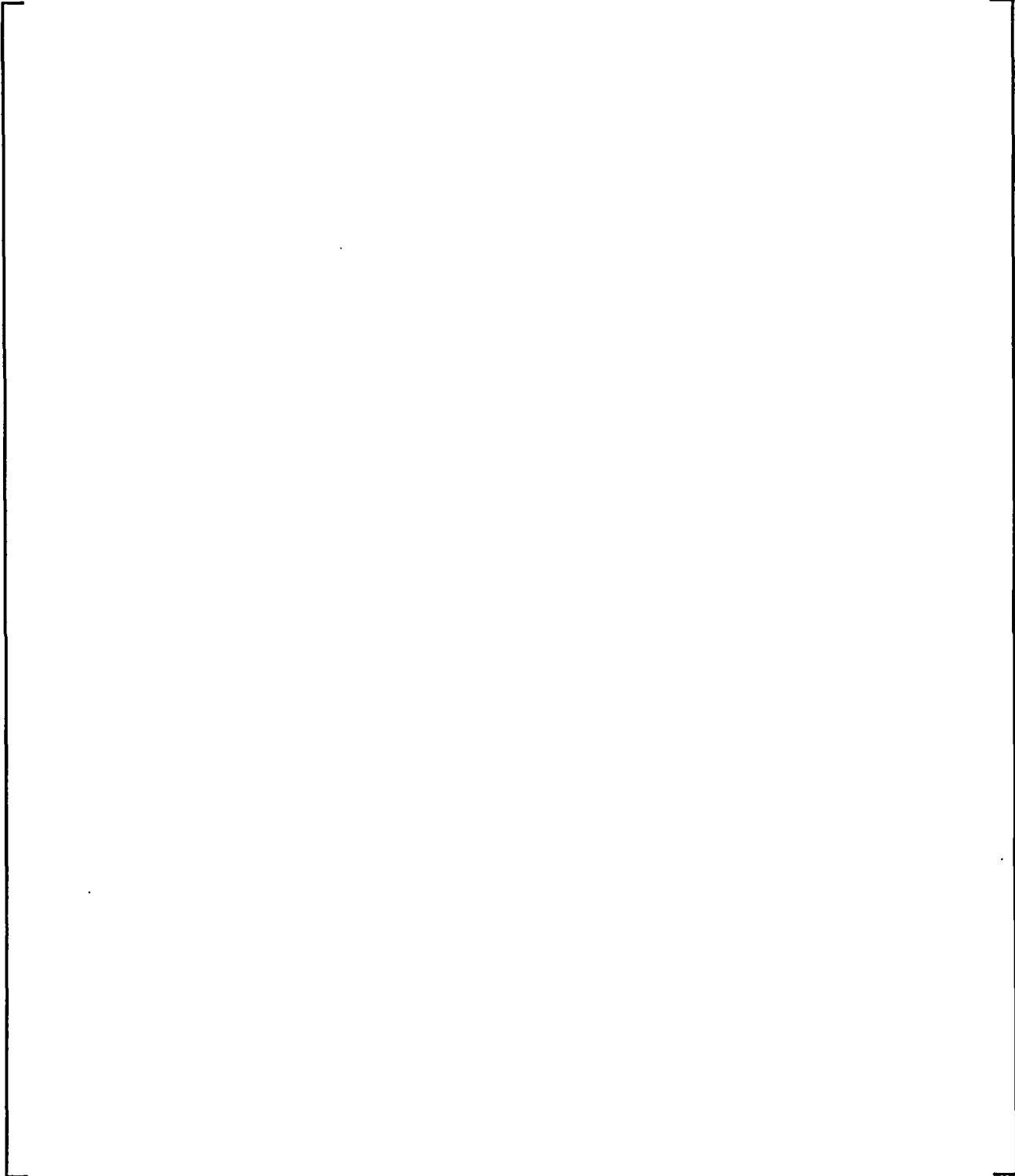


Figure 9-60 WGOTHIC Calculated AP600 Containment Steam Pressure Ratio for MSLB Above-Deck

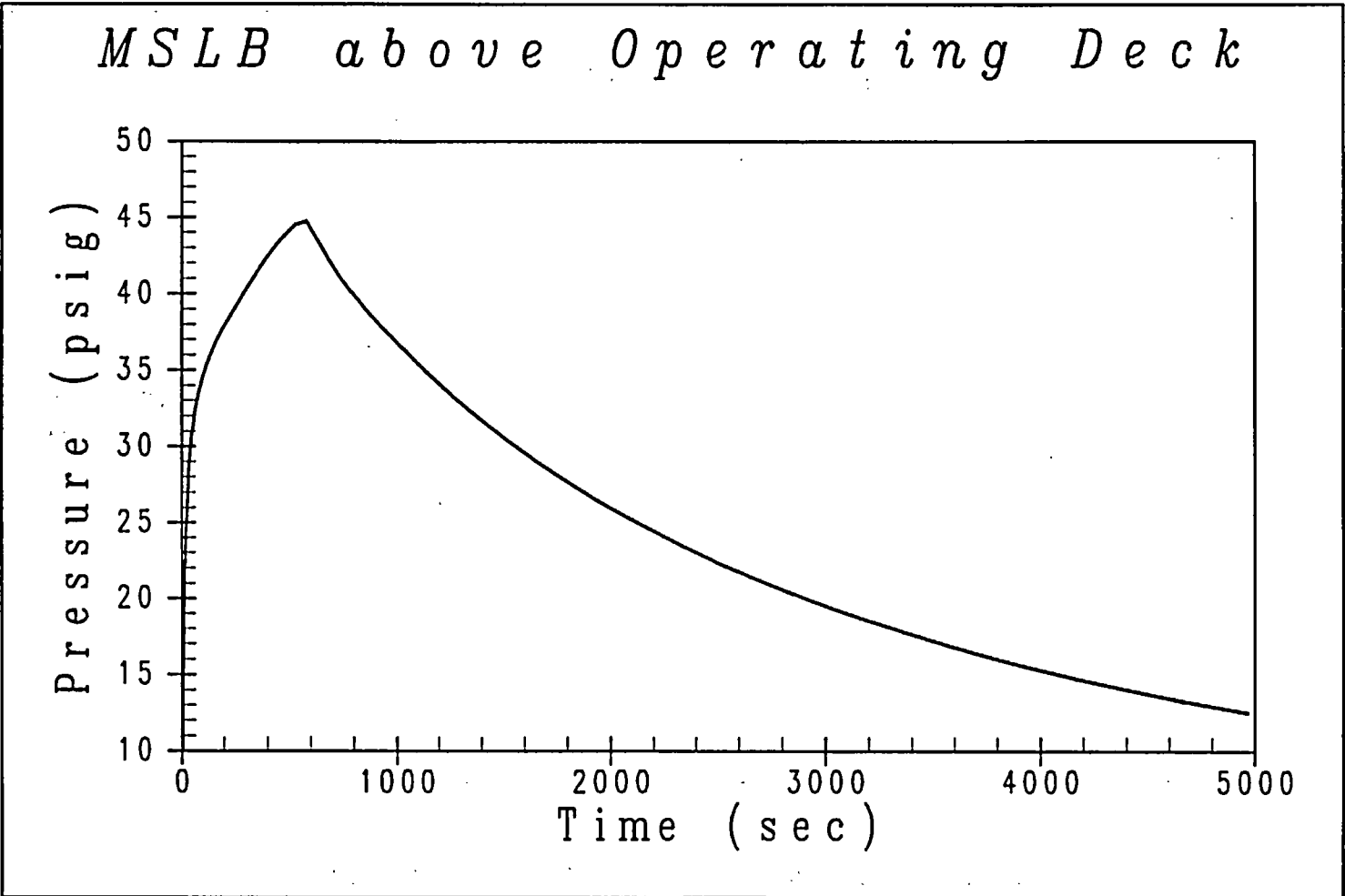


Figure 9-61

WGOOTHIC Calculated AP600 Containment Pressure - MSLB Above Operating Deck

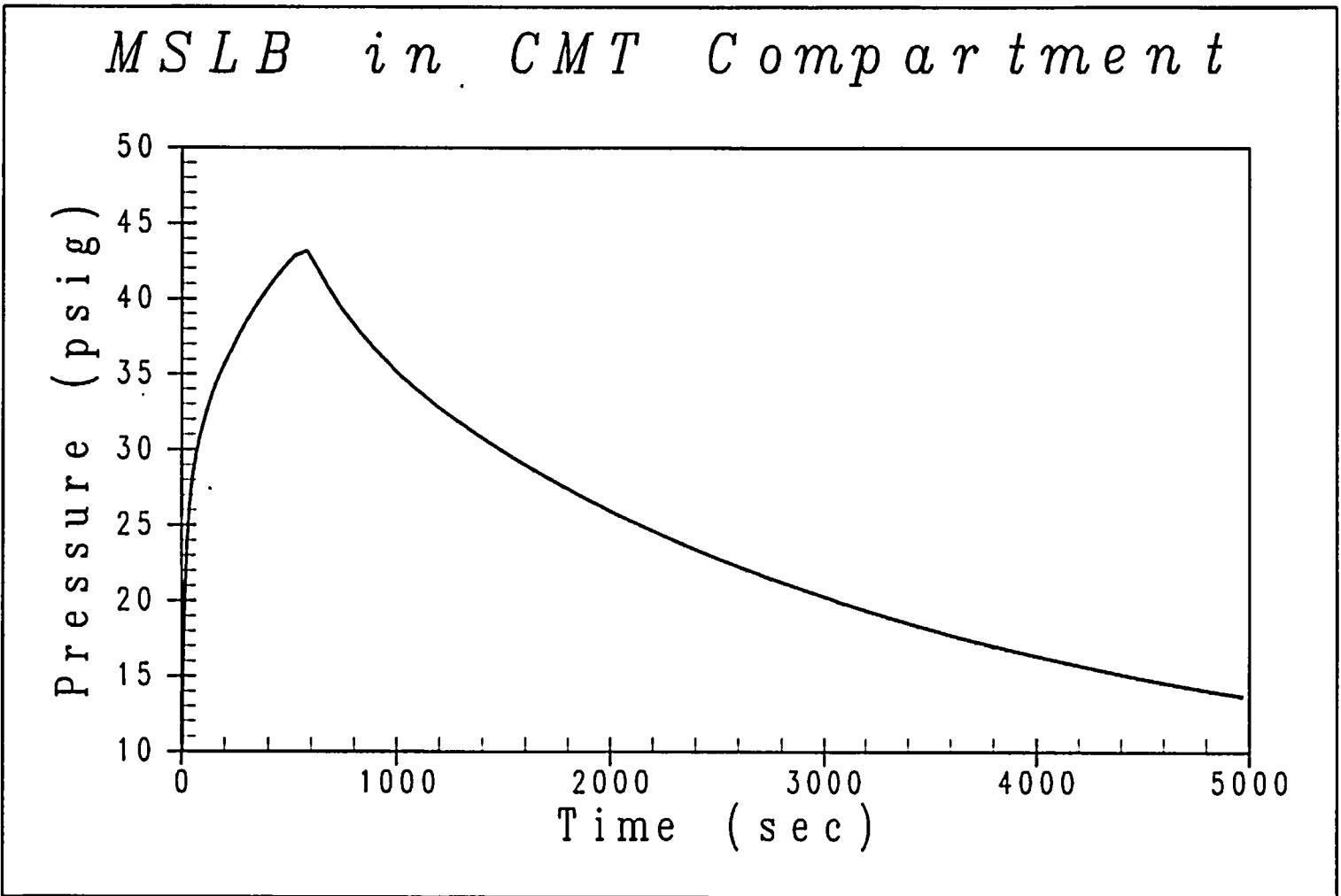


Figure 9-62

WCGOTHIC Calculated AP600 Containment Pressure - MSLB in CMT Room

Appendix 9.A

**Thermal and Circulation Effects of Drops
During a LOCA**

TABLE OF CONTENTS

9.A THERMAL AND CIRCULATION EFFECTS OF DROPS DURING A LOCA 9.A-2

LIST OF TABLES

9.A-1 Estimated Drop Fall Times 9.A-2

9.A THERMAL AND CIRCULATION EFFECTS OF DROPS DURING A LOCA

Drops, or fog particles, are created when the blowdown break source steam velocity is large enough to disperse a fraction of the break liquid along with the gas. As discussed in Section 4.4.2D of Reference 9.A.1 and Section 7.1 of Reference 9.A.2, drops will be formed during the LOCA blowdown phase. For the post-blowdown phases of a LOCA and for the MSLB, there will not be any significant drop formation. The thermal and circulation effects of drops on LOCA containment pressure are examined in this section.

The limiting DBA analysis LOCA is a DECLG break. The source flow from the reactor side of the break has more energy than the source flow from the steam generator side of the break, so more drops are expected from the reactor side. During blowdown, a range of drop sizes will be produced. The percentage of liquid converted to drops will also be within some range, the theoretical limits being 0 and 100 percent, although it is anticipated that a significant fraction of the liquid will form drops.

Many factors affect the length of time that the drops will be present in the atmosphere, such as shear coupling to the moving gas, coalescence, de-entrainment at walls and other surfaces, and the drop size (affecting its fall time). To estimate the fall time for various size drops, a simple calculation was performed which only accounts for the gravitational effects on the drops. Using the terminal velocity versus drop diameter information in Section 7.6 of Reference 9.A.3, fall times range from seconds to hours depending on the drop size and fall height. Table 9.A-1 shows estimated fall times for drops with diameters of 0.001, 0.01, and 0.1 inches. This provides an indication that the drops will exist long enough that their effect on containment pressure must be considered.

Drop Size (in)	Terminal Velocity (ft/sec)	Fall Time (sec)	
		30 ft	100 ft
0.001	.08	375	1250
0.01	8	3.8	12.5
0.1	20	1.5	5

Thermal Effects

The drops flash when they enter the containment atmosphere, reaching saturation very quickly. Section 7.1 of Reference 9.A.2 estimates 3.5 percent of a given drop flashes to steam. Section 7.1 also estimates that the drop diameter only decreases 5 percent due to evaporation in later phases. The drops are strongly coupled to the containment atmosphere temperature due to the large surface area of the total drop population. This strong coupling results in the drop temperature closely following the containment atmosphere temperature as it changes during the transient. Sensitivities using WGOTHIC show that if 5 percent or more of the liquid is converted into drops, then the containment atmosphere will be saturated quickly. Given the high velocity of the blowdown releases, much greater than 5 percent is anticipated to be converted into drops. With the atmosphere saturated, thermal effects such as superheating will not occur and the effect of larger drop fractions does not significantly affect the pressure response. The effects of drops on the Evaluation Model calculation of containment pressure is investigated with a sensitivity study described in Section 5.8.

Circulation and Stratification Effects

The presence of drops increases the density of the containment atmosphere, which makes the post-blowdown steam release relatively more buoyant. An estimate of the effect of drops on circulation and stratification is made by calculating the plume entrainment rate and resulting circulation time constant for the conditions at the end of the blowdown phase of the DBA LOCA. As discussed in Section 7.1 of Reference 9.A.2, well-accepted models are not available to predict the mass of the drops created during blowdown, so the bounds of 0 percent and 100 percent of the liquid will be considered.

To estimate the volume entrained into the plume (Q_{ent} , in ft³/sec), Peterson's equations (Reference 9.A.4) can be used:

$$Q_{ent} = 0.15 * B^{1/3} * Z^{5/3}$$

where: Z = elevation (ft.)

$$B = g * Q_{st} * (\rho_{amb} - \rho_{st}) / \rho_{amb}$$

$$g = \text{gravitational acceleration} = 32.2 \text{ ft/sec}^2$$

$$Q_{st} = \text{volumetric steam flow (ft}^3\text{/sec)}$$

$$\rho_{amb} = \text{containment ambient density (lbm/ft}^3\text{)}$$

$$\rho_{st} = \text{steam density (lbm/ft}^3\text{)}$$

The entrainment is calculated for a height of 100 feet above the top of the steam generator compartment, so Z = 100 ft. The steam release at the beginning of the peak pressure phase is estimated to be 1870 ft³/sec (Q_{st}). For the case assuming 0 percent of the liquid is released as drops, the $(\rho_{amb} - \rho_{st}) / \rho_{amb}$ term is approximately 0.275. For the case assuming 100 percent of the liquid is released as drops, the density term

is approximately 0.60. Using the above equation, the estimated entrainment rate is $Q_{ent} = 8239 \text{ ft}^3/\text{sec}$ (0 percent drops) and $10695 \text{ ft}^3/\text{sec}$ (100 percent drops). The estimated entrainment at the end of blowdown is approximately four times the steam flow (Q_s) for the case without drops, and slightly less than six times the steam flow for the case with drops.

Knowing the entrainment rate, a circulation time constant can be calculated for the containment free volume. This time constant will change with time, but it provides an indication of the amount of circulation expected for the releases after the refill phase. The circulation time constant is the volume divided by the entrainment rate, and for 0 percent drops it is 206 seconds and for 100 percent drops it is 159 seconds. It should be noted that the estimated times conservatively neglect volumetric entrainment into the wall layers. These time constants increase as the steam flow decreases, but this estimation shows that a large fraction of the containment volume will be entrained in the plume within a few minutes, which is relatively short compared to the time to reach maximum pressure (at approximately 1200 seconds), and very short compared to long-term cooling. A relatively large entrainment rate within the above-deck region indicates that the steam density gradients above-deck are not large whether drops exist or not. Therefore, the presence of drops will not significantly affect the general circulation and stratification patterns in the containment atmosphere.

Evaluation Model Drop Sensitivity Study

The AP600 Containment Evaluation Model, with the jet dissipated in the steam generator compartment, was used to determine the effect of drops on the calculation of containment pressure. The treatment of drops in the AP600 Containment Evaluation Model is described in Section 4.5.2.1. The Evaluation Model converts all of the liquid from the reactor side of the break to drops, and none of the liquid from the steam generator side of the break. Sensitivity cases were analyzed for comparison to the Evaluation Model results. The sensitivity cases are discussed in Section 5.8. One case modeled no drop formation and one case modeled 100 percent of the liquid converted into drops.

The containment pressure, as a function of time, was calculated for the sensitivity case. The maximum containment pressure, calculated with the Evaluation Model, is greater than the maximum pressure calculated assuming no drop formation. The presence of drops does have a slight influence on the Evaluation Model pressure calculation. Drop formation is expected during the blowdown phase and the sensitivity study indicates that drop formation should be modeled to provide a bounding calculation for containment pressure.

Conclusions

The formation of drops during the LOCA blowdown phase is a physically real phenomenon that may influence the maximum containment pressure calculated by the Evaluation Model. Drop formation increases the density of the containment atmosphere making the post-blowdown releases relatively more buoyant. A small percentage of the blowdown break liquid formed into drops is sufficient to saturate the containment atmosphere, at which point additional drop density has a minor thermal effect. The Evaluation Model treatment of drops provides a sufficient bounding calculation for maximum and long-term containment pressure.

References

- 9.A.1. WCAP-14812, "Accident Specification and Phenomena Evaluation for AP600 Passive Containment Cooling System," Revision 2, April 1998.
- 9.A.2. WCAP-14845, "Scaling Analysis for AP600 Containment Pressure During Design Basis Accidents," Revision 3, March 1998.
- 9.A.3. NTD-NRC-95-4563, "GOTHIC Version 4.0 Documentation, Enclosure 2: Technical Manual," September 21, 1995.
- 9.A.4. Peterson, P., "Scaling and Analysis of Mixing in Large Stratified Volumes," *International Journal of Heat and Mass Transfer*, Vol. 37, Supplement 1, pp 97-106, 1994.

Appendix 9.B

Effects of Stratification on Heat Sink Utilization

TABLE OF CONTENTS

9.B.1 INTRODUCTION 9.B-2
9.B.2 HEAT SINK ANALYSIS 9.B-2
9.B.3 CONDENSATION BOUNDARY CONDITIONS 9.B-2
9.B.4 HEAT CONDUCTION MODELS 9.B-5
9.B.5 RESULTS 9.B-7
9.B.6 CONCLUSIONS 9.B-11

LIST OF TABLES

9.B-1 Concrete Model Nodal Thickness 9.B-6
9.B-2 AP600 Assumed Room Heat Sink Distribution 9.B-9

LIST OF FIGURES

9.B-1 Condensation Heat Transfer Coefficients vs. T_{surf} 9.B-13
9.B-2 Containment Shell Heat Sink Results 9.B-14
9.B-3 CMT Room Heat Sink Results 9.B-15

9.B.1 INTRODUCTION

An analysis was performed to determine the impact of stratification on the relative effectiveness of containment heat sinks during a postulated LOCA. Models were developed to study transient heat conduction effects for steel and concrete structures under a variety of containment atmosphere boundary conditions. The models were then used to determine the effects of stratification of steam in the containment atmosphere on heat sink utilization in the CMT room and in the above-deck region.

9.B.2 HEAT SINK ANALYSIS

The condensation heat transfer in the containment atmosphere has been characterized as a function of the steam fraction, and has been used as boundary conditions to determine the transient heat absorption rate of the heat sink structures. The results of these analyses are used to estimate the relative effects of stratification on the heat sinks located on the PCS steel shell and in the CMT room.

The purpose of the analysis is to obtain relative effects of stratification for reasonably representative conditions to assess the magnitude of the bias. An extreme stratification gradient is assumed from which the relative effect of stratification on total heat sink energy removal in a region can be assessed. A bias is developed to bound the non-conservative effects of stratification.

9.B.3 CONDENSATION BOUNDARY CONDITIONS

These sensitivity calculations are performed to examine the relative effect of a gas mixture that is homogeneous (as in a lumped parameter node) and a gas mixture that is stratified. To keep the calculations simple, boundary conditions are assumed constant with time, and the following homogenous atmosphere conditions are assumed:

$$T_{\text{atm}} = 276^{\circ}\text{F}$$

$$P_{\text{atm}} = 59.7 \text{ psia}$$

$$f_{\text{st}} = 0.63 \text{ (homogeneous steam mole fraction)}$$

These parameters represent approximately time-averaged values over the first hour of the LOCA, since the CMT room steam concentration is relatively constant (Figure 9-44).

The heat transfer from the containment atmosphere and the structure is assumed to be dominated by condensation so that convection and radiation are neglected. The condensation heat transfer is determined by first determining the mass transfer for turbulent free convection (Reference 9.B.1, Section 4.3):

$$m'' = 0.13 \cdot \frac{\rho_{stm} D_v \Delta P_{stm}}{(v^2/g)^{1/3} P_{lm,air}} \left(\frac{\Delta \rho Sc}{\rho} \right)^{1/3} \quad (9.B-1)$$

where

- m'' is the condensation mass flux
- ρ_{stm} is the density of steam at the total pressure and boundary layer temperature
- ΔP_{stm} is the difference in the steam partial pressure atmosphere - surface
- v is the mixture kinematic viscosity
- g is gravity
- $P_{lm,air}$ is the log mean pressure difference atmosphere - surface
- $\Delta \rho$ is the mixture density difference atmosphere - surface
- ρ is the bulk mixture density
- Sc is the mixture Schmidt number (typically ~0.51)

and D_v is the air-steam diffusion coefficient which is given by (Reference 9.B-1, Section 4.3.2)

$$D_v = 0.892 \frac{14.2 \text{ psi}}{P} \left(\frac{T_{surf} + T_{atm}}{2 \times 460^\circ R} \right)^{1.81} \quad (9.B-2)$$

The steam partial pressure in the atmosphere is given by:

$$P_{stm-atm} = f_{st} * P \quad (9.B-3)$$

where f_{st} is the steam mole fraction in the atmosphere and P is the total pressure.

The steam partial pressure at the condensing surface is given by:

$$P_{stm-surf} = P_{sat}(T_{surf}) \quad (9.B-4)$$

where P_{sat} is the saturation pressure corresponding to T_{surf} .

The log mean pressure difference between the atmosphere air pressure and the air pressure at the surface is given by:

$$P_{tm-air} = \frac{(P_{air-surf} - P_{air-atm})}{\ln(P_{air-surf} / P_{air-atm})} \quad (9.B-5)$$

where $P_{air-surf}$ is the air partial pressure at the heat sink surface, $P - P_{stm-surf}$ and $P_{air-atm}$ is the air partial pressure in the atmosphere, $(1 - f_{st}) * P$.

The densities of air and steam at the atmospheric and surface pressures and temperatures are determined from the ideal gas law.

To determine the effect of the steam fraction, three distinct regions based on equal volume are assumed. The top region is assumed to be nearly all steam with $f_{st-top} = 0.98$. The middle region is assumed to be at the nominal conditions with $f_{st-mid} = 0.63$. The bottom region steam fraction is determined by conserving the total amount of steam in the total volume.

$$f_{st-bot} = 3 * f_{st-nom} - f_{st-top} - f_{st-mid} = 0.28 \quad (9.B-6)$$

Applying these three steam mole fractions along with the above containment atmosphere conditions, a relationship can be determined for the condensation heat transfer coefficient as a function of heat sink surface temperature. An equivalent condensation heat transfer coefficient is calculated from m'' for use as a boundary condition for heat sink condensation, described later. The equivalent condensation heat transfer coefficient is calculated by:

$$h_{cond} = \frac{m * h_{fg}}{(T_{atm} - T_{surf})} \quad (9.B-7)$$

where h_{fg} is the difference between the steam and liquid saturation enthalpy. The relationships for equivalent heat transfer coefficient are shown graphically in Figure 9.B-1.

The condensation heat transfer coefficient varies considerably with respect to the steam fraction in the containment atmosphere, f_{st} , and the surface temperature, T_{surf} . For each steam fraction, the heat transfer coefficient increases with increasing T_{surf} until the saturation temperature that corresponds to the steam partial

pressure at the surface is reached. At this point the condensation heat transfer drops to zero, and is zero for all surface temperatures greater than this temperature.

For the case of $f_{st} = 0.98$, $T_{sat} = 291^\circ\text{F}$, which is greater than the containment atmosphere temperature. Thus, the condensation heat transfer coefficient increases with surface temperature and no cutoff is reached. For the case of $f_{st} = 0.63$, $T_{sat} = 264^\circ\text{F}$, and the heat transfer coefficient drops to zero at this temperature. For the case of $f_{st} = 0.28$, 217°F , the heat transfer coefficient drops to zero.

9.B.4 HEAT CONDUCTION MODELS

Several models were developed to calculate heat transfer to the heat sinks. These include:

- Steel structures of varying thickness
- Concrete structures
- Steel-jacketed concrete structures
- Steel containment shell

A description of each model is given as follows.

Steel Structures

The one-dimensional model consists of a 1 ft. by 1 ft. section of steel, modeled by ten nodes of equal thickness, representing one-half the heat sink thickness. For example, for a one-half inch thick steel plate, the model has ten nodes, each 0.025 in. thick. A convective boundary condition is applied to one surface, while the other surface is assumed to be adiabatic. Connections between the nodes are defined by the area of the interface (1 ft²), and the distance from the node center to the interface (0.0125 in.). The properties for steel are listed below:

$$\begin{aligned}\rho &= 490.7 \text{ lbm/ft}^3 \\ C &= 0.107 \text{ Btu/lbm-}^\circ\text{F} \\ k &= 30 \text{ Btu/hr-ft-}^\circ\text{F}\end{aligned}$$

A zero-volume node is attached to the steel at the surface exposed to the atmosphere. The boundary conditions for the three steam fractions are described in the previous section.

Concrete Heat Sinks

The concrete heat sinks have much lower thermal conductivity and are modeled differently than the steel heat sink. The thermal properties of the concrete are given as:

$$\begin{aligned}\rho &= 140 \text{ lbm/ft}^3 \\ C &= 0.19 \text{ Btu/lbm-}^\circ\text{F} \\ k &= 0.83 \text{ Btu/hr-ft-}^\circ\text{F}\end{aligned}$$

where δ_{gap} is the gap thickness
 and k_{mix} is the thermal conductivity of the containment atmosphere mixture

$$k_{mix} = 0.5 \cdot (k_{air} + k_{stm}) \quad (9.B-9)$$

For $T_{stm} = 276^\circ\text{F}$, and $f_{st} = 0.5$, $k_{mix} = 0.03 \text{ Btu/hr-ft}^\circ\text{F}$, and $h_{gap} = 10 \text{ Btu/hr-ft}^2\text{-}^\circ\text{F}$.

The concrete is represented by 10 nodes with thicknesses shown in Table 9.B-1.

Steel Containment Shell

The steel containment shell model is somewhat more complex in that the inside boundary condition is the same as the other models while the outside boundary condition is not adiabatic, but is representative of the outer shell evaporative heat transfer. The steel shell is assumed to be []^{ac} thick. For this case, a []^{ac} The inner-most node is connected to a zero-volume node upon which the condensation boundary condition is assumed. The outer-most node is also connected to a zero-volume node upon which an evaporation boundary condition is assumed. The outside boundary temperature is assumed to be an average between the inlet air temperature at the bottom of the Passive Containment Cooling System annulus, and the outlet air temperature at the top.

$$T_{air-avg} = 142^\circ\text{F}$$

and $h_{evap} = 113 \text{ Btu/hr-ft}^2\text{-}^\circ\text{F}$

Note that the assumption of a constant value of h over the entire shell surface is very conservative, since in the stratified case, the shell adjacent to the steam-rich top would heat up and significantly increase the evaporation rate on the outside. No credit is taken in this analysis for the associated increase in external heat transfer coefficient.

For this model, there is a short period of time during which the shell heats up from the initial temperature. After this time, a steady-state condition is established as heat is transferred at a nearly constant rate from the inside to the outside of the shell.

9.B.5 RESULTS

For each of the models described above, three transient calculations were performed representing each of the three steam fraction conditions. The results of these calculations were used to examine heat absorption effects for each of the conditions. Since the models represent one square foot of heat sink area, the results

can be used to estimate the heat sink behavior in a typical room by multiplying the integrated heat removal by the total area for a particular heat sink type.

Containment Steel Shell Heat Sink Stratification Sensitivity

Figure 9.B-2 shows the heat removal rate for the containment shell. The areas for the top, middle, and bottom of the shell are not weighted equally (as in Equation 9.B-10). The volume of the containment above the operating deck is divided into three regions of equal volume, and the associated surface area for each volume is used. For the AP600 containment,

Elevation of operating deck = 135.25 ft

Elevation of spring line = 218.71 ft

Elevation of top of dome = 256.4 ft

Containment radius = 65 ft

Gas Volume in dome = 336,963 ft³

Surface area of dome = 15,552 ft²

Total volume of gas above deck = 1.45 x 10⁶ ft³

The two lower regions both consist of a cylindrical gas volume = 481,582 ft³. This corresponds to a cylindrical section 36.28 feet in length with a surface area = 14,776 ft². The upper region gas volume is also 481,582 ft³, and consists of the dome and a cylindrical section 11.1 feet in length. The total surface area associated with this volume is 19,898 ft².

Thus, the equivalent integrated heat removal rate through one square foot of the shell is weighted by surface area as

$$Q_{3\text{-Region}} = (19,898 \cdot Q_{\text{top}} + 14,776 \cdot Q_{\text{mid}} + 14,776 \cdot Q_{\text{bot}}) / 49,450 \quad (9.B-10)$$

The results show that the higher weighting of the upper, steam-rich region nearly compensates for the lower heat removal rates in the bottom region, and the heat removal rate is slightly (~0.5% after 200 seconds) higher for the homogeneous case.

Results for the steel shell assessment are presented in terms of instantaneous rate since the external boundary condition never allows the steel to saturate. The results also allow interpretation of stratification effects during the quasi-steady, long-term, while the steel shell is the dominant heat sink and the balance between instantaneous source and sink heat rates governs the containment pressure. Since the stratification penalty on the steel shell heat removal rate is nearly negligible, a simple bias is introduced into the Evaluation Model by removing the non-grating operating deck floors to bound the effect. The stratification effect is exaggerated due to the use of an extreme gradient, well beyond what has been observed in the LST (Section 9.2.1 and 9.2.3) and in the international containment database (Appendix 9.C.2).

Simulated Room Heat Sink Stratification Sensitivity

These models were applied to heat sinks which reasonably represent the AP600 CMT room. The heat sinks for the AP600 CMT room (North and South sections) are summarized in Table 9.B-2.

Table 9.B-2 AP600 Assumed Room Heat Sink Distribution			
Heat Sinks in Simulated Room	Thickness	Surface Area	Region
Steel-Jacketed Concrete - Ceiling (single-sided)	0.5 in. / 24 in.	5398.87 ft ²	Top
Steel-Jacketed Concrete - Floors (single-sided)	0.5 in. / 24 in.	5601.44 ft ²	Bottom
Steel-Jacketed Concrete - Walls (double-sided)	0.5 in. / 24 in.	4596.11 ft ²	1/3 in each region
Steel-Jacketed Concrete - Wall (double-sided)	0.5 in / 48 in	673.99 ft ²	1/3 in each region
Concrete - Bulk (double-sided)	48 in.	3287.36 ft ²	1/3 in each region
Steel - CMT (single-sided)	4.874 in.	1848.8 ft ²	1/3 in each region
Steel - Containment Shell Wall (single-sided)	1.57 in.	11385.53 ft ²	1/3 in each region
Steel - Columns (double-sided)	0.39 in.	1656.5 ft ²	1/3 in each region
Steel - Floor Grating (double-sided)	0.39 in.	3781.69 ft ²	1/3 in each region
Steel - Elevator (double-sided)	0.2 in.	218.96 ft ²	1/3 in each region
Steel - Platform (double-sided)	0.144 in.	11254.2 ft ²	1/3 in each region
Steel - Stair & Rails (double-sided)	0.132 in.	181.59 ft ²	1/3 in each region

As was discussed previously, each heat sink was analyzed using three different steam fractions representing the top, middle, and bottom thirds of the room which is a bounding gradient when the plume rises through the CMT compartment. There is expected to be no significant stratification penalty in the CMT room with

downflow in the Evaluation Model, where the plume rises from the steam generator compartment. For each individual heat sink, a homogeneous case and three-region averaged result was obtained for a 1 ft² section of the heat sink. The energy removal by each heat sink is determined by calculating the heat removal for 1 ft², and multiplying by the appropriate surface area.

Where appropriate, the heat sinks that are located in a specific volume (i.e., ceilings and floors) are not averaged for the three-region, but are analyzed solely with the steam fraction of that volume. This becomes important for the ceilings since these heat sinks are located within the high steam fraction volume and higher heat transfer is expected when the room is stratified. The opposite is expected when considering floors. Refer to Table 9.B-2 for the region designation.

Figure 9.B-3 shows the integrated heat removal by all the heat sinks in the CMT room for a one hour transient. As will be discussed below, the stratification bias for this case is a function of the total energy absorbed. This is because the adiabatic boundary condition results in heat sinks reaching a maximum thermal absorption governed by the saturation temperature for the given steam concentration in a volume. Therefore, results for this scenario are presented in terms of integrated total heat absorption.

The results show the CMT room heat sinks including the floors for the homogeneous and stratified cases. In addition, the case where the floors are not included for the homogeneous case is also shown. The stratified, three-region results are lower than the homogeneous case results by 10-15% when all heat sinks are considered. The homogeneous case with floors excluded is slightly conservative when compared to the stratified case with the floors included. Thus, the combination of assuming homogeneous conditions and neglecting the floors in the total heat sink area results in total heat sink utilization that is neutral at the time of peak pressure, and over the longer term is slightly conservative relative to the expected conditions.

The assessment of stratification effects is very conservative because a conservatively low benefit for the uppermost region is used, and the gradient is much more extreme than what has been observed in the LST (9.2.1 and 9.2.3) and in the international containment database (Appendix 9.C.2). The choice of stratified conditions to examine for this sensitivity are conservative and the results bound other, less extreme postulated stratification gradients. The room temperature is assumed to be 276°F in the stratified case, the same temperature as in the base case homogeneous room. One could, for example, postulate a less extreme, thermodynamically consistent, gradient of 0.77 for the top, 0.63 for the middle, and 0.49 for the bottom. The saturation temperature for a region at 59.7 psia and a steam mole fraction of 0.98 (psat of 58.5 psia) is 291°F. The upper region then would be about 15°F hotter than assumed. Therefore, the upper region conditions are thermodynamically inconsistent in a way that minimizes heat absorption in the upper region of the room, and thus maximizes the stratification bias.

The bias for the CMT room is governed by the air content in the lowest region. Results indicate that steel heat sinks, and the steel on jacketed concrete, reach a maximum for integrated heat absorption well within

the one-hour time frame of the calculation. The concrete continues to absorb heat over a very long term, on the order of days. However, the transient skin temperature of concrete increases due to its relatively poor thermal conductivity and a gap between the steel jacket and concrete reduces concrete effectiveness, so that the magnitude of concrete heat absorption is not significant relative to the steel. The integrated heat absorption by heat sinks is then primarily a function of the maximum bulk steel temperature rise, which is related to the saturation temperature of the adjacent region. While a less severe assumed stratification gradient would result in less rapid heat absorption by sinks in the upper region, the upper heat sinks would still reach their maximum well within the one-hour time frame. The lower region integrated heat absorption is limited by the saturation temperature for the assumed steam concentration. Therefore, the stratification bias is controlled by the lower region steam concentration and is maximized by the assumption of the extreme stratification gradient.

Since the exaggerated effect of stratification for the case of a plume rising through the CMT shows a bias on total integrated heat removal, a bias is introduced into the Evaluation Model by removing heat sinks associated with floors in compartments. As an additional conservatism, that bias is retained for the Evaluation Model with a plume rising through the steam generator compartment, as well as all sensitivity cases performed, even though most situations result in downflow through the CMT compartment.

For the case of the steel containment shell above the operating deck, the dome surface area weights the upper, steam-rich volume more heavily than the lower volumes, and compensates for the lower heat removal rates. Thus, the homogeneous case results are nearly equal to those for the stratified case, with the homogeneous case giving less than 0.5% less instantaneous heat removal rates. A simple bias of removing operating deck floors is included in the Evaluation Model to bound this effect.

9.B.6 CONCLUSIONS

For the case of the steel containment shell above the operating deck, the dome surface area weights the upper, steam-rich volume more heavily than the lower volumes, and compensates for the lower heat removal rates. Thus, the homogeneous case results are nearly equal to the stratified case, with the homogeneous case giving less than 0.5 percent less instantaneous heat removal rates. A simple bias of removing operating deck floors is included in the Evaluation Model to bound this effect.

The results of the heat sink utilization analysis for below-deck compartments indicate that in general, the assumption of homogeneous compartment volumes predicts higher overall heat removal by the heat sinks compared to stratified volumes. This is primarily due to the propensity of the condensation heat transfer to fall off as the heat sink surface temperature approaches the local saturation temperature in the lower steam fraction volumes. Stratification gradients are not expected to be nearly as extreme as assumed in this evaluation. The results of the homogeneous case gives 15-20% higher integrated heat removal than the

stratified results. Therefore, a bias is introduced in the Evaluation Model to account for this difference, implemented by removing heat sinks representing floors from the Evaluation Model.

References

- 9.B-1. WCAP-14845, "Scaling Analysis for AP600 Containment Pressure During Design Basis Accidents,"
Revision 3, March 1998.

Heat Sink Utilization - Heat Transfer Coefficients

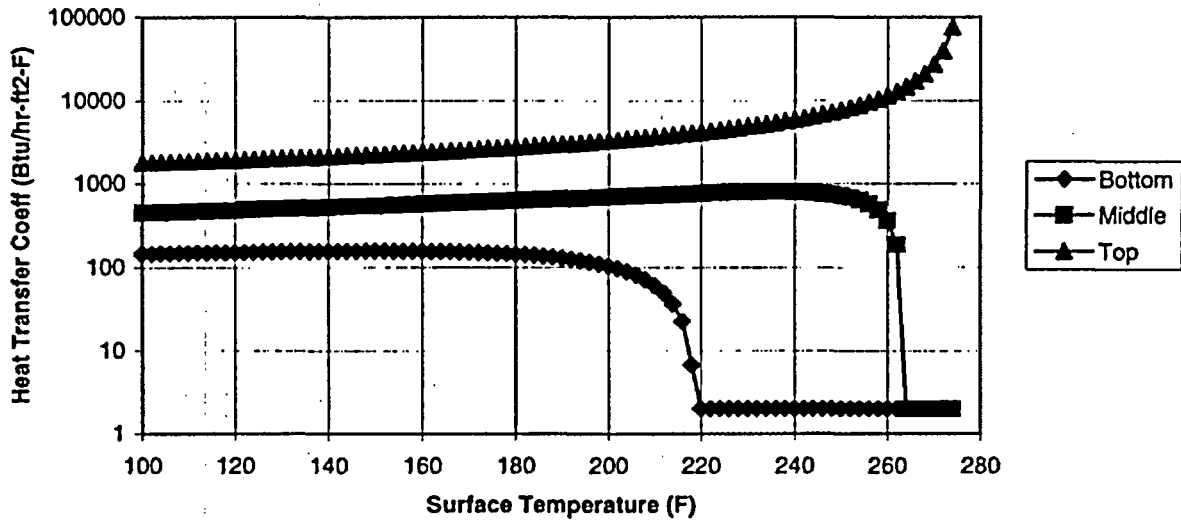


Figure 9.B-1: Condensation Heat Transfer Coefficients vs. T_{surf}

Heat Sink Utilization - Containment Shell Heat Flux

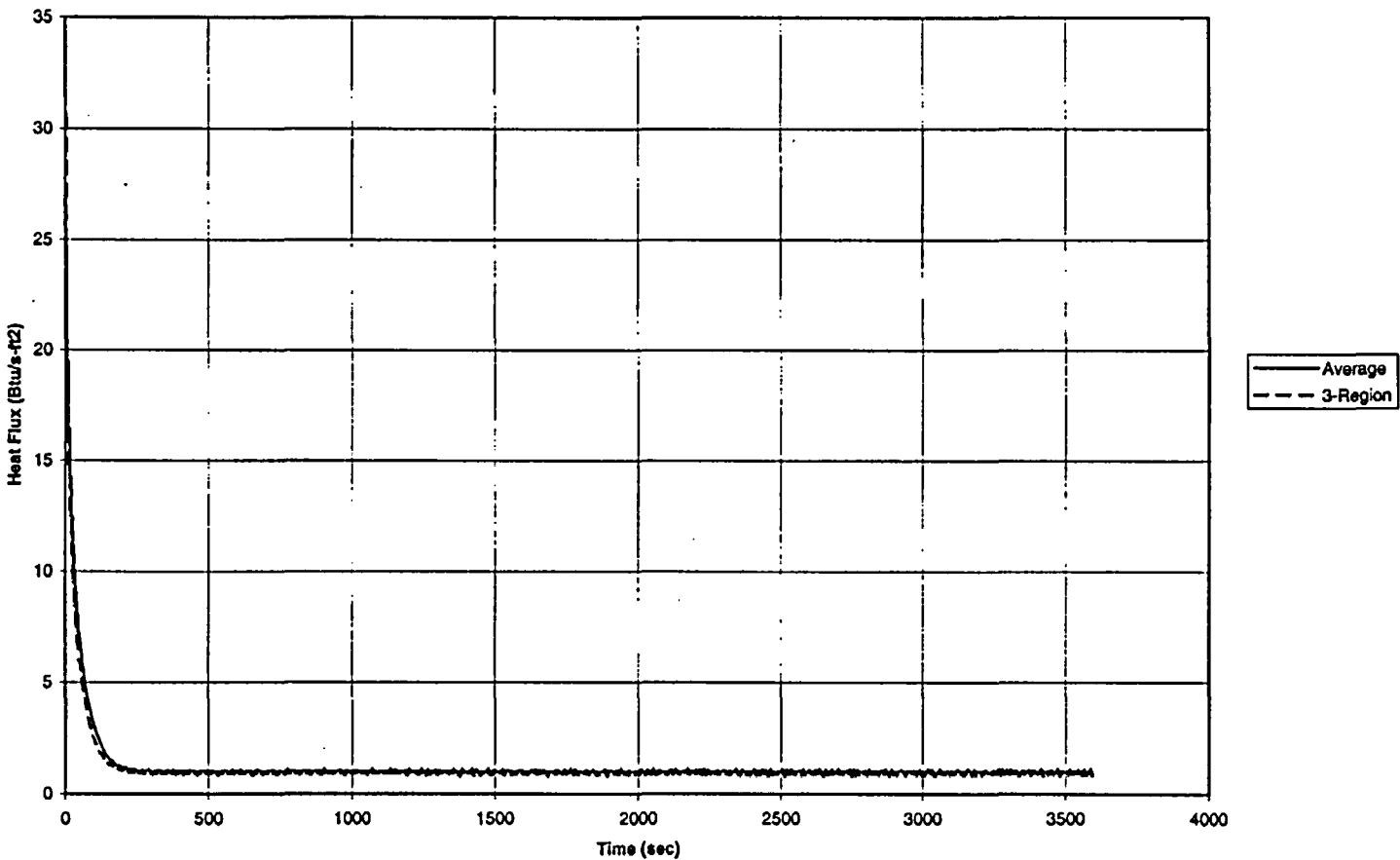


Figure 9.B-2: Containment Shell Heat Sink Results

CMT Room Heat Sink Utilization

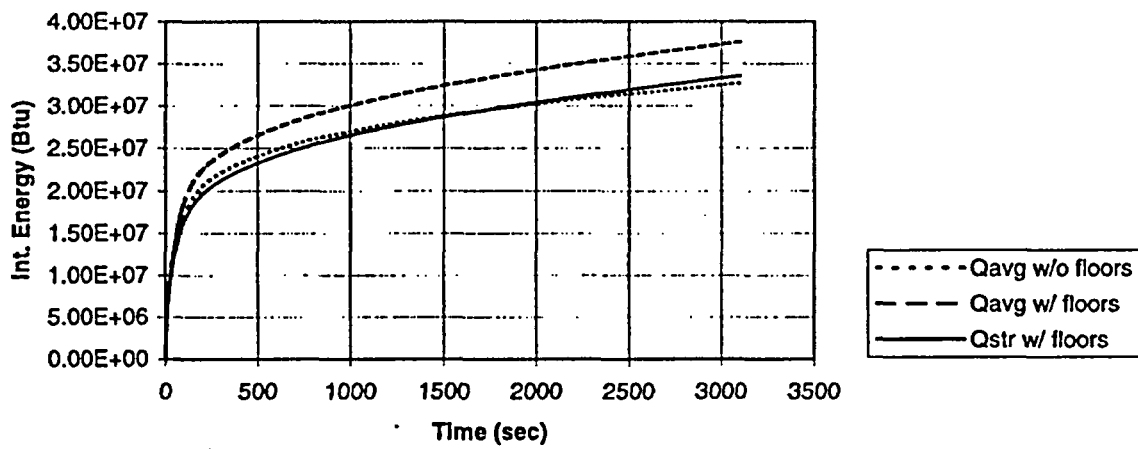


Figure 9.B-3: CMT Room Heat Sink Results

Appendix 9.C

**Additional Information on
Containment Circulation and Stratification**

**J. Woodcock
M. DzoDzo**

TABLE OF CONTENTS

Section	Title	Page
	LIST OF TABLES	9.C-iii
	LIST OF FIGURES	9.C-iv
9.C.1	DEVELOPMENT OF EXPECTED FLOW PATTERNS FOR AP600 AND AP1000 BASED ON SEPARATE FLOW TESTS IN ENCLOSURES	9.C-1
9.C.1.1	STRATIFICATION PHENOMENA	9.C-1
9.C.1.1.1	Static Stratification	9.C-3
9.C.1.1.2	Stratification and Circulation	9.C-5
9.C.1.1.3	References	9.C-21
9.C.1.2	CIRCULATION PHENOMENA	9.C-25
9.C.1.2.1	Circulation Phenomena Due to the Presence of Boundary Layers (Wall Jets) and Buoyant Plumes Formed as a Consequence of Natural Convection Effects	9.C-26
9.C.1.2.2	Circulation Phenomena Due to the Interaction With the Hot Buoyant Plumes and Jets	9.C-28
9.C.1.2.3	References	9.C-36
9.C.1.3	IMPORTANT DIMENSIONLESS GROUPS	9.C-38
9.C.1.3.1	Important Dimensionless Groups for Stratification and Circulation Phenomena Inside Enclosures	9.C-38
9.C.1.3.2	References	9.C-42
9.C.1.4	EXPECTED FLOW PATTERNS FOR AP600 AND AP1000	9.C-43
9.C.1.4.1	Simplified Representation of Circulation Regions During Post- Blowdown LOCA in AP600 and LST	9.C-43
9.C.1.4.2	A Qualitative Model for Recirculating Stratified Region II	9.C-46
9.C.1.4.3	References	9.C-58
9.C.2	OVERVIEW OF THE INTERNATIONAL CONTAINMENT EXPERIMENTAL DATA BASE	9.C-59
9.C.2.1	DESCRIPTION OF THE AVAILABLE BATTELLE MODEL CONTAINMENT (BMC) DATABASE	9.C-65
9.C.2.1.1	Natural Convection Phenomena Inside the Multi-Compartment Containment (F2 Experiments)	9.C-66
9.C.2.1.2	The Influence of Initial Temperature Distribution, Location of Hydrogen Injection, Duration of Injection, and Size of Vent Openings on the Hydrogen Distribution BMC Tests 2, 4, 6, 12 and 20)	9.C-86
9.C.2.1.3	Effects of Sump Heatup on Global Natural Circulation (Experiments RX1 - RX5)	9.C-98
9.C.2.1.4	References	9.C-111

TABLE OF CONTENTS (Cont.)

Section	Title	Page
9.C.2.2	DESCRIPTION OF THE AVAILABLE NUPEC DATA BASE	9.C-112
9.C.2.2.1	M-7-1 Test	9.C-112
9.C.2.2.2	M-4-3 Test	9.C-112
9.C.2.2.3	References	9.C-122
9.C.2.3	DESCRIPTION OF THE AVAILABLE CAROLINAS VIRGINIA TUBE REACTOR CONTAINMENT (CVTR) DATABASE	9.C-123
9.C.2.4	DESCRIPTION OF THE AVAILABLE HDR DATABASE	9.C-139
9.C.2.4.1	HDR E11 Test Series	9.C-139
9.C.2.4.2	HDR Large LOCA Experimental Data Base	9.C-175
9.C.2.4.3	References	9.C-223
9.C.2.5	CONCLUSION	9.C-225
9.C.3	APPLICATION OF LUMPED-PARAMETER CODES FOR MODELING LARGE CONTAINMENT FACILITIES	9.C-227
9.C.3.1	VALIDATION OF THE LUMPED PARAMETER CONTAINMENT ANALYSIS COMPUTER CODES BASED ON BMC EXPERIMENTAL RESULTS	9.C-227
9.C.3.1.1	F2 Experiments - Natural Convection Phenomena Inside the Multi- Compartment Containment	9.C-227
9.C.3.1.2	Influence of Initial Temperature Distribution, Location of Hydrogen Injection, Duration of Injection, and Size of Vent Openings on Hydrogen Distribution (BMC Tests 2, 4, 6, 12, and 20)	9.C-228
9.C.3.2	VALIDATION OF THE LUMPED PARAMETER CONTAINMENT ANALYSIS COMPUTER CODES BASED ON NUPEC EXPERIMENTAL RESULTS	9.C-230
9.C.3.2.1	M-7-1 Test	9.C-230
9.C.3.2.2	M-4-1 Test	9.C-230
9.C.3.3	VALIDATION OF THE LUMPED-PARAMETER CONTAINMENT ANALYSIS COMPUTER CODES BASED ON HDR EXPERIMENTAL RESULTS	9.C-241
9.C.3.4	CONCLUSIONS	9.C-251
9.C.3.5	REFERENCES	9.C-253

LIST OF TABLES

Table	Title	Page
Table 9.C-1	Comparison of Various Facilities	9.C-61
Table 9.C-2	Overviewed Tests from International Database	9.C-62
Table 9.C-3	Representative Velocity in [m/s] in Opening from R3 to R6 in the Different Experimental Phases of Experiment F2, Phases 2-4	9.C-69
Table 9.C-4	Test Matrix of Battelle Sump Heatup Experiments	9.C-100
Table 9.C-5	Events for E11.4 Experiment	9.C-163
Table 9.C-6	HDR-V21.1 Test Conditions	9.C-188

LIST OF FIGURES

Figure	Title	Page
Figure 9.C.1-1a	The formation of the horizontal layers of the constant density due to the stratification	9.C-9
Figure 9C.1-1b	Interaction of jets, plumes and wall boundary layers with stratified regions	9.C-10
Figure 9C.1-2	Combination of the constant temperature boundary conditions at the outside and inside surfaces which will produce stratification inside the enclosure	9.C-11
Figure 9C.1-3	Stratification inside the upper and lower corners of the romb-shaped enclosure	9.C-12
Figure 9C.1-4	Experimental and numerical results for the romb-shaped enclosure with the romb angle 44° and $Ra=3.5 \cdot 10^4$, $Pr=5270$	9.C-13
Figure 9.C.1-5	a) The square enclosure with vertical walls at the different temperatures and horizontal walls adiabatic, b) Streamlines for $Ra=10^6$ and $Pr=0.71$, c) Isotherms for $Ra=10^6$ and $Pr=0.71$	9.C-14
Figure 9.C.1-6	Average Nusselt numbers as a function of the Rayleigh numbers for the square enclosure with opposite vertical walls at the different temperature and $Pr=0.71$ (air)	9.C-15
Figure 9.C.1-7	Formation of the stratified core in between two opposite vertical line jets (after Baines and Turner, 1969)	9.C-16
Figure 9.C.1-8	Flow in an enclosure with vertical opposite walls at different temperatures ($Ra=10^5$, $Pr=0.71$)	9.C-17
Figure 9.C.1-9	Internal waves in the square cavity - fluctuations in the temperature field at $Ra=2 \cdot 10^8$ and $Pr=0.71$ (air)	9.C-18

LIST OF FIGURES (Cont.)

Figure	Title	Page
Figure 9.C.1-10	Temperatures for the initial solution with the hot and cold intrusions and boundary layer waves presented (after Armfield and Janssen, 1996)	9.C-19
Figure 9.C.1-11	Formation of the downward negatively buoyant jets	9.C-20
Figure 9.C.1-12	Rayleigh-Benard convection example	9.C-29
Figure 9.C.1-13	Hele-Shaw cell	9.C-30
Figure 9.C.1-14	Steady and oscillatory convection in Hele-Shaw cell (after Buhler et al., 1987)	9.C-31
Figure 9.C.1-15	Turbulent (chaotical) flow with hot and cold plumes interactions (plane cross-section of the three-dimensional enclosure is presented)	9.C-32
Figure 9.C.1-16	Interaction of hot and cold plumes (after Aqino et al., 1989)	9.C-33
Figure 9.C.1-17a	Vertical temperature distribution inside the cylindrical enclosure with lower and upper horizontal plate at higher and lower temperatures, respectively ($Ra=9.38 \cdot 10^7$, $Pr=200$)	9.C-34
Figure 9.C.1-17b	Generation of the cold plumes due to the brake (separation) of the vertical boundary layers near the cold vertical walls	9.C-35
Figure 9.C.1-18	Primary flow regions and volumetric flow rates for quasi-steady containment conditions	9.C-52
Figure 9.C.1-19	The volumetric flow between the upper and lower deck regions Q_c	9.C-53

LIST OF FIGURES (Cont.)

Figure	Title	Page
Figure 9.C.1-20	Primary flow regions and volumetric flow rates for quasi-steady containment conditions in LST case	9.C-54
Figure 9.C.1-21	Inflows and outflows from the Region II	9.C-55
Figure 9.C.1-22	Recirculating flow paths inside the Region II	9.C-56
Figure 9.C.1-23	Mass conservation for thin horizontal layer inside the Region II	9.C-57
Figure 9.C.2-1	Comparison of different facilities	9.C-60
Figure 9.C.2-2	Model Containment: vertical cross-section 0/180°, horizontal cross-sections at +02 m and +1.7 m for configuration in experiment F2	9.C-70
Figure 9.C.2-3	Model Containment: vertical cross-section 0/180°, horizontal cross-sections at +4.01 m and +5.05 m for configuration in experiment F2	9.C-71
Figure 9.C.2-4	Injections and convective flow loop directions (+ sign for flow indicates the same direction of the flow as arrow in R9)	9.C-72
Figure 9.C.2-5	Experiment F2, Phases 2-8, experimental procedures, total and partial pressures	9.C-73
Figure 9.C.2-6	Number of compartments, locations of measurement transducers and steam releases	9.C-74
Figure 9.C.2-7	Test group F2, Phase 1 (heatup), total pressure in the containment	9.C-75
Figure 9.C.2-8	Test group F2, Phase 1 (heatup), atmospheric temperature in the compartment R9, H=1.0 m and 21 m	9.C-76

LIST OF FIGURES (Cont.)

Figure	Title	Page
Figure 9.C.2-9	Scheme of multi-compartment containment geometry in experiment F2	9.C-77
Figure 9.C.2-10	Test group F2, phase 2: atmospheric temperatures in zones 1, 2 and 3 (R5 + R6, R1 + R4, R7 + R8)	9.C-78
Figure 9.C.2-11	Test group F2, phase 3 and 4: atmospheric temperatures in zones 1, 2 and 3 (R5 + R6, R1 + R4, R7 + R8)	9.C-79
Figure 9.C.2-12	Thermodynamic state of steam-air atmosphere in R9 top (H=7.6 m)	9.C-80
Figure 9.C.2-13	Thermodynamic state of steam-air atmosphere in R9 bottom (H=1 m)	9.C-81
Figure 9.C.2-14	Test group F2, phase 2: atmospheric temperatures in R9 (Zone 4)	9.C-82
Figure 9.C.2-15	Test group F2, phase 3 and 4: atmospheric temperatures in R9 (Zone 4)	9.C-83
Figure 9.C.2-16	Velocities in opening from compartment R7 to compartment R9	9.C-84
Figure 9.C.2-17	Velocities in opening from compartment R3 to compartment R6	9.C-85
Figure 9.C.2-18	Vertical cut through BMC with orifice in between R2 and R1	9.C-89
Figure 9.C.2-19a	BMC test no. 2: Comparison between experimental data and 2-d GOTHIC computations for hydrogen concentrations	9.C-90
Figure 9.C.2-19b	BMC test no. 4: Comparison between experimental data and 2-d GOTHIC computations for hydrogen concentrations	9.C-91

LIST OF FIGURES (Cont.)

Figure	Title	Page
Figure 9.C.2-19c	BMC test no. 6: Comparison between experimental data and 2-d GOTHIC computations for hydrogen concentrations	9.C-92
Figure 9.C.2-20	BMC test no. 12: Comparison between experimental data and GOTHIC-lp computations for hydrogen concentrations	9.C-94
Figure 9.C.2-21a	BMC test no. 20: Comparison between experimental data and 2-d GOTHIC computations for hydrogen concentrations	9.C-95
Figure 9.C.2-21b	BMC test no. 20: Comparison between experimental data and 2-d GOTHIC computations for hydrogen concentrations	9.C-96
Figure 9.C.2-21c	BMC test no. 20: Comparison between experimental data and 2-d GOTHIC computations for hydrogen concentrations	9.C-97
Figure 9.C.2-22	Perspective view, vertical and upper horizontal cross-sections through BMC with main steam feedline	9.C-101
Figure 9.C.2-23	Perspective view, vertical and upper horizontal cross-sections through BMC with auxiliary steam feedline	9.C-102
Figure 9.C.2-24	Instrumentation plan for BMC - sump heatup test RX4	9.C-103
Figure 9.C.2-25	Battelle-Experiment RX4: Sump and atmospheric temperatures	9.C-104
Figure 9.C.2-26	Battelle-Experiment RX4: Velocities in side vents	9.C-105

LIST OF FIGURES (Cont.)

Figure	Title	Page
Figure 9.C.2-27	Battelle-Experiment RX4: Temperatures in center compartment and dome	9.C-106
Figure 9.C.2-28	Battelle-Experiment RX4: Temperatures in external annulus	9.C-107
Figure 9.C.2-29	Battelle-Experiment RX4: Hydrogen concentration along circulation path	9.C-108
Figure 9.C.2-30	Battelle-Experiment RX4: Hydrogen concentrations in intermediate subcompartments	9.C-109
Figure 9.C.2-31	Battelle-Experiment RX4: Relative humidity in the containment atmosphere	9.C-110
Figure 9.C.2-32	Model containment used in the test, break-release position, and circulation flow paths (see arrows)	9.C-115
Figure 9.C.2-33	Detailed arrangement of each floor	9.C-116
Figure 9.C.2-34	Distribution of the compartments at each floor	9.C-117
Figure 9.C.2-35	Pressure history	9.C-118
Figure 9.C.2-36	Dome temperature history	9.C-119
Figure 9.C.2-37	Dome Helium Concentration history	9.C-120
Figure 9.C.2-38	a) Temperature histories for compartments forming a circulation path (8, 15, dome and 7) b) Helium concentration histories for compartments forming a circulation path (8, 15, dome and 7)	9.C-121
Figure 9.C.2-39	Carolinas Virginia Tube Reactor (CVTR) containment structure	9.C-126

LIST OF FIGURES (Cont.)

Figure	Title	Page
Figure 9.C.2-40	CVTR steam line diffuser	9.C-127
Figure 9.C.2-41a	Steam injection histories test 1	9.C-128
Figure 9.C.2-41b	Steam injection histories test 2	9.C-129
Figure 9.C.2-41c	Steam injection histories test 3	9.C-130
Figure 9.C.2-42	CVTR containment pressure response (Heise gauge)	9.C-131
Figure 9.C.2-43	Atmospheric vertical temperature profile, test 1	9.C-132
Figure 9.C.2-44	Atmospheric vertical temperature profile, test 2	9.C-133
Figure 9.C.2-45	Atmospheric vertical temperature profile, test 3	9.C-134
Figure 9.C.2-46	Surface and atmosphere temperatures - intermediate region, test 1	9.C-135
Figure 9.C.2-47	Surface and atmosphere temperatures - basement region, test 1	9.C-136
Figure 9.C.2-48	Concrete surface temperatures, test 1	9.C-137
Figure 9.C.2-49	Isolated containment region temperatures	9.C-138
Figure 9.C.2-50	Cross-sections, elevations and numbers of compartments of the HDR containment, left (180°-0° cross-section), right (270°-90° cross-section)	9.C-142
Figure 9.C.2-51	Locations and Enumerations of Thermocouples (left) and Anemomenters (right) of HDR-E-test Series	9.C-143
Figure 9.C.2-52	HDR-E11.2 Sequence of Experimental Test Procedures	9.C-144

LIST OF FIGURES (Cont.)

Figure	Title	Page
Figure 9.C.2-53	HDR-E11.2 Containment pressure history	9.C-145
Figure 9.C.2-54	HDR-E11.2 Atmospheric temperatures along main stairway	9.C-146
Figure 9.C.2-55	HDR-E11.2 Steam concentrations along main stairway	9.C-147
Figure 9.C.2-56	HDR-E11.2 H ₂ /He Gas concentrations along main stairway	9.C-148
Figure 9.C.2-57	HDR-E11.2 Comparison between temperatures in main and spiral stairways at +31.0 m level	9.C-149
Figure 9.C.2-58	HDR-E11.2 Comparison between temperatures in main and spiral stairways at +26.5 m level	9.C-150
Figure 9.C.2-59	HDR-E11.2 Comparison between temperatures in main and spiral stairways at +16.5 m level	9.C-151
Figure 9.C.2-60	HDR-E11.2 Comparison between temperatures in main and spiral stairways at +6 m level	9.C-152
Figure 9.C.2-61	HDR-E11.2 Axial temperature profiles in both major flow paths at specific times, left in spiral stairway, right in main stairway	9.C-153
Figure 9.C.2-62	HDR-E11.3 Velocities in both major flow paths at different axial positions during containment heatup	9.C-155
Figure 9.C.2-63	HDR-E11.3 Velocities in both major flow paths at different axial positions during H ₂ /He gas mixture release	9.C-156
Figure 9.C.2-64	HDR-E11.3 Comparison between temperatures in main and spiral stairways at +31.0 m level	9.C-157

LIST OF FIGURES (Cont.)

Figure	Title	Page
Figure 9.C.2-65	HDR-E11.3 Comparison between temperatures in main and spiral stairways at +26.5 m level	9.C-158
Figure 9.C.2-66	HDR-E11.3 Comparison between temperatures in main and spiral stairways at +16.5 m level	9.C-159
Figure 9.C.2-67	HDR-E11.3 Comparison between temperatures in main and spiral stairways at +6 m level	9.C-160
Figure 9.C.2-68	HDR-E11.3 Axial temperature profiles in both major flow paths at specific times, left in spiral stairway, right in main stairway	9.C-161
Figure 9.C.2-69	HDR-E11.4 Sequence of Experimental Test Procedures	9.C-164
Figure 9.C.2-70	HDR-E11.4 Containment pressure history	9.C-165
Figure 9.C.2-71	HDR-E11.4 Atmospheric temperatures along main stairway	9.C-166
Figure 9.C.2-72	HDR-E11.4 Steam concentrations along main stairway	9.C-167
Figure 9.C.2-73	HDR-E11.4 H ₂ /He gas concentrations along main stairway	9.C-168
Figure 9.C.2-74a	HDR-E11.4 Comparison between temperatures in main and spiral stairways at +31.0 m level	9.C-169
Figure 9.C.2-74b	HDR-E11.4 Comparison between temperatures in main and spiral stairways at +31.0 m level	9.C-170
Figure 9.C.2-75	HDR-E11.4 Comparison between temperatures in main and spiral stairways at +26.5 m level	9.C-171
Figure 9.C.2-76	HDR-E11.4 Comparison between temperatures in main and spiral stairways at +16.5 m level	9.C-172

LIST OF FIGURES (Cont.)

Figure	Title	Page
Figure 9.C.2-77	HDR-E11.4 Comparison between temperatures in main and spiral stairways at +6 m level	9.C-173
Figure 9.C.2-78	HDR-E11.4 Axial temperature profiles in both major flow paths at specific times, left in spiral stairway, right in main stairway	9.C-174
Figure 9.C.2-79	HDR-T31.5 Blowdown mass flow rate into the containment	9.C-178
Figure 9.C.2-80	HDR-T31.5 Steam and H ₂ /He gas mass flow rates into containment	9.C-179
Figure 9.C.2-81	HDR-T31.5 Pressure history after large LOCA over 1200 minutes	9.C-180
Figure 9.C.2-82	HDR-T31.5 Axial temperature profiles along spiral stairway (left) and main stairway (right) for different instants in time	9.C-181
Figure 9.C.2-83	HDR-T31.5 Axial gas concentration profiles along spiral stairway (left) and main stairway (right) in upper containment region at different instants in time	9.C-182
Figure 9.C.2-84	HDR-T31.5 Gas concentrations inside the containment dome	9.C-183
Figure 9.C.2-85a	HDR-T31.5 Velocities over 60 minutes along spiral stairways and associated dome regions	9.C-184
Figure 9.C.2-85b	HDR-T31.5 Velocities over 60 minutes along main stairways and associated dome regions	9.C-185
Figure 9.C.2-86	HDR-V21.1 Arrangement of reactor pressure vessel, blowdown pipe and jet impingement plate for water blowdown test	9.C-189

LIST OF FIGURES (Cont.)

Figure	Title	Page
Figure 9.C.2-87	HDR-V21.1 Containment pressure history	9.C-190
Figure 9.C.2-88	HDR-V21.1 Temperatures in the containment dome	9.C-191
Figure 9.C.2-89	HDR-V21.1 Temperature along the main staircase at different axial positions	9.C-192
Figure 9.C.2-90	HDR-V21.1 Temperatures along spiral staircase at different axial positions	9.C-193
Figure 9.C.2-91	HDR-V21.1 Comparison between temperatures in spiral staircase (H=22.5 m) and main staircase (H=25 m)	9.C-194
Figure 9.C.2-92a	HDR-E11.5 Sequence of Experimental Test Procedures	9.C-198
Figure 9.C.2-92b	HDR-E11.5 Sequence of Experimental Test Procedures	9.C-199
Figure 9.C.2-93	HDR-E11.5 Containment pressure	9.C-200
Figure 9.C.2-94	HDR-E11.5 Containment pressure history	9.C-201
Figure 9.C.2-95	HDR-E11.5 Containment temperatures along main stairway during containment heatup phase	9.C-202
Figure 9.C.2-96a	HDR-E11.5 Temperatures in both major flow paths at the same axial positions for three heights in the containment	9.C-203
Figure 9.C.2-96b	HDR-E11.5 Temperatures in both major flow paths at the same axial positions for three heights in the containment	9.C-204

LIST OF FIGURES (Cont.)

Figure	Title	Page
Figure 9.C.2-96c	HDR-E11.5 Temperatures in both major flow paths at the same axial positions for three heights in the containment	9.C-205
Figure 9.C.2-97a	HDR-E11.5 Axial steam concentration in spiral (left) and main (right) stairways for different instants in time for large break LOCA release in lower containment region	9.C-206
Figure 9.C.2-97b	HDR-E11.5 Axial temperature profiles in spiral (left) and main (right) stairways for different instants in time for large break LOCA release in lower containment region	9.C-207
Figure 9.C.2-98a	HDR-E11.5 Axial H ₂ -He gas mixture concentration profiles along spiral (left) and main (right) stairways during gas release phase (total mass 291 kg)	9.C-208
Figure 9.C.2-98b	HDR-E11.5 Axial steam concentration profiles along spiral (left) and main (right) stairways during gas release phase (total mass 291 kg)	9.C-209
Figure 9.C.2-98c	HDR-E11.5 Axial temperature profiles along spiral (left) and main (right) stairways during gas release phase (total mass 291 kg)	9.C-210
Figure 9.C.2-99a	HDR-E11.5 Gas concentrations in the major flow paths and in regions and subcompartments away from the stairways (H=22m up to 27 m)	9.C-211
Figure 9.C.2-99b	HDR-E11.5 Gas concentrations in the major flow paths and in regions and subcompartments away from the stairways (H=22m up to 27 m)	9.C-212

LIST OF FIGURES (Cont.)

Figure	Title	Page
Figure 9.C.2-100a	HDR-E11.5 Gas concentrations in the major flow paths and in regions and subcompartments away from the stairways (H=-4.5m up to +2.0 m)	9.C-213
Figure 9.C.2-100b	HDR-E11.5 Gas concentrations in the major flow paths and in regions and subcompartments away from the stairways (H=-4.5m up to +2.0 m)	9.C-214
Figure 9.C.2-101a	HDR-E11.5 Velocities in the main stairway during blowdown	9.C-215
Figure 9.C.2-101b	HDR-E11.5 Velocities in the spiral stairway during blowdown	9.C-216
Figure 9.C.2-102a	HDR-E11.5 Velocities in the main stairway during containment heatup phase	9.C-217
Figure 9.C.2-102b	HDR-E11.5 Velocities in the spiral stairway during containment heatup phase	9.C-218
Figure 9.C.2-103a	HDR-E11.5 Velocities in the main stairway during H ₂ -He gas mixture release phase	9.C-219
Figure 9.C.2-103b	HDR-E11.5 Velocities in the spiral stairway during H ₂ -He gas mixture release phase	9.C-220
Figure 9.C.2-104a	HDR-E11.5 Velocities in the main stairway during sump heatup and boiling phase	9.C-221
Figure 9.C.2-104b	HDR-E11.5 Velocities in the spiral stairway during sump heatup and boiling phase	9.C-222
Figure 9.C.3-1	Dome pressure history	9.C-232
Figure 9.C.3-2a	Temperature history inside node 8	9.C-233

LIST OF FIGURES (Cont.)

Figure	Title	Page
Figure 9.C.3-2b	Helium concentration inside node 8	9.C-234
Figure 9.C.3-3a	Temperature history inside node 15	9.C-235
Figure 9.C.3-3b	Helium concentration inside node 15	9.C-236
Figure 9.C.3-4a	Temperature history inside dome	9.C-237
Figure 9.C.3-4b	Helium concentration history inside dome	9.C-238
Figure 9.C.3-5a	Temperature history inside node 7	9.C-239
Figure 9.C.3-5b	Helium concentration inside node 7	9.C-240
Figure 9.C.3-6	HDR-E11.5: Comparison between measured long-term containment pressure and GOTHIC open post-test prediction	9.C-243
Figure 9.C.3-7	HDR-E11.5: Comparison between measured sump temperature and GOTHIC open post-test prediction	9.C-244
Figure 9.C.3-8	HDR-E11.5: Comparison between measured temperature in main stairway (6m) and GOTHIC open post-test prediction	9.C-245
Figure 9.C.3-9	HDR-E11.5: Comparison between measured temperature in spiral stairway (6m) and GOTHIC open post-test prediction	9.C-246
Figure 9.C.3-10	HDR-E11.5: Comparison between measured gas mixture concentration in main stairway (6m) and GOTHIC open post-test prediction	9.C-247
Figure 9.C.3-11	HDR-E11.5: Comparison between measured gas mixture concentration in spiral stairway (6m) and GOTHIC open post-test prediction	9.C-248

LIST OF FIGURES (Cont.)

Figure	Title	Page
Figure 9.C.3-12	HDR-E11.5: Comparison between measured velocity in main stairway (15m) and GOTHIC open post-test prediction	9.C-249
Figure 9.C.3-13	HDR-E11.2: Comparison between measured long-term containment pressure and various "optimized" open post-test predictions	9.C-250

9.C.1 DEVELOPMENT OF EXPECTED FLOW PATTERNS FOR AP600 AND AP1000 BASED ON SEPARATE FLOW TESTS IN ENCLOSURES

9.C.1.1 STRATIFICATION PHENOMENA

Stratification is the formation of horizontal layers of constant density. Stratified layers are stable if the density of the layers decreases in the upward vertical direction (the gradients of density are negative in z direction according to Figure 9.C.1-1a) and if forced convection mixing is not sufficiently strong to disrupt the stable fluid layers.

Another more general definition of stratified conditions is that gradients of density in the horizontal direction are small, except in jets, buoyant plumes, and small regions near the vertical walls inside boundary layers (wall jets). In most of the volume, the density gradients in z direction are negative, while inside the jets, wall jets, and buoyant plumes they could be positive (see Figure 9.C.1-1b).

Stratification occurs as a consequence of the temperature or concentration gradients in the vertical direction. Increasing temperatures or decreasing concentrations of heavier mixture components with increasing elevation promote stratification. The existence of flow structures, such as jets, plumes, and vertical wall boundary layers, decreases the "steepness" of the vertical density gradients.

Examples of stratified conditions are numerous. Stratified layers are observed as large-scale geophysical phenomena (in lakes, sea, and oceans, in atmosphere - stratus clouds), as well as inside the enclosures. For example, warmer air tends to gather below ceilings in energy storage devices, nuclear reactors, solar collectors, and enclosures under the influence of the spread of fire and smoke.

This appendix discusses the stratification phenomena inside a nuclear reactor containment. Possible reasons for the stratification will be specified. Stratification may occur if:

- 1) The upper boundary is at the higher temperature than the lower boundary (see Figure 9.C.1-2a), as well as for other similar combinations of temperature boundary conditions at the outside and inside surfaces (see Figure 9.C.1-2b - d).
- 2) A higher concentration of the heavier or lighter components of the mixtures is maintained (by injecting and removing) near the lower or upper boundaries of the enclosure, respectively.
- 3) A lighter fluid is released (permanently, or from time to time) and captured below the ceiling of the containment.

- 4) The release point of the lighter/heavier fluid is closer to the top/bottom.
- 5) The shape of the enclosure promotes stratification (tall elongated enclosure).
- 6) The distribution of the non-complete vertical partitions suppresses fluid flow in the upper portions of the enclosure.
- 7) The distribution and size of the horizontal openings suppresses the fluid flow in vertical direction.
- 8) The internal heat sources (sinks) are positioned in the upper (lower) portions of the enclosure.

Under the conditions above (or a combination of them), the stratification may be stable. The presence of stratified layers inhibits circulation, that otherwise could be induced by a jet, plume, or boundary layers. The conduction and diffusion, heat and mass transfer processes, respectively, are dominant. As a result, the overall heat and mass transfer decreases and the heat transfer through the containment shell is slowed.

One way to avoid the stratification is to generate fluid flow patterns inside the enclosure using forced convection. Additional devices such as fans, sprays, or nozzles are necessary, as well as associated power supplies and controls.

Since the AP600 and AP1000 rely on a passive containment cooling system (PCS), only the effects of fluid circulation due to the interaction of natural convection with the stratified field are discussed.

Modifications to the shape of the enclosure, the distribution and size of the internal partitions, and the openings could be made to avoid stratification. A different distribution of heat sources could also be applied to generate natural convection effects. The fluid flows due to natural convection promote better circulation inside the enclosure. The introduction of jets may also interrupt stably stratified layers through better mixing of the layers of various densities and concentrations. With a jet stratification may become unstable or, at least, the vertical gradient reduced. With only natural convection if the generated buoyancy forces are strong enough, the entire volume of the enclosure will be affected, resulting in the relatively uniform values of temperature and concentration fields. Natural convection heat transfer is dominant and the more intensive circulation improves the transfer of heat from the containment. Natural convection flow effects are generated spontaneously due to the gravity (buoyancy forces) when heated sources exist, so that additional control and other devices are not necessary.

9.C.1.1.1 Static Stratification

Static stratification occurs if the upper horizontal boundary of the domain is maintained at a higher temperature than lower boundary, as in Fig. 9.C.1-1a. Stratification also occurs if the concentration of heavy components is low in the mixture in the upper portion of the domain. The fluid layers are undisturbed and fluid motion is negligible. The temperature or density distribution in the vertical direction is linear. Heat transfer is predominantly governed by conduction, while mass transfer is driven by diffusion. The formed fluid layers are stable and communicate only with the neighboring upper and lower layers. The resulting heat and mass transfer rates are low.

Corresponding experimental results are found in Akino et al., 1989 and Hiller et al., 1988. In both papers, stable stratified layers are identified using various colors reflected by liquid crystals (suspended in the fluid).

Static stratification exists inside a containment vessel if the temperature distribution of the vertical walls is the same as in the surrounding stratified fluid (adiabatic vertical walls, as in Fig 9.C.1-1a). Since, the top of the passive containment, as well as the vertical walls, are exposed to the surrounding air and cooled by natural convection, stable stratification is not present. Even small temperature differences between the air inside and outside the containment produce large Grashof (Rayleigh) numbers, due to the height of the containment ($H_T=109$ ft). For example, a temperature difference of 9°F between the air at the deck level and the air below the dome ceiling results in $Gr_T = 2.2 \cdot 10^{13}$. This is in the range of chaotic turbulent flow, characterized by upward and downward plumes (see experimental results by Akino et al., 1989).

Static stratified layers are also generated by releasing a lighter gas, e.g., steam or hydrogen, into the upper portion of the containment and capturing the gas beneath the dome.

Hydrogen distribution experiments performed in the HDR facility, test group E11, combine high hydrogen release rates with superheated steam injection into the containment (see Wolf et al., 1994a). A comparison of influences of the axial break and gas release positions is obtained with E11.2 (high release position) and E11.4 (low release position) experiments. Although these two specific experiments simulate severe accident scenarios, comparison of results from the two experiments provides insights into the physics of stratification. The tests are characterized by boundary conditions that can promote circulation (especially test E11.4). They also show that relatively small concentration gradients can exist in the presence of circulation.

Steam release from small breaks generates thermal stratification for break positions located at the higher level, with the hot zone above the break locations. Two mechanisms are used to break up the established thermal stratification. The first mechanism used subsequent steam releases at positions lower than the original release to break up the established thermal stratification. This mechanism did not produce

homogeneously mixed conditions. The second method is the application of external sprays on the upper dome. This causes condensation on the inner surface and a decrease in the temperature in the upper part of the dome. Convective flows form and affect the whole volume of the dome and lower compartments, resulting in a completely homogenized atmosphere.

As in the HDR E11.2 experiment, condensation on the dome of the passive containment breaks up stratification. The condensation on the vertical walls also contributes to breaking of stratified layers and to entrainment in the vertical boundary layers. The circulation inside the containment affects the lower compartments and promotes circulation due to the natural convection.

The shape of an enclosure could also promote stratification. One example is natural convection inside romb shaped enclosures (see Figure 9.C.1-3). Stratification is generated if the upper vertical side is at a high temperature and the inclined top and bottom sides are adiabatic (see, Dzodzo, 1993). The overall heat and mass transfer are suppressed by the presence of the stratified fluid in the upper and lower corners of the romb shaped enclosures. When the boundary conditions are reversed, i.e., the lower vertical side is at the higher temperature, the entire volume of the enclosure is effected by circulation. Heat transfer is intensified and stratified layers are not present in the upper and lower corners. A comparison of experimentally and numerically obtained temperature and velocity fields for these two cases is presented in Figure 9.C.1-4. An overview of the numerical results for various angles of the romb (parallelogram-shaped) enclosures, Prandtl numbers, and aspect ratios is presented by (Hyun and Choi, 1990).

Although the top of the passive containment is somewhat conical in shape, stratification in the upper portion of the dome would not exist because of the natural convection due to the lower temperatures of the ceiling and vertical walls. Stratification effects are promoted if the containment ceiling is insulated or at a higher temperature.

The distribution of the internal heat sources in the upper part and heat sinks in the lower part of enclosures promotes the formation of the stratified layers (see Figure 9.C.1-2 b, c, d). Examples of the influence of the position and distance between the heat source and heat sink are provided by A. Kurosawa et al., 1993 and C. J. Ho et al., 1994. An example of the influence of an array of discrete heat sources on natural convection is presented by T. J. Heindel et al., 1995.

Vertical non-complete partitions inside an enclosure contribute to the stratification. If the non-complete vertical partition is positioned near the ceiling, flow in the upper part of the enclosure is obstructed and a stagnant stratified region near the ceiling is formed (see Hanjalic et al., 1996, and Nowak and Novak, 1994 for examples of the two-dimensional numerical simulation, and T. Fusegi et al., 1992, for the

three-dimensional simulation). This is of special interest for the analysis of the spread of fire and smoke inside the buildings. Such partitions do not exist above the operating deck level in the passive containment.

Narrow horizontal openings between upper and lower compartments also suppress circulation and cause stratification. The results of a two-dimensional numerical simulation (R. Frederick and A. Valencia, 1995) show the influence of the size of the horizontal openings on the natural convection inside the vertically connected enclosures.

The potential for stratification in compartments below the operating deck of containments, due to the various sizes of the openings is also studied (see ref. Wolf et al., 1994b).

9.C.1.1.2 Stratification and Circulation

Figure 9.C.1-1b illustrates conditions where a portion of an enclosure is stratified and other portions are affected by strong recirculation zones and currents. Due to the circulation effects, shallow vertical density gradients are present inside the stratified portion of the enclosure volume.

Convective heat and mass transfer that results from communication between the stratified and flow-affected zones, contributes to the mixing between the zones with different temperatures, concentrations, and densities. Flow inside the enclosure is promoted by the existence of the entraining wall layers (which are a consequence of the heat transfer), penetrating jets, and buoyant plumes (see reference, Peterson, 1994 and Figure 9.C.1-1b).

To gain insight into passive containment physics, we will start with small-scale enclosure examples and progress to larger scale.

9.C.1.1.2.1 Interaction of Wall Jets (Boundary Layers) with Stratified Layers

One example of interaction of wall jets with stratified layers is the natural convection inside a square enclosure (see Figure 9.C.1-5). The opposite vertical walls of the enclosure are at the different temperatures and the horizontal walls are adiabatic (see Markatos and Pericleous, 1984 and Figure 9.C.1-5a). With high Rayleigh numbers (over 10^6), $Pr=0.71$, turbulent flow exists inside the enclosure. Velocity and temperature gradients are large in the boundary layers. Velocities have maximum values near the walls, while inside the core of the enclosure they are small. The temperature (density) field in the core of the enclosure is stratified (see Figure 9.C.1-5c). Communication exists between the boundary layer region and core of the enclosure through the vortices (see Figure 9.C.1-5b), which change in number, position, and intensity for various temperature differences between the opposite walls (various Ra numbers). Temperature gradients are highest

in the boundary layers near the vertical and horizontal walls (see Figure 9.C.1-5c). For the laminar convection ($Ra=10^{+4}$ and $Ra=10^{+5}$), the temperature difference between the highest and lowest points at the vertical axis of the stratified core is $0.6*(T_h - T_c)$, while for the turbulent regime ($Ra= 10^{+8}$, 10^{+12} , 10^{+16}) it is $0.4*(T_h - T_c)$. The decrease in the vertical temperature gradients inside the stratified core for the turbulent regime is the result of higher velocities and stronger circulation inside the cavity. The temperature field inside the core of the enclosure is stratified, while recirculation due to convection inside the enclosure is predominantly near the walls. Despite the presence of the stratified core, for high Ra numbers, a fluid particle travels the entire enclosure (due to the convection) and contributes to better mixing and decreases the vertical gradients inside the core.

The increase of the Rayleigh number corresponds with a decrease in the thickness of the boundary layers, an increase in the temperature gradients inside the boundary layers, and an increase in the heat transfer rate. The dependence of the average Nusselt numbers on the Rayleigh numbers is presented in Figure 9.C.1-6.

A similar two-dimensional flow pattern and stratified temperature (density) field is also obtained between two opposite vertical line jets (see Figure 9.C.1-7) as discussed in Baines and Turner, 1969.

A numerical analysis (Markatos and Pericleous, 1984) is performed for a two-dimensional plane, assuming that the influence of the front and back walls of real three-dimensional enclosures is not significant. For Rayleigh numbers greater than 10^6 , the k- ϵ turbulence model is used. Due to time-averaging, the numerical results do not show either the instability mechanisms during the transition from laminar to turbulent flow, or the resulting oscillations that would result from solving the time dependent Navier-Stokes equations.

Experimental and numerical results for three-dimensional enclosures are provided by Hiller et al. 1989, Mallinson and de Vhal Davis, 1977, respectively. The results indicate that observed vortices, which affect mixing inside the core of the enclosure, communicate between the front and back walls through the middle of the enclosure, thus enhancing mixing due to three-dimensional circulation effects (see Figure 9.C.1-8).

Reviews of various aspects of confined convective flows, including the interactions between boundary layers near the bounding walls and core and the effects of the cavity aspect ratio, inclination angle, and thermal boundary conditions on flow patterns, are presented by Ostrach 1972, 1982, Catton, 1978, Hoogendoorn, 1986 and Allard, 1992. A state of the art review of the analyses of two-dimensional and three-dimensional transient effects on the natural convection flows in sidewall heated enclosures is presented by T. Fusegi and J. M. Hyun, 1994.

R. J. Janssen and R.A.W.M Henkes, 1995 simulated the instability mechanisms and the transition from laminar to turbulent (oscillatory and finally chaotic) flow regimes inside a two-dimensional square enclosure with differentially heated vertical walls and adiabatic horizontal walls by solving the time-dependent Navier-Stokes equations. The results indicate that the transition from laminar to chaotic flow (for $Pr < 2.0$) is through periodic and quasi-periodic flow regimes. The periodic, quasi-periodic and chaotic flow regimes are established for Prandtl number 0.71 and Rayleigh numbers $2 \cdot 10^8$, $3 \cdot 10^8$ and $7.5 \cdot 10^8$. Internal waves corresponding to fluctuations in the temperatures at $Ra = 2 \cdot 10^8$ are presented in Figure 9.C.1-9. The temperature differences in the entire core of the enclosure are small, $0.004 \cdot (T_h - T_c)$. The predicted temperature differences inside the core of the enclosure are much smaller than those predicted by $k-\epsilon$ turbulence model (Markatos and Pericleous, 1984). This indicates that temperature gradients inside the boundary layers are greater (isotherms inside the thermal boundary layer are not presented in Figure 9.C.1-9) and heat transfer is more intensive than calculated by $k-\epsilon$ model.

Two instability mechanisms influence the transition to turbulent (chaotic) flow regime. The first instability is a Kelvin-Helmholtz type instability (as in a plane jet with inflection points in the velocity profile) in the fluid layer exiting from the corners (where the vertical boundary layers are turned horizontal). The second source of the instability is related to the instability in the boundary layer near the vertical walls. The instability inside the enclosure vertical boundary layers is mechanically (shear) driven. Both regions of the instability origins (hot and cold intrusions from corners and boundary layer waves) are presented in the Figure 9.C.1-10 (from S. Armfield and R. Janssen, 1996). The figure presents temperatures for the initial solution, i.e., immediately after setting the left and right vertical boundaries to $\Delta T/2$ and $-\Delta T/2$, respectively. For values of Rayleigh numbers greater than 10^9 , the turbulent oscillatory and chaotic flow affects the stratified layers inside the core of the enclosure. If the radius ($H_v = 65$ ft) of the containment is taken as a characteristic length (as a distance between the hot buoyant jet plume in the center and cold vertical wall boundary layers), a 9°F temperature difference results in a Grashof number $Gr_v = 4.7 \cdot 10^{12}$.

9.C.1.1.2.2 Interaction of jets or plumes with the stratified layers

The penetration of a stratified layer by a jet is another example where a portion of an enclosure is stratified and another portion is affected by strong recirculating zones (Figure 9.C.1-1b). Depending upon the strength of the jet and the depth of the stratified layers, portions of the enclosure are affected by interaction between the jet and stratified layers. A portion of the stratified fluid is entrained by the jet, decreasing the average jet velocity. The jet penetrates upward (Garrad and Patrick, 1983, So and Aksoy, 1993, and Porterie et al., 1996), or downward (Markatos and Pericleous, 1984, see Figure 9.C.1-5 b and c near the cool wall). A negatively buoyant jet, as presented in Kapoor and Jaluria, 1993, is also possible.

The upward penetrating jet is of interest for LOCA or MSLB accident scenarios. Scaling and analysis of mixing in large stratified volumes for the cases of upward penetrating jets is presented by Peterson, 1994.

If the strength of the jet is strong enough, it produces fluid flow below the ceiling. After reaching the vertical side walls, the flow results in downward negatively buoyant jets (see Figure 9.C.1-11 a and b).

The downward, negatively buoyant penetrating jet (Kapoor and Jaluria, 1993, see Figure 9.C.1-11a and 1-11b) is of interest for the analysis of the flow patterns inside the upper-deck region (Figure 9.C.1-11a), as well as for the compartments below the dome floor (Figure 9.C.1-11b). If the strength of the negatively buoyant jet is not high, it is not able to reach compartments below the deck. The direction of the flow changes as presented in Figure 9.C.1-11a. The redirection of the flow causes additional entrainment of the surrounding fluid, thus contributing towards the increase of the circulation (and mixing) inside the upper-deck region. The correlations for entrainment rates in the negatively buoyant jets are presented in Kapoor and Jaluria, 1993.

If the strength of the negatively buoyant jets is high, it is able to penetrate into the below-deck compartments. There are indications from large-scale tests conducted by Westinghouse (tests 222.3 and 222.4, 3-inch pipe, elevated 6 ft, pointed at the wall and up, respectively, see F. E. Peters, WCAP-14135, July 1994) which simulate the MSLB, that the entire volume of the containment has almost the same steam concentration. This occurs despite the fact that formation of the global circulation loop between the lower-deck compartments and upper dome regions is not possible. An explanation is that the kinetic energy of the jets is high enough to provide downward penetration of the negatively buoyant jets into the below-deck compartments.

Depending upon the distribution of compartments below the dome floor and the number, size and distribution of openings between the compartments and the dome region, various flow patterns are possible inside the compartments. A portion of the downward vertical plumes produced by natural convection (wall boundary layers) or the negatively buoyant jets produced by strong vertical upward penetrating jet into the dome region enters horizontal openings in the compartments, thus promoting circulation and flow inside the compartments below the deck. Fluid flows upward to the dome through other compartment horizontal openings to preserve overall mass continuity and to close the global circulation loop (see Figure 9.C.1-11b).

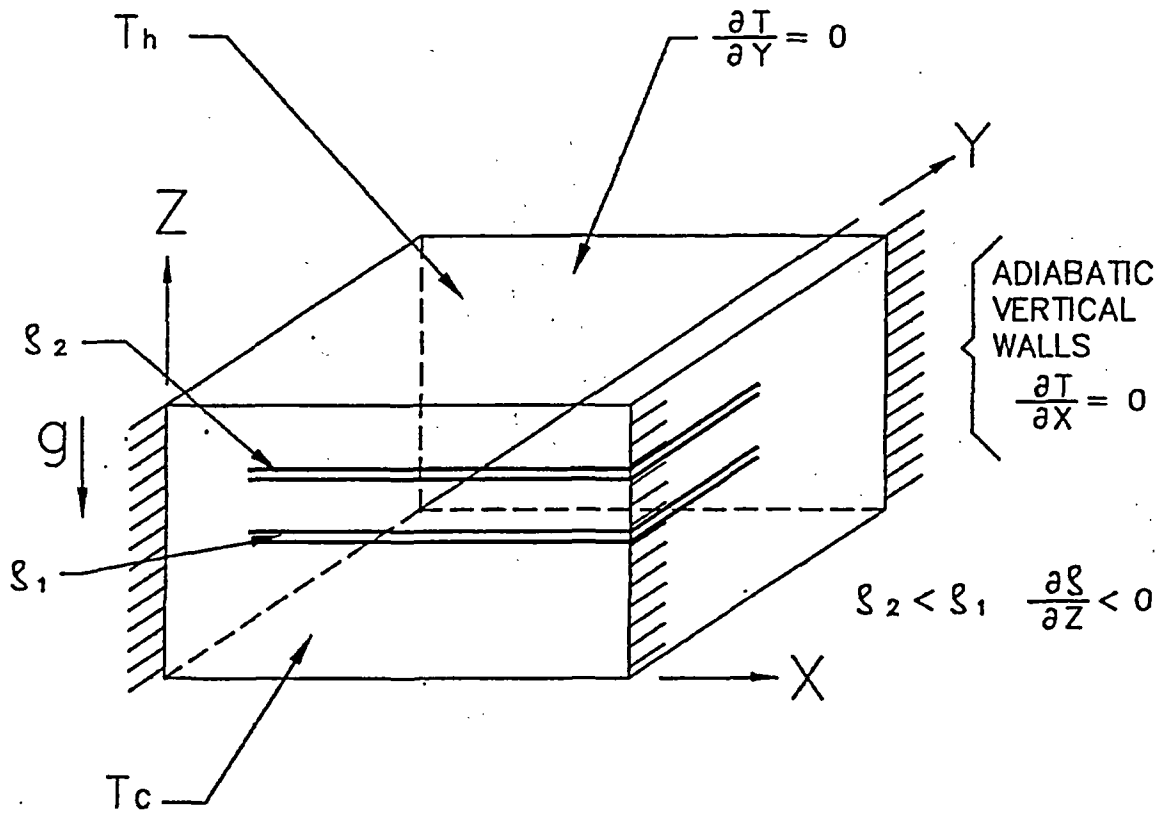
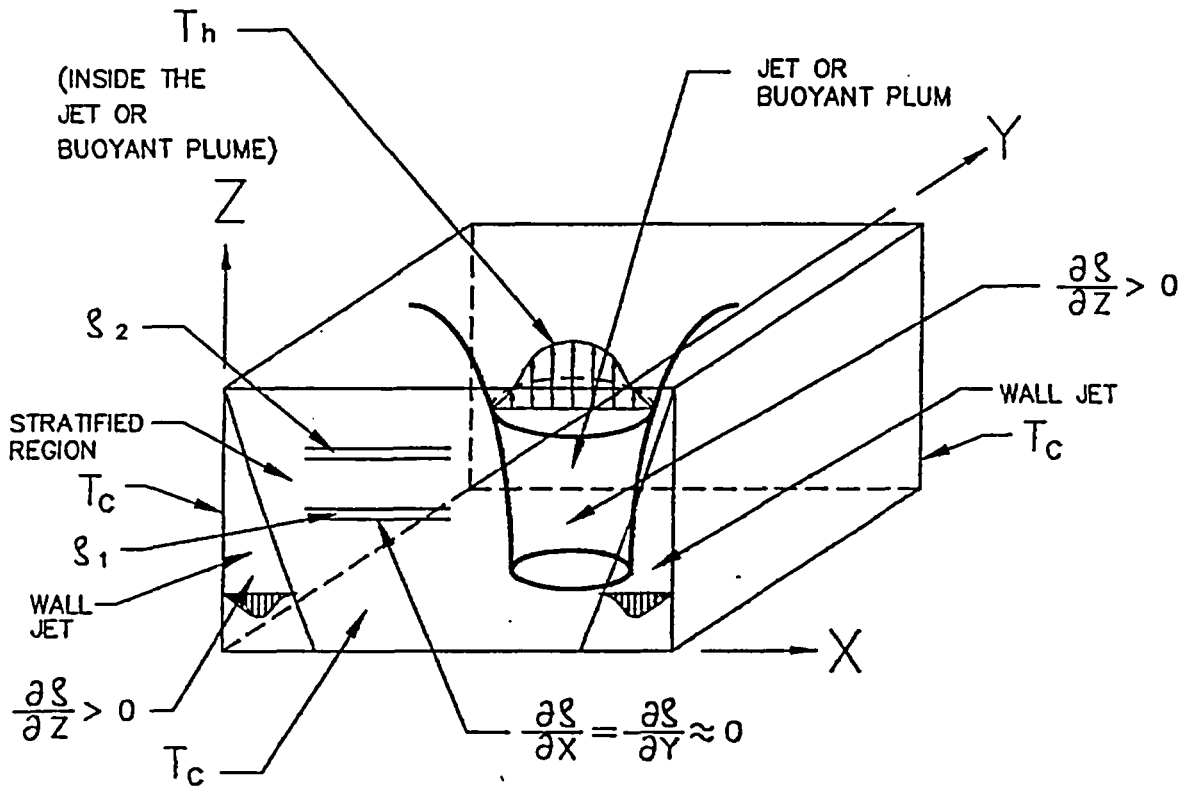


Figure 9.C.1-1a The formation of the horizontal layers of the constant density due to the stratification



STRATIFIED REGIONS $\left(\frac{\partial \rho}{\partial X} = \frac{\partial \rho}{\partial Y} = 0, \frac{\partial \rho}{\partial Z} < 0 \right)$ AND
 JET REGIONS $\left(\frac{\partial \rho}{\partial X} \neq 0, \frac{\partial \rho}{\partial Y} \neq 0, \frac{\partial \rho}{\partial Z} > 0 \right)$ INSIDE
 THE ENCLOSURE.

Figure 9.C.1-1b Interaction of jets, plumes and wall boundary layers with stratified regions

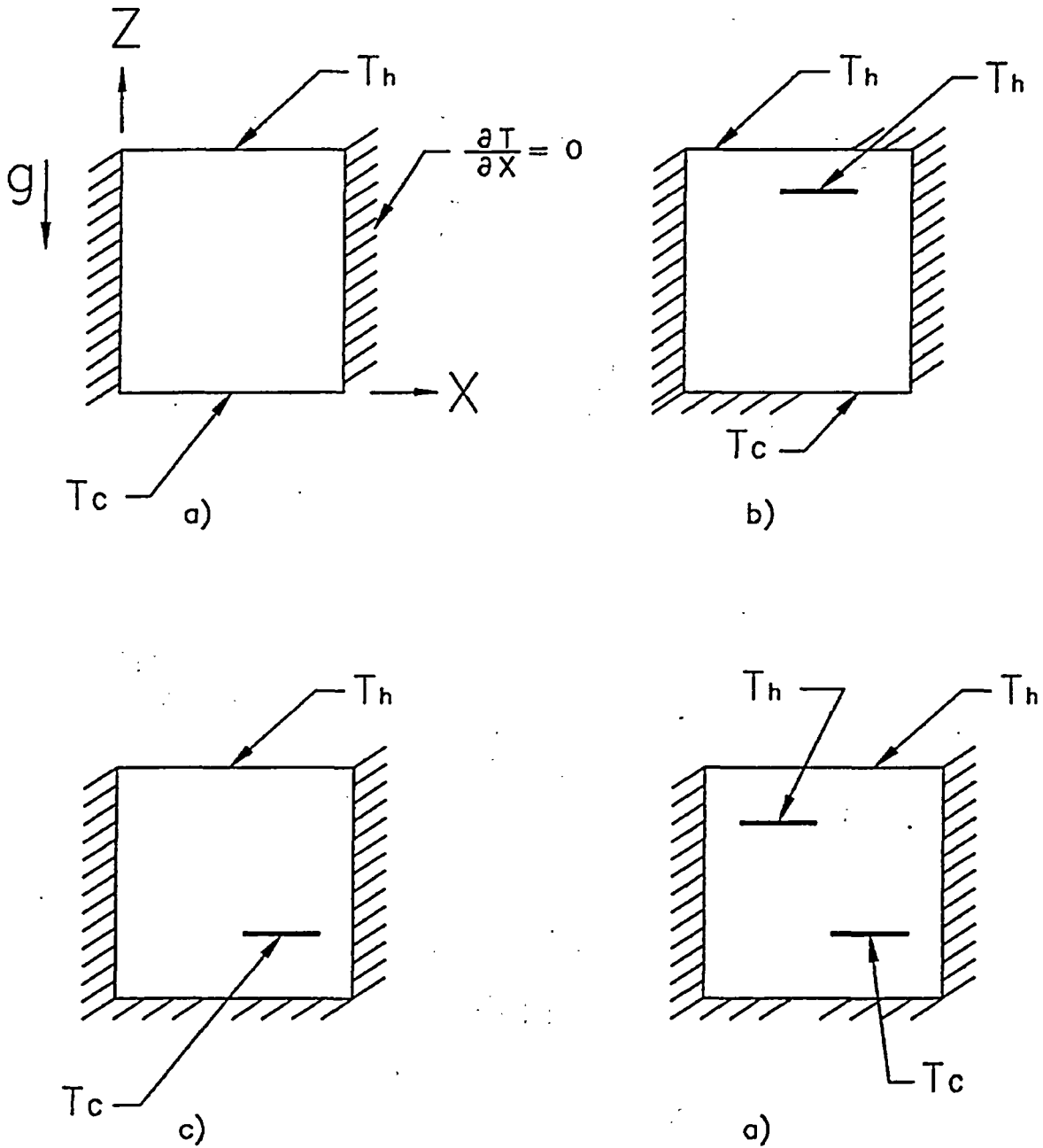


Figure 9.C.1-2 Combination of the constant temperature boundary conditions at the outside and inside surfaces which will produce stratification inside the enclosure

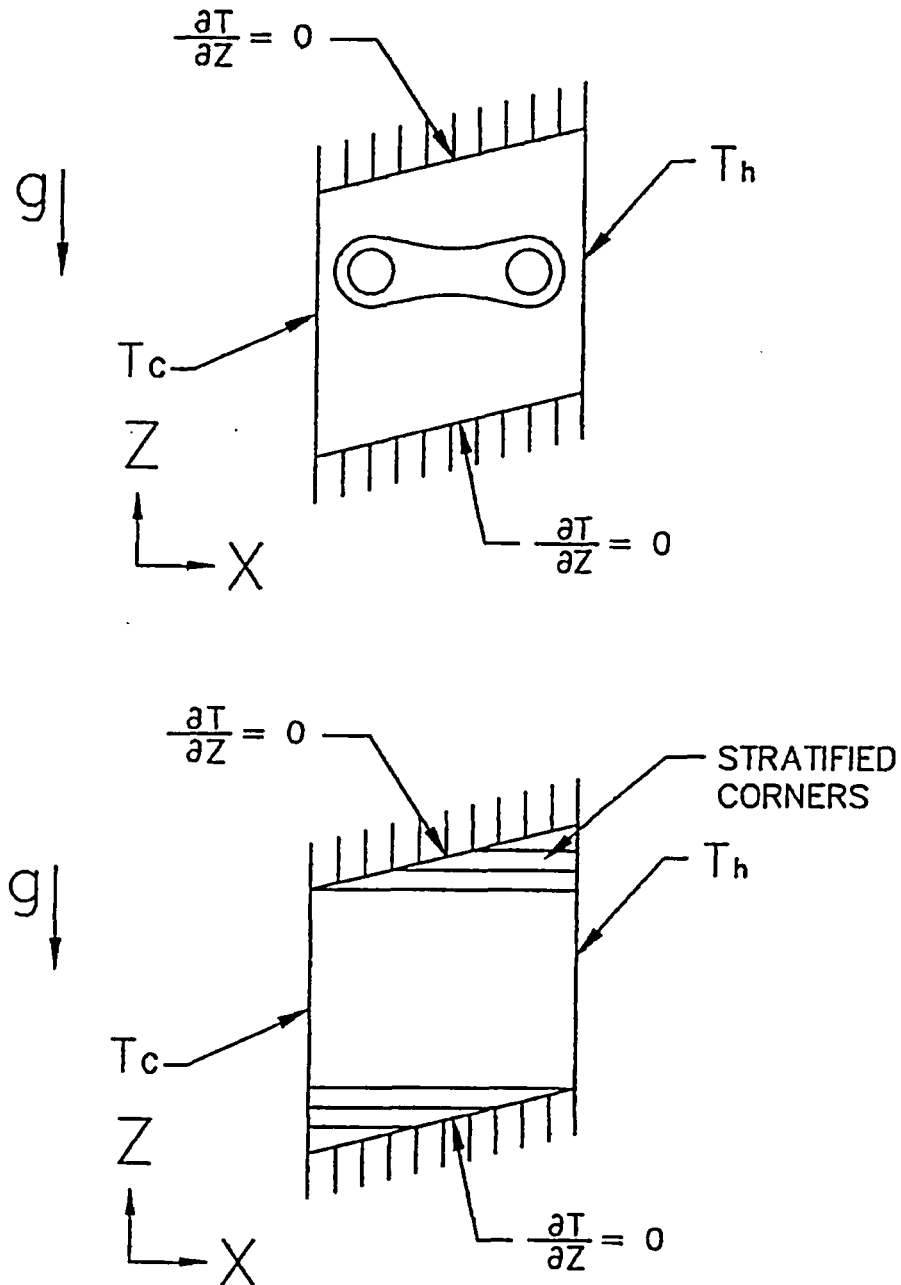


Figure 9.C.1-3 Stratification inside the upper and lower corners of the romb-shaped enclosure

Example of the Stratification Caused by the Shape of the Enclosure and Distribution of the Boundary Conditions

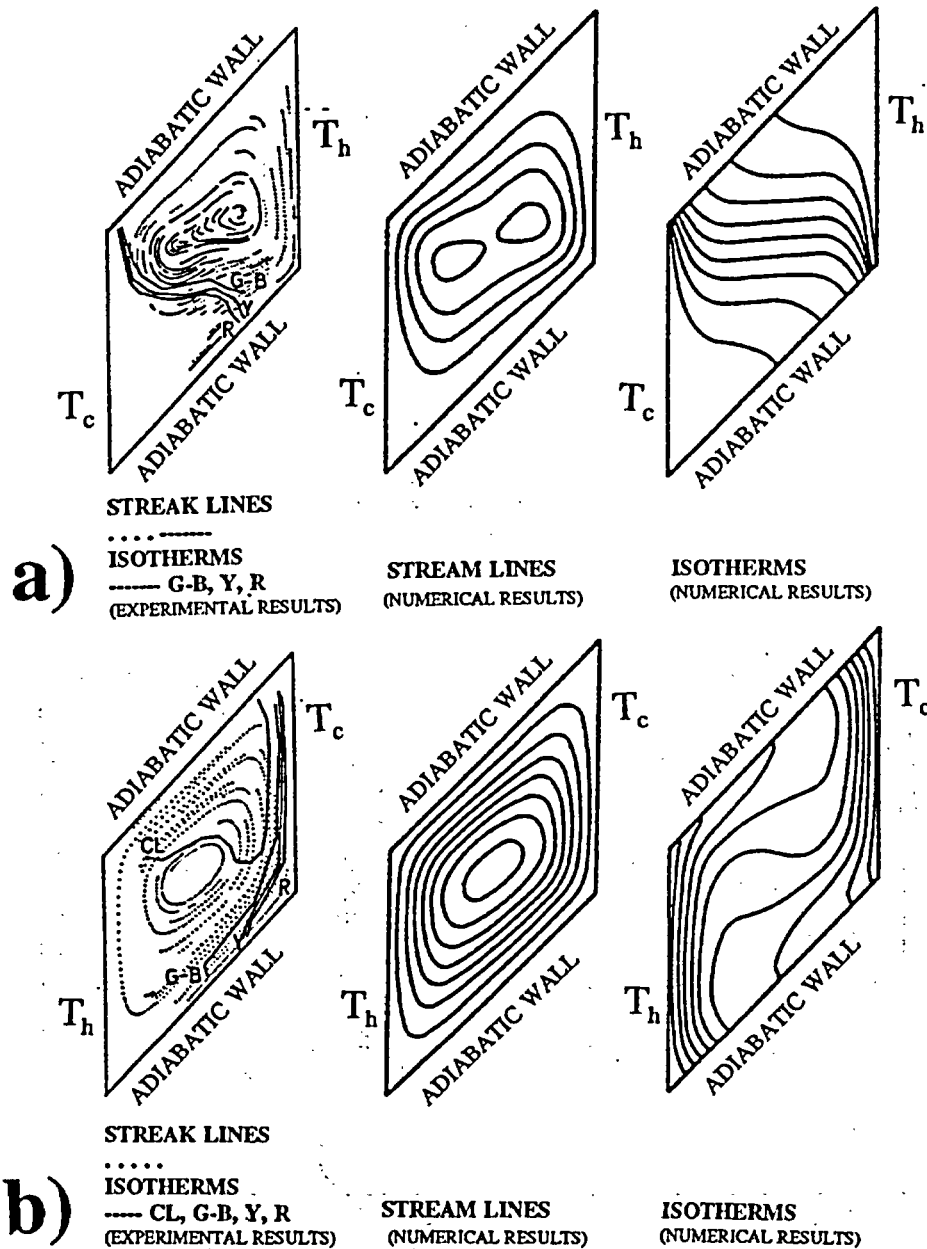


Figure 9.C.1-4 Experimental and numerical results for the romb-shaped enclosure with the romb angle 44° and $Ra=3.5 \cdot 10^4$, $Pr=5270$.

- a) results for the upper vertical wall at the higher temperature
- b) results for the lower vertical wall at the higher temperature

(Reprinted from: M.B. Dzodzo, "Visualization of laminar natural convection in romb-shaped enclosures by means of liquid crystals", in Imaging in transport processes (ed. S. Sideman and K. Hijikata), Begel House, Inc., 1993, pp. 183-193)

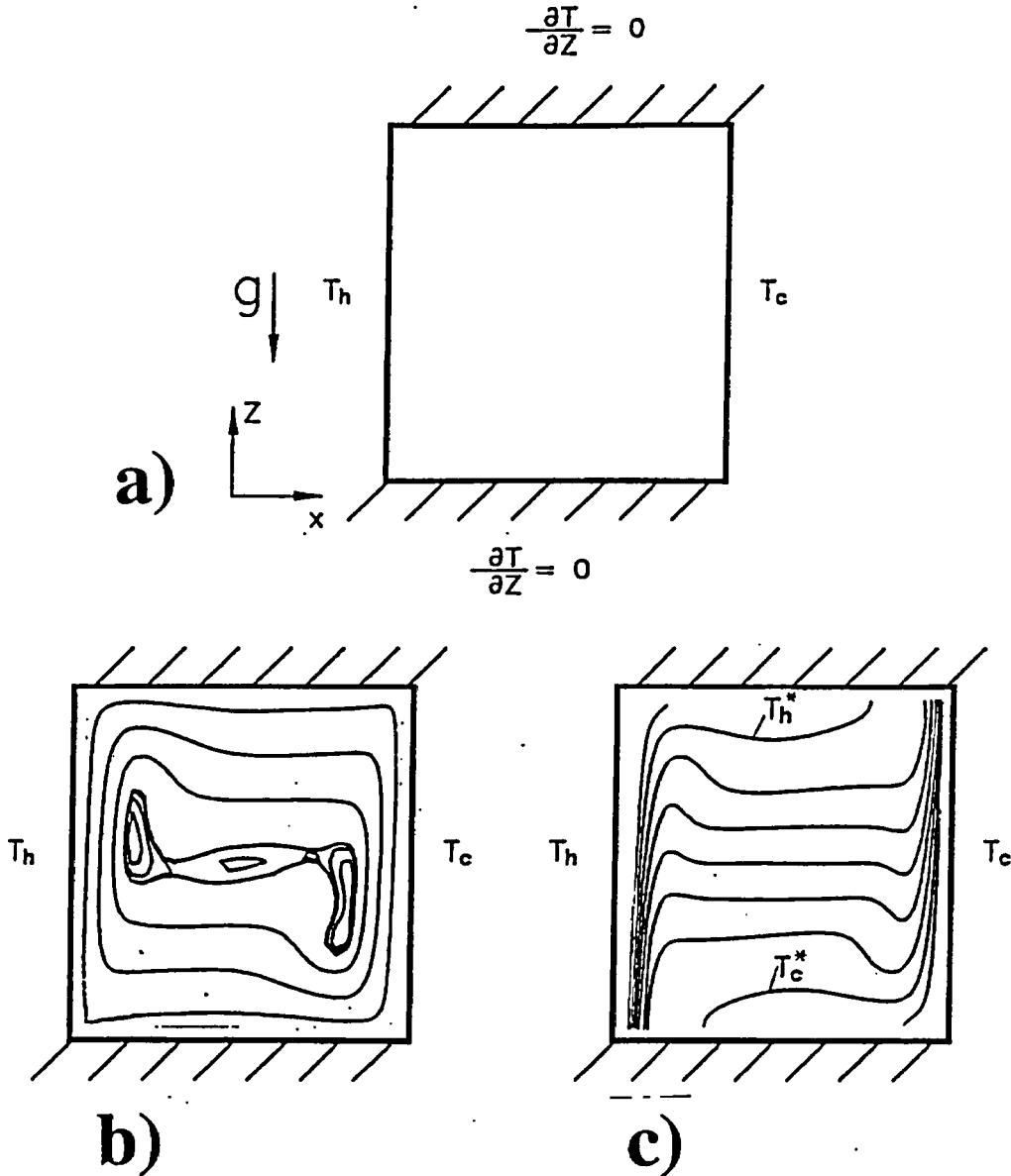


Figure 9.C.1-5 a) The square enclosure with vertical walls at the different temperatures and horizontal walls adiabatic, b) Streamlines for $Ra=10^6$ and $Pr=0.71$, c) Isotherms for $Ra=10^6$ and $Pr=0.71$

"Reprinted from N.C. Markatos and K.A. Pericleous/Laminar and Turbulent Natural Convection in an Enclosed Cavity, Int. J. Heat Mass Transfer, Vol. 27, No. 5, pp. 755-772, 1984, Copyright 1984, Figure 9.C.5(d) and 6(d), with kind permission from Elsevier Science Ltd, The Boulevard, Langford Lane, Kidlington OX5 1GB, UK"

Ra	10^3	10^4	10^5	10^6	10^8	10^{10}	10^{12}	10^{14}	10^{16}
Nu	1.108	2.201	4.430	8.754	32.045	156.85	840.13	3624.4	11226

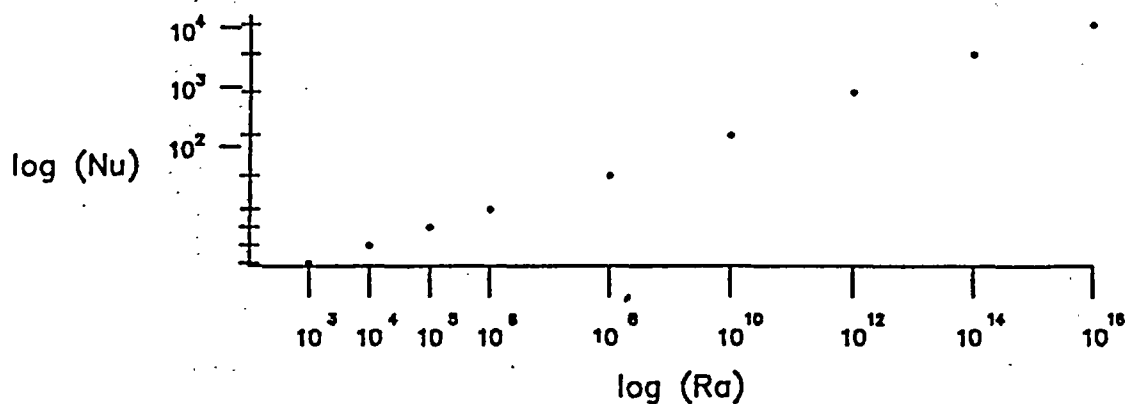


Figure 9.C.1-6 Average Nusselt numbers as a function of the Rayleigh numbers for the square enclosure with opposite vertical walls at the different temperature and Pr=0.71 (air)

(according to N.C. Markatos and K.A. Pericleous/Laminar and Turbulent Natural Convection in an Enclosed Cavity, Int. J. Heat Mass Transfer, Vol. 27, No. 5, pp. 755-772, 1984)

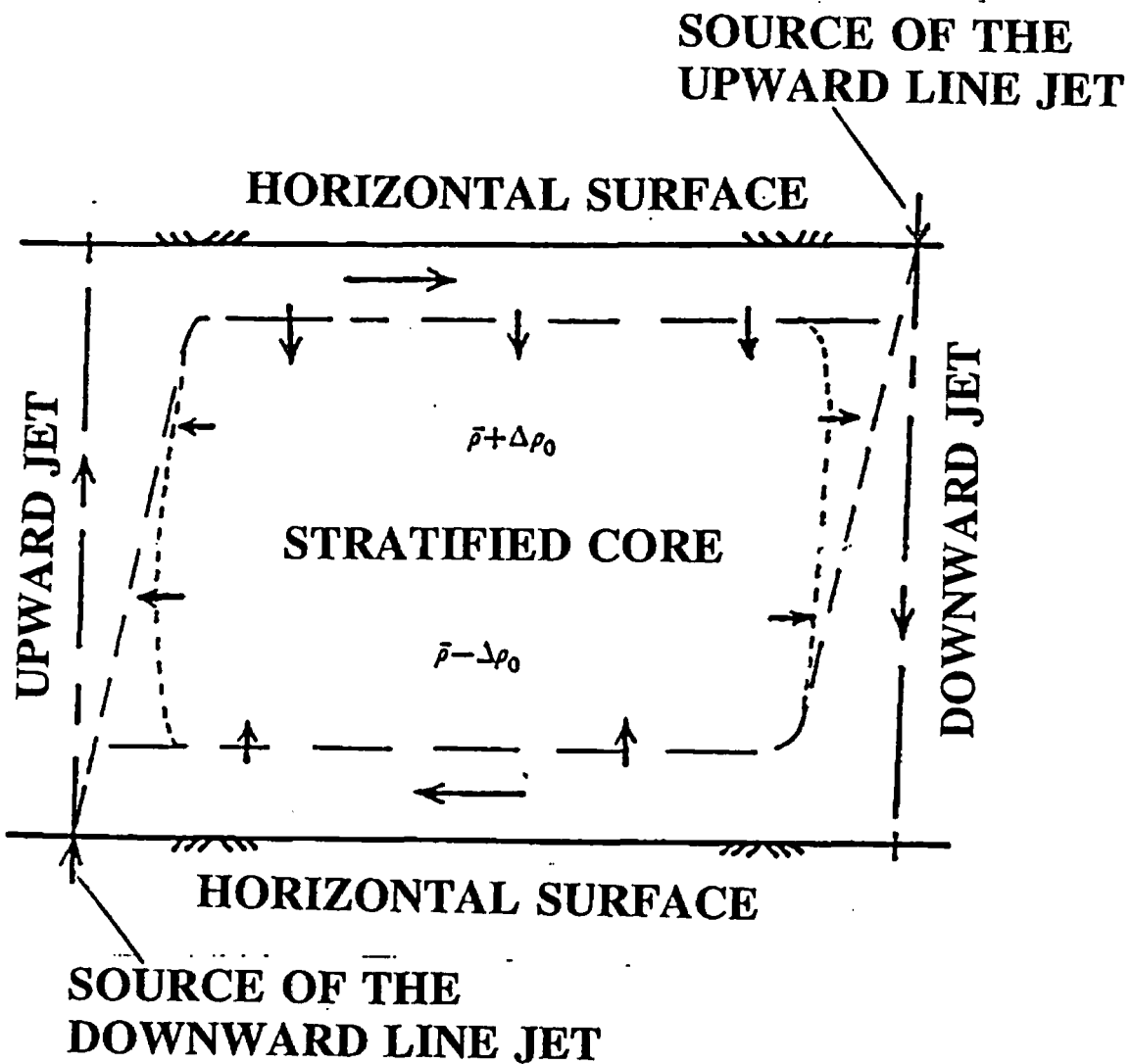


Figure 9.C.1-7 Formation of the stratified core in between two opposite vertical line jets (after Baines and Turner, 1969)

"Reprinted with the permission of Cambridge University Press from Baines W.D. and Turner, J. S./Turbulent buoyant convection from a source in a confined region, Journal of Fluid Mechanics, Vol. 37, 1969; pp. 51-80, Copyright 1969, Figure 9.C.10"

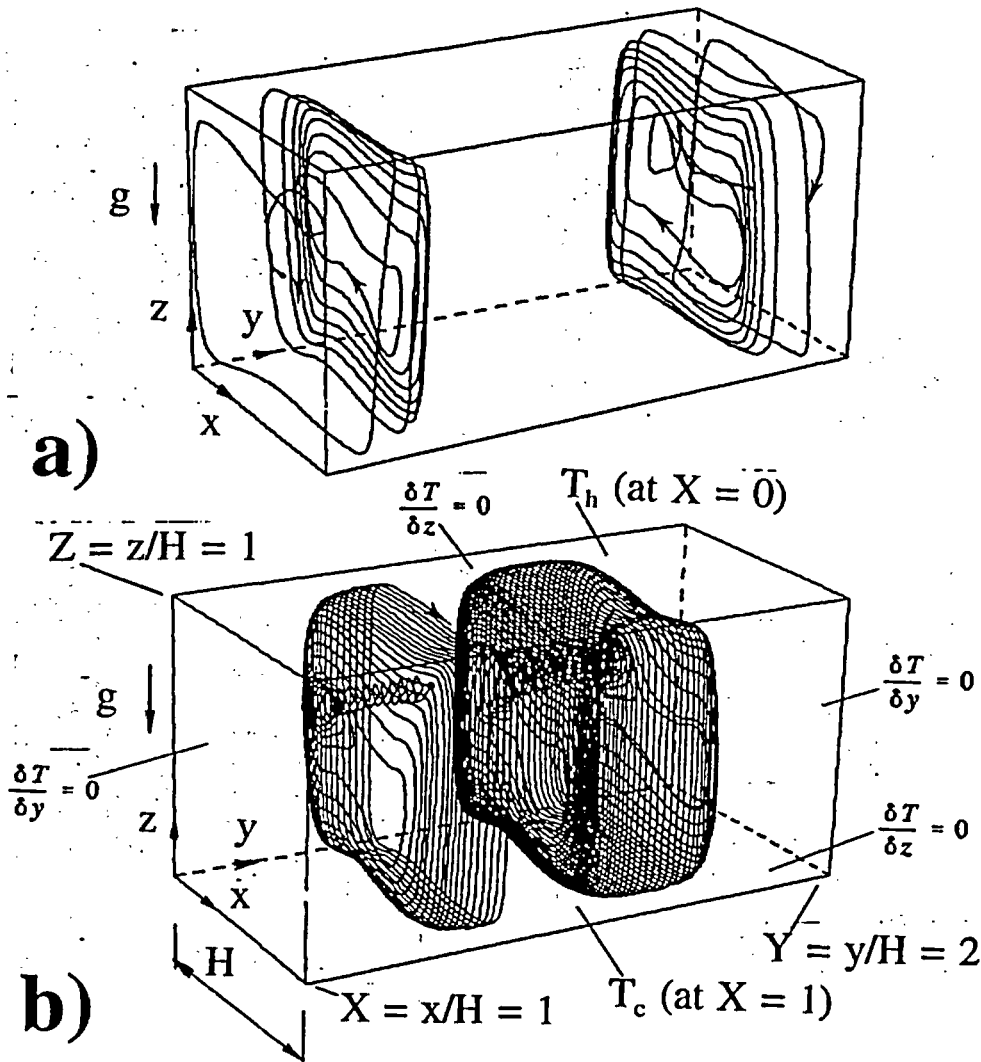


Figure 9.C.1-8 Flow in an enclosure with vertical opposite walls at different temperatures ($Ra = 10^5$, $Pr = 0.71$)

- a) forward flow (towards $Y=0$ and $Y=2$) - streamlines through the points $(X=0.5, Y=0.1, Z=0.49)$ and $(X=0.5, Y=1.9, Z=0.49)$
- b) reverse flow (towards $Y=1.0$) - streamlines through the points $(X=0.3, Y=0.8, Z=0.65)$ and $(X=0.3, Y=1.2, Z=0.65)$ after (Mallinson and deVahl Davis, 1977)

"Reprinted with the permission of Cambridge University Press from Mallinson, G.D. and G. de Vahl Davis/Three-dimensional natural convection in a box: a numerical study, *Journal of Fluid Mechanics*, Vol. 83, 1977; pp.1-31, Copyright 1977, Figure 9.C.8"

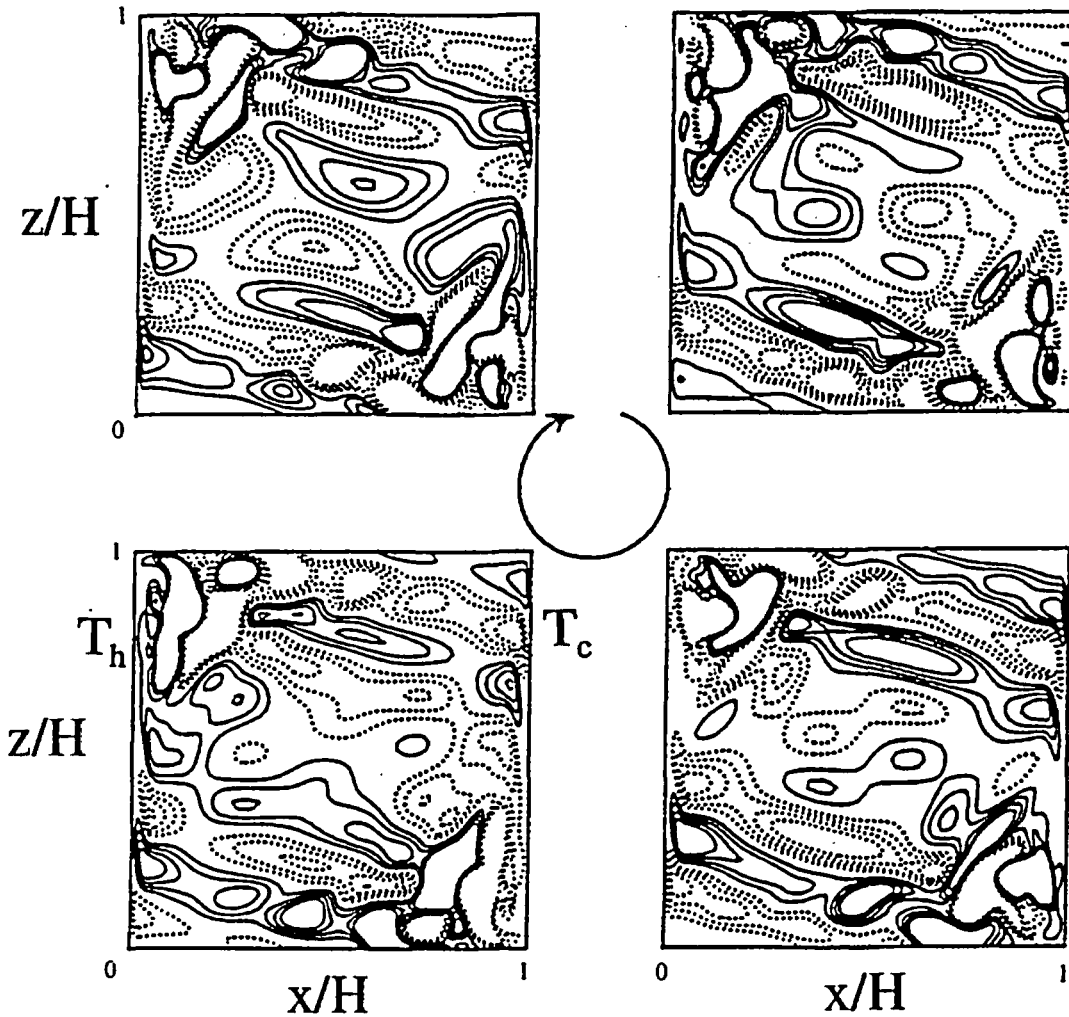


Figure 9.C.1-9 Internal waves in the square cavity - fluctuations in the temperature field at $Ra = 2 \cdot 10^8$ and $Pr = 0.71$ (air)

Circle with the arrow (in the middle) presents the direction of the consecutive temperature fields. Contour lines correspond to $\pm 0.0005 \Delta T$, $\pm 0.001 \Delta T$, $\pm 0.0015 \Delta T$ and $\pm 0.002 \Delta T$ (the dotted contour lines correspond to negative values, where $T_h = \Delta T/2$ and $T_c = -\Delta T/2$). (After Janssen and Henkes, 1995)

"Reprinted with the permission of Cambridge University Press from Janssen, R.J.A. and R.A.W. Henkes/Influence of Prandtl number on stability mechanisms and transition in a differentially heated square cavity, Journal of Fluid Mechanics, Vol. 290, 1995; pp.319-344, Copyright 1995, Figure 9.C.4"

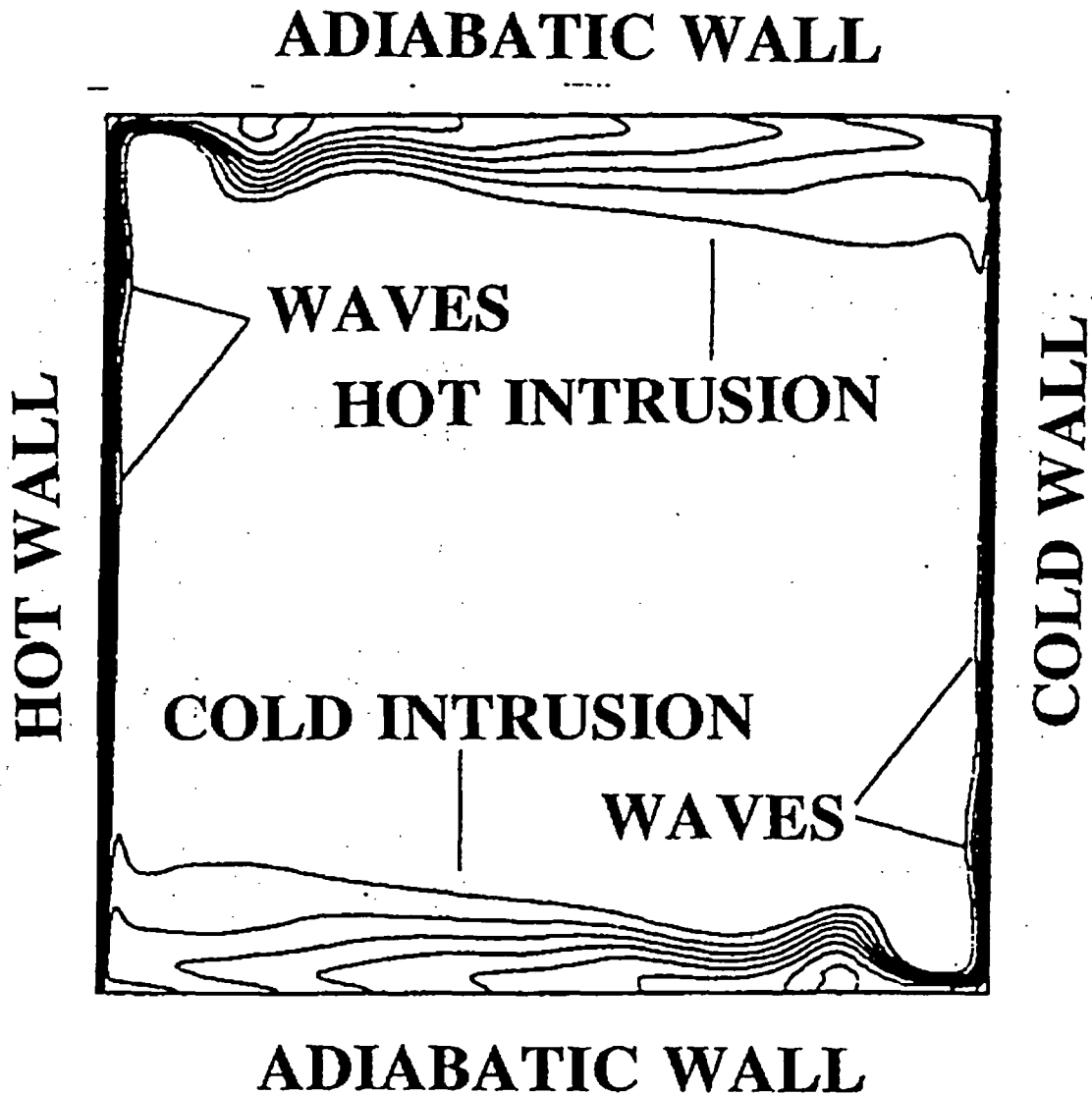


Figure 9.C.1-10 Temperatures for the initial solution with the hot and cold intrusions and boundary layer waves presented (after Armfield and Janssen, 1996)

"Reprinted with permission from Int. J. Heat and Fluid Flow, Vol. 17, S. Armfield and R. Janssen/A direct boundary-layer stability analysis of steady-state cavity convection flow, pp. 539-546, 1996. Elsevier Science Inc."

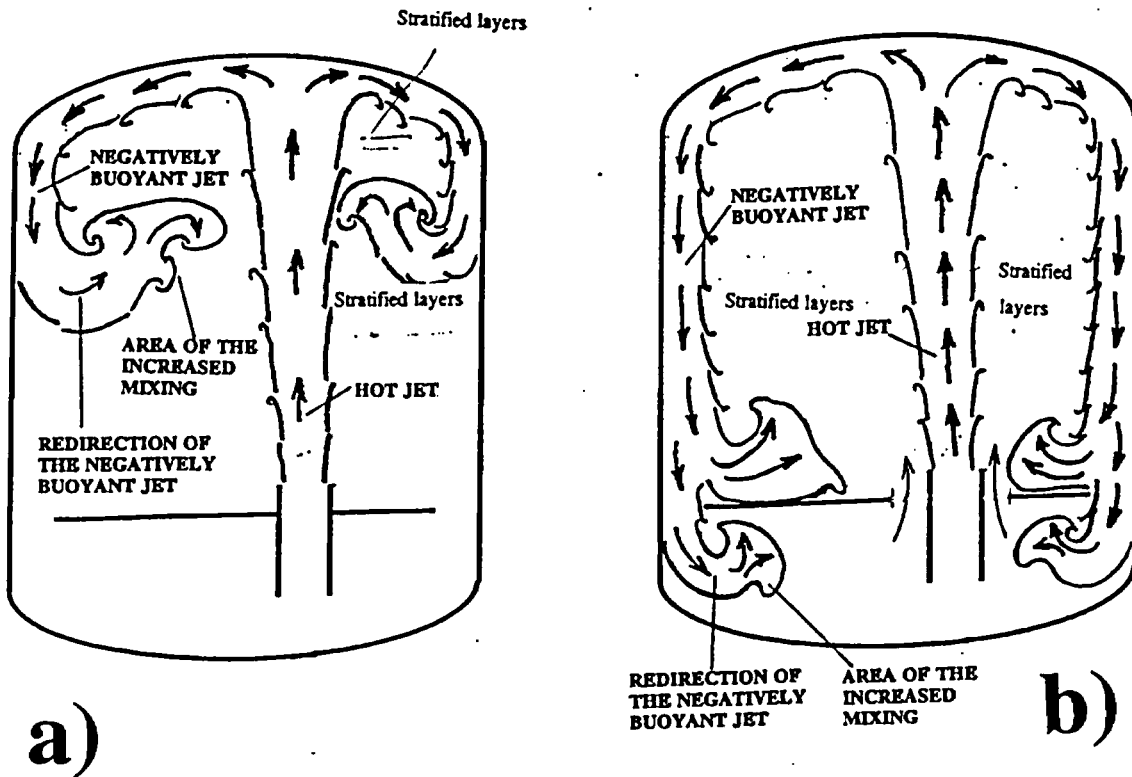


Figure 9.C.1-11 Formation of the downward negatively buoyant jets

- a) negatively buoyant jet redirected inside the dome region
- b) negatively buoyant jet penetrating the below deck region

9.C.1.1.3 References

1. Akino, N., Kunugi, T., Shiina, Y., Seki, M. and Okamoto, Y. (1989)
"Natural convection in a horizontal silicone oil layer in a circular cylinder heated from below and cooled from above", (in Japanese), *Trans. Jpn. Soc. of Mech. Eng.* 55 509 no. 1989-1), no. 88-0901 B: 152-158, 1989.
2. Allard, F., (1992)
"Effects of thermal boundary conditions on natural convection in thermally driven cavities", in-Turbulent Natural Convection in Enclosures, A Computational and Experimental Benchmark Study, (Eds.) R.A.W.M Henkes and C.J. Hoogendoorn, Editions Europeennes Thermique et Industrie, Paris, pp. 234-256.
3. S. Armfield and R. Janssen (1996)
"A direct boundary-layer stability analysis of steady-state cavity convection flow" *Int. J. Heat and Fluid Flow*, Vol. 17, No. 6, December 1996.
4. W.D. Baines and J.S. Turner (1969)
"Turbulent buoyant convection from a source in a confined region" *J. Fluid Mech.*, Vol. 37, part 1, pp. 51-80.
5. Catton, I., (1978)
"Natural convection in enclosures" *Proc. 6th Int. Heat Transfer Conf.*, Vol. 6, pp. 13-31.
6. Dzodzo M. B., (1993)
"Visualization of laminar natural convection in romb-shaped enclosures by means of liquid crystals" in "Imaging in transport processes", (ed. S. Sideman and K. Hijikata), Chapter 15, pp. 183-193., Begel House, Inc., 1993.
7. R. Frederick and A. Valencia, (1995), "Natural Convection in Central Microcavities of Vertical Pinned Enclosures of very High Aspect Ratios," *Int. J. Heat and Fluid Flow*, Vol. 16, No. 2, April 1995, pp. 114-124.
8. T. Fusegi, J. M. Hyun, K. Kuwahara, (1992)
"Numerical simulations of natural convection in a differentially heated cubical enclosure with a partition" *Int. J. Heat and Fluid Flow*, Vol. 13, No. 2, June 1992, pp 176-183.

9. T. Fusegi, T. M. Hyun, (1994) "Laminar and Transitional Natural Convection in an enclosure with complex and realistic conditions," *Int. J. Heat and Fluid Flow*, Vol. 15, No. 4, August 1994, pp. 258-268.
10. A. D. Garrad and M.A. Patrick, (1983)
"The velocity field produced by a submerged jet directed upwards at a free surface" *Int. J. Heat Mass Transfer*, Vol. 26, No. 7, pp. 1029-1036.
11. K. Hanjalic, S. Kernjeres and F. Durst, (1996)
"Natural convection in partitioned two-dimensional enclosures at higher Rayleigh numbers" *Int J. Heat Mass Transfer*, Vol. 39, No. 7, pp. 1407-1427, 1996
12. T. J. Heindel, S. Ramadhyani, and F. P. Incropera (1995)
"Conjugate natural convection from an array of discrete heat sources: part 1 - two and three-dimensional model validation" *Int. J. Heat and Fluid Flow*, Vol. 16, No. 6, December 1995, pp. 01-510.
13. Hiller W.J., Koch St., Kowalewski T.A., (1988)
"Simultane erfassung von temperatur und geschwindigkeitsfeldern in einer thermischen konvektionsstromung mit ungekapselten flussigkristalltracern, DGLR - Workshop, 2D-Mesttechnik, 1988.
14. Hiller W.J., Koch St., Kowalewski T.A., (1989)
"Three-dimensional structures in laminar natural convection in a cube enclosure" *Exp. Therm. Fluid Sci.*, Vol. 2, pp. 34-44.
15. C. J. Ho, Y. T. Cheng and C. C. Wang, (1994)
"Natural convection between two horizontal cylinders inside a circular enclosure subjected to external convection" *Int. J. Heat and Fluid Flow*, Vol. 15, No. 4, August 1994, pp 299-306.
16. Hoogendoorn, C.J., (1986)
"Natural convection in enclosures" *Proc. 8th Int. Heat Transfer Conf.*, Vol. 1, pp. 111-120.
17. J.M. Hyun and B.S. Choi, (1990)
"Transient natural convection in a parallelogram-shaped enclosure", *Int. J. Heat and Fluid Flow*, Vol. 11, No. 2, June 1990, pp. 129-134.

18. R. J. A. Janssen and R.A.W.M. Henkes, (1995)
"Influence of Prandtl number on instability mechanisms and transition in a differentially heated square cavity," J. Fluid Mech., Vol. 290, pp. 319-344., 1995
19. K. Kapoor and Y. Jaluria, (1993)
"Penetrative convection of a plane turbulent wall jet in a two-layer thermally stable environment: a problem in enclosure fires" Int. J. Heat Mass Transfer, Vol. 36, No. 1, pp. 155-167, 1993.
20. A. Kurosawa, N. Akino, T. Otsuji, S. Kizu, K. Kobayashi, K. Iwahori, T. Takeda and Y. Ito, (1993)
"Fundamental study on thermo-hydraulic phenomena concerning passive safety of advanced marine reactor" Journal of Nuclear Science and Technology, Vol 30 [2], pp. 131-142, February 1993.
21. G.D. Mallinson and G. de Vahl Davis, (1977)
"Three-dimensional natural convection in a box: a numerical study" J. Fluid Mech., Vol. 83, pp. 1-31.
22. N.C. Markatos and K.A. Pericleous, (1984)
"Laminar and turbulent natural convection in an enclosed cavity" Int. J. Heat Mass Transfer, Vol. 27, No. 5, pp. 755-772.
23. E. S. Nowak and M. H. Novak, (1994)
"Vertical partitions in slender rectangular cavities" Int. J. Heat and Fluid Flow, Vol. 15, No. 2, April 1994, pp. 104-110.
24. Ostrach, S., (1972)
"Natural convection in enclosures" Advances in Heat Transfer, Vol. 8, Academic Press, New York, pp. 161-227.
25. Ostrach, S., (1982)
"Natural convection heat transfer in cavities and cells" Proc. 7th Int. Heat Transfer Conf., Vol 1, pp.365-379.
26. F.E. Peters, (1994)
WCAP-14135, "Final Data Report for PCS Large-Scale Tests, Phase 2 and Phase 3", Revision 1, April 1997.
27. P.F. Peterson, (1994)
"Scaling and analysis of mixing in large stratified volumes" Int. J. Heat Mass Transfer, Vol. 37, Suppl. 1, pp. 97-106.

28. B. Porterie, M. Larini, F. Giroud and J.C. Loraud (1996)
"Solid-propellant fire in an enclosure fitted with a ceiling safety-vent" *Int. J. Heat Mass Transfer*, Vol. 39, No. 3, pp. 575-601.
29. R.M. C So and H. Aksoy, (1993)
"On vertical turbulent buoyant jets" *Int. J. Heat Mass Transfer*, Vol. 36, No. 13, pp. 3187-3200.
30. L. Wolf, H. Holzbauer, T. Cron, (1994a)
"Detailed Assessment of the HDR-Hydrogen Mixing Experiments E11" International Conference on New Trends in Nuclear System Thermohydraulics, Pisa, Italy, May 30th - June 2nd, vol. 2, pp. 91-103.
31. L. Wolf, H. Holzbauer, M. Schall, (1994b)
"Comparisons between multi-dimensional and lumped-parameter Gothic-containment analyses with data" International Conference on New Trends in Nuclear System Thermohydraulics, Pisa, Italy, May 30th - June 2nd, vol. 2, pp. 321 - 330.

9.C.1.2 CIRCULATION PHENOMENA

Circulation processes inside enclosures are the result of natural or forced convection effects. Forced convection inside an enclosure is promoted using devices such as fans, nozzles, or sprays of liquid droplets. PCS applications are of primary interest, since no credit is taken for active systems in the design basis analysis.

A review of possible flow patterns due to natural convection effects is presented. Natural convection is generated if:

- 1) The upper boundary is at a lower temperature than the lower boundary or opposite vertical boundaries are at different temperature, as well as for other similar combinations of temperature boundary conditions (or imposed heat flux conditions) at the outside and inside surfaces.
- 2) A higher concentration of the lighter or heavier components of a mixture is maintained near the lower or upper boundaries of the enclosure, respectively.
- 3) A lighter fluid is released (permanently, or from time to time) from a source which is closer to the bottom of the enclosure.
- 4) The shape of the enclosure promotes natural convection (together with the distribution of other boundary conditions).
- 5) The distribution and size of the horizontal and vertical internal openings allows or enhances (as with a chimney or staircase effects) the formation of fluid flow patterns due to the natural convection.
- 6) If the internal heat sources (sinks) are positioned in the lower (upper) portions of the enclosure.

Under the conditions above (or a combination of them), natural convection causes circulation inside the enclosure. The convection increases the intensity of heat and mass transfer, therefore increasing the heat released from the containment. The intensity of heat transfer depends upon the location of the heat sinks and sources, which can exchange positions due to the transient effects. The velocity and temperature profiles inside the formed boundary layers (wall jets) influence the rate of heat transfer due to the convection. Wall jets entrain the surrounding atmosphere and contribute to better mixing. In the regions with a higher steam concentration, the increase in the heat transfer rate and the effects of entrainment occur due to the condensation inside the boundary layers.

Another contributing factor that promotes circulation inside an enclosure is the interaction of the enclosure atmosphere with the penetrating buoyant plumes or jets and wall layers. In the case of a containment vessel, the plumes or jets could be generated by a LOCA or MSLB. If the break position is inside a narrow corridor or surrounded by additional equipment, the kinetic energy of the jet is dissipated and steam rises in the form of a buoyant plume. The rising plume entrains the surrounding gas and results in circulation inside the volume of the enclosure.

If the break position is open and the jet is directed upward, both the kinetic energy of the jet and the buoyancy forces contribute to penetration into the atmosphere. The higher speeds of the jet affect a greater portion of the volume and both entrainment of the surrounding gas and circulation is stronger.

9.C.1.2.1 Circulation Phenomena Due to the Presence of Boundary Layers (Wall Jets) and Buoyant Plumes Formed as a Consequence of Natural Convection Effects

Natural convection flow is the most often generated by different temperatures or heat fluxes imposed on the boundaries of an enclosure. Various distributions on the boundaries produce various flow patterns and temperature fields.

Section 9.C.1.1 discusses boundary temperature distributions (upper/lower horizontal plates at the higher/lower temperatures) that produce static stratification. Section 9.C.1.2 discusses the case where vertical opposite sides are at constant, but different temperatures. If Rayleigh numbers are greater than 10^4 , this condition produces a recirculated region near the walls and a stratified core of the enclosure.

Figure 9.C.1-12 presents a case known as Rayleigh-Benard convection. The upper horizontal boundaries are at the lower temperatures (or cooled). The flow patterns formed depend upon the temperature difference and geometry of the enclosure (in fact the value of the Rayleigh number).

For the smaller Ra numbers, vortical cells are formed. An increase in the Ra numbers produces a greater number of vortical cells that start to oscillate, periodically changing the size and intensity. A further increase in the Ra number results in chaotic flow, and produces vertical plumes which reach the opposing horizontal sides of the enclosure. The flow patterns and possible bifurcations produced during the transition from the laminar to turbulent (chaotical) flow regimes are described in Koschmieder, 1993, Yang, 1988, and Ozawa et al., 1992. Some experimental results (flow patterns and temperature fields) are presented for laminar flow regimes by M. Dzodzo et al., 1994 and M.J. Braun et al., 1993. Flow patterns for turbulent and chaotic flow between two horizontal plates at different temperatures are described in Akino et al., 1989.

Flow in the Hele-Shaw cell is presented as an example of natural convection between two horizontal plates. A Hele-Shaw cell has a square cross-section, but it is narrow in one of the horizontal directions so that three-dimensional convection effects are suppressed (see Figure 9.C.1-13). The upper and lower horizontal sides are at the lower and higher temperatures, respectively.

Consecutive flow patterns and temperature fields for a Hele-Shaw cell with various Rayleigh numbers are presented in Figure 9.C.1-14 (after Buhler et al., 1987). If the value of the Rayleigh number is greater than 4×10^6 , oscillatory flow patterns with four vortical cells are present. The large and small vortices expand and contract periodically (see Figure 9.C.1-14). At high Rayleigh numbers (above 5.9×10^7), a reverse transition from the oscillatory to the steady flow patterns occurs. This phenomena is probably due to suppressed three-dimensional convection effects.

For cubic or cylindrical enclosures, with the upper and lower horizontal surfaces at the lower and higher temperatures, respectively, three-dimensional convection effects produce turbulent (chaotical) flow (see Figure 9.C.1-15). In the paper by Akino et al., 1989, the turbulent flow regime starts at a Rayleigh number of 2×10^6 ($Pr = 200$). For fluids with a Prandtl number close to one, the transition to turbulent flow regime occurs at a smaller Rayleigh number ($Ra \sim 10^4$).

The flow pattern consists of vertical buoyant plumes detached from the horizontal sides. The vertical plumes reach opposite sides of the enclosure and generate opposing plumes (see Figure 9.C.1-16). Temperature gradients near the horizontal surfaces are high, while temperatures in the core of the containment are almost uniform. Figure 9.C.1-17a illustrates an example where the temperature in the middle of the enclosure oscillates between 26 and 29°C with $Ra = 9.38 \times 10^7$ ($T_h = 35^\circ\text{C}$ and $T_c = 20^\circ\text{C}$). The highest temperature is registered during the rise of the hot plume and the lowest temperature is registered during the downward penetration of the cold plume. The amplitude of the temperature oscillations in the middle of the enclosure is three degree Celsius. The temperature interval between 26 and 29°C represents $0.2 \times (T_h - T_c)$ or 20 percent of the maximum temperature difference. The temperature in the middle of the enclosure is (27.5°C) $\pm 1.5^\circ\text{C}$.

Rayleigh-Benard convection is relevant to the containment. In the case of a LOCA or MSLB, the upper portion of the dome and vertical sides are cooled. If the temperature below the ceiling is 9°F lower than temperature of the incoming steam (at the deck level), the Grashof number (based on the height of the containment, $H_i = 109$ ft) is $Gr_i = 2.2 \times 10^{13}$. This Grashof number is in the range of the chaotic flow, with the upward and downward plumes (because $Gr_i > 10^4/0.71$).

Maintaining the vertical walls of the containment at the lower temperature also promotes downward vertical plumes near the walls due to separation of the vertical boundary layers (see Figure 9.C.1-17b).

9.C.1.2.2 Circulation Phenomena Due to the Interaction With the Hot Buoyant Plumes and Jets

The presence of a hot buoyant plume or a jet of the hot steam during a LOCA or MSLB contributes to the circulation of the containment atmosphere by entraining the surrounding air and other gases. In the case of jet inflow, additional entrainment and circulation are generated by the jet kinetic energy.

Depending upon the strength (initial velocity and mass flow) and direction of the plume or jet, various flow patterns inside the containment are possible. Interaction of the vertical downward plumes generated due to the natural convection (cooling of the shell) produce turbulent flow. This results in good mixing of the dome atmosphere. Examples of vertical plumes and jets are presented by Garrad and Patrick, 1983, So an Aksoy, 1993, and Porterie et al. 1996. The scaling and analysis of circulation in large stratified volumes is presented by Peterson, 1994.

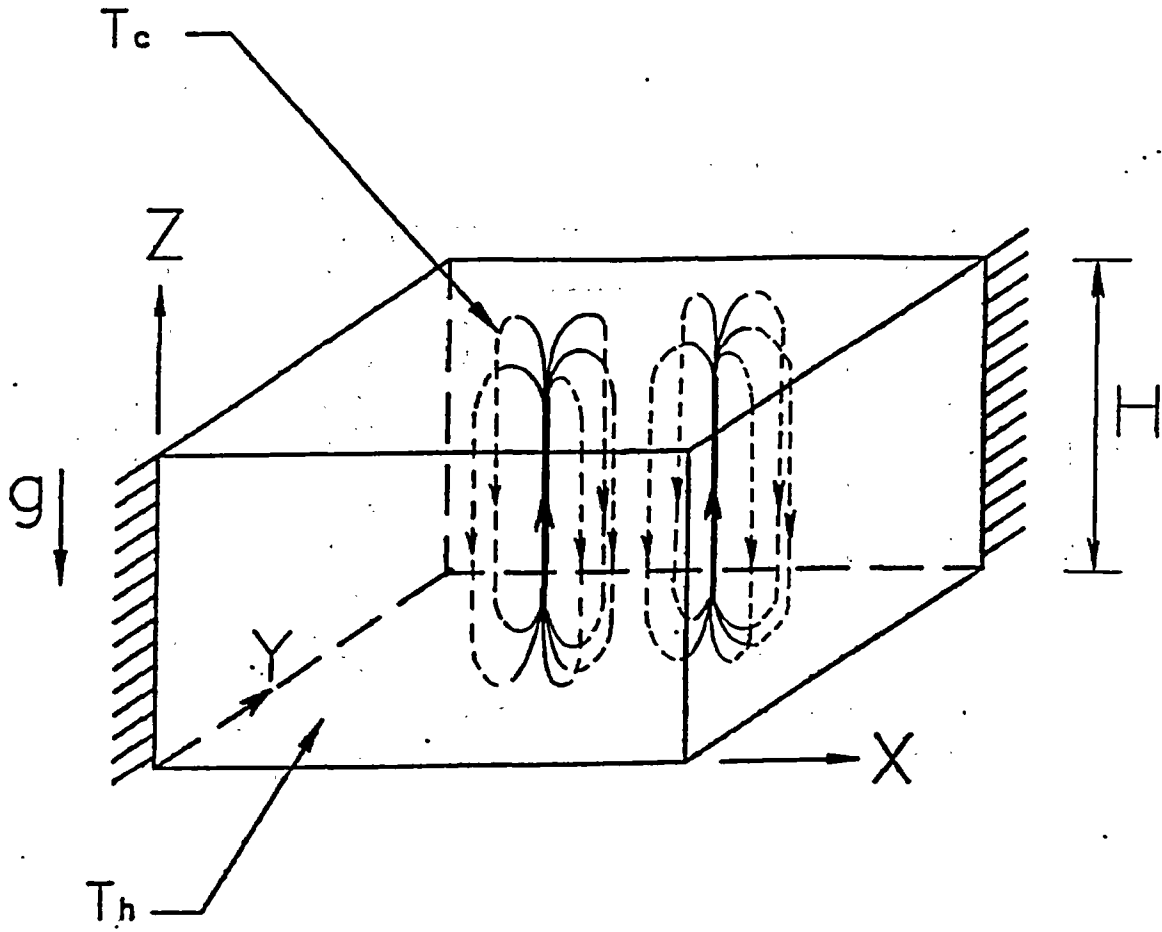


Figure 9.C.1-12 Rayleigh-Benard convection example

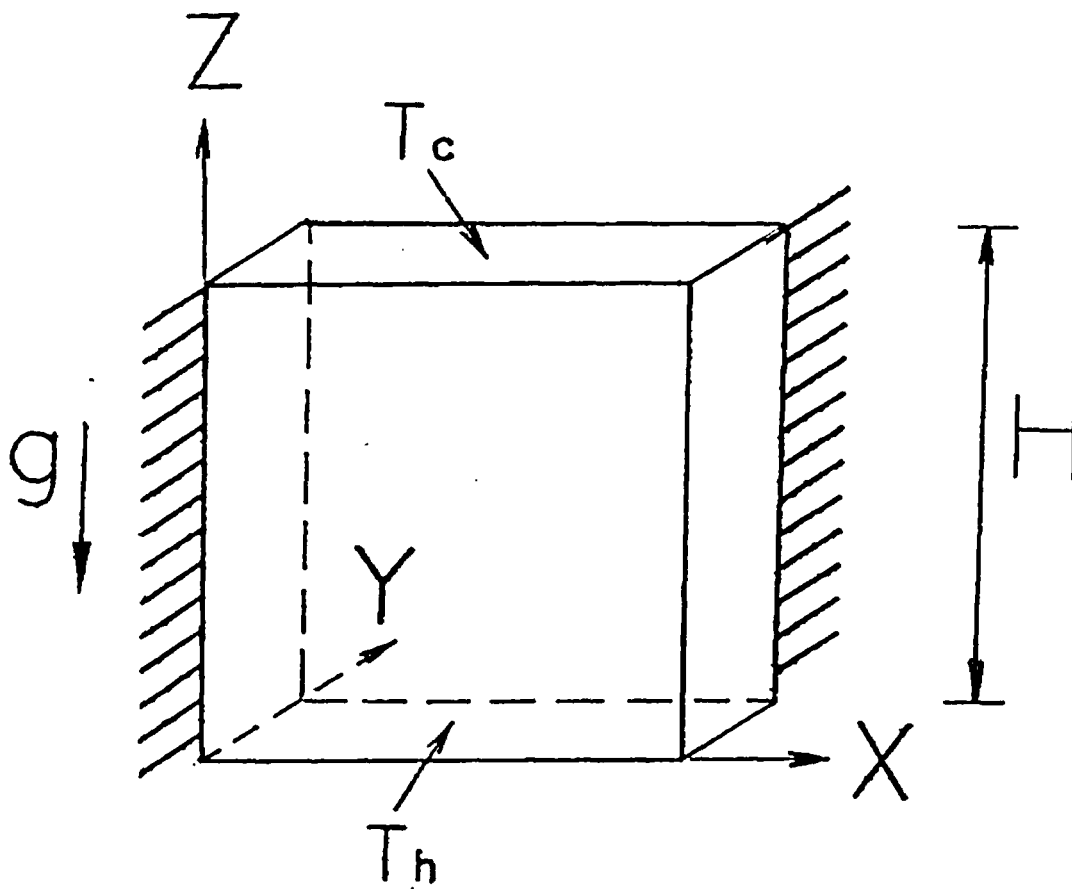


Figure 9.C.1-13 Hele-Shaw cell

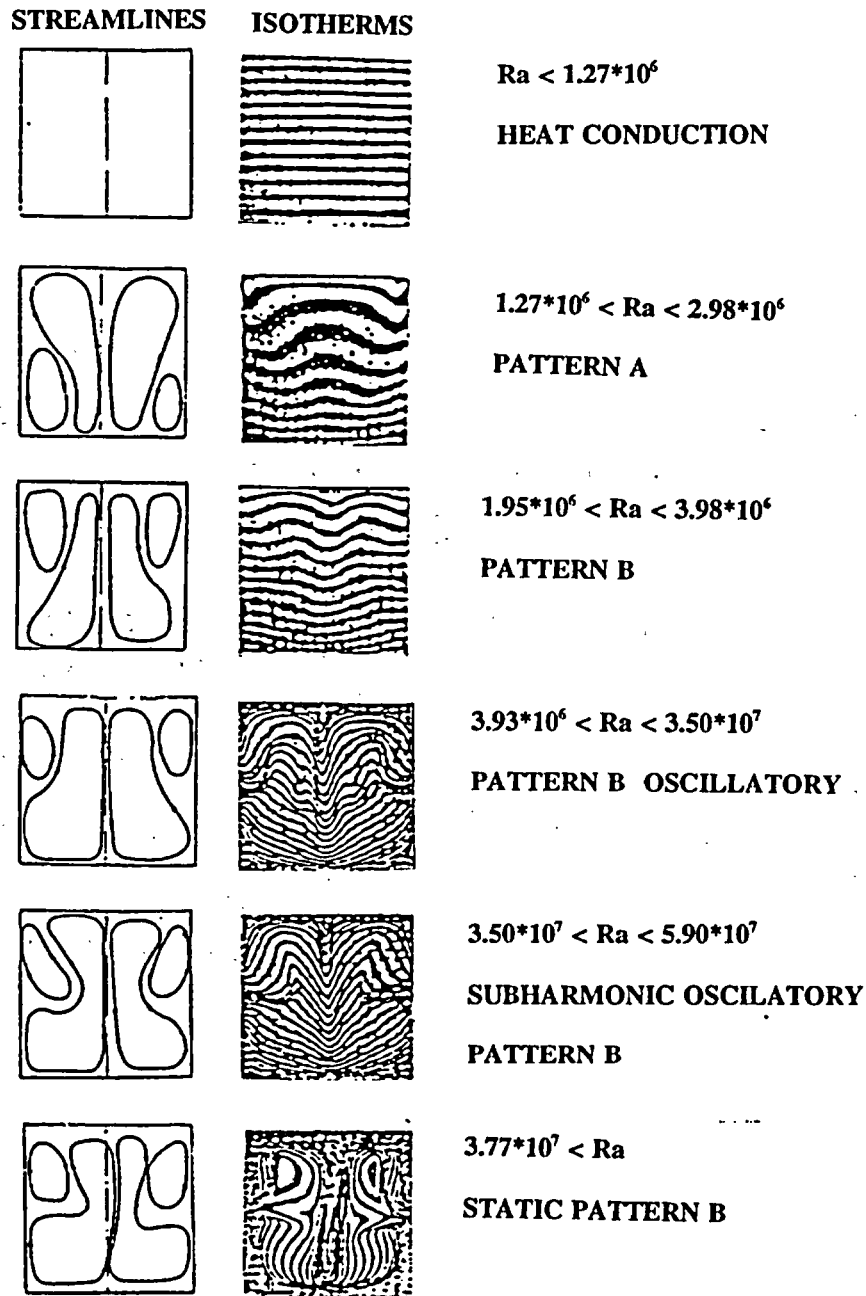


Figure 9.C.1-14 Steady and oscillatory convection in Hele-Shaw cell (after Buhler et al., 1987)

"Reprinted from L.Buhler, P. Ehrhard, C. Gunther, U. Muller and G. Zimmermann/Natural convection in vertical gaps heated at the lower side - an experimental and numerical study, HTD-Vol. 94, AMD-Vol. 89, Bifurcation Phenomena in Thermal Processes and Convection, Winter Annual Meeting of the American Society of Mechanical Engineers, Boston, Massachusetts, December 13-20, 1987"

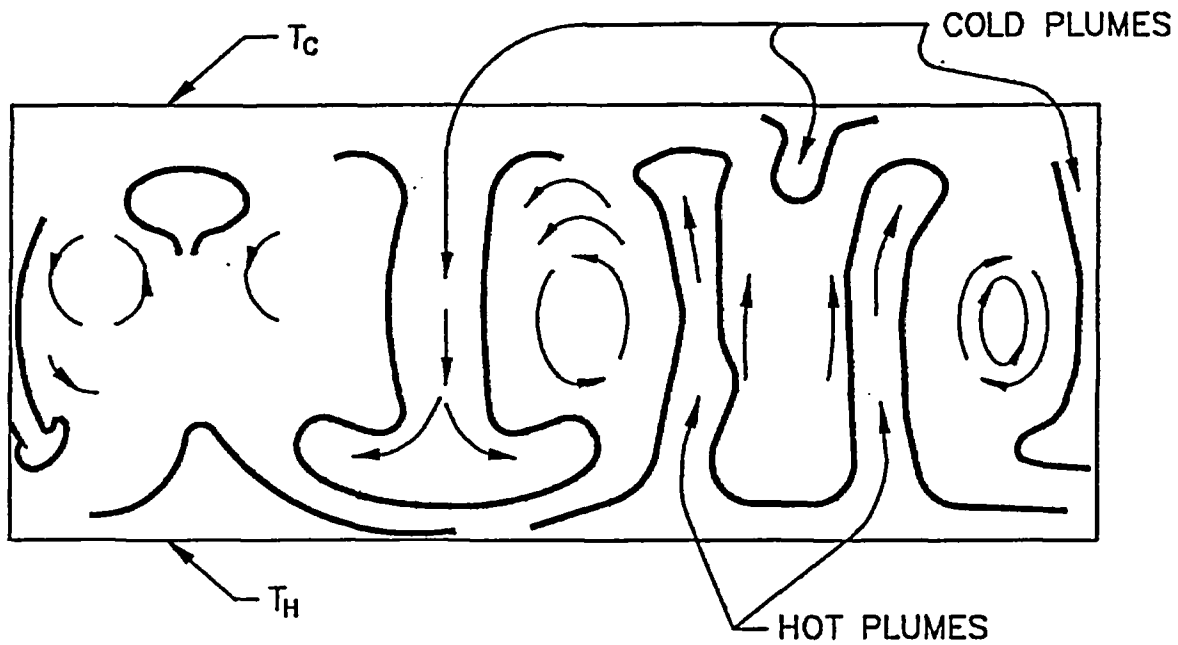


Figure 9.C.1-15 Turbulent (chaotical) flow with hot and cold plumes interactions (plane cross-section of the three-dimensional enclosure is presented)

(according to Figure 6 in N. Akino, T. Kunugi, Y. Shiina, M. Seki, Y. Okamoto/Natural convection in a horizontal silicone oil layer in a circular cylinder heated from below and cooled from above", Trans. Jpn. Soc. of Mech. Eng. 55 509 no. 1989-1), no. 88-0901 B:, pp. 152-158, 1989 -with permission from Norio Akino)

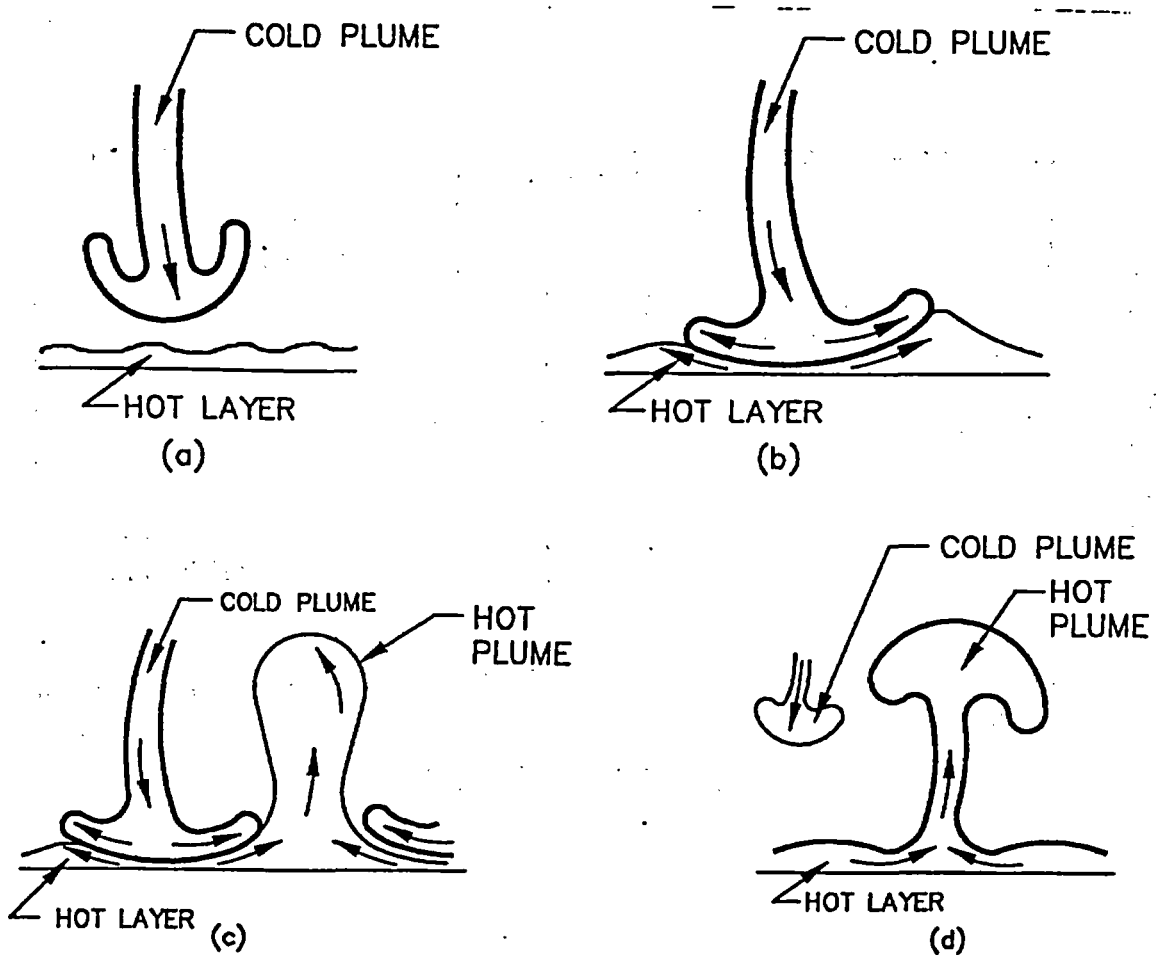


Figure 9.C.1-16 Interaction of hot and cold plumes (after Aqino et al., 1989)

(according to Figure 12 in N. Akino, T. Kunugi, Y. Shiina, M. Seki, Y. Okamoto/Natural convection in a horizontal silicone oil layer in a circular cylinder heated from below and cooled from above", Trans. Jpn. Soc. of Mech. Eng. 55 509 no. 1989-1), no. 88-0901 B:, pp. 152-158, 1989 - with permission from Norio Akino)

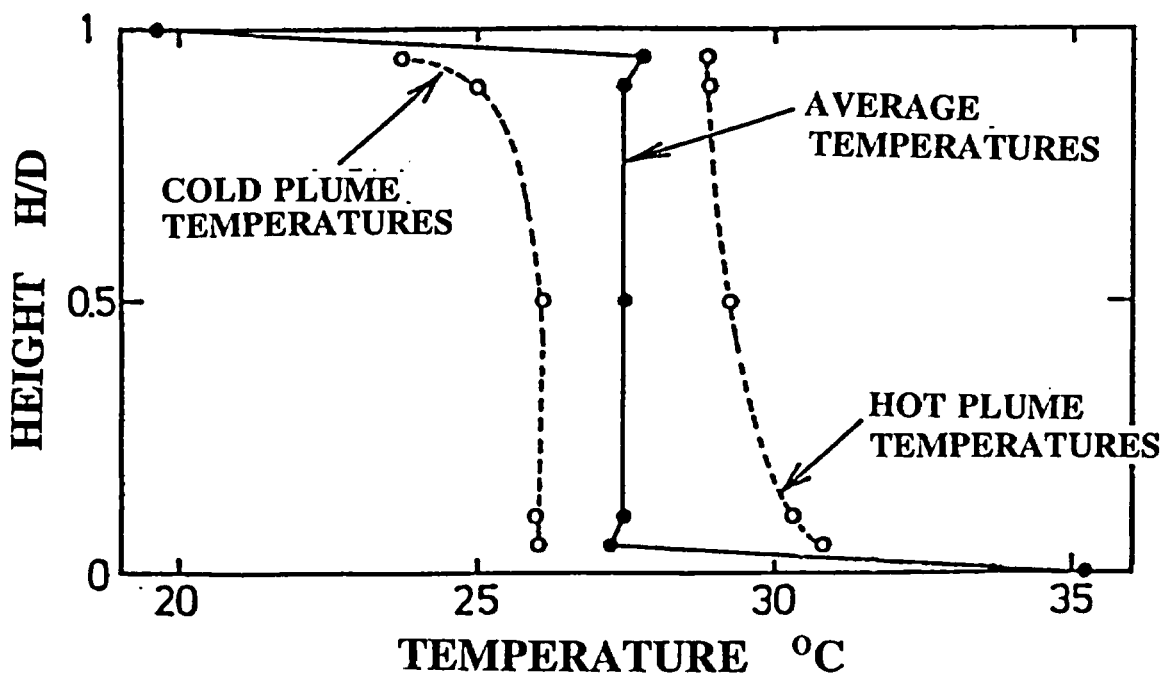


Figure 9.C.1-17a Vertical temperature distribution inside the cylindrical enclosure with lower and upper horizontal plate at higher and lower temperatures, respectively ($Ra = 9.38 \times 10^7$, $Pr = 200$)

(according to Figure 14 in N. Akino, T. Kunugi, Y. Shiina, M. Seki, Y. Okamoto/Natural convection in a horizontal silicone oil layer in a circular cylinder heated from below and cooled from above", Trans. Jpn. Soc. of Mech. Eng. 55 509 no. 1989-1), no. 88-0901 B; pp. 152-158, 1989 - with permission from Norio Akino)

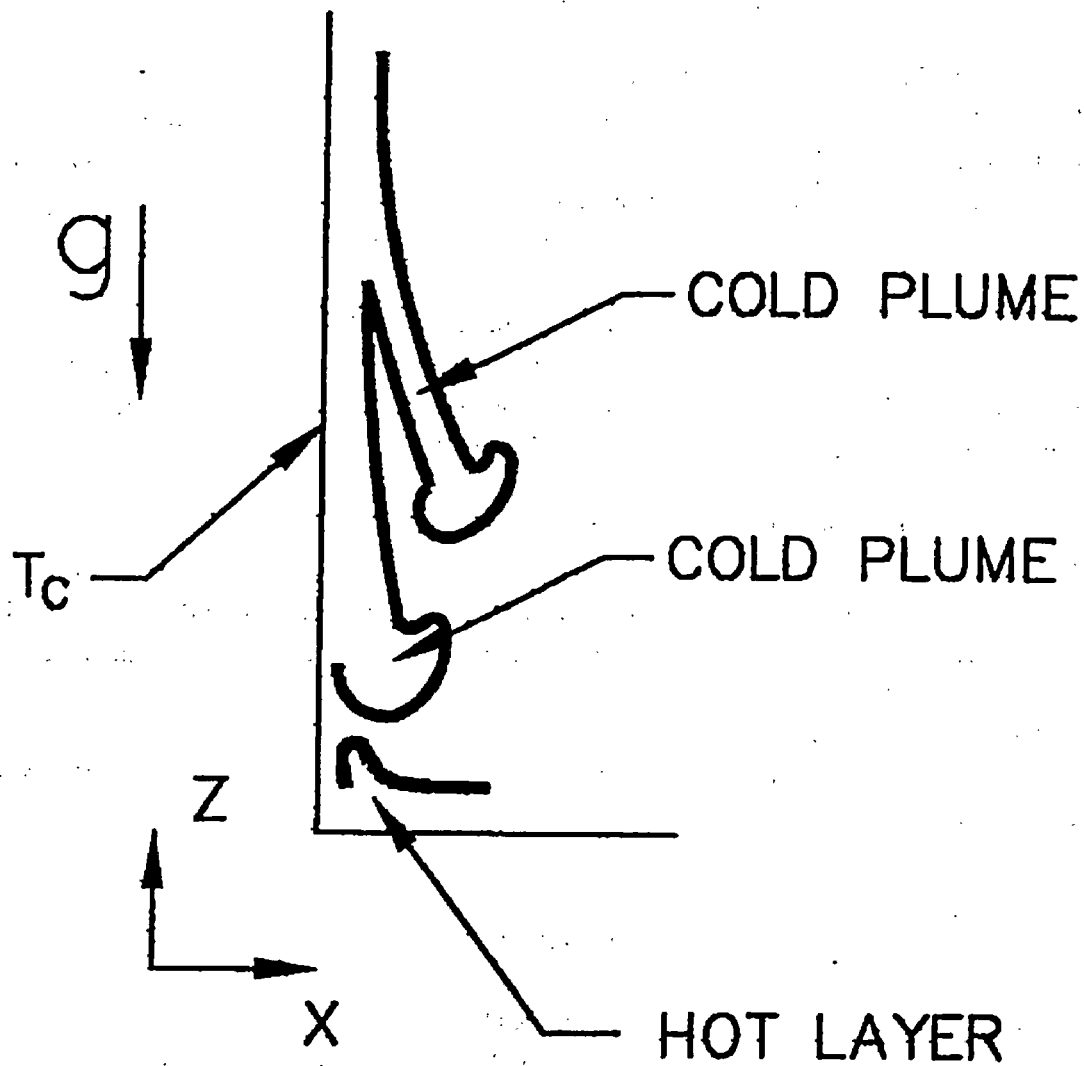


Figure 9.C.1-17b Generation of the cold plumes due to the brake (separation) of the vertical boundary layers near the cold vertical walls

9.C.1.2.3 References

1. N. Akino, T. Kunugi, Y. Shina, M. Seki, Y. Okamoto, (1989)
"Natural Convection in a Horizontal Silicone Oil Layer in a Circular Cylinder Heated from Below and Cooled from Above" Nippon Kikai Gakkai Ronbunchyu, 55 Vol. 509 (1989-1), pp. 152 -158.
2. M. J. Braun , M. B. Dzodzo, S. B. Lattime, (1993)
"Automatic computer based non-intrusive temperature measurements in laminar natural convection using thermochromic liquid crystals in enclosures with variable aspect ratio" FED-Vol. 172, Experimental and numerical flow visualization, The 1993 ASME Winter Annual Meeting, New Orleans, Louisiana, November 28 - December 3, 1993, pp. 111-119.
3. L. Buhler, P. Erhard, G. Gunther, U. Muller, G. Zimmermann, (1987)
"Natural convection in vertical gaps heated at the lower side - an experimental and numerical study. In: Bifurcation Phenomena in Thermal Processes and Convections (eds.H.M. Bau, L.A. Bertram, S.A. Lorpela) ASME, HTD-Vol. 94/AMD-Vol.89, 67-74.
4. M. Dzodzo, M.J. Braun, S.B. Lattime, (1994)
"A non-intrusive computer automated investigation of natural convection using thermochromic liquid crystals and comparison with numerical simulation" (ed. G.F. Hewitt) Proceedings of The Tenth International Heat Transfer Conference, Brighton, UK, Volume 2, 2-MT-6, pp. 225-230.
5. A.D. Garrad and M.A. Patrick, (1983)
"The velocity field produced by submerged jet directed upwards at a free surface", Int. J. Heat Mass Transfer, Vol. 26, No. 7, pp. 1029-1036.
6. E. L. Koschmieder, (1993)
"Benard Cells and Taylor Vorticies" Cambridge University Press
7. M. Ozawa, U. Muller, I. Kimura and T. Takamori, (1992)
"Flow and temperature measurements of natural convection in a Hele-Shaw cell using a thermo-sensitive liquid-crystal tracer" Experiments in Fluids, Vol 12, pp. 213-222.
8. P.F. Peterson, (1994)
"Scaling and analysis of mixing in large stratified volumes" Int. J. Heat Mass Transfer, Vol. 37, Suppl. 1, pp. 97-106.

9. B. Porterie, M. Larini, F. Giroud and J.C. Loraud, (1996)
"Solid-propellant fire in an enclosure fitted with a ceiling safety-vent" *Int. J. Heat Mass Transfer*,
Vol. 39, No. 3, pp. 575-601.
10. R.M.C. So and H. Aksoy, (1993)
"On vertical turbulent buoyant jets" *Int. J. Heat Mass Transfer*, Vol. 36, No. 13, pp. 3187-3200.
11. K.T. Yang, (1988)
"Transitions and Bifurcations in Laminar Buoyant Flows in Confined Enclosures" *J. of Heat
Transfer*, November 1988, Vol. 110, pp. 1191-1204.

9.C.1.3 IMPORTANT DIMENSIONLESS GROUPS

9.C.1.3.1 Important Dimensionless Groups for Stratification and Circulation Phenomena Inside Enclosures

For natural convection, the ratio of the buoyancy to viscosity forces is the most important dimensionless group. The Grashof number defines the ratio of the buoyancy to viscosity forces:

$$Gr = \frac{g\beta(T_h - T_c)H^3}{\nu^2} = \frac{g(\rho_c - \rho_h)H^3}{\rho_c \nu^2}$$

Natural convection correlations often use the Rayleigh number instead of Grashof number, where the Rayleigh number Ra is defined as:

$$Ra = \frac{g\beta(T_h - T_c)H^3}{\alpha \nu} = \frac{g(\rho_c - \rho_h)H^3}{\rho_c \alpha \nu} = Gr \frac{\nu}{\alpha} = Gr Pr$$

Using the Rayleigh number reduces the number of dimensionless groups in the correlations for natural convection. The appearance of Prandtl number inside some correlations could be avoided.

The Prandtl number is based on fluid properties, i.e., the ratio of kinematic viscosity to thermal diffusivity.

$$Pr = \frac{\nu}{\alpha}$$

When considering the interaction between the hot buoyant plume and the cold vertical wall boundary layer, the Grashof and Rayleigh numbers are defined with H_v as the characteristic length.

$$Gr_v = \frac{g(\rho_v - \rho_c)H_v^3}{\rho_v \nu^2}$$

This applies to flows generated inside the enclosures with the opposite vertical walls at the different temperatures. It also applies to flow caused by two opposing vertical jets (between the two horizontal plates). The AP600 and AP1000 have a combination of the two cases.

Upward flow is caused by the buoyant plume, while downward flow is caused by the lower temperatures of the vertical wall. If the initial kinetic energy of the plume is small, this Grashof number gives an indication of the formed flow pattern and heat transfer due to the two opposing vertical flow paths. The formation of a recirculating stratified core between the vertical jets is related to this parameter as well.

When considering the interaction between the cold ceiling and the hot rising plume (at the bottom of the enclosure), the height of the upper-deck region H_t can be used as a characteristic length. The Grashof number is:

$$Gr_t = \frac{g(\rho_t - \rho_o) H_t^3}{\rho_t v^2}$$

The value of this Grashof number indicates the status of the Rayleigh-Benard convection. If the values are above 10^4 , it is possible to form periodic vertical downward plumes which detach from the ceiling.

The conditions described above interact. The overall flow pattern is expected to be a superposition of the flow patterns described for enclosures with horizontal and vertical temperature gradients. The prevailing flow pattern is estimated from the ratio of the two Grashof numbers already defined:

$$\frac{Gr_t}{Gr_v} = \frac{(\rho_t - \rho_o) H_t^3 \rho_v}{(\rho_v - \rho_o) H_v^3 \rho_t}$$

Note that both dimensions of the large-scale test (LST) installation (H_t and H_v) are scaled to AP600 dimensions. Therefore, if the ratio of relative densities (in vertical and horizontal directions) is the same, the flow patterns obtained in LST experiments can be applied to the AP600.

Even small temperature differences between the shell and the atmosphere inside a containment produce large Grashof numbers. For example, a temperature difference of 9°F results in $Gr_t = 2.2 \cdot 10^{13}$ and $Gr_v = 4.7 \cdot 10^{12}$ for $H_t = 109$ ft and $H_v = 65$ ft, respectively.

In the case of LST, a temperature difference of 9°F results in $Gr_t = 3.9 \cdot 10^{10}$ and $Gr_v = 7.2 \cdot 10^9$ for $H_t = 13.2$ ft and $H_v = 7.5$ ft, respectively.

If the Grashof numbers are greater than 10^8 , the Nusselt number can be obtained by applying the correlation for turbulent free convection.

For jets and buoyant plumes that penetrate the containment, the ratio of inertia forces and buoyant forces influences the entrainment of surrounding gases. If the initial velocities are high, a constant spreading angle indicates a jet. As the jet velocities decrease, upward motion results from buoyant forces. Buoyant plume behavior is indicated by different spreading angles at each level.

The Froude number represents the ratio of the inertia to gravity forces, or the ratio of kinetic energy to potential energy:

$$Fr = \frac{U^2}{gH} = \frac{\rho U^2}{g \Delta \rho H} = \frac{\left(\frac{U H}{\nu}\right)^2}{\frac{g \Delta \rho H^3}{\rho \nu^2}} = \frac{Re^2}{Gr}$$

For buoyant plumes and jets, the Froude number can be defined as:

$$Fr_{j,o} = \frac{\rho_o U_o^2}{g(\rho_a - \rho_o) d_o}$$

where the characteristic length is the initial diameter of the jet or plume. The source velocity and density have the subscript (o), while the ambient density has the subscript (a). The elevation of the transition from a forced jet to a buoyant plume is calculated (Peterson, 1994 and Spencer, 1997) from the expression:

$$\frac{z_{trans}}{d_o} = Fr_{j,o}^{1/4} \left(\frac{\rho_o}{\rho_a}\right)^{1/4}$$

The ratio of the square of the jet Reynolds number to the containment Grashof number is a volumetric Froude number:

$$Fr_v = \frac{\rho_a U_o^2 d_o^2}{g(\rho_a - \rho_o) H^3}$$

If the volumetric Froude numbers are much greater than one, the inertia forces dominate. The inertia forces unstratify stratified layers, promote circulation inside the containment, and contribute towards the better mixing.

However, Peterson, 1994, proposes that the jet or plume is not able to disturb the stratified vertical density gradients if:

$$Fr_v < \left(1 + \frac{d_o}{4 \sqrt{2} \alpha H}\right)^2$$

where (α) is Taylor's jet entrainment parameter and where $\alpha = 0.05 = \text{constant}$.

For volumetric Froude numbers less than one, the inertia forces are not dominant and are not able to unstratify stratified layers inside the containment. Therefore, the buoyancy effects are more important than inertia effects. The reciprocal value of the Froude number or Richardson number is the appropriate dimensionless group.

$$Ri_v = \frac{g(\rho_a - \rho_o)H^3}{\rho_a U_o^2 d_o^2}$$

Since inertia effects of the plume are not important (Reynolds number of the plume is small), only Grashof numbers Gr_j and Gr_r will influence the flow pattern.

Another important factor is the position of the jet (plume) or heat source release location. The ratio of the release point level, H_r , to the height of the containment, H_t , describes the relative position of the jet (plume) or heat source:

$$\frac{H_r}{H_t}$$

If H_r/H_t is less than 0.2, the release location is considered low. A global circulation flow pattern affecting the entire containment is most likely formed. If H_r/H_t is greater than 0.5, the release elevation is high and stratification effects may occur in a portion of the volume. The result may be that only the upper portion of the enclosure is affected by global circulation, while the lower may be stratified. Such stratification may be stagnant. In stagnantly stratified regions, no entrainment into wall boundary layers or buoyant plumes

occurs, and thus little or no vertical mixing occurs, while in recirculating stratified regions vertical mixing can be strong and can greatly reduce vertical density gradients.

Specified criteria for the H_2/H_1 ratio are based on the international experimental database which is presented in the next chapter.

9.C.1.3.2 References

P. F. Peterson, (1994), "Scaling and Analysis of Mixing in Large Stratified Volumes," Int. J. of Heat and Mass Transfer, Vol. 37, Supplement 1, pp. 97-106, 1994.

D. R. Spencer, (1997), "Scaling Analysis for AP600 Containments Pressure During Design Basis Accidents," WCAP-14845, Revision 3, March 1998.

9.C.1.4 EXPECTED FLOW PATTERNS FOR AP600 AND AP1000

9.C.1.4.1 Simplified Representation of Circulation Regions During Post-Blowdown LOCA in AP600 and LST

The AP600 containment and the large-scale test (LST) facility include five primary flow regions (Peterson, 1997 - letter to Woodcock). The regions are presented in Figure 9.C.1-18 showing a control volume that extends to the condensed fluid film surfaces. This figure is useful for structuring a discussion of circulation and stratification phenomena and for relating separate effects of enclosures tests to the various regions.

The volumetric flow rates presented in Figure 9.C.1-18 at "quasi-steady" conditions are:

- Q_o , the steam volumetric flow rate from the break,
- Q_e , the flow rate of fluid entrained from inside the below-deck region into the steam generator compartment (equivalent to the flow rate delivered to the below-deck region due to the penetration of a portion of the wall boundary layers through the deck gap near the walls),
- Q_p , the flow rate of fluid entrained into the plume in the above-deck region,
- Q_w , the flow rate of fluid entrained into the vertical wall boundary layers,
- Q_v , the flow rate of steam condensed on the vertical walls (shown leaving the control volume), and
- Q_i , the flow rate of steam condensed on the dome ceiling (shown leaving the control volume)

For the quasi-steady conditions, the steam flow rate entering in the containment volume Q_o is equal to the summation of the steam flow rates condensed on the dome ceiling Q_i and vertical walls Q_v .

The distances presented in Figure 9.C.1-18 are:

- H_p , the distance between the jet inflow position into the upper-deck region and the dome springline elevation (in vertical direction),

- H_{EF} , the distance between the break location and the jet inflow position into the upper-deck region (in vertical direction), and
- H_v , the distance between the vertical wall and the jet center (in horizontal direction).

The definitions of the regions relate well to the separate effects of the enclosure tests.

Region I is below the operating deck level. In the AP600 and AP1000 configuration, connections exist between the below-deck compartments and the upper-deck region (dome). These connections allow the steam jet (plume) generated-entrainment into the break compartment to produce circulation through Region I. The volumetric flow from the lower to the upper deck regions is Q_e . Jet entrainment and the slots around the circumference of the deck floor enable this circulation (see Figure 9.C.1-19).

In the LST - LOCA experiments, the release point is also below the operating deck level. However, the compartment containing the release is not connected with the other below-deck compartments (see Figure 9.C.1-20). The simulated steam generator compartment is connected only with the upper portion (dome) of the containment. Therefore, the jet injection location for the LST LOCA experiments is effectively at the top of the simulated steam generator compartment, where the flow enters the above-deck region, and entrained volumetric flow Q_e is equal to zero (see Figure 9.C.1-20). The atmosphere in the below-deck compartment is a stably stratified region without recirculation. The heat and mass transfer in the below deck compartments are governed primarily by molecular diffusion.

Region II is defined as the volume between the springline elevation and a horizontal line above the operating deck elevation, and between the wall boundary layers (Region IV) and the plume (Region III). Two entrainment mechanisms remove fluid from Region II. Entrainments into the vertical jet (or buoyant plume) and the wall boundary layers are compensated for by the inflows from the upper and lower horizontal boundaries. In order to preserve mass continuity and to obtain inflow into Region II, the vertical velocity components (see Figure 9.C.1-21) are negative and positive at the upper and lower horizontal boundaries, respectively. The fluid inside the Region II is recirculating (see Figure 9.C.1-22), yet has a quasi-steady dp/dz maintained by balance between the buoyancy and the two entrainment mechanisms. Therefore, Region II can be called a recirculating stratified region. The horizontal density and concentration gradients are small, but significant recirculation flow exists due to the entrainment into the free and wall jets (see Peterson, 1997). Region II can be considered as a region where the vertical density, temperature and concentration gradients are dependent on the values of the volumetric Froude numbers (for free jets or plumes) and Grashof (Rayleigh) numbers (for wall boundary layers). This is similar to the case of an enclosure with opposite vertical walls at different temperatures (see section 9.C.1.1.2.1). The recirculation and entrainment from the Region II contributes to a decrease in the vertical temperature, density, and concentration gradients.

Region III contains free jets (plumes) which transport fluid in the vertical direction. The upward motion of a jet (or plume) produces entrainment from Region II. As a result, the jet (or plume) spreads, reduces velocity, and dilutes (decreases the temperature and concentration difference between the core of the jet and the surrounding atmosphere - Region II).

Region IV contains wall boundary layers which also provide transport in the vertical direction. The entrainment into the wall boundary layer transports steam into Region IV. The entrainment from Region II into the wall boundary layers enhances recirculation inside the Region II. This contributes to a decrease in the vertical temperature, density, and concentration gradients inside Region II.

Region V, the dome region, is between the containment ceiling and the elevation of the springline. Because the temperature of the containment ceiling is lower than the temperature of the atmosphere below the ceiling, downward flowing "ceiling plumes" are formed (see the Rayleigh-Benard convection example of section 9.C.1.2.1). The difference in the steam concentrations between the top of the Region V (immediately below the ceiling where condensation occurs) and the top of Region II are small due to the circulation (interaction) within Region V, caused by cold plumes falling from the ceiling and the hot plume reaching the ceiling of the dome. The downward plumes increase circulation and reduce gradients inside the dome, Region V. The downward "ceiling plumes" interact with the uprising plume (from the Region III). If the strength of the jet (plume) from the Region III is high, interactions occur inside Region V and the influence of the downward plumes does not spread towards the lower regions.

However, if the plume from Region III is not strong enough to produce good mixing inside Region V, the penetration of the downward "ceiling plumes" into the lower regions can disturb (from time to time) the recirculating stratified layers inside Region II. This tends to reduce the vertical gradients within Region II.

If the plume is very weak or does not exist, the vertical downward "ceiling plumes" affect the entire volume of the upper-deck region. The flow patterns formed are the result of superposition of Rayleigh-Benard convection (described for the enclosure with cold upper and hot lower surface) and recirculating stratification (described for the enclosure with opposite vertical walls at different temperatures).

The cold dome ceiling produces downward vertical plumes as in Rayleigh-Benard convection case, while cold vertical walls produce downward wall boundary layers. Due to continuity, the downward wall boundary layers tend to generate upward flow in the middle of the above-deck region. The wall boundary layer and the upward flow in the middle of the containment form a recirculation zone. Between the wall boundary layers and the upward flow in the middle of the containment, a recirculating stratified core is formed. This is similar to enclosures with opposite vertical walls at different temperatures. Note that although there is

evidence from enclosure tests that a stable non-zero vertical density gradient could exist in Region II, entrainment flows cause circulation of fluid. Region II is not considered as stagnant.

The prevailing flow pattern can be postulated (Rayleigh-Benard or recirculating stratified) from the ratio of Grashof numbers Gr_v/Gr_h , [defined for vertical $\Delta\rho$ and distance H_v (for Gr_v) and horizontal $\Delta\rho$ and distance H_h (for Gr_h)]. Note that turbulent Rayleigh-Benard convection starts at $Ra_v = Gr_v Pr > 10^4$ (for $Pr = 0.71$, based on 3D enclosure experiments - see section 9.C.1.2.1), while turbulent flow (with thin boundary layers and recirculating stratified but almost homogenized core) in enclosures with vertical walls at opposite temperatures starts at $Ra_h = Gr_h Pr > 10^8$ (for $Pr = 0.71$, based on 2D numerical simulations, see section 9.C.1.1.2.1). This indicates that for small values of Rayleigh numbers ($10^4 < Ra_v$ and $Ra_h < 10^8$), Rayleigh-Benard convection is dominant. Turbulent and chaotic flow are dominated by falling vertical plumes (see Figure 9.C.1-15).

For higher Rayleigh numbers (Ra_v and $Ra_h > 10^8$) combined with a weak source plume, in fact smaller Rayleigh number in horizontal direction, falling vertical plumes (see Figure 9.C.1-15) dominate the flow patterns. For the dominant jet (or plume), or high Rayleigh number in horizontal direction (Gr_h high) and moderate Froude number, a recirculating stratified flow pattern prevails in Region II (see Figure 9.C.1-5). Higher and similar magnitude values of both Rayleigh numbers (in vertical and horizontal direction) result in a flow pattern that is a superposition of the two described patterns (shown in Figures 9.C.1-15 and 9.C.1-5). Finally, for the case of the momentum-dominated jet (with high Froude number), the circulation flow pattern will be present in the entire volume of the containment (see Figure 9.C.1-11).

9.C.1.4.2 A Qualitative Model for Recirculating Stratified Region II

A qualitative model of Region II is used to address the issue of recirculating stratification and circulation (Peterson, 1997). The model is a coarse, first-principle representation of the effects of various volumetric flows and entrainment rates. It qualitatively examines the influence of various parameters on the difference in steam concentrations from the bottom to the top of the Region II (ΔX).

Because of the complexity of the physics, two simplifying assumptions are used. It is assumed that Region II is not influenced by falling plumes from Region V and that the recirculation effects inside Region II can be neglected. Both assumptions cause overestimated vertical steam gradients ΔX . Interactions between Region II and Region V that result from the penetration of the cold falling plumes (from Region V), improve mixing and decrease vertical steam gradients ΔX . Recirculation inside Region II (established experimentally and numerically inside the core of enclosures) further decreases the vertical steam gradients.

Peterson, 1997, provides the following mass conservation equation for the thin horizontal layer inside Region II with area $A(z)$ (see Figure 9.C.1-23):

$$\rho(z)A(z)dv(z) = -\rho_p(z)u_p(z)p_p(z)dz - \rho_w(z)u_w(z)p_w(z)dz$$

where $v(z)$ is the vertical velocity, and $u_p(z)$ and $u_w(z)$ are the entrainment velocities into the steam plume and wall boundary layer, respectively. The vertical coordinate is z , while p_p and p_w are the perimeters of the plume (or jet) and wall boundary layer, respectively.

Since molar densities are dependent only on the temperature (assuming constant pressure in the entire volume), the differences between the molar densities $\rho(z)$, ρ_p and ρ_w are small. To simplify the analysis, the equation is written without densities. A balance of the volumetric flow rates is then used for the remainder of the analysis (instead of a mass balance).

To further simplify the analysis (considering only global effects), u_p , u_w , p_p , p_w , and A are assumed to be constant, or independent of z (Peterson, 1997). This assumption results in a linear, vertical velocity distribution. Although the actual entrainment varies with height, the integrated total should be reasonably close to the average constant values.

The calculations of the entrained volumetric flow into the plume Q_p and wall boundary layer Q_w are simplified as:

$$Q_p = \int_0^H u_p(z)p_p(z)dz = u_p p_p H$$

and

$$Q_w = \int_0^H u_w(z)p_w(z)dz = u_w p_w H$$

respectively. The total inflow to the top and bottom of Region II (see Figure 9.C.1-21) provides the boundary conditions for the vertical velocities $v(0)$ and $v(H)$ at the bottom and at the top of the Region II, respectively:

$$A v(0) = Q_w - Q_v - Q_e$$

$$A v(H) = - (Q_v + Q_p + Q_e)$$

where Q_e is the volumetric rate of flow into the below-deck region (see Figures 9.C.1-18 and 9.C.1-19). Due to mass continuity (conservation) for the below-deck region, this flow rate is equal to the volumetric flow rate (Q_e) entrained into the steam generator compartment by the steam jet (plume).

The volumetric flow rate of steam condensed on the vertical wall is Q_v . Q_t is the flow rate of steam condensed on the dome. The total steam volumetric inflow into the containment is $Q_o = Q_v + Q_t$ (see Figure 9.C.1-18 and 9.C.1-23).

The linear, vertical velocity distribution in Region II is:

$$Av(z) = (Q_w - Q_v - Q_e) - \frac{z}{H}(Q_p + Q_w)$$

Downflow exists in the top part of Region II, while in the lower portion, the velocities are positive (upwards flow). This agrees with the previous discussion of Region II inflow horizontal boundaries (see Figure 9.C.1-21). Because the continuity-driven velocities are assumed horizontally uniform upward at the bottom and downward at the top of Region II, there will be an elevation, z , where the two meet and vertical velocity is zero. The z coordinate where the vertical velocity is zero in this model is:

$$z = \frac{Q_w - Q_v - Q_e}{Q_p + Q_w} H$$

The average gas mole fraction in Region II is:

$$\bar{x}_g = \frac{1}{V} \int_0^H A(z) x_g(z) dz = \frac{1}{H} \int_0^H x_g(z) dz$$

The mole fraction of gas at the bottom of Region II is found from a mass balance on the wall boundary layer. (Note that Q_v is the volumetric flow of steam that condenses on the vertical wall. It contains no noncondensable gas.)

$$x_g(0) = \frac{\int_0^H x_g(z) u_w(z) p_w(z) dz}{Q_w - Q_v} = \frac{u_w p_w \int_0^H x_g(z) dz}{Q_w - Q_v} = \frac{u_w p_w H \bar{x}_g}{Q_w - Q_v} = \frac{Q_w \bar{x}_g}{Q_w - Q_v}$$

Similarly the gas mole fraction at the top of the Region II is:

$$x_g(H) = \frac{x_g(0) Q_e + \int_0^H x_g(z) u_p(z) p_p(z) dz}{Q_v + Q_p + Q_e} = \frac{\frac{Q_w \bar{x}_g}{Q_w - Q_v} Q_e + u_p p_p \int_0^H x_g(z) dz}{Q_v + Q_p + Q_e} = \frac{\frac{Q_w \bar{x}_g}{Q_w - Q_v} Q_e + Q_p \bar{x}_g}{Q_v + Q_p + Q_e}$$

The relative difference in the concentrations from the bottom to the top of Region II is:

$$\frac{\Delta x}{\bar{x}_g} = \frac{x_g(0) - x_g(H)}{\bar{x}_g} = \frac{Q_w}{Q_w - Q_v} - \frac{\frac{Q_w Q_e}{Q_w - Q_v} + Q_p}{Q_v + Q_p + Q_e}$$

The final form of the equation, which is more suitable for qualitative understanding of the influence of various volumetric flow rates, is:

$$\frac{\Delta x}{\bar{x}_g} = \frac{x_g(0) - x_g(H)}{\bar{x}_g} = \frac{Q_v (Q_w + Q_p)}{(Q_w - Q_v)(Q_p + Q_v + Q_e)}$$

The influence of the various volumetric flow rates under various assumed conditions will now be examined.

9.C.1.4.2.1 Case 1: Strong Plume, Wall Boundary Layer and Plume Entrainments are Equal

If the entrainment volumetric flow rates are approximately equal ($Q_p \sim Q_w$) and are large compared to Q_v and Q_e , the relative concentration difference is simplified to:

$$\frac{\Delta x}{\bar{x}_g} = \frac{x_g(0) - x_g(H)}{\bar{x}_g} \approx \frac{Q_v (2Q_w)}{(Q_w)(Q_w)} = \frac{2Q_v}{Q_w}$$

These assumptions are valid for the case of the jet-dominated flow. The large plume and wall boundary layer entrainment volumetric flow rates act to reduce the relative, vertical steam concentration gradient.

Even if the flow pattern cannot be defined as jet-dominated (i.e., the equation for the relative difference in the concentration from the bottom to the top of Region II cannot be simplified), the recirculating stratified Region II interacts with the plume and wall jets, Regions III, and IV (see Figure 9.C.1-23). The relative

concentration difference will still decrease if the entrainments in both the wall layer Q_w and plume Q_p are large.

It has been shown (Enclosure to Westinghouse Letter NSD-NRC-97-4978, February 7, 1997) that during the quasi-steady portion of a LOCA, jet entrainment rates (Q_p) in the AP600 are about a factor of 10 greater than the condensation rate (Q_v+Q_d).

9.C.1.4.2.2 Case 2: Equal Entrainment into the Wall Boundary Layer Q_w and the Rate of the Steam Condensed at the Vertical Walls Q_v

A small difference between the entrainment volumetric flow rate into the wall boundary layer Q_w and volumetric flow rate of the steam condensed at the vertical walls Q_v produces an increase in the relative difference of the concentrations. If all the steam entrained into the wall boundary layer is condensed at the vertical walls, nothing is left to be redistributed through the lower horizontal boundary of Region II and contribute towards a decrease in the vertical concentration gradients.

9.C.1.4.2.3 Case 3: High Dome Condensation Rate Q_d

The volumetric flow of the steam condensed on the dome of the containment Q_d does not directly affect the relative concentration difference in Region II (it is not present in the equation). However, indirect effects are possible. If the condensation on the dome is high, the ratio of Q_d/Q_v is high, and the volumetric flow of steam condensing on the vertical walls Q_v decreases. In contrast, a small ratio of Q_d/Q_v represents an increased volumetric flow rate condensing on the vertical walls, Q_v . A decrease in the rate of steam condensing on the vertical walls Q_v (in fact the increase of steam volumetric flow rate condensing on the dome, Q_d), decreases the relative concentration difference.

9.C.1.4.2.4 Case 4: Influence of the Below Deck Entrainment Q_e

Region I also interacts with the stratified Region II. The effects of this interaction on the relative concentration difference change are captured by the Q_e term. A large below-deck entrainment, Q_e , reduces the concentration difference. In the AP600 and AP1000, below-deck entrainment contributes to a decrease in the relative concentration difference. This effect is not present in the LST case, where $Q_e = 0$.

9.C.1.4.2.5 Case 5: Dominant Entrainment into the Wall Boundary Layer Q_w

If $Q_v = 0.5 Q_o$, as observed in phase 3 of the LST experiments where Q_v is between $0.4Q_o$ and $0.6Q_o$ (see WCAP-14135), and if $Q_w = 2Q_p$, i.e., the wall boundary layer entrainment is twice as strong as plume entrainment (weak plume scenario), if the entrainment in the below-deck region is negligible, $Q_e = 0$, and if we assume $Q_p = 10Q_o$ the relative steam concentration is:

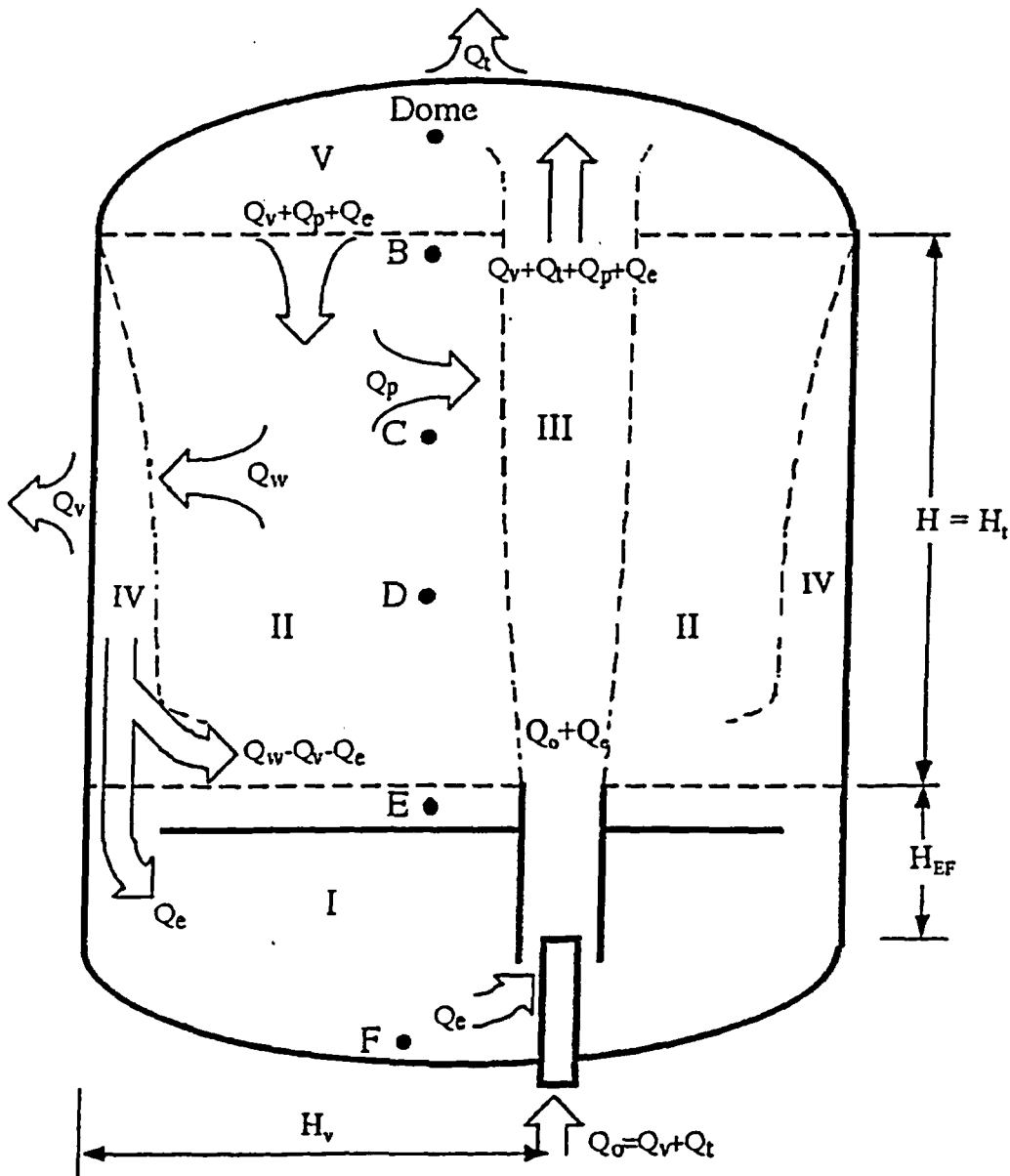
$$\frac{\Delta x}{\bar{x}_g} = \frac{x_g(0) - x_g(H)}{\bar{x}_g} = \frac{0.5Q_o (2Q_p + Q_p)}{(2Q_p - 0.5Q_o)(Q_p + 0.5Q_o + 0)} = 0.073$$

A further increase in the entrainment into the wall boundary layers causes an additional decrease in the relative difference between steam concentrations in the bottom and the top of Region II (e.g., if $Q_w=3Q_p$, the relative concentration is 0.064). The increase in the entrainment into the wall boundary layers contributes to the homogenization of the containment atmosphere.

9.C.1.4.2.6 Conclusion

The expected circulation within the AP600 and AP1000 containment is segregated into five regions that relate to separate effects tests (SETs) in enclosures. Given the presence of the externally cooled shell, which is assumed in a DBA analysis, there are no regions of stagnant stratification in containment.

The proposed conceptual model can be used to structure the containment into regions for comparison to relevant enclosures SETs. The mathematical representation provides insight into the influence of various volumetric flows on the axial steam concentration gradients in the AP600 and AP1000.



VOLUMETRIC FLOW RATES

- Q_v steam volumetric flow rate from the brake
- Q_e flow rate entrained by the jet inside the below deck region
- Q_p flow rate entrained into the plume in the above deck region
- Q_w flow rate entrained into the vertical wall boundary layers
- Q_c steam flow rate condensed on the vertical walls
- Q_t steam flow rate condensed on the dome ceiling

REGIONS

- I below deck region
- II region of recirculating stratification
- III region of jets or plumes
- IV region of wall boundary layers
- V region below dome ceiling

Figure 9.C.1-18

Primary flow regions and volumetric flow rates for quasi-steady containment conditions

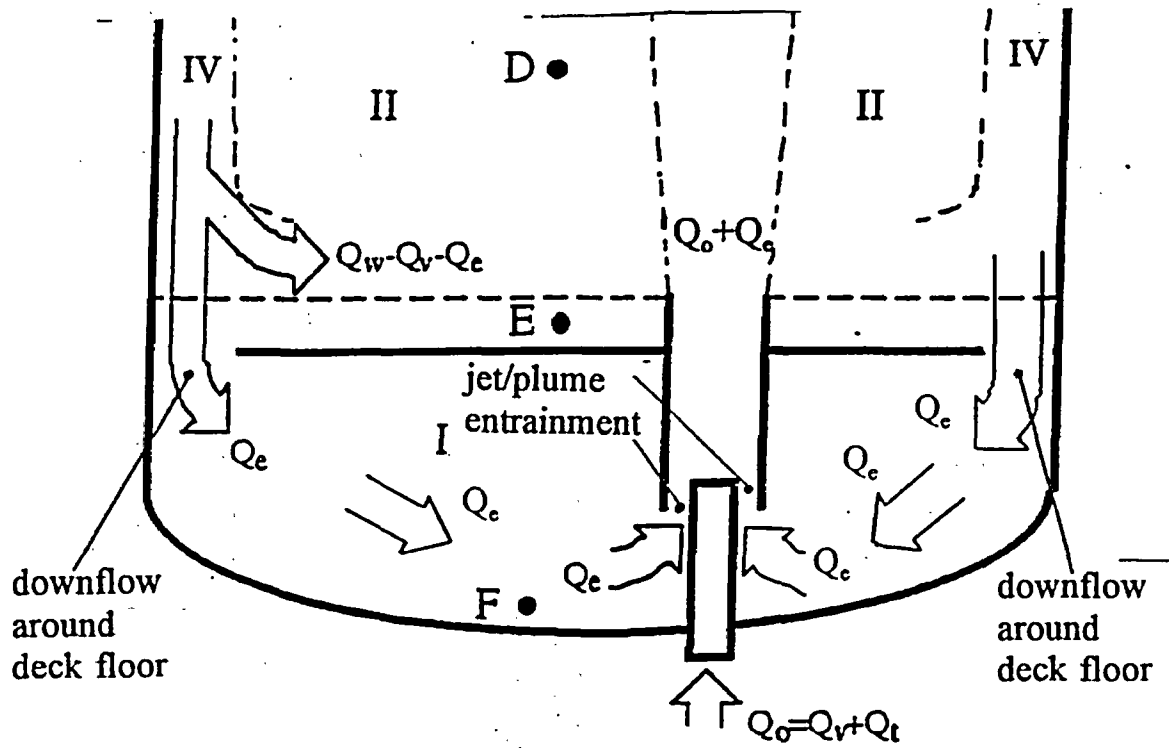
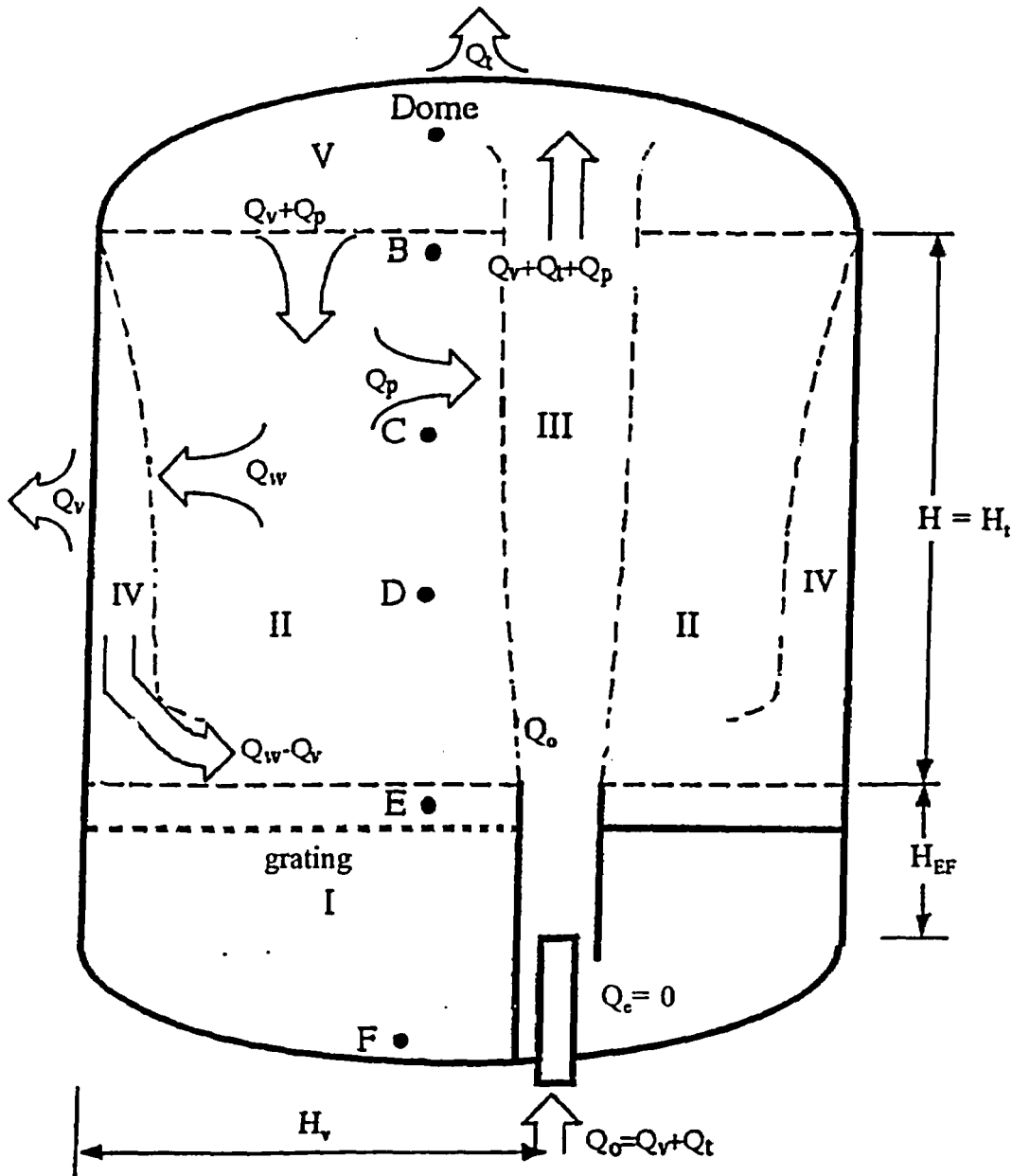


Figure 9.C.1-19 The volumetric flow between the upper and lower deck regions Q_e .



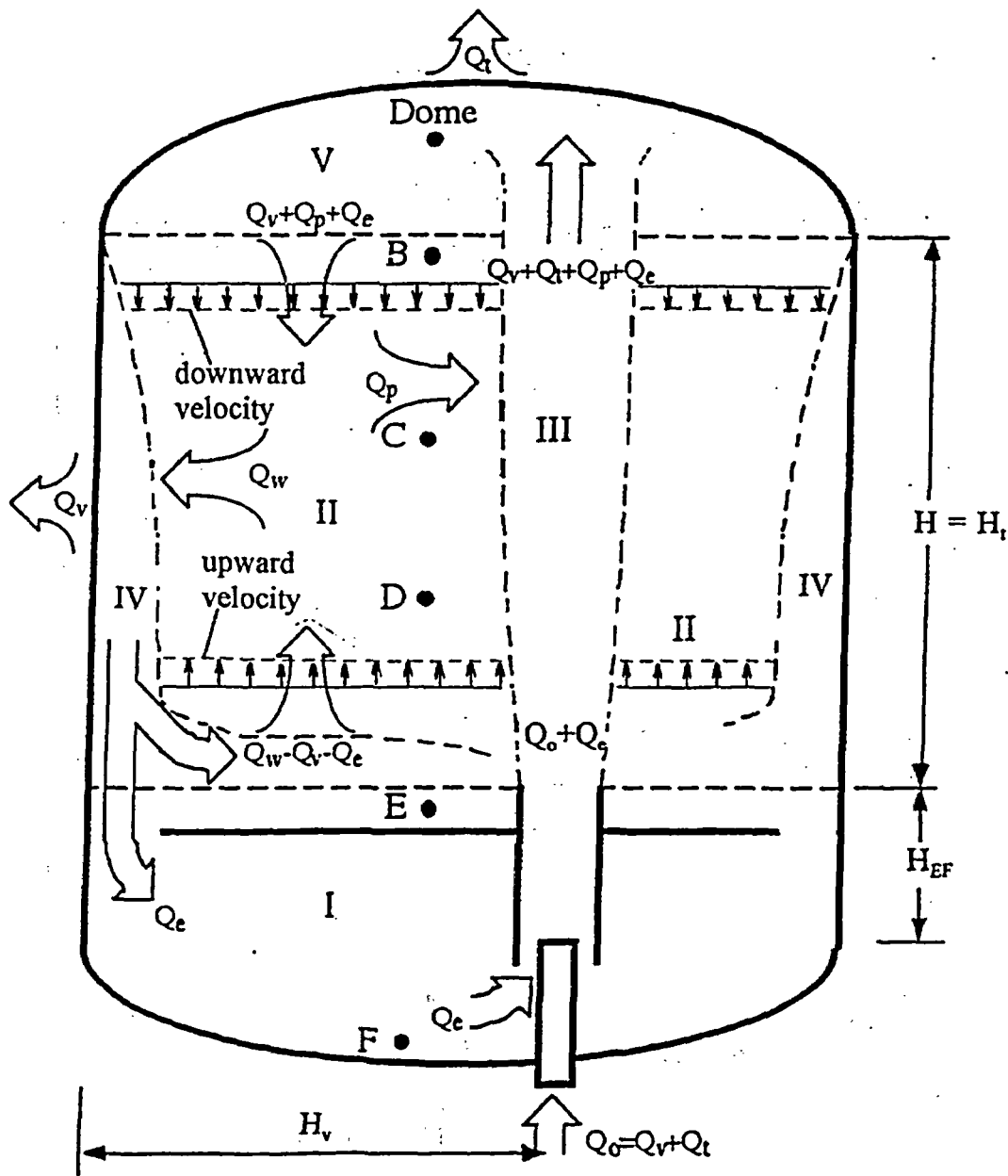
VOLUMETRIC FLOW RATES

- Q_o steam volumetric flow rate from the brake
- $Q_e = 0$ flow rate entrained by the jet inside the below deck region
- Q_p flow rate entrained into the plume in the above deck region
- Q_w flow rate entrained into the vertical wall boundary layers
- Q_v steam flow rate condensed on the vertical walls
- Q_t steam flow rate condensed on the dome ceiling

REGIONS

- I below deck region
- II region of recirculating stratification
- III region of jets or plumes
- IV region of wall boundary layers
- V region below dome ceiling

Figure 9.C.1-20 Primary flow regions and volumetric flow rates for quasi-steady containment conditions in LST case



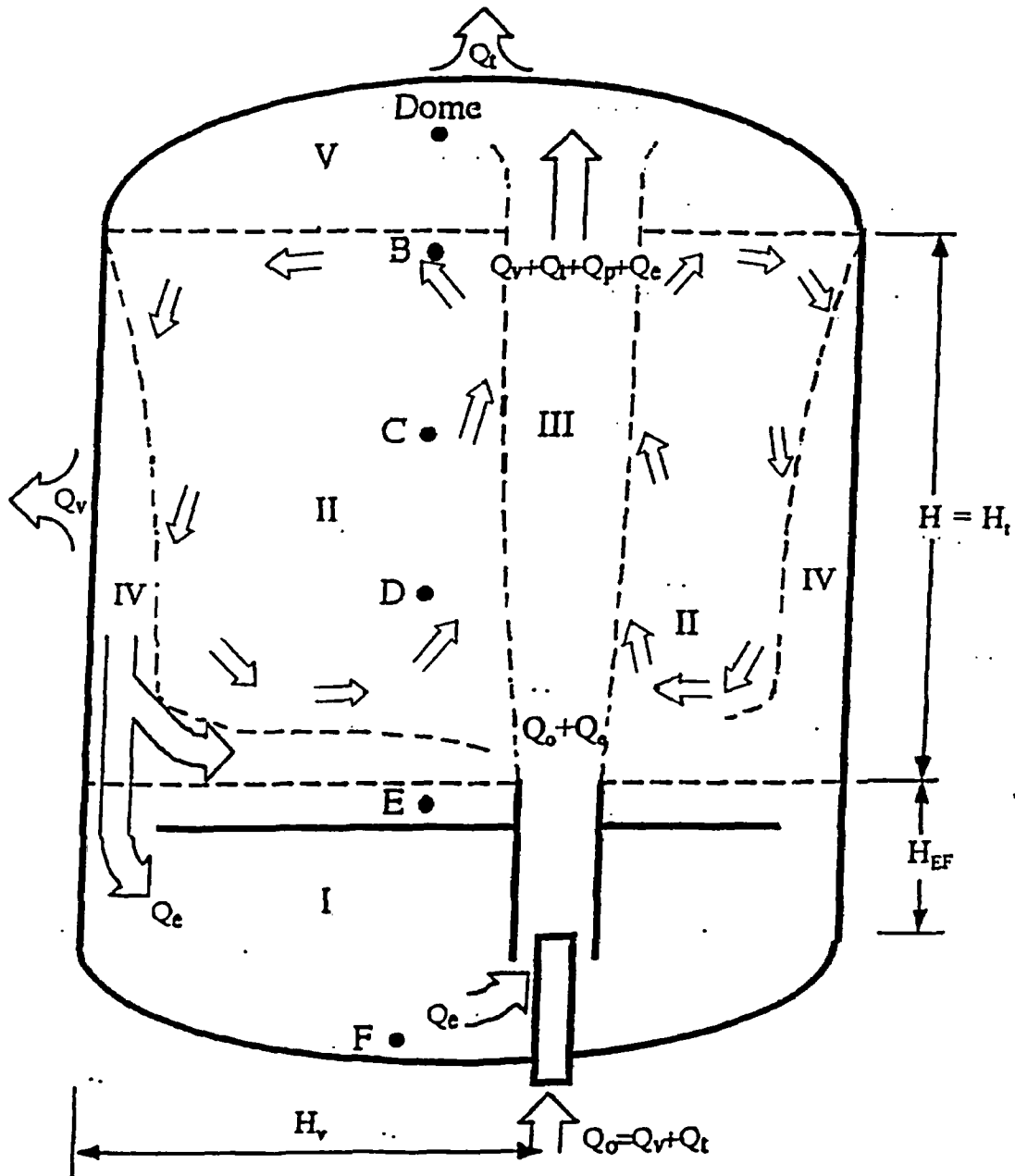
VOLUMETRIC FLOW RATES

- Q_o steam volumetric flow rate from the brake
- Q_e flow rate entrained by the jet inside the below deck region
- Q_p flow rate entrained into the plume in the above deck region
- Q_w flow rate entrained into the vertical wall boundary layers
- Q_v steam flow rate condensed on the vertical walls
- Q_t steam flow rate condensed on the dome ceiling

REGIONS

- I below deck region
- II region of recirculating stratification
- III region of jets or plumes
- IV region of wall boundary layers
- V region below dome ceiling

Figure 9.C.1-21 Inflows and outflows from the Region II



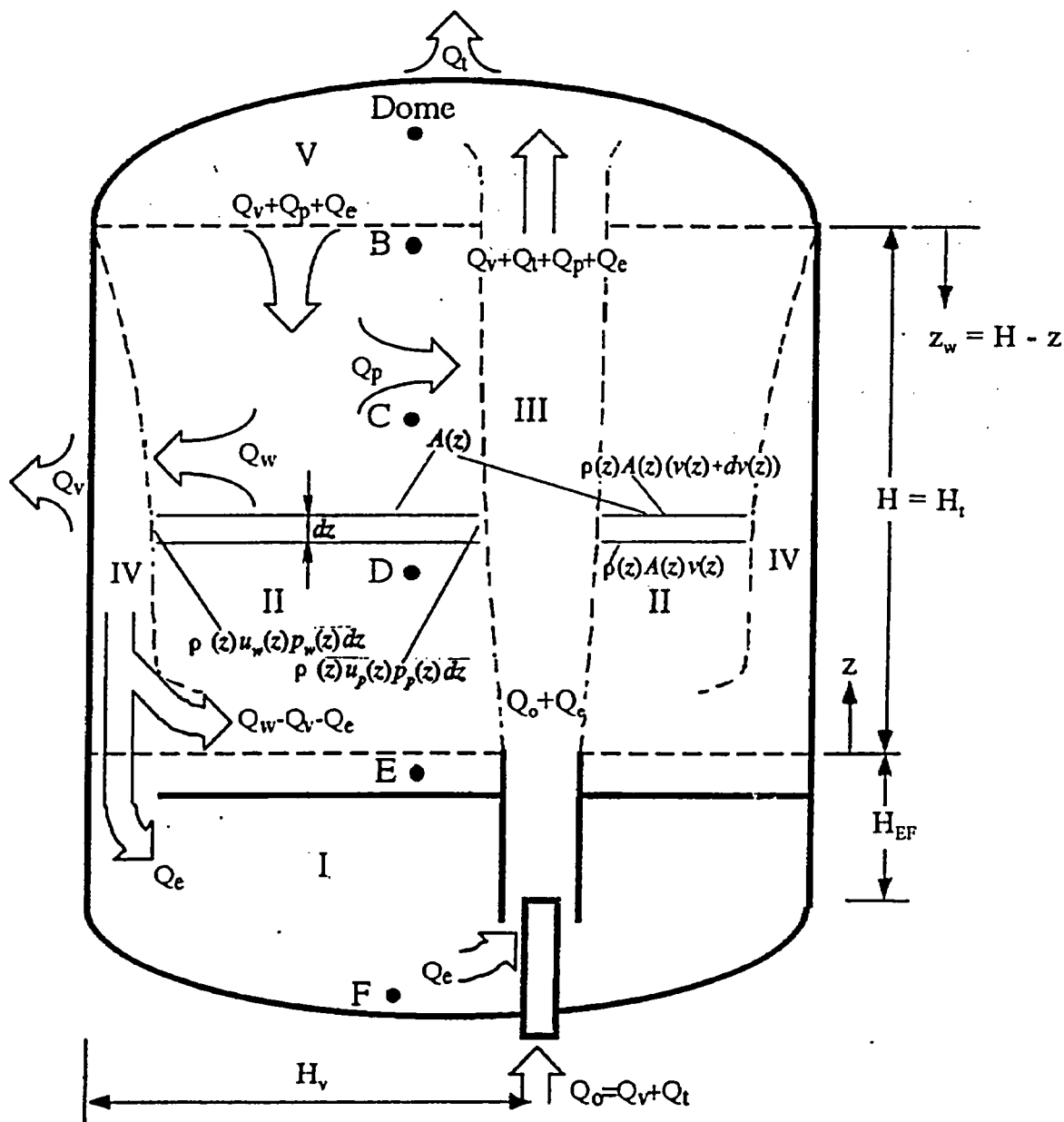
VOLUMETRIC FLOW RATES

- Q_o , steam volumetric flow rate from the brake
- Q_e , flow rate entrained by the jet inside the below deck region
- Q_s , flow rate entrained into the plume in the above deck region
- Q_v , flow rate entrained into the vertical wall boundary layers
- Q_c , steam flow rate condensed on the vertical walls
- Q_d , steam flow rate condensed on the dome ceiling

REGIONS

- I below deck region
- II region of recirculating stratification
- III region of jets or plumes
- IV region of wall boundary layers
- V region below dome ceiling

Figure 9.C.1-22 Recirculating flow paths inside the Region II



VOLUMETRIC FLOW RATES

- Q_o steam volumetric flow rate from the brake
- Q_e flow rate entrained by the jet inside the below deck region
- Q_p flow rate entrained into the plume in the above deck region
- Q_w flow rate entrained into the vertical wall boundary layers
- Q_v steam flow rate condensed on the vertical walls
- Q_c steam flow rate condensed on the dome ceiling

REGIONS

- I below deck region
- II region of recirculating stratification
- III region of jets or plumes
- IV region of wall boundary layers
- V region below dome ceiling

Figure 9.C.1-23 Mass conservation for thin horizontal layer inside the Region II

9.C.1.4.3 References

1. P.F. Peterson, 1997
LST Mixing Model Writeup - letter to J. Woodcock, 02/24/97
2. Enclosure to Westinghouse Letter NSD-NRC-97-4978
Subject: Position paper in support of the assumption of complete mixing of aerosols in the AP600 containment atmosphere following a loss of coolant accident
February 7, 1997
3. WCAP-14135, F. E. Peters, April 1997
"Final Data Report for PCS Large-Scale Tests, Phase 2 and Phase 3", Revision 1
Westinghouse Energy Systems

9.C.2 OVERVIEW OF THE INTERNATIONAL CONTAINMENT EXPERIMENTAL DATA BASE

Tests from the available international containment experimental database that are relevant to the passive containment design, are presented in this chapter. Some tests are very close to possible passive containment cases. Others are presented to emphasize the difference between the passive containment design and the test conditions that lead towards stratification.

Four experimental facilities are considered to supplement LST data. Table 9.C-1 specifies characteristics of each experimental facility and provides a comparison with the LST, the AP600 and the AP1000. A comparison of the sizes of various test facilities is provided in Figure 9.C.2-1. Scaled cross-sections of each facility are shown.

A list of the facilities and the overviewed experiments is provided in Table 9.C.2-2, as well as the main characteristics of each experiment.

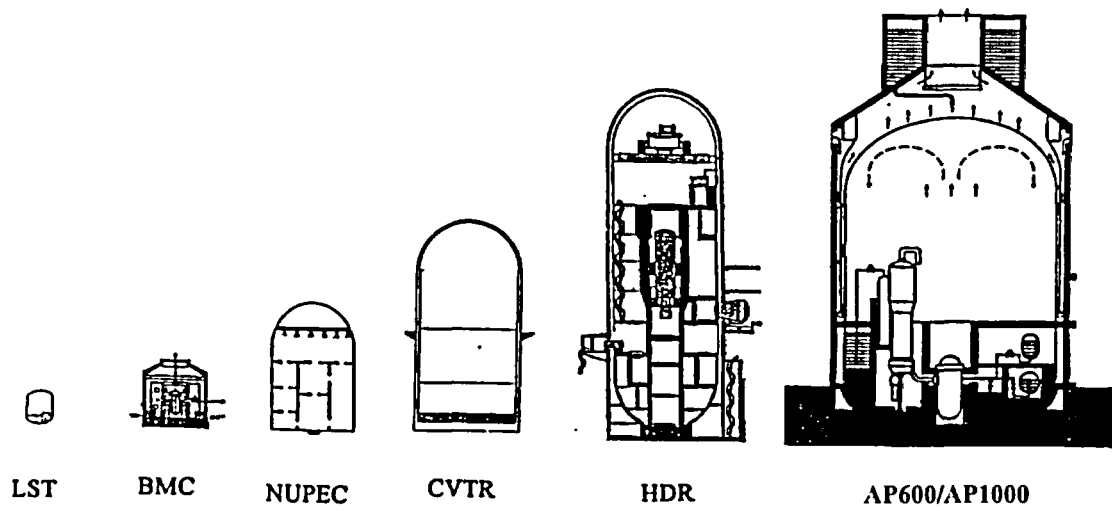


Figure 9.C.2-1 Comparison of different facilities

Table 9.C-1 Comparison of Various Facilities							
Facility	LST	BMC	NUPEC	CVTR	HDR	AP600	AP1000
Volume m ³	83.1	640	1300 (used)	6428	11300	48710	58333
Height m	6.1	9	17.4	34.7	60	57.9	65.6
Diameter m	4.57	11.25	10.8	17.7	20	39.6	39.6
Number of compartments	3	9	25	3	62-72	11	11
Volume of the dome	79%		70%	41%	44%	81%	83%
Containment walls	steel	concrete	steel	concrete	steel shell concrete and steel	steel shell concrete and steel	steel shell concrete and steel

Table 9.C-2 Overviewed Tests from International Database				
Facility	Experiment	Main Feature	Position of the Release Point and Other Relevant Data	Stratification or Circulation
BMC	F2 set First Phase	stepwise steam addition	release point is high Hr/Ht=0.444	circulation through the majority of compartments, external annulus stratified
BMC	F2 set Phase 2	inducing the natural circulation with steam injection	steam release point is low Hr/Ht = 0.111	circulation through the majority of compartments, external annulus stratified
BMC	F2 set Phase 3	heater on in R6 to reverse circulation	heat source location is low Hr/Ht = 0.111	circulation through the majority of compartments, external annulus stratified
BMC	F2 set Phase 4	steam injection in R6 compartment	steam release point is low Hr/Ht = 0.111	circulation through the majority of compartments, external annulus stratified
BMC	Test 2 Two compartments (Phase I)	hydrogen injection, uniform initial temperature, orifice present, low feed rate	low position of hydrogen source Hr/Ht = 0.06	hydrogen uniformly distributed, circulation present
BMC	Test 4 Two compartments (Phase I)	hydrogen injection, uniform initial temperature, no orifice	high position of hydrogen source Hr/Ht = 0.57	concentration stratification occurs
BMC	Test 6 Two compartments (Phase I)	hydrogen injection, stratified initial temperature, orifice present	low position of hydrogen source Hr/Ht = 0.06	stratification present, highest hydrogen concentration in the lower compartments

Table 9.C-2 Overviewed Tests from International Database (cont.)				
Facility	Experiment	Main Feature	Position of the Release Point and Other Relevant Data	Stratification or Circulation
BMC	Test 12 Six compartments (Phase II)	hydrogen injection in R2 room (high), uniform initial temperatures	high release point $H_i/H_1 = 0.69$	hydrogen uniformly distributed, circulation present
BMC	Test 20 Six compartments (Phase II)	hydrogen injection in R6 room (low), stratified initial temperature	low position of hydrogen source $H_i/H_1 = 0.06$	stratification present, highest hydrogen concentration in the lower compartments
BMC	RX4	sump heat up and three hydrogen injections	low position of the heat and hydrogen source $H_i/H_1 = 0.0$	circulation present, homogenization of temperature and concentrations
NUPEC	M-4-3	simulated break inside the low steam generator compartment, steam and hydrogen release, containment shell insulated	low position of the heat and hydrogen source $H_i/H_1 = 0.0$	circulation present during release, temperature stratifies and concentration homogenizes after the end of release
CVTR	First test without the internal water sprays	steam release in the upper compartment, concrete shell	high position of the steam release $H_i/H_1 = 0.525$	temperature field stratifies
CVTR	The second and third test with internal water sprays	steam release in the upper compartment, concrete shell	high position of the steam release $H_i/H_1 = 0.525$	temperature field stratifies but not as strong as in the previous case
HDR	E11.2	high positioned release point (small break) and active external spray	high position of the steam release $H_i/H_1 = 0.555$	stratification exists, external sprays promoted circulation
HDR	E11.3	low positioned small break closed spiral stairway entrance		global circulation pattern formed

Table 9.C-2 Overviewed Tests from International Database (cont.)				
Facility	Experiment	Main Feature	Position of the Release Point and Other Relevant Data	Stratification or Circulation
HDR	E11.4	low positioned release point (small break) and active external spray	low position of the steam release $H_1/H_0 = 0.18$	global circulation formed almost uniform temperature distribution except below release point
HDR	T31.5	simulates DBA large LOCA in the upper section of the containment	high position of the steam release $H_1/H_0 = 0.526$	temperatures and gas concentrations first stratify and latter homogenize
HDR	V21.1	simulates DBA large LOCA in the middle section of the containment (in both staircases)	middle position of the steam release $H_1/H_0 = 0.38$	Equal heating of both staircases first suppressed circulation. Slight global circulation was generated later.
HDR	E11.5	simulates DBA large LOCA in the lowest section of the containment with effects of dry heat release and sump boiling	low position of the steam release $H_1/H_0 = 0.18$	global circulation due to the steam release, gas mixture injection and sump boiling contributed towards homogenization

9.C.2.1 DESCRIPTION OF THE AVAILABLE BATTELLE MODEL CONTAINMENT (BMC) DATABASE

The objective of the Battelle Model Containment (BMC) tests is to obtain data to analyze design basis accidents (DBAs), hydrogen distribution, and aerosol depletion. The total volume of the containment is 640 m³ and represents 1/64 of the BIBLIS B containment. Its interior is divided into nine compartments and its walls are made of reinforced concrete. The sizes and locations of openings between the compartments can be adjusted by opening (or closing) the openings with steel plates or mobile concrete structures.

Three sets of tests are presented.

- The first set, the F2 experiments, tests natural convection as a function of release location and type of release (steam, air, dry heat).
- The second set of tests studies the influence of the initial temperature distribution, the location of hydrogen injection, the injection rates, and the size of the vent openings on hydrogen distribution, stratification and global circulation.
- The third set of tests examines the effect of sump heatup on global natural circulation.

9.C.2.1.1 Natural Convection Phenomena Inside the Multi-Compartment Containment (F2 Experiments)

The F2 experiments, performed by Kanzleiter in 1988, study natural convection inside a multi-compartment containment as a function of release location (room) and type (steam, air, dry heat). The BMC configuration used for experiment F2 is shown in Figures 9.C.2-2 and 9.C.2-3. A 48-hour heatup period is the first phase of the experiment - see Figure 9.C.2-4, (Fischer et al., 1989, and Fischer et al., 1991). This is followed by a three-part, natural circulation phase (phases 2, 3, and 4) within the 48- to 75-hour time period see Figure 9.C.2-5, (Fischer et al., 1990 and Fischer et al., 1993).

An overview of the results and a comparison with analysis codes is presented by Wolf et al, 1996. Data for pressure, temperature, sump temperature, and liquid level, as well as partial steam pressure is presented for phases 1-4 (up to 75 hours).

9.C.2.1.1.1 F2 - Experiment Heatup Phase - Phase 1

Phase 1 is from 0-48 hours. A steam release inside the R2 compartment provides the heatup (see Figures 9.C.2-6 and 9.C.2-4). The stepwise steam addition results in a stepwise increase of the containment pressure (see Figure 9.C.2-7 for GP 9117 location).

During the 48 hours of heatup, the atmosphere in the external annulus (the lower portion of R9 surrounding compartment) stratifies, Figure 9.C.2-8. Since there is no driving force for the circulation of steam into the lower air-rich regions of R9, the two experimental curves in Figure 9.C.2-8 (for temperatures GT9004 and GT9037) show that the heatup was delayed in lower positions in the external annulus behind the missile shield. The lower portion of R9 heats up over a longer period (Figure 9.C.2-8) because of global circulation induced by entrainment in the release. The entrainment is fed by flow from R9, R4 and R1.

Over a period of time, the atmosphere of the containment in the external annulus stratifies (after 16 hours it is already stratified). However, after 36 hours the stratification is not as pronounced, i.e., the temperature differences are not greater than 10°C in the external annulus. The initial stratification in the external annulus results from the high position of the steam release, which is inside the R2 compartment, and the closed circulation paths in the lower portion of the external annulus (see Figure 9.C.2-9).

The experimental curves for temperature histories of the other subcompartments (except for R4 and R3) are not presented in Wolf et al., 1996. However, consecutive phases of other experiments performed in the BMC indicate that natural circulation effects are present and contribute towards homogenization of the temperature fields among the majority of compartments. The only exception is the external annulus.

Application to the AP600 and AP1000

There is evidence that a release high in the steam generator compartment can induce global circulation flow by entrainment through the CMT room openings. It is difficult to compare time scales due to significant differences between the BMC and the passive containment compartment arrangement.

9.C.2.1.1.2 Phases 2-4 of the F2 Experiment (Natural Circulation)

After the heatup, the experiment continues through three additional phases (see Figures 9.C.2-4 and 9.C.2-5 for phases 2, 3 and 4) that use the following methods to induce or amplify circulation:

- Steam injection to induce natural circulation,
- Activation of the heater to reverse circulation,
- Injection of steam to amplify reversed circulation.

Figure 9.C.2-5 illustrates four additional phases (5, 6, 7, and 8) that are not discussed. The circled numbers in Figure 9.C.2-5 represent the type of injection (see also Figure 9.C.2-4). The flow patterns formed during the particular injection are presented below the circled numbers. Figure 9.C.2-9 shows the two different locations for the steam injection, the location of the heater and the positions of the anemometers.

In addition to the measured velocities in the openings (see Table 9.C-3), the fluctuations in measured temperatures indicate natural circulation (see Figures 9.C.2-10 and 9.C.2-11). Due to natural circulation, complex flow patterns form and temperatures in the compartments are nearly homogeneous (i.e., temperature differences are not greater than 4°C, see Figures 9.C.2-10 and 9.C.2-11). The detailed temperatures and velocities during each subphase are given by Kanzleiter, 1988.

Figure 9.C.2-12 presents the thermodynamic states of the containment dome atmosphere at a high position ($H = 7.6$ m) during various time periods, while Figure 9.C.2-13 presents the conditions at a low position in the external annulus ($H = 1.0$ m). Except during air injection times, the steam partial pressure in the high position follows the shape of the total pressure curve (0.5 to 1.0 bar lower values than p_{tot}). At the low position, the steam partial pressure is almost constant (0.5 bar) after 60 hours. This indicates steam stratification inside the external annulus (lower portion of the R9 compartment) behind the missile shield.

The temperature distribution inside the external annulus is presented in Figure 9.C.2-14 for the second phase and in Figure 9.C.2-15 for the third and fourth phases. Both figures indicate stratification of the temperature fields. The temperature difference between the upper dome and the lowest position in the external annulus is 30°C at the end of the second phase and 18°C at the end of the fourth phase.

All other compartments have almost homogeneous temperatures (the greatest temperature differences are 4°C), which indicate the presence of the natural circulation (see Figures 9.C.2-10 and 9.C.2-11).

The values of the measured velocities in the vent between the R3 and R6 compartments during the individual phases are presented in Table 9.C-3. The histories of the velocities in the R7-R9 and R3-R6 vent paths are presented in Figures 9.C.2-16 and 9.C.2-17, respectively. The directions of the convective flow loops as a function of steam and air injections into the various compartments and the applications of the dry heater are presented in Figure 9.C.2-4 (arrow in R9 compartment represents positive flow loop direction). The upward (positive) velocities in Figure 9.C.2-16 produce a positive flow direction loop. The upward (positive) velocities in Figure 9.C.2-17 produce a negative flow direction loop.

The various injections and the application of the dry heat source generate natural circulation and homogenize temperatures in the majority of the containment compartments.

Table 9.C-3 Representative Velocity in [m/s] in Opening from R3 to R6 in the Different Experimental Phases of Experiment F2, Phases 2-4

	Phase No.										
	2.1	2.2	2.3	2.4	3.1	3.2	3.3	4.1	4.2	4.3	4.4
	0.35	-0.4	0.4	-0.4	+/-0.1	+/-0.1	+/-0.1	-0.35	0/0.6	0.35	-0.4

(reprinted from L. Wolf, M. Gavrilas, K. Mun, "Overview of experimental results for long-term, large-scale natural circulations in LWR-containments after large LOCAS," University of Maryland at College Park, Final Report for DOE - Project, Order Number: DE-AP07-96ID10765")

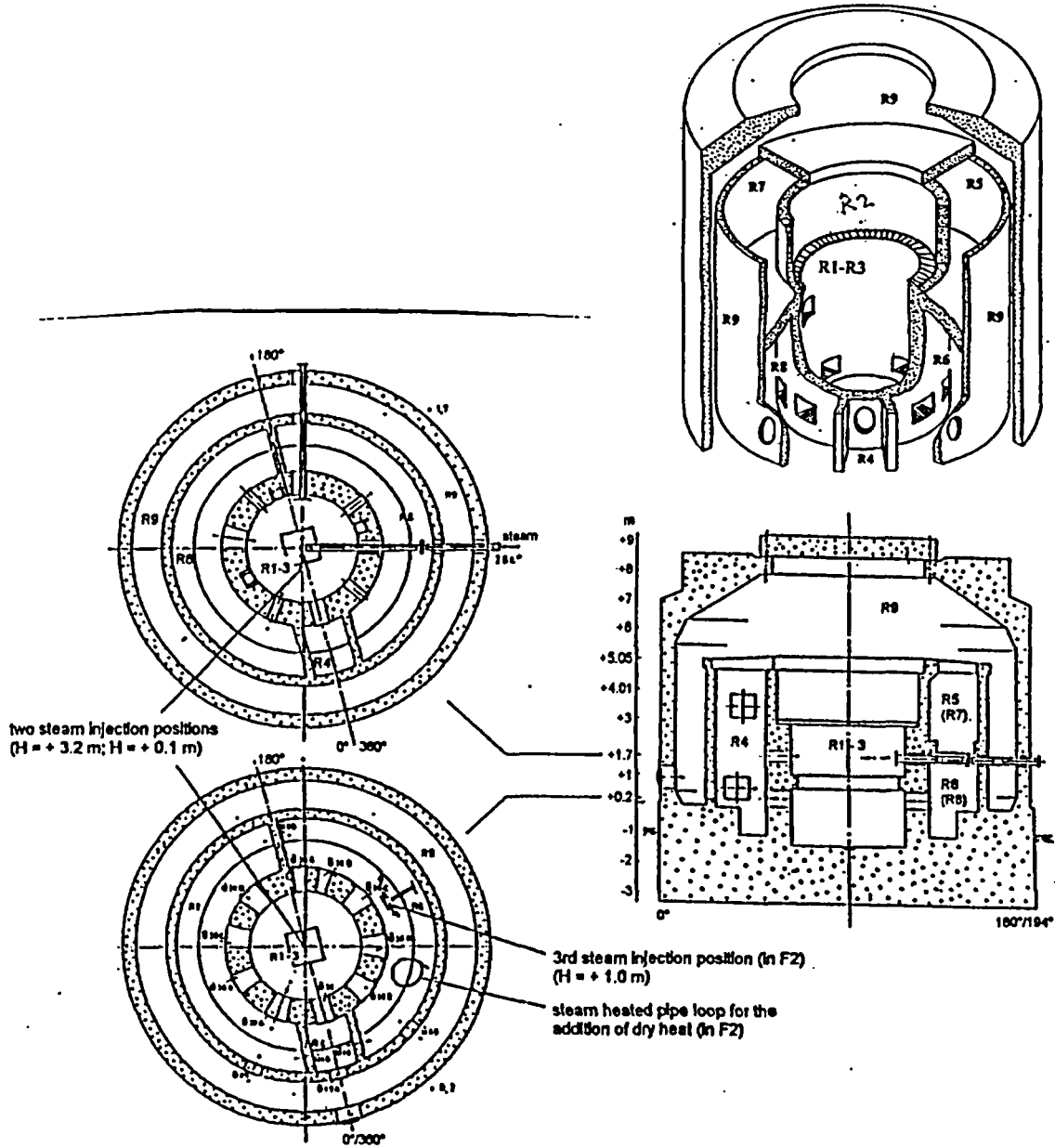


Figure 9.C.2-2 Model Containment: vertical cross-section 0/180°, horizontal cross-sections at +0.2 m and +1.7 m for configuration in experiment F2

(reprinted from L.Wolf, M.Gavrilas, K. Mun, "Overview of experimental results for long-term, large-scale natural circulations in LWR-containments after large LOCAs", University of Maryland at College Park, Final Report for DOE - Project, Order Number: DE-AP07-96ID10765")

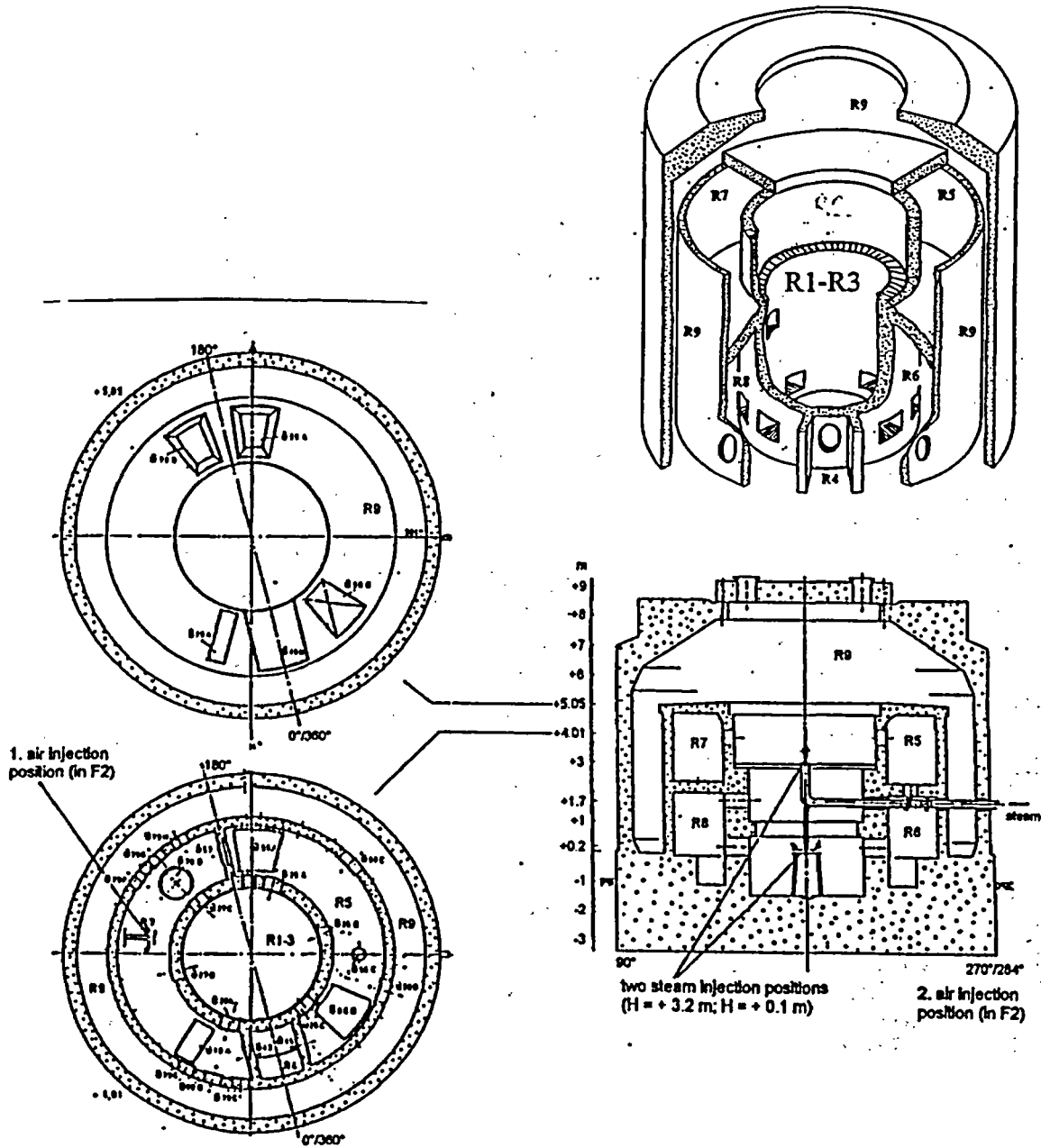
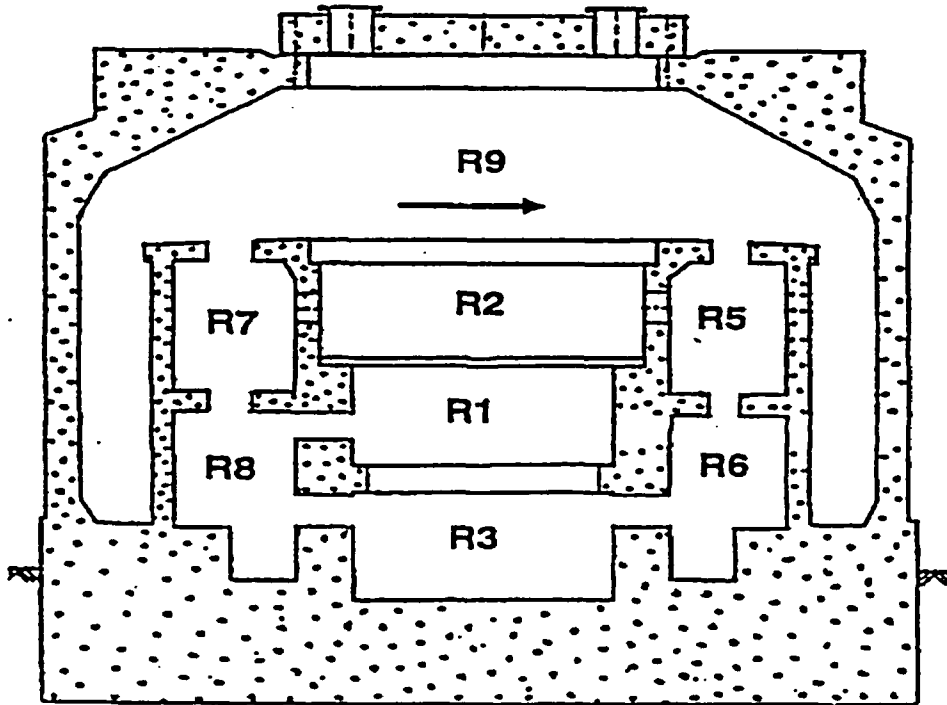


Figure 9.C.2-3 Model Containment: vertical cross-section 0/180°, horizontal cross-sections at +4.01 m and +5.05 m for configuration in experiment F2

(reprinted from L. Wolf, M. Gavrilas, K. Mun, "Overview of experimental results for long-term, large-scale natural circulations in LWR-containments after large LOCAS", University of Maryland at College Park, Final Report for DOE - Project, Order Number: DE-AP07-96ID10765")



Phase	Pressure	Steam	Air	Heat	Drainage	Flow	Injection
1	1-3 bar	R2			R9		
2.1	3 bar	R3	R7		R3	-	1 +
2.2	3 bar	R3		R6	R3	+	2
2.3	3 bar	R6				-	3
2.4	3 bar	R3				+	1
3.1	3 bar						
3.2	to			R6		-	2
3.3	1.8 bar					-	
4.1	1.8 bar	R3				+	2
4.2	1.8 bar	R3		R6		+ -	1
4.3	1.8 bar	R6				-	2
4.4	1.8 bar	R3				+	3

Figure 9.C.2-4 Injections and convective flow loop directions (+ sign for flow indicates the same direction of the flow as arrow in R9)

(reprinted from L.Wolf, M.Gavrilas, K. Mun, "Overview of experimental results for long-term, large-scale natural circulations in LWR-containments after large LOCAS", University of Maryland at College Park, Final Report for DOE - Project, Order Number: DE-AP07-96ID10765")

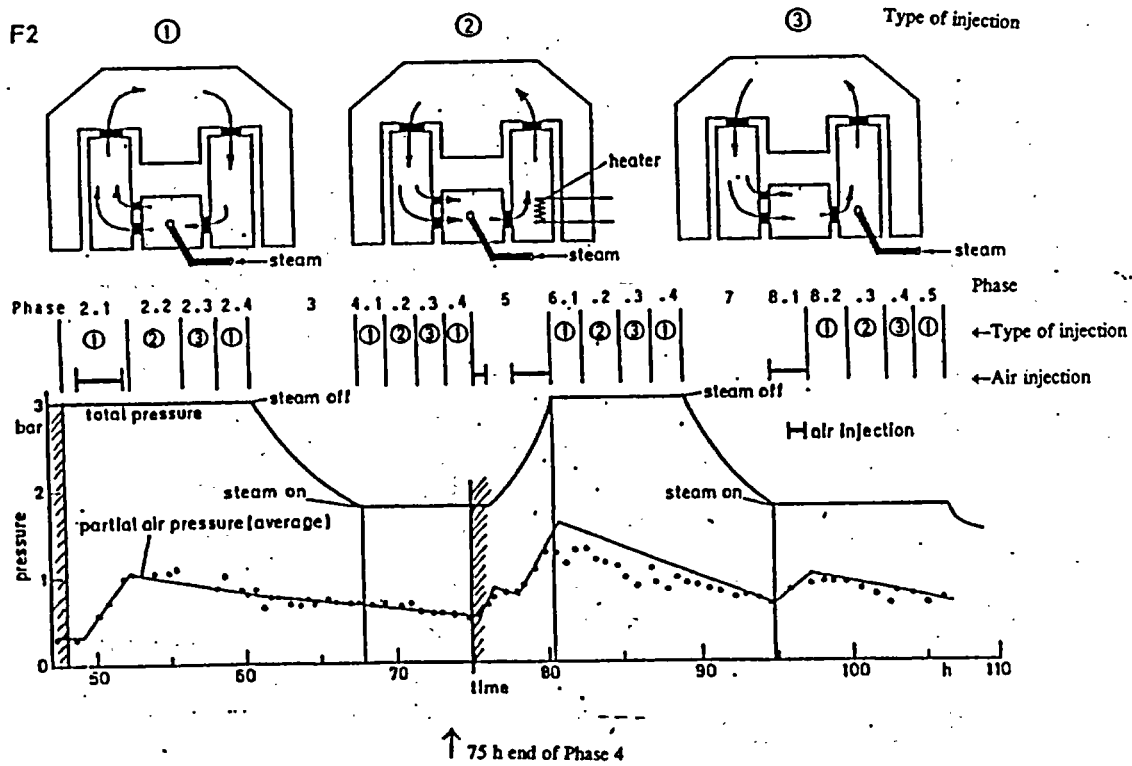


Figure 9.C.2-5 Experiment F2, Phases 2-8, experimental procedures, total and partial pressures

(reprinted from L.Wolf, M.Gavrilas, K. Mun, "Overview of experimental results for long-term, large-scale natural circulations in LWR-containments after large LOCAS", University of Maryland at College Park, Final Report for DOE - Project, Order Number: DE-AP07-96ID10765")

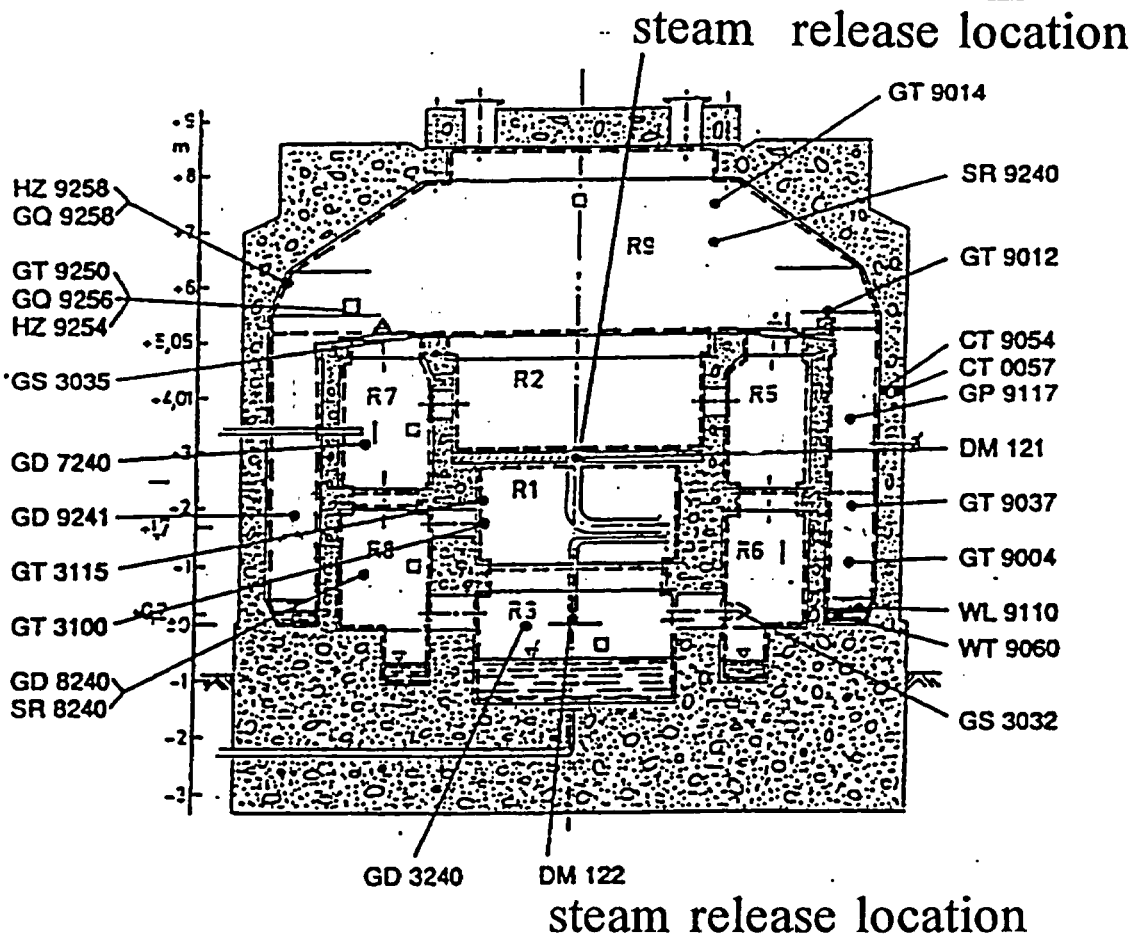


Figure 9.C.2-6 Number of compartments, locations of measurement transducers and steam releases

(reprinted from L.Wolf, M.Gavrilas, K. Mun, "Overview of experimental results for long-term, large-scale natural circulations in LWR-containments after large LOCAS", University of Maryland at College Park, Final Report for DOE - Project, Order Number: DE-AP07-96ID10765")

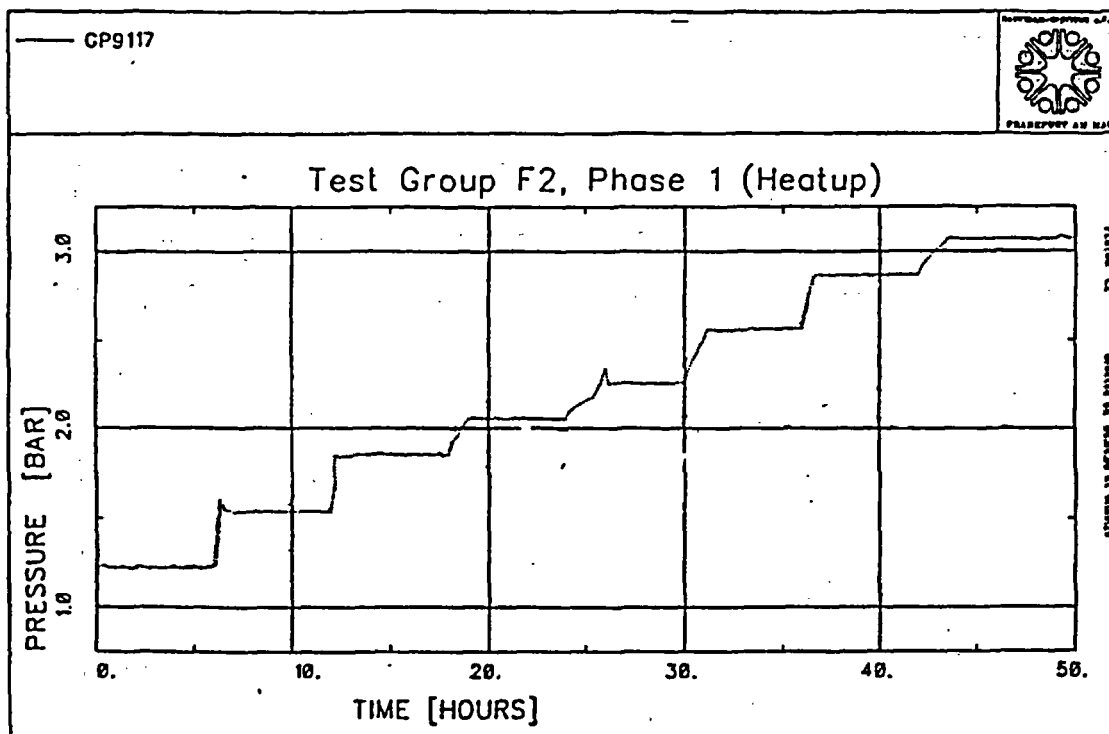
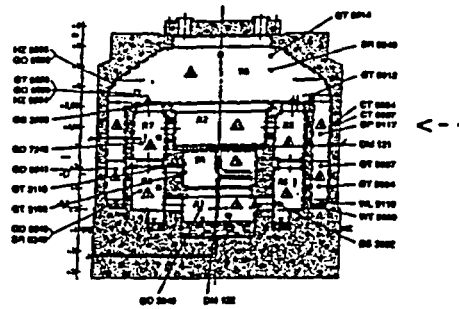


Figure 9.C.2-7 Test group F2, Phase 1 (heatup), total pressure in the containment

(reprinted from L.Wolf, M.Gavrilas, K. Mun, "Overview of experimental results for long-term, large-scale natural circulations in LWR-containments after large LOCAS", University of Maryland at College Park, Final Report for DOE - Project, Order Number: DE-AP07-96ID10765")

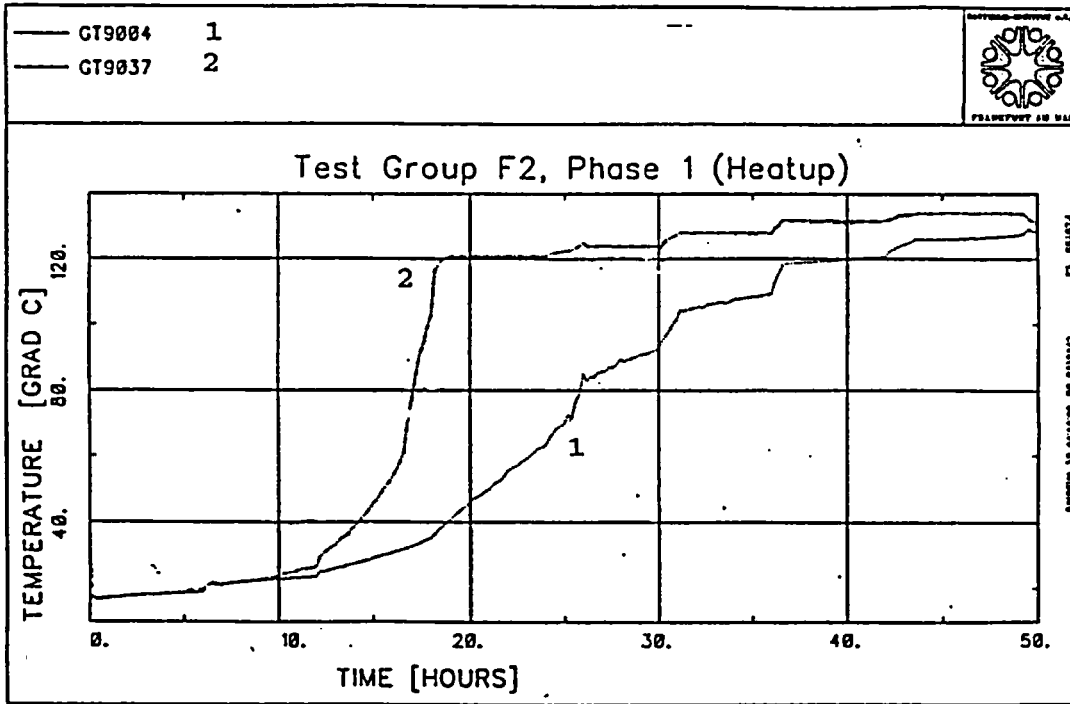
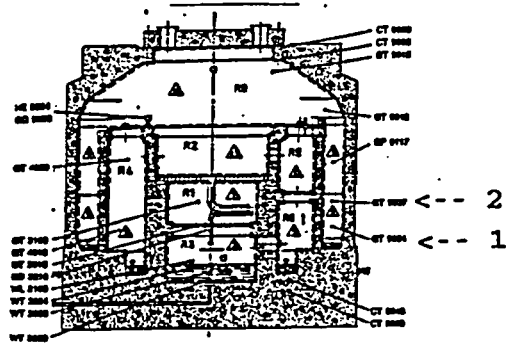
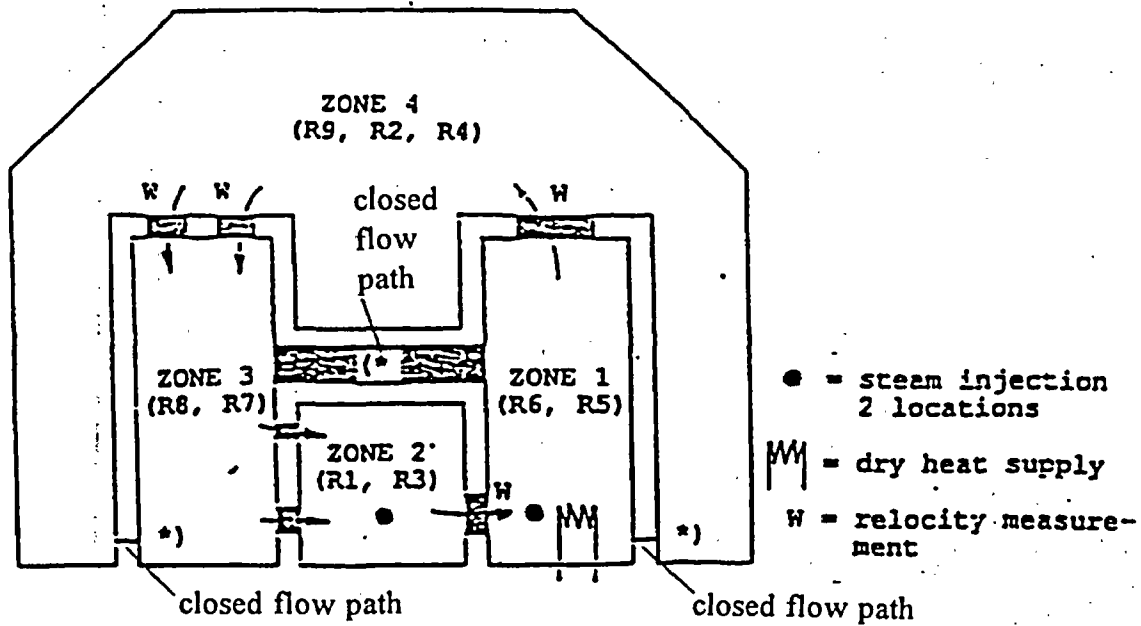


Figure 9.C.2-8 Test group F2, Phase 1 (heatup), atmospheric temperature in the compartment R9, H=1.0 m and 2.1 m.

(reprinted from L.Wolf, M.Gavrilas, K. Mun, "Overview of experimental results for long-term, large-scale natural circulations in LWR-containments after large LOCAS", University of Maryland at College Park, Final Report for DOE - Project, Order Number: DE-AP07-96ID10765")



circulation for phases 3 and 4 are shown

Figure 9.C.2-9 Scheme of multi-compartment containment geometry in experiment F2

(reprinted from L.Wolf, M.Gavrilas, K. Mun, "Overview of experimental results for long-term, large-scale natural circulations in LWR-containments after large LOCAS", University of Maryland at College Park, Final Report for DOE - Project, Order Number: DE-AP07-96ID10765")

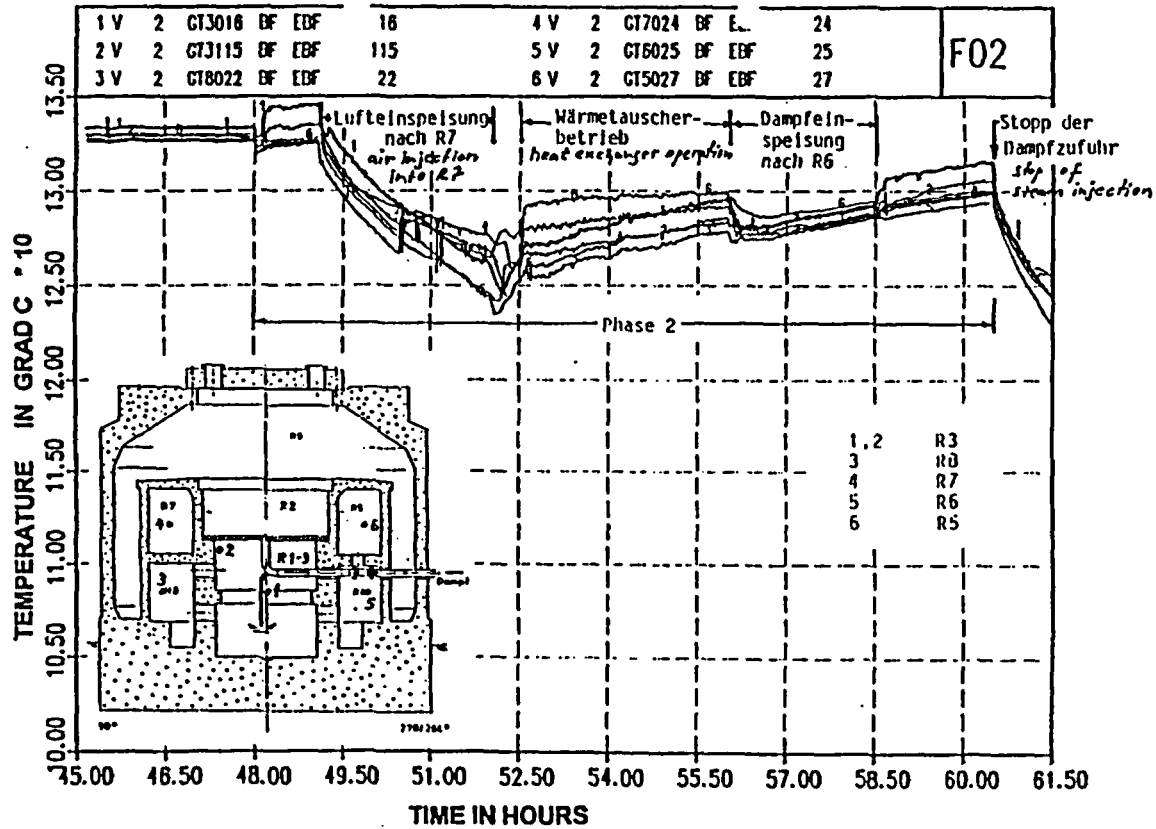


Figure 9.C.2-10 Test group F2, phase 2: atmospheric temperatures in zones 1, 2 and 3 (R5 + R6, R1 + R4, R7 + R8)

(reprinted from L.Wolf, M.Gavrilas, K. Mun, "Overview of experimental results for long-term, large-scale natural circulations in LWR-containments after large LOCAS", University of Maryland at College Park, Final Report for DOE - Project, Order Number: DE-AP07-96ID10765")

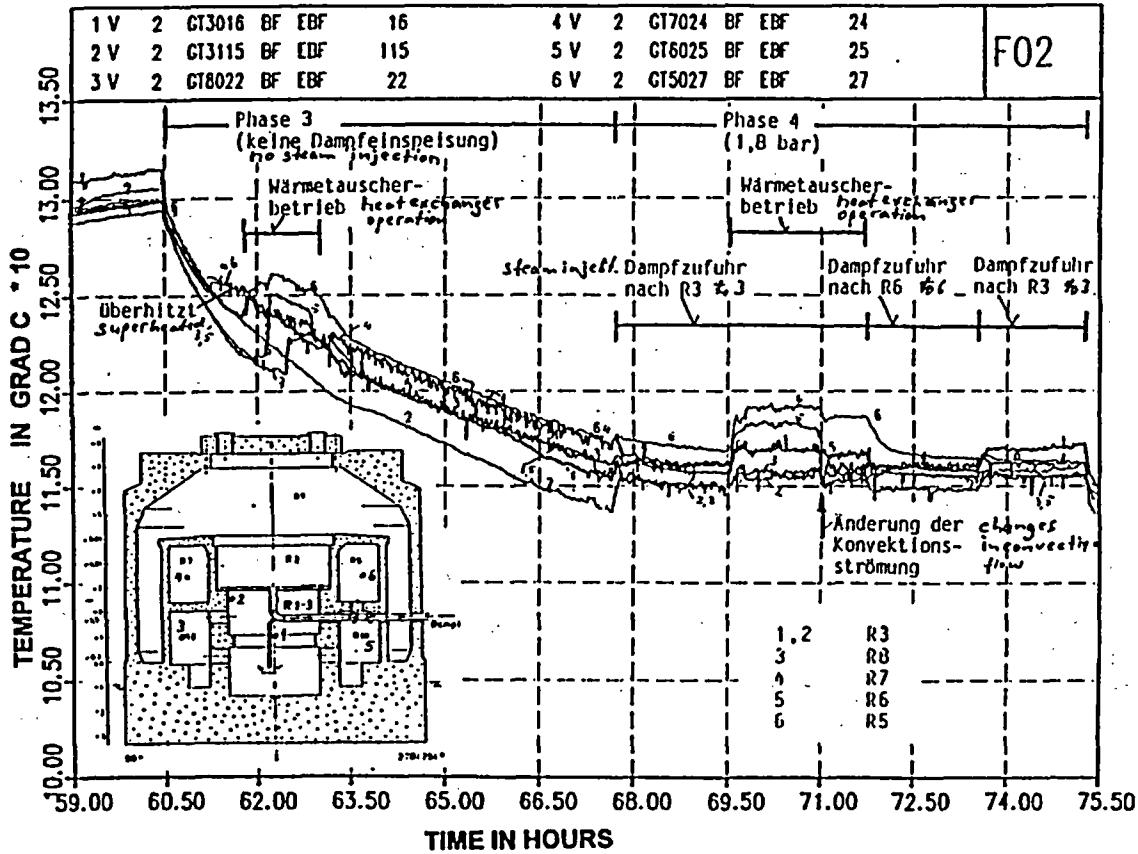


Figure 9.C.2-11 Test group F2, phase 3 and 4: atmospheric temperatures in zone 1, 2 and 3 (R5 + R6, R1 + R4, R7 + R8)

(reprinted from L.Wolf, M.Gavrilas, K. Mun, "Overview of experimental results for long-term, large-scale natural circulations in LWR-containments after large LOCAS", University of Maryland at College Park, Final Report for DOE - Project, Order Number: DE-AP07-96ID10765")

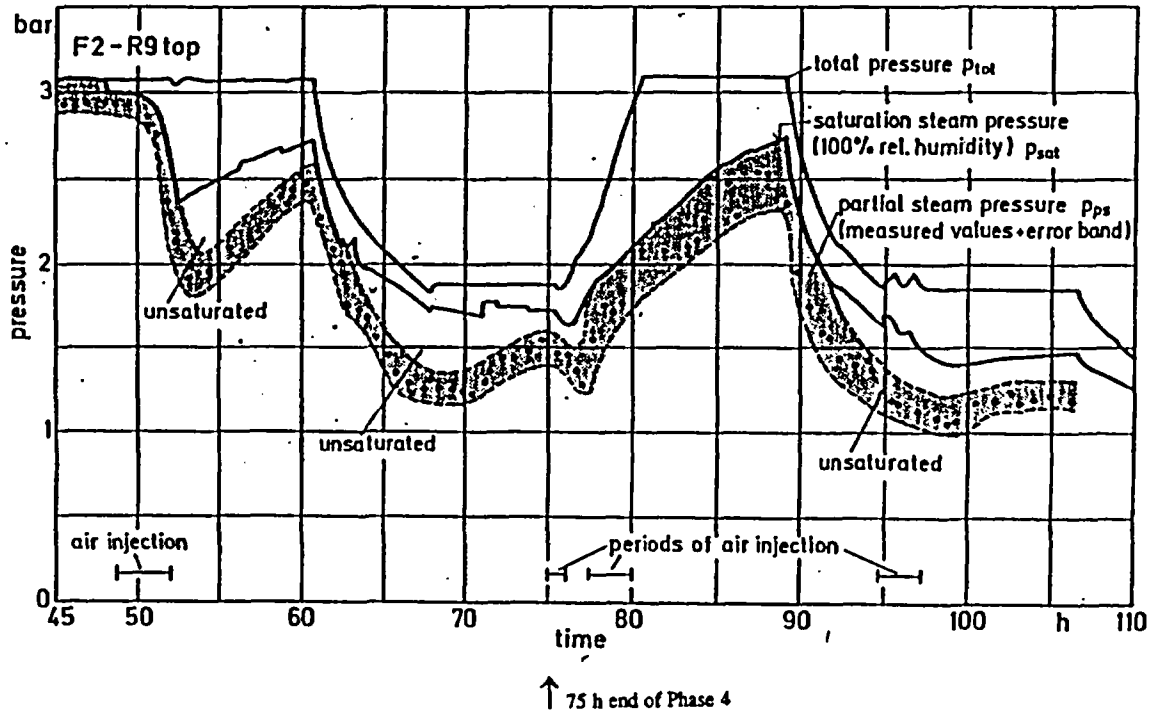


Figure 9.C.2-12 Thermodynamic state of steam-air atmosphere in R9 top (H=7.6 m)

(reprinted from L. Wolf, M. Gavrilas, K. Mun, "Overview of experimental results for long-term, large-scale natural circulations in LWR-containments after large LOCAs", University of Maryland at College Park, Final Report for DOE - Project, Order Number: DE-AP07-96ID10765")

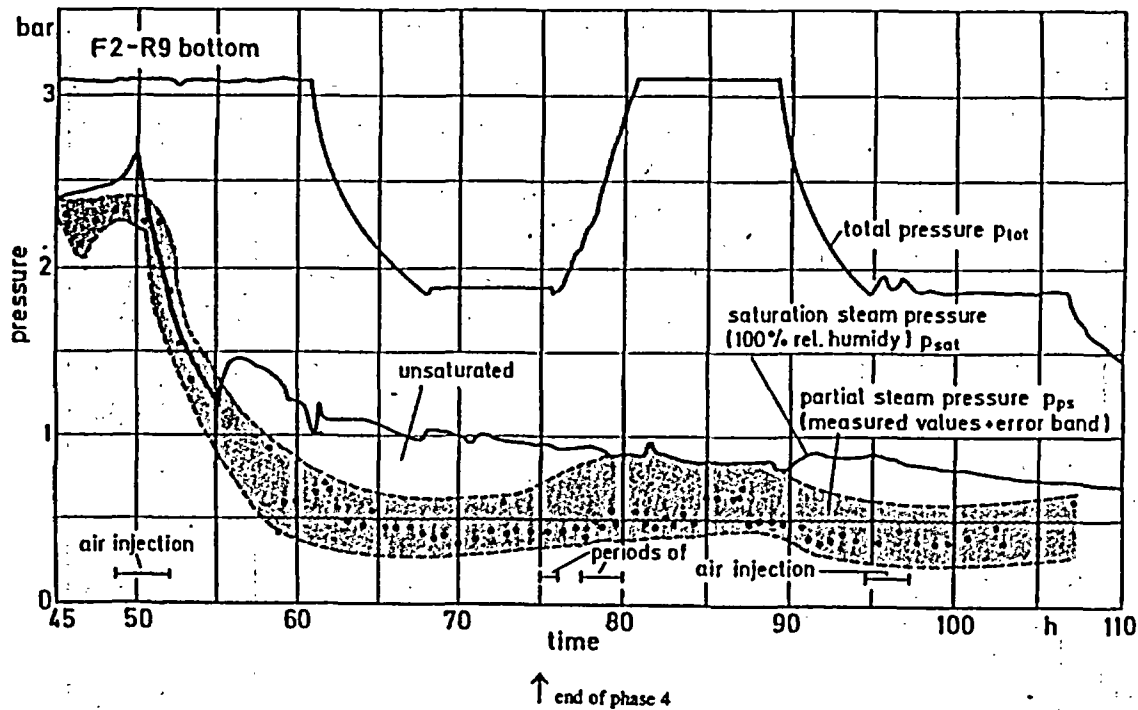


Figure 9.C.2-13 Thermodynamic state of steam-air atmosphere in R9 bottom (H=1 m)

(reprinted from L.Wolf, M.Gavrilas, K. Mun, "Overview of experimental results for long-term, large-scale natural circulations in LWR-containments after large LOCAS", University of Maryland at College Park, Final Report for DOE - Project, Order Number: DE-AP07-96ID10765")

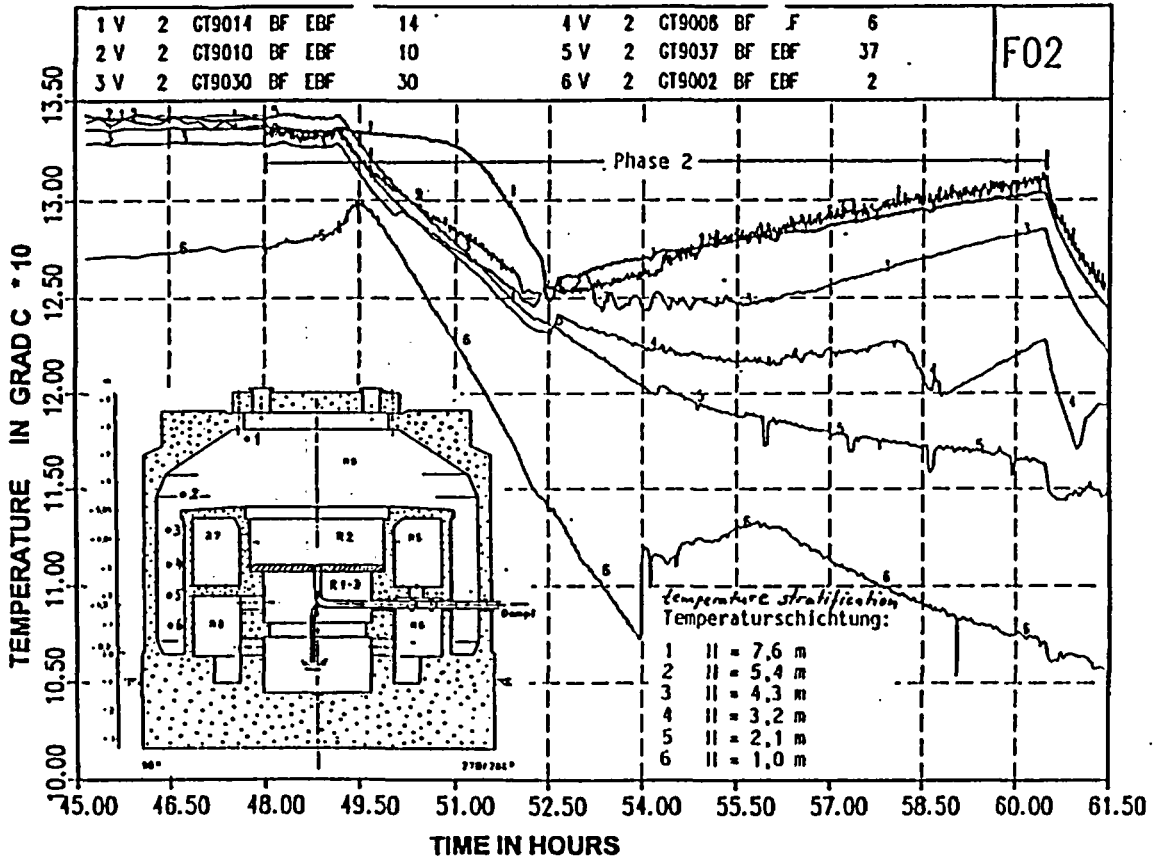


Figure 9.C.2-14 Test group F2, phase 2: atmospheric temperatures in R9 (Zone 4)

(reprinted from L.Wolf, M.Gavrilas, K.Mun, "Overview of experimental results for long-term, large-scale natural circulations in LWR-containments after large LOCAS", University of Maryland at College Park, Final Report for DOE - Project, Order Number: DE-AP07-96ID10765")

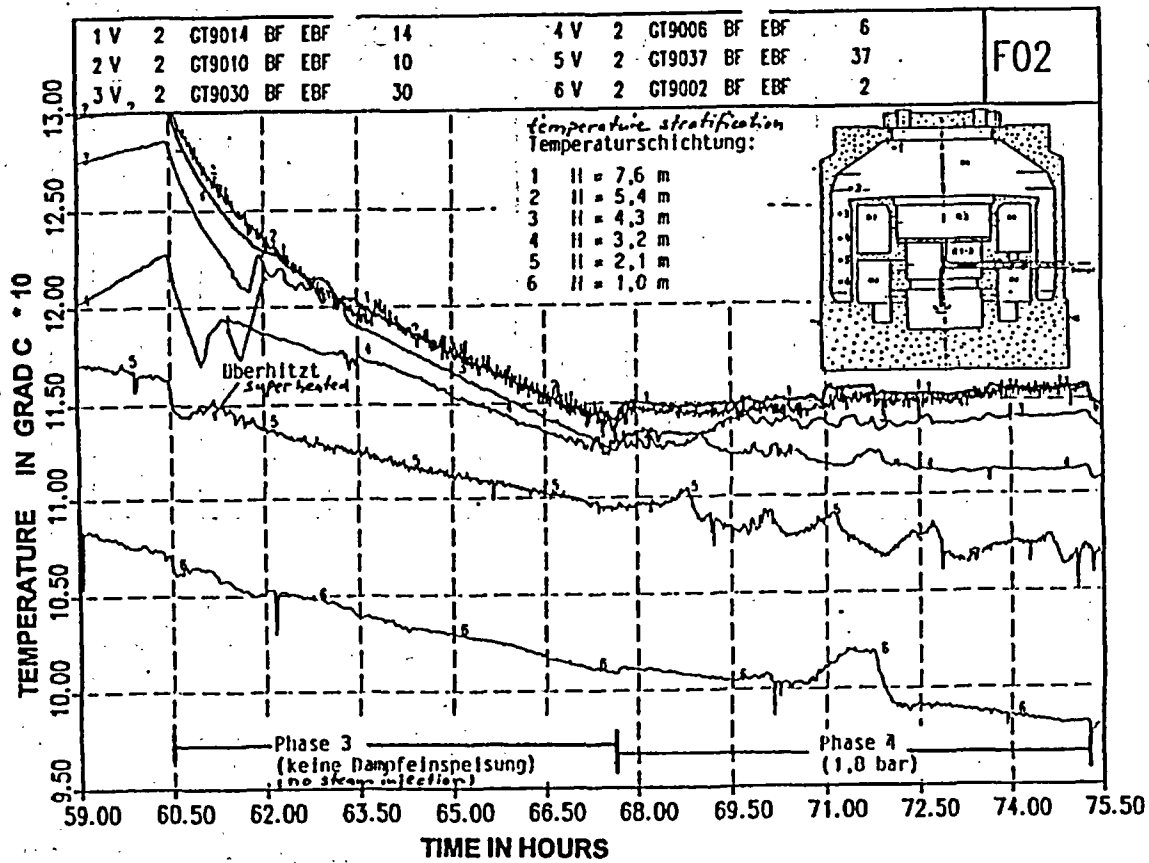


Figure 9.C.2-15 Test group F2, phase 3 and 4: atmospheric temperatures in R9 (Zone 4)

(reprinted from L. Wolf, M. Gavrilas, K. Mun, "Overview of experimental results for long-term, large-scale natural circulations in LWR-containments after large LOCAS", University of Maryland at College Park, Final Report for DOE - Project, Order Number: DE-AP07-96ID10765")

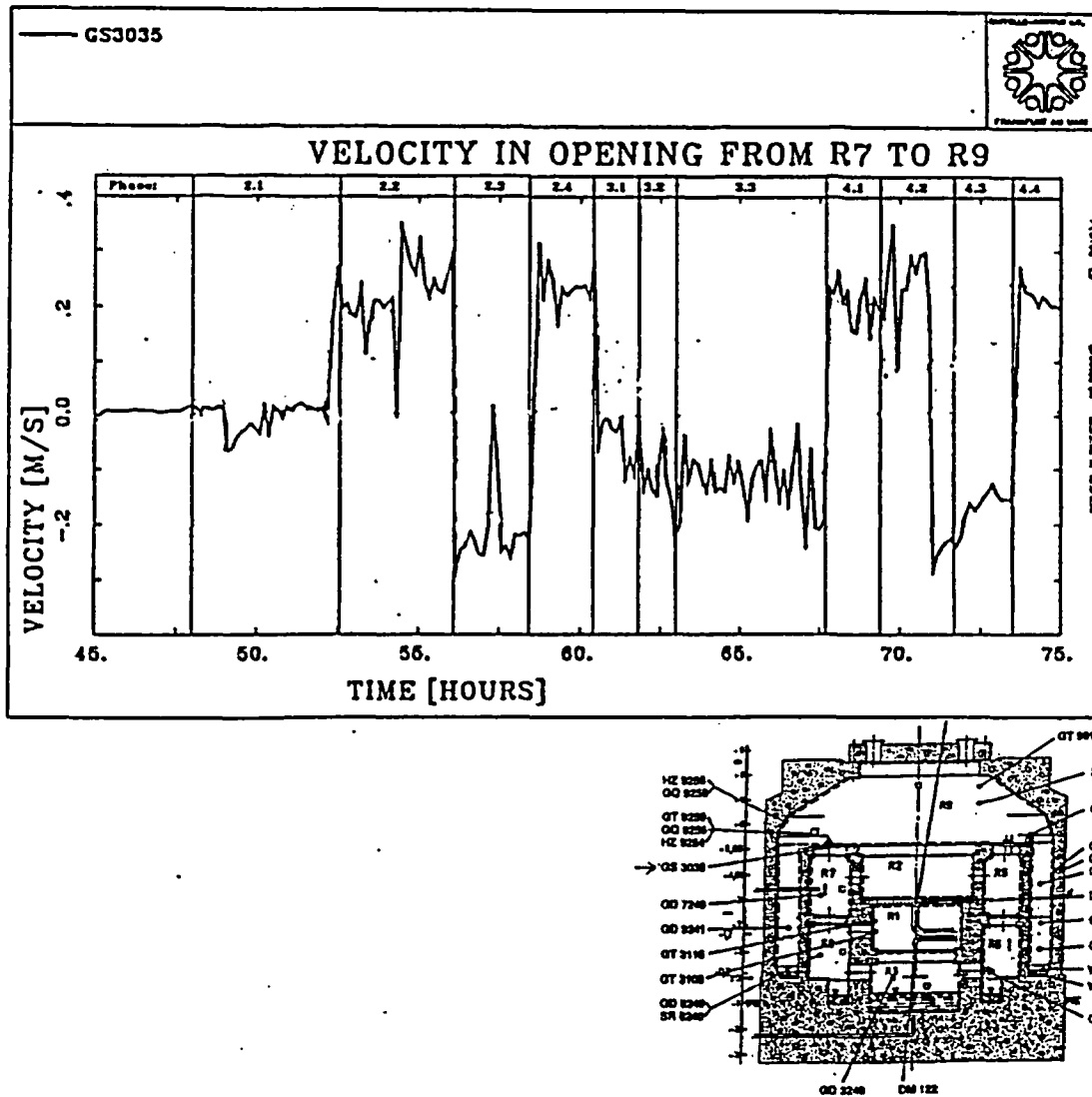


Figure 9.C.2-16 Velocities in opening from compartment R7 to compartment R9

(reprinted from L.Wolf, M.Gavrilas, K. Mun, "Overview of experimental results for long-term, large-scale natural circulations in LWR-containments after large LOCAs", University of Maryland at College Park, Final Report for DOE - Project, Order Number: DE-AP07-96ID10765")

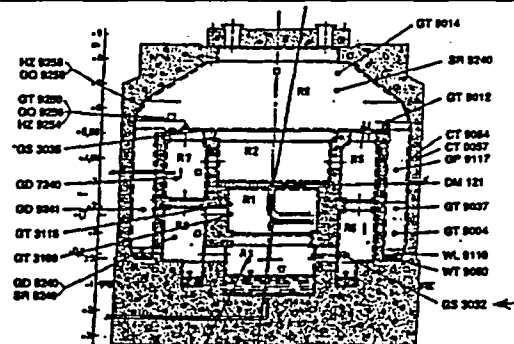
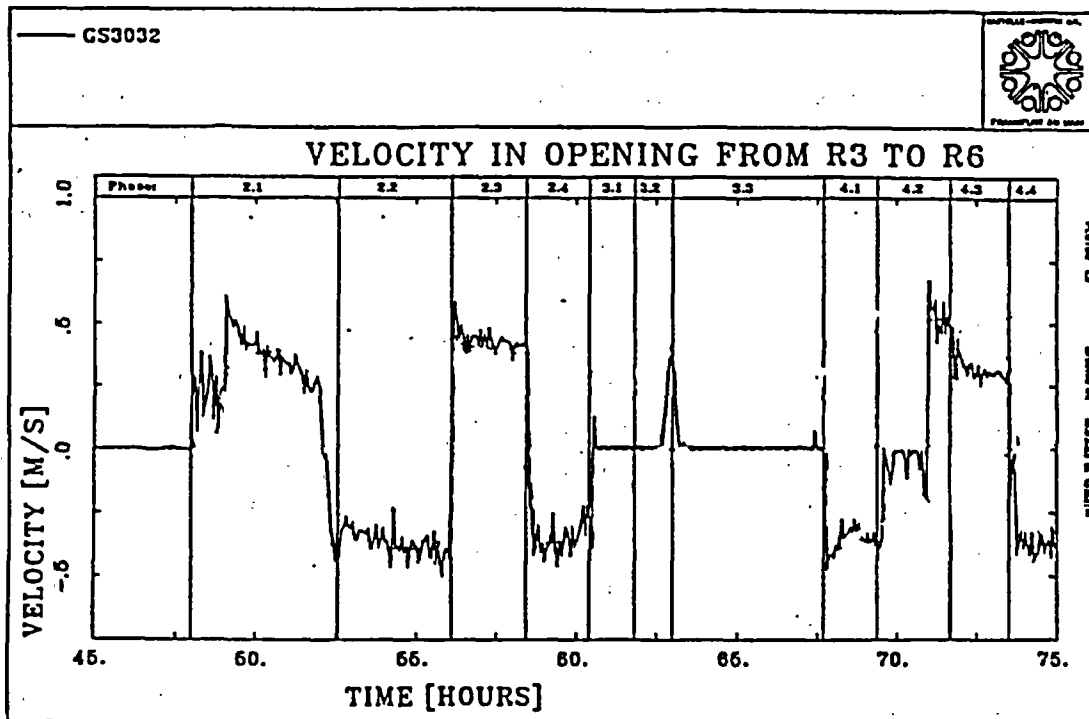


Figure 9.C. 2-17 Velocities in opening from compartment R3 to compartment R6

(reprinted from L.Wolf, M.Gavrilas, K. Mun, "Overview of experimental results for long-term, large-scale natural circulations in LWR-containments after large LOCAs", University of Maryland at College Park, Final Report for DOE - Project, Order Number: DE-AP07-96ID10765")

9.C.2.1.2 The Influence of Initial Temperature Distribution, Location of Hydrogen Injection, Duration of Injection, and Size of Vent Openings on the Hydrogen Distribution (BMC Tests 2, 4, 6, 12 and 20)

Another set of experimental results obtained in BMC is presented in Wolf et al., 1994. The temperature and hydrogen distribution are studied first for two compartments (Phase I) and later for the whole containment (Phase II). These experiments are not directly related to LOCA and MSLB situations, but contribute toward a better understanding of the influence of stratification and circulation phenomena on the hydrogen distribution inside containments. Although Wolf et al., 1994, compared the experimental results with the GOTHIC containment code, the comparisons are not discussed because of the non-prototypical nature of the experiment relative to the passive containment design.

The results of the experiments with only two compartments (upper and lower) are first presented by Langer et al., 1979. The total volume of the two compartments is 72 m³. The central compartments R1, R3 (form lower compartment) and R2 (upper - see Figure 9.C.2-2, 9.C.2-3 and 9.C.2-18) are used for the test. The opening size between the two compartments can be adjusted. Experiments are performed both with and without orifice (with an effective circular opening of 1 m²) between compartments R1 and R2 (see Fig 9.C.2-18). Uniform injection of hydrogen-nitrogen gas is provided by a flat circular plate with a diameter of 2.5 m. The upper containment is preheated with warm air for several days before the start of some experiments to provide stratification .

Tests 2, 4 and 6 (presented by Wolf et al., 1994) investigate the effects of the vertical hydrogen distribution. The measurement positions are located near the bottom (levels 1 m and 1.85 m) and at the top (levels 5 and 5.5 m) of the containment.

The experiments study the effects of

- The hydrogen injection rates
 - Test 2 has a longer time duration than test 6
- The locations of hydrogen injections
 - The hydrogen-nitrogen source is located above the pool surface in tests 2 and 6
 - The hydrogen-nitrogen source is at the 3.4 m elevation (above the mid-elevation of room R1) in test 4

- The vent flow area (between two compartments)
 - An orifice plate is present between R1 and R2 in tests 2 and 6
 - Test 4 is performed without the orifice plate
- The initial temperature distribution in the containment (homogeneous versus stratified)
 - A uniform temperature of 19°C is applied in test 2
 - The temperature is a uniform 22°C in test 4
 - A temperature stratification of 19°C in the R3 and R1 (lower rooms) and 35°C in the R2 (upper room) exist in test 6

The hydrogen pressure ratios at the top and bottom of the compartments are presented in Figure 9.C.2-19a, b, c for the second, fourth, and sixth experiments. A comparison of the hydrogen partial pressures shows the effects of the hydrogen release position (test 4) and the initially stratified temperature field (test 6) on the hydrogen concentration stratification.

The experimental findings presented in Wolf et al., 1994 are:

- 1) The hydrogen is homogeneously distributed through a compartment if the hydrogen source is at the floor and the feed rate is low, even if an orifice plate is installed (see the results for test 2, Figure 9.C.2-19a). Note that the feed rate in the second experiment is lower than in the fourth and sixth experiment. Also, hydrogen is released for 225 minutes in test 2 and for 125 minutes in test 4 and 6.
- 2) Vertical concentration stratification occurs if the source is located above the floor (see results for test 4, Figure 9.C.2-19b). For low kinetic energy, the diffusion process slowly equalizes concentrations.
- 3) If the openings between compartments are relatively small, the transport of hydrogen may be obstructed (see results for test 6, Figure 9.C.2-19c).
- 4) If an initial thermal stratification of air exists and an orifice is installed between the lower and upper compartments, the transport of the lighter H_2/N_2 gas mixture is prevented. The highest hydrogen concentrations exist in the lower, cooler part of the compartments, where circulation and mixing occurs (see results for test 6, Figure 9.C.2-19c). The initially stratified temperature field is provided by keeping the upper compartment R2 at a higher temperature (35°C) for several days before the start of the experiment.

Figure 9.C.2-19a (see results for test 2) shows that the buoyancy of the rising plume and the circulation resulting from entrainment into the introduced lighter H_2/N_2 gas mixture lead to a relatively homogenized atmosphere. Circulation and mixing are present in both the upper and lower compartments.

Test 4, with an elevated source and reasonably low kinetic energy (Fr is not reported for the tests), shows that there is no significant driving force for circulation below the break elevation. Stratification into two regions occurs, one below and one above the break elevation. The lower region is almost stagnant, while circulation and mixing is present in the upper region (see GOTHIC numerical simulation results by L.Wolf, H. Holzbauer, M. Schall, 1994).

In comparison, test 6, which includes an orifice between R1 and R2 and a stratified temperature field in the upper R2 compartment, shows an almost stagnant upper region. It also shows an increase in the concentration of the lighter H_2/N_2 gas mixture in the lower region (a result of the circulation and mixing in the lower regions R1 and R3). The lighter gas mixture is not able to penetrate into the upper stratified layers due to the presence of the narrow orifice. The circulation cell formed by the gas mixture injection into the lower compartments does not communicate with the stratified layers in the upper compartment (see also GOTHIC numerical simulation results by L.Wolf, H. Holzbauer, M. Schall, 1994).

Application to the AP600 and AP1000

These tests are not relevant to the passive containment design. The cold dome prevents the stratification that results from higher temperatures of either the vertical walls at the high elevations or the ceiling. In the BMC case, the higher temperatures of the wall surfaces are maintained for a long period of time due to the heat accumulated in the concrete walls (which are heated for several days before the start of the experiment). The passive containment shell is made of steel. Natural convection at the outer surface of the containment walls keeps their temperature low, so that a highly stratified initial temperature field is not possible. Even if initial stratification exists, the application of water on the outer containment surface decreases wall temperatures and causes circulation inside the containment.

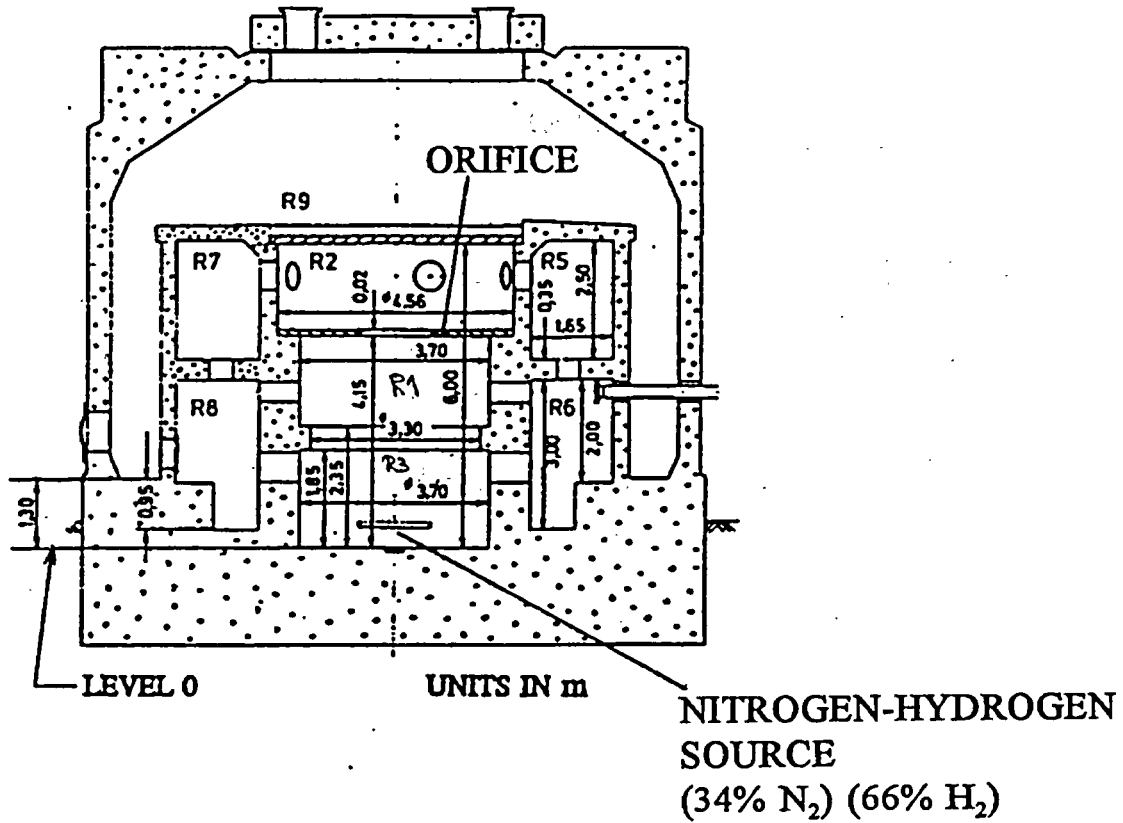
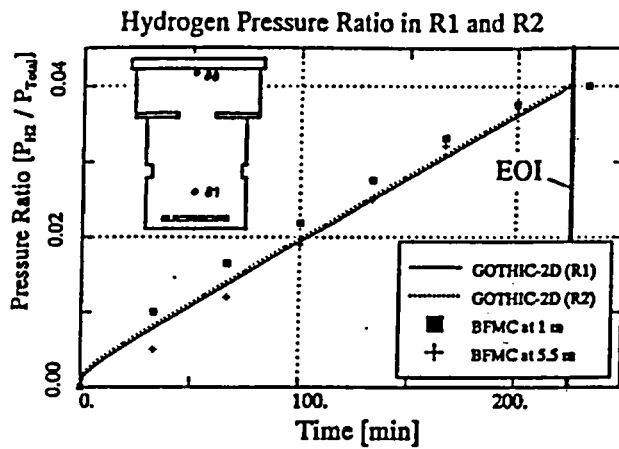


Figure 9.C.2-18 Vertical cut through BMC with orifice in between R2 and R1

(reprinted with permission from authors from L. Wolf, H. Holzbauer, M. Schall, "Comparison between multi-dimensional and lumped-parameter GOthic-containment analyses with data", Proceedings, Volume II - Thermohydraulics of Containment and Severe Accidents, May 30th - June 2nd, 1994, pp. 321-330.)

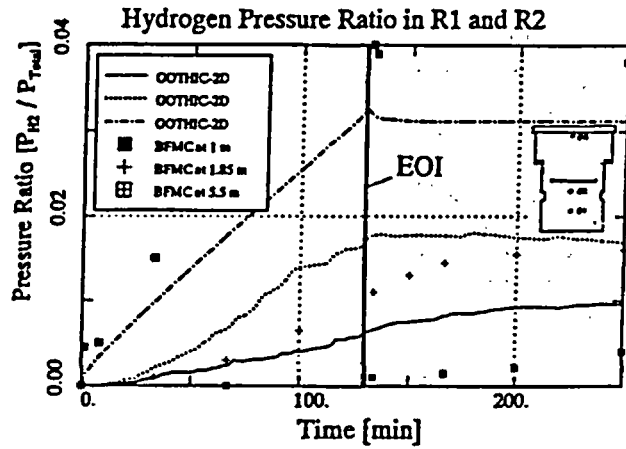


Battelle Test No. 2

EOI - End of Injection

Figure 9.C.2-19a BMC test no. 2: Comparison between experimental data and 2-d GOTHIC computations for hydrogen concentrations

(reprinted with permission from authors from L.Wolf, H. Holzbauer, M. Schall, "Comparison between multi-dimensional and lumped-parameter GOTHIC-containment analyses with data", Proceedings, Volume II - Thermohydraulics of Containment and Severe Accidents, May 30th - June 2nd, 1994, pp. 321-330.)

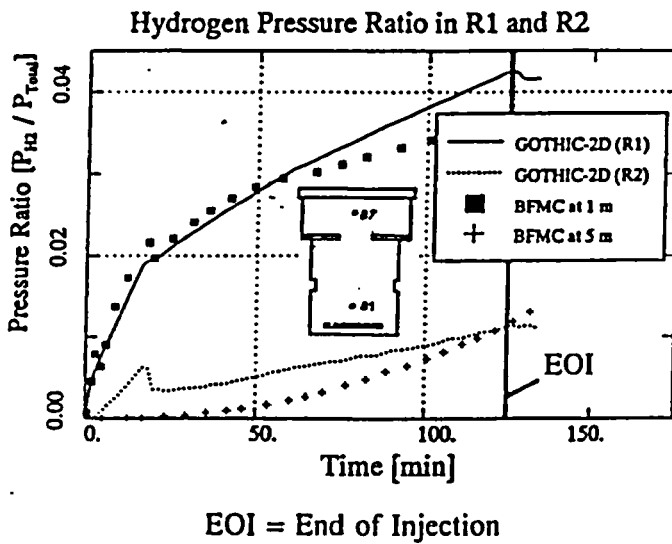


Battelle Test No. 4

EOI - End of Injection

Figure 9.C.2-19b BMC test no. 4: Comparison between experimental data and 2-d GOTHIC computations for hydrogen concentrations

(reprinted with permission from authors from L.Wolf, H. Holzbauer, M. Schall, "Comparison between multi-dimensional and lumped-parameter GOTHIC-containment analyses with data", Proceedings, Volume II - Thermohydraulics of Containment and Severe Accidents, May 30th - June 2nd, 1994, pp. 321-330.)



Battelle Test No. 6

Figure 9.C.2-19c BMC test no. 6: Comparison between experimental data and 2-d GOTHIC computations for hydrogen concentrations

(reprinted with permission from authors from L. Wolf, H. Holzbauer, M. Schall, "Comparison between multi-dimensional and lumped-parameter GOTHIC-containment analyses with data", Proceedings, Volume II - Thermohydraulics of Containment and Severe Accidents, May 30th - June 2nd, 1994, pp. 321-330.)

In the second phase (Langer and Baukal, 1982), the full model containment is used for experiments. The effects of: (1) the initial temperatures and humidities, (2) the geometry of the containment, and (3) the location and rate of hydrogen release are investigated.

The results of tests 12 and 20 are presented in Wolf et al., 1994 and are compared with the results of three GOTHIC modeling strategies. Tests 12 and 20 are performed with six compartments (R1-2, R5-8, see Figures 9.C.2-2 and 9.C.2-3). The hydrogen-nitrogen mixture is injected into rooms R2 and R6 in tests no.12 and 20, respectively.

Test no. 12 is performed with a uniform initial temperature. It results in a homogenized hydrogen distribution in the containment (see Figure 9.C.2-20). The stratified initial temperature distribution in test 20 results in higher hydrogen distribution in the lower level compartments (R1, R6 and R8 - see Figure 9.C.2-21a, b, c). An explanation for this unexpected result is that the circulation cell formed by the injection of the lighter gas mixture is not able to penetrate upper stratified layers at the beginning of the experiment. This is similar to test 6, which includes an orifice and stratified initial temperature field in the upper compartment. After three hours, there is a tendency toward decreased gradients in the concentration field, especially between R1 and R2 compartments. This indicates that global circulation affects the upper stratified layers.

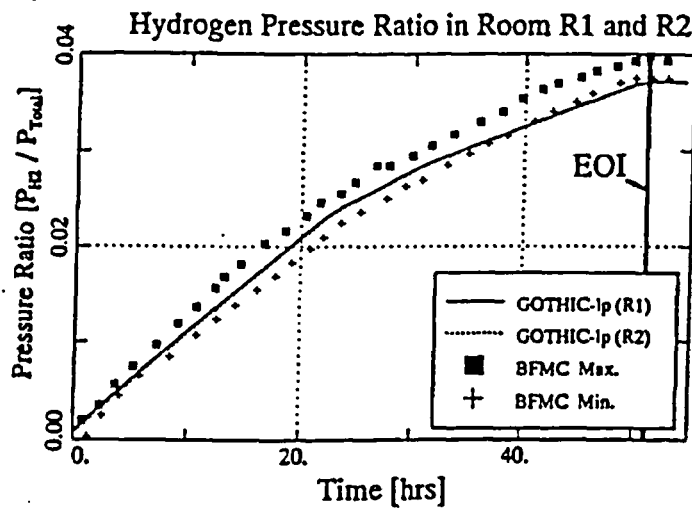
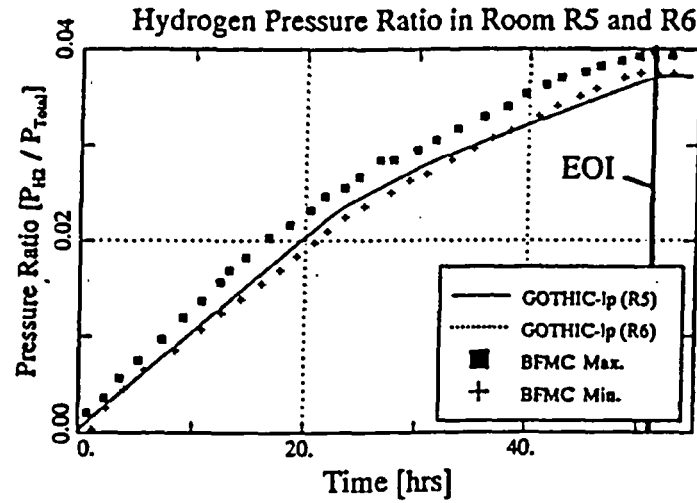
A summary of the experimental results is:

- 1) If the temperature field was uniform (test 12), hydrogen was homogeneously distributed inside the containments.
- 2) For an initially thermally stratified field (test 20), higher hydrogen concentrations are present in the lower (cooler) compartments at the beginning of the experiment.

Both groups of experiments indicate that good air circulation inside the containment (in fact a uniform temperature field) is crucial for homogeneous hydrogen distribution. Note that in the first group of tests, the stratification is obtained by preheating the upper room with warm air for several days before the start of the experiments.

A comparison between this experimental data and the numerical results obtained with GOTHIC (with lumped-parameter and multi-dimensional analyses) is presented in Wolf et. al, 1994.

Battelle Test No. 12



EOI = End of Injection

Figure 9.C.2-20 BMC test no. 12: Comparison between experimental data and GOTHIC-lp computations for hydrogen concentrations

(reprinted with permission from authors from L. Wolf, H. Holzbauer, M. Schall, "Comparison between multi-dimensional and lumped-parameter GOTHIC-containment analyses with data", Proceedings, Volume II - Thermohydraulics of Containment and Severe Accidents, May 30th - June 2nd, 1994, pp. 321-330.)

Battelle Test No. 20

Hydrogen Pressure Ratio in Room R1 and R2

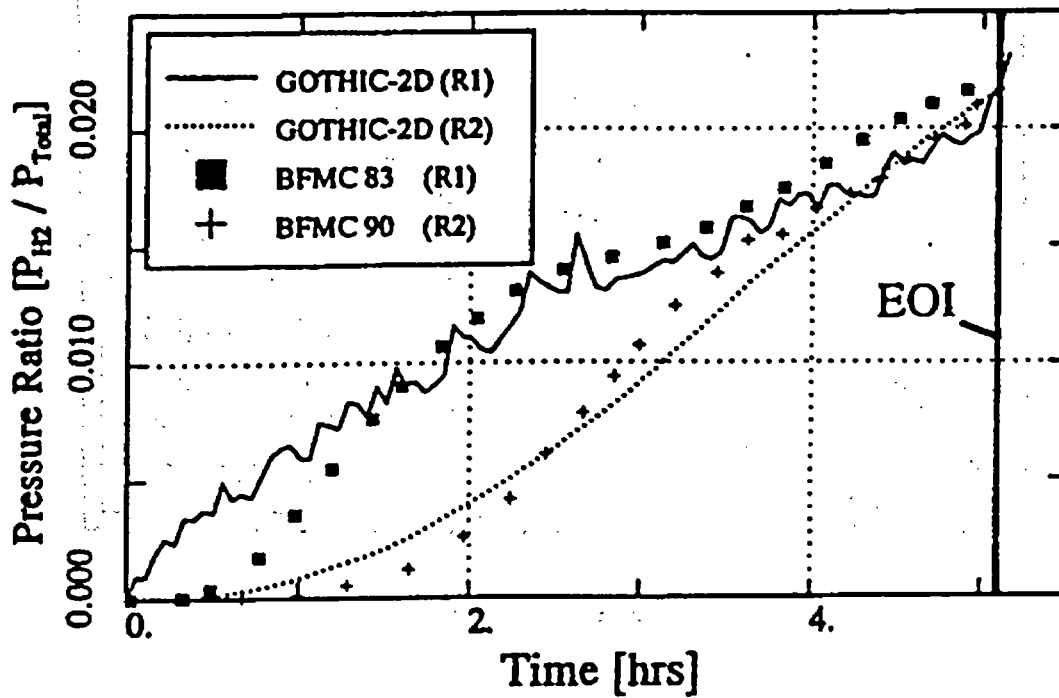


Figure 9.C.2-21a BMC test no. 20: Comparison between experimental data and 2-d GOTHIC computations for hydrogen concentrations

(reprinted with permission from authors from L.Wolf, H. Holzbauer, M. Schall, "Comparison between multi-dimensional and lumped-parameter GOTHIC-containment analyses with data", Proceedings, Volume II - Thermohydraulics of Containment and Severe Accidents, May 30th - June 2nd, 1994, pp. 321-330.)

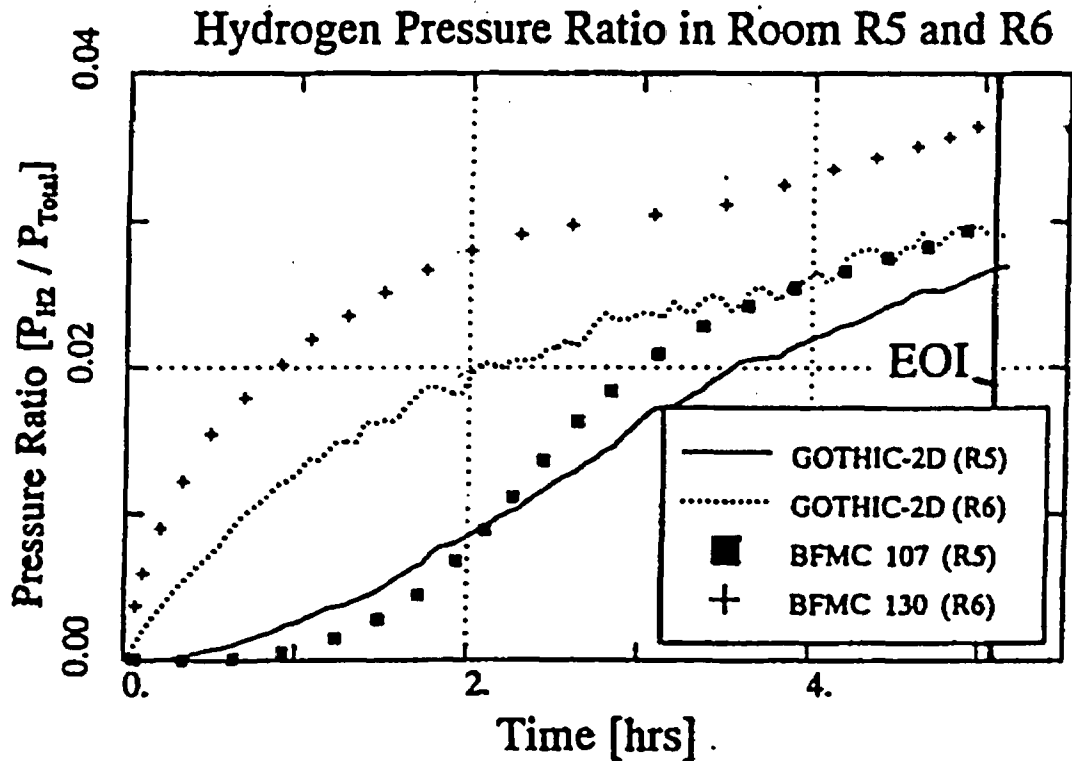


Figure 9.C.2-21b BMC test no. 20: Comparison between experimental data and 2-d GOTHIC computations for hydrogen concentrations

(reprinted with permission from authors from L. Wolf, H. Holzbauer, M. Schall, "Comparison between multi-dimensional and lumped-parameter GOTHIC-containment analyses with data", Proceedings, Volume II - Thermohydraulics of Containment and Severe Accidents, May 30th - June 2nd, 1994, pp. 321-330.)

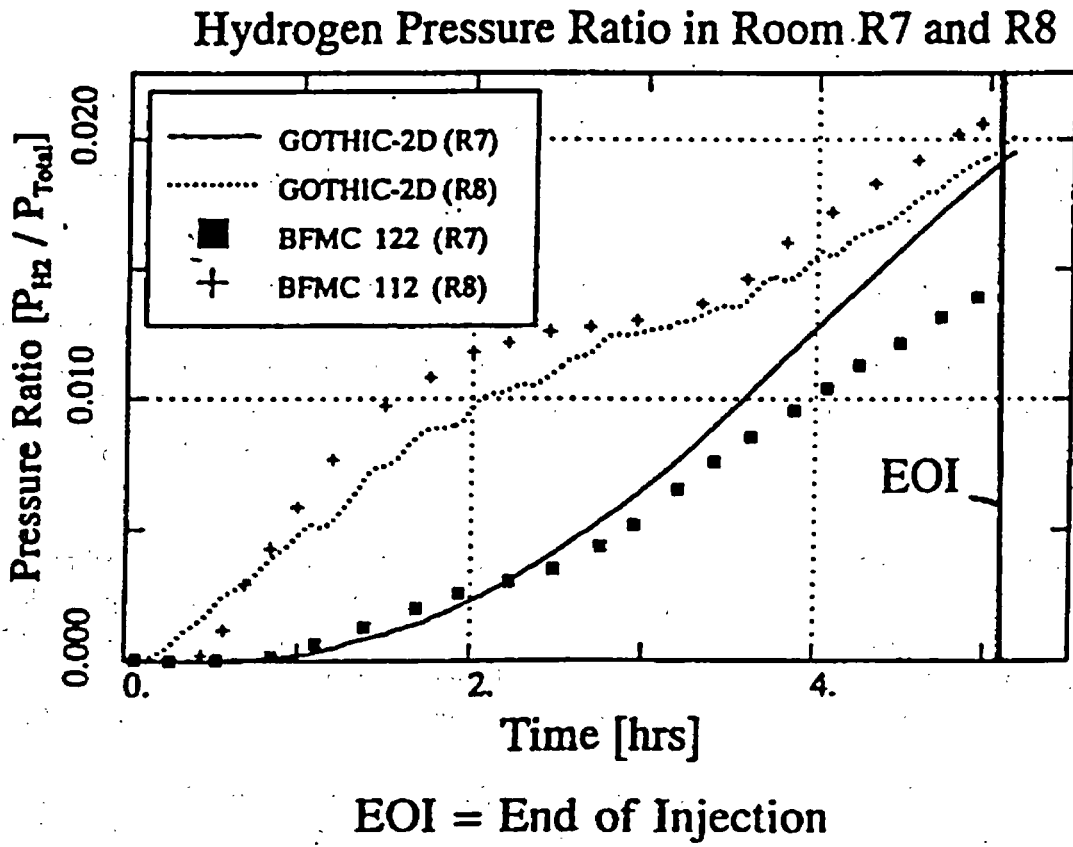


Figure 9.C.2-21c BMC test no. 20: Comparison between experimental data and 2-d GOTHIC computations for hydrogen concentrations

9.C.2.1.3 Effects of Sump Heatup on Global Natural Circulation (Experiments RX1 - RX5)

The third set of experiments performed in the BMC (Fischer et al., 1994 and Petersen et al., 1994) examine the effect of sump heatup on global natural circulation inside the containment. The starting and transient behavior of natural circulation for small temperature differences, the influence of natural circulation on mixing of hydrogen released during accident conditions, and the effects of stratification on the natural convection formation are also studied.

A total of five experiments are performed (RX1 to RX5) at atmospheric pressure. Temperatures are recorded in the sump, in the containment atmosphere, and in the concrete structures. The relative humidity, containment pressure, liquid sump level, velocities (in the vents), and hydrogen concentration are also measured.

The objective of long-term experiments is to establish at what sump temperature global circulation exists. During these experiments, the containment atmosphere, structure, and sump have nearly identical temperatures. Circulation effects inside the containment are already present with a sump temperature as low as 25°C. Experiments RX2 (without hydrogen injection) and RX4 (with multiple hydrogen injections) are performed as long-term tests. The respective initial and boundary conditions for all experiments are given in Table 9.C-4.

Results are provided for only the RX4 experiment, since the hydrogen distribution is available for this test. A summary of the results for the RX4 experiment, with the cold containment and multiple hydrogen injections, is presented in Wolf et al., 1996. The perspective view and cross-sections of the BMC containment, illustrating the compartment numbers and the location of the hydrogen injection, are presented in Figures 9.C.2-22 and 9.C.2-23. The instrumentation plan for the RX4 test is specified in Figure 9.C.2-24.

At the beginning of the experiment, the temperatures of the structure range from 20-26°C. The sump temperature is 20°C (see Figure 9.C.2-25). Several consecutive characteristic periods evolve during the experiment. The sump heat up is divided into three periods:

- 1) 0 to 1:48 hr - the sump is heated to 50°C
- 2) 2:43 to 3:39 hr - continuation of sump heating to 60°C
- 3) 3:34 to 4:52 hr - continued sump heating to maintain the temperature at 60°C until the end of experiment (5 hr)

Three hydrogen injections occur:

- 1) 1:11-1:24 hr, 236 g of hydrogen is released
- 2) 2:11-2:23 hr, 215 g of hydrogen is released
- 3) 4:06-4:33 hr, 319 g of hydrogen is released

At the beginning of the sump heatup, the anemometers register velocities between 0.2-0.3 m/s (for sump temperatures 24-27°C), while at the end of the experiment, velocities are 0.6-0.8 m/s (see Figure 9.C.2-26). At the end, the temperature of the dome is 30°C (see Figure 9.C.2-27). Shaded areas in Figures 9.C.2-26 and 9.C.2-27 represent periods of hydrogen injection. Velocities increase during periods of hydrogen injection.

Sump and atmosphere temperatures are presented in Figures 9.C.2-25, 9.C.2-27, and 9.C.2-28. Temperature differences in the area of the center compartment and dome are not greater than 2°C (Figure 9.C.2-27). The temperature difference in the external annulus is smaller than 3°C (Figure 9.C.2-28), indicating the presence of natural circulation effects.

Due to the natural circulation, the hydrogen distribution is almost uniform in the whole containment, see (Figures 9.C.2-29 and 9.C.2-30). After two hours, the relative humidity of the whole containment atmosphere is 100 percent (see Figure 9.C.2-31). Even low natural circulation flows provide complete mixing of the hydrogen and steam (evaporated from sump). The heated sump provides sufficient buoyancy force for natural circulation flow.

Table 9.C-4 Test Matrix of Battelle Sump Heatup Experiments

Test No.	Containment-Atmosphere			Structure-Temperature [°C]	Sump-Temperature [°C]	H ₂ -Mass [g]
	Containment Media	Initial Temperature [°C]	Total Pressure [bar]			
RX1	air	23.5 - 28.5	1.011	24 - 26	1) ≈ 40 2) ≈ 50 3) ≈ 55 4) ≈ 60	-----
RX2	air	22 - 28.5	1.009	24.5 - 28	1) ≈ 40 2) ≈ 50 3) ≈ 60	-----
RX3	air + steam	48 - 58.5	1.008	42 - 61	60 - 100	-----
RX4	air + H ₂	24 - 27	1.014	22.5 - 26.5	1) ≈ 48 2) ≈ 60	1) 236 2) +215 3) +319
RX5	air + steam + H ₂	55 - 69	1.001	39 - 64	1) 62 - 49 2) 63 - 58	1) 371 2) +390 3) +406

(reprinted from L. Wolf, M. Gavrilas, K. Mun, "Overview of experimental results for long-term, large-scale natural circulations in LWR-containments after large LOCAS," University of Maryland at College Park, Final Report for DOE - Project, Order Number: DE-AP07-96ID10765")